DIGITAL COMMONS
@ UNIVERSITY OF SOUTH FLORIDA

University of South Florida
Digital Commons @ University of South Florida

6-28-2024

The discovery of first RET PROTAC with *in vivo* activity

Yafeng Wang
University of South Florida

Follow this and additional works at: https://digitalcommons.usf.edu/etd

Part of the Chemistry Commons

Scholar Commons Citation
Wang, Yafeng, "The discovery of first RET PROTAC with *in vivo* activity" (2024). *USF Tampa Graduate Theses and Dissertations.*
https://digitalcommons.usf.edu/etd/10574

This Dissertation is brought to you for free and open access by the USF Graduate Theses and Dissertations at Digital Commons @ University of South Florida. It has been accepted for inclusion in USF Tampa Graduate Theses and Dissertations by an authorized administrator of Digital Commons @ University of South Florida. For more information, please contact digitalcommons@usf.edu.

The Discovery of First RET PROTAC with *in vivo* Activity

by

Yafeng Wang

A dissertation submitted in partial fulfillment
of the requirements for the degree of
Doctor of Philosophy
Department of Chemistry
College of Arts and Sciences
University of South Florida

Major Professor: Jianfeng Cai, Ph.D.
David Merkler, Ph.D.
Feng Cheng, Ph.D.
Wenqi Liu, Ph.D.

Date of Approval:
June 28, 2024

Keywords: PROTAC, Sulfono-γ-AApepdtide, SPPS, Michael receptor, HPLC purification, Cleavage cocktail

Copyright © 2024, Yafeng Wang

ACKNOWLEDGEMENTS

I would like to thank my major professor, Dr. Jianfeng Cai, for his guidance and patience during these five years. Whenever I was stuck with my project, he would offer help, was very patient with my slow progress, and encouraged me to learn to solve research problems. It is my great honor to work in this lab and I have learnt so much from him.

Moreover, I would like to thank all my committee members, Dr. David Merkler, Dr. Feng Cheng, and Dr. Wenqi Liu. They have encouraged me and given me suggestions since my first year in 2020. Also, I must thank my previous committee member, Dr. Wayne Guida. I attended his advanced organic class that helped me learn deeper about organic chemistry. As a committee member, he shared his great vast treasure of knowledge to help me pass each milestone.

In our lab, I must thank Dr. Lulu Wei, she taught me how to run reactions and do research. I also need to thank Dr. Yizhan Zhai, and previous senior graduate students, such as Dr. Lei Wang, Dr. Songyi Xue, Huaxuan Yu, Jun Ou, Yu Yu Win, Haohui Ye. They offered great help and convenience for lab research and life. Furthermore, I would like to thank the undergrade student, Ting Chao, she helped me prepare important intermediates and taught me new generation fancy techniques.

I would like to thank all my collaborators, Dr. Jie Wu, Dr. Jiandong Chen, Dr. Danny Chou. I appreciate their sticking and biologycal experiment help with my research projects.

I am also grateful for other graduate students and faculty members in the chemistry department who shared their happy time and experience with me.

Finally, I really appreciate the help from my family and my high school friend, Jun Cao. They are the spark, the inspiration, the guide, and the candle in my life.

TABLE OF CONTENTS

List of Tables ... iv

List of Figures ... v

List of Abbreviation ... vii

Abstract ... viii

Chapter One: First Ret Degrader With *In Vivo* Activity ... 1
- 1.1. Introduction ... 1
- 1.2. Results ... 3
  - 1.2.1. Design of RET PROTAC ... 3
  - 1.2.2. SAR study ... 5
  - 1.2.3. LOXO-292 and BLU-667 treatment. ... 7
  - 1.2.4. Lenalidomide-based PROTAC degradation result ... 8
  - 1.2.5. Phenyl glutarimide-based PROTAC for RET protein degradation ... 9
  - 1.2.6. The cytotoxicity of YW-L-13, YW-N-7 and YW-N-11 ... 10
  - 1.2.7. YW-N-7 RET degradation with Proteasome inhibitor ... 10
  - 1.2.8. Pharmacokinetics (PK) Test ... 11
  - 1.2.9. YW-N-7 inhibits B/KR CDX tumor growth in animals ... 11
- 1.3. Discussion ... 13
- 1.4. Conclusion ... 15
- 1.5. Synthesis and biological test ... 16
  - 1.5.1. Synthesis of L-1-3 ... 16
  - 1.5.2. Synthesis of L-2-2 ... 17
  - 1.5.3. Synthesis of L-3-2 ... 18
  - 1.5.4. Synthesis of W-1-4 ... 18
  - 1.5.5. Synthesis of W-2-3 ... 20
  - 1.5.6. Synthesis of H-1-1 to H-1-3 ... 21
- 1.6. Cell and animal test material ... 22
  - 1.6.1. Antibodies ... 22
  - 1.6.2. Cell lines and cell culture ... 22
  - 1.6.3. Cell-based assays and immunoblotting analysis ... 22
  - 1.6.4. PK study ... 23
  - 1.6.5. Cell-derived xenograft (CDX) tumor study ... 23
- 1.7. Additional compounds ... 24

Chapter Two: Covalent Inhibitor To Target Ret G810c Mutation ... 26
- 2.1 Introduction ... 26

2.2. Design of RET covalent inhibitors ... 29
2.3. Result ... 29
2.4. Chemistry synthesis ... 30

Chapter Three: Dendrimeric Peptidomimetic As Antimicrobial ... 33
3.1. Introduction ... 33
3.2. Examples of HDP and mimics ... 35
3.3. Results and discussion ... 36
3.4. Materials and methods ... 39
3.4.1. Membrane depolarization study ... 39
3.4.2 Outer membrane (OM) permeabilization ... 40
3.4.3. Inner membrane (IM) permeabilization ... 41
3.4.4. Fluorescence microscopy ... 41
3.4.5. Transmission electron microscopy (TEM) ... 42
3.4.6. Bacterial killing efficiency ... 43
3.5. Experiment Procedure ... 44
3.5.1. General experiment methods ... 44
3.5.2. MIC ... 45
3.5.3. Hemolytic activity ... 45
3.5.4. Drug resistance study ... 46
3.5.5. TEM ... 46
3.5.6. Inner membrane permeability ... 46
3.5.7. Fluorescence microscopy ... 46
3.5.8. Time-kill kinetics study ... 47
3.6. Conclusions ... 47
3.7. General synthesis of compound ... 47

Chapter Four: Bcl-9 P-Protac To Degrade B-Catenin ... 49
4.1. Fmoc SPPS ... 49
4.1.1. Background of Fmoc SPPS ... 49
4.1.2. Coupling reagents and limitations for Fmoc SPPS ... 50
4.1.3. Resins in Fmoc-SPPS ... 54
4.1.4. Cleavage cocktails ... 56
4.1.5. HPLC analysis and purification ... 58
4.2. Introduction ... 59
4.3. Design ... 62
4.4. Synthesis ... 63
4.4.1. Building preparation ... 63
4.4.2. Fmoc-SPPS synthesis ... 69

Chapter Five: S597 Peptidomimetic To Activate Insulin Receptor ... 71
5.1. Background ... 71
5.2. Functional roles of α-helix ... 76
5.2.1. DNA binding ... 76
5.2.2. Membrane spanning ... 76

  - 5.3. Unnatural helical peptide foldamers 77
  - 5.4. Sulfono-γ-AApeptide 78
  - 5.5. S597 insulin peptidomimetic 79
    - 5.5.1. Design of S597 sulfono-γ-AApeptide 80

References 84

Appendices 92
  - Appendix A: ^{1}H-NMR, ^{13}C-NMR, and HRMS 92
  - Appendix B: ^{1}H-NMR and ^{13}C-NMR 172
  - Appendix C: HPLC data, ^{1}H-NMR, and ^{13}C-NMR 176
  - Appendix D: ESI-MS data 188
  - Appendix E: LC-MS and ESI-MS data 194

LIST OF TABLES

Table 1.1. PROTAC compounds and their ability to degrade RET at 50 nM 5

Table 1.2. HRMS data..24

Table 2.1. SAR of different Michael Receptors...30

Table 3.1. IC_{50}; hemolytic activity; and selectivity of dendrimeric γ-AApeptides 39

Table 3.2. HRMS data..48

Table 4.1. Swelling factor of 1% cross-linked polystyrene resins in different solvents..........56

Table 4.2. High concentration of TFA Fmoc-SPPS cleavage cocktail..................................57

Table 4.3. Comparison of p-PROTAC and small molecule PROTAC..................................61

Table 5.1. L-AA α-helix propensities; Difference in free energy change 75

LIST OF FIGURES

Figure 1.1. Design of PROTAC 4
Figure 1.2. Evaluation of RET PROTACs 8
Figure 1.3. YW-N-7 inhibits cell-derived xenograft (CDX) tumors in animals 12
Figure 1.4. Synthesis route of L-1-1, L-2-2, L-3-2 16
Figure 1.5. Synthesis of different methylene linkers of W-2-3 19
Figure 1.6. Synthesis of various E3 ligands with different heterocycle linkers 21
Figure 1.7 Additional compounds 25
Figure 2.1. Examples of covalent inhibitor 28
Figure 2.2. Design of RET covalent inhibitor 29
Figure 2.3. WB data of YW-D-50-2, YW-D-50-6 30
Figure 2.4. Synthesis route of covalent inhibitor 31
Figure 3.1. Structure of α-peptides, γ-AA peptides, and dendrimeric γ-AA peptides 34
Figure 3.2. Example of HDPs 35
Figure 3.3. Examples of recently developed γ-AA peptides to mimic HDPs 36
Figure 3.4. Structures of lipidated dendrimeric γ-AApeptides 38
Figure 3.5. Membrane depolarization study of YW-1 40
Figure 3.6. Outer membrane (OM) permeabilization 40
Figure 3.7. Fluorescence microscopy of the bacteria MRSA and E. coli 42
Figure 3.8. TEM graphs of MRSA and E. coli in the presence and absence of YW-1 43
Figure 3.9. Time-kill kinetics of YW-1 toward MRSA (A) and E. coli (B) 43

Figure 3.10. Drug resistance study of YW-1 toward MRSA 44

Figure 4.1. Deprotection mechanism of Fmoc-SPPS 50

Figure 4.2. Coupling reagents and mechanism 52

Figure 4.3. Base and additives for coupling 53

Figure 4.4. Structure of polystyrene 54

Figure 4.5. Structure of AM resin 55

Figure 4.6. Various kinds of Merrifield resin 56

Figure 4.7. Design of Sulfono-γ-AApeptide PROTAC 62

Figure 4.8. Building block preparation 63

Figure 4.9. Synthesis procedure of Sulfono-γ-AApeptide PROTAC 70

Figure 4.10. Synthesis design 71

Figure 4.11. WB data of YW-D-103-2 and previously reported xStAx-VHLL 72

Figure 4.12. Structure of PG Sulfono-γ-AApeptide PROTAC 73

Figure 5.1. A tripeptide consists of Val, Ala, and Leu AA 74

Figure 5.2. Transcriptional factor Max DNA binding with leucine zipper coil-coil....................................76

Figure 5.3. Structure of Bovine Rhodopsin in a trigonal crystal form 77

Figure 5.4. Structure of natural residues and unnatural helical foldamer residues 78

Figure: 5.5. Chemical structure of 13, 14, 15, 16 79

Figure 5.6. Sequence of S597 80

Figure 5.7. Crystal structure of S597 bind with IR 81

Figure 5.8. Crystal structure of S597 bind with IR 82

Figure 5.9. Structure of site-1 sulfono-γ-AApeptide mimic 83

LIST OF ABBREVIATIONS

Abbreviations	**Definitions**
AA	Amino acid
BB	Building block
Boc	*tert*-Butoxycarbonyl
Bn	Benzyl
DCM	Dichloromethane
Cbz	Benzyloxycarbonyl
DCC	1,3-Dicyclohexylcarbodiimide
DIC	*N, N*-Di(propan-2-yl) methanediimine
DMF	*N, N*-Dimethylformamide
DIPEA	Diisopropylethylamine
DMAP	4-Methylaminopyridine
DMSO	Dimethylsulfoxide
EDCI	1-ethyl-3-[3-(dimethylamino)propyl] carbodiimide
$Pd_2(dba)_3$	Tris(dibenzylideneacetone)dipalladium (0)
$Pd_2Cl_2(PPh_3)$	Bis(triphenylphosphine)palladium chloride
Fmoc	9-Fluorenylmethoxycarbonyl
HOBt	1H-1,2,3-Benzotriazol-1-ol
HPLC	High-performance liquid chromatography
IC_{50}	Half-maximal inhibitory concentration
MIC	Minimum inhibitory concentration
NMM	N-methylmorpholine
Pbf	2,2,4,6,7-pentamethyldihydrobenzofuran-5-sulfonyl
PG	Protecting group
PROTAC	Proteolysis targeting chimera
SNAr	Nucleophilic aromatic substitution
SPPS	Solid phase peptide synthesis
TEA	Triethylamine
THF	Tetrahydrofuran
$T_{1/2}$	Half life
Ts	Tosyl
Trt	Trityl
Xantphos	(9,9-Dimethyl-9H-xanthene-4,5-diyl) Bis(diphenylphosphane)

ABSTRACT

This report discusses the development of RET Proteolysis targeting chimera PROTAC molecules based on Selpercatinib (LOXO-292) and Sulfono-γ-AApeptide PROTAC. A PROTAC molecule is a bifunctional molecule composed of two active domains and a linker. It works by inducing selective protein intracellular degradation. This technology was first discussed by Kathleen Sakamoto, Ray Deshaies and Craig Crews in 2001. Using various E3 Ligase, such as CRBN, pVHL, beta-TrCP1, Mdm2, DCAF15, DCAF16, RNF114, and c-IAP1, the PROTAC technology has been applied to several novel drug development,. Yale University licensed the PROTAC technology to Arvinas in 2013–14. For my research, Chapter one summarizes our development of RET PROTAC in detail. Using Selpercatinib as warhead binding to RET protein, different methylene, PEG and heterocycle linkers, various E_3 ligases are also tried to develop RET proteac molecues. Chapter two discusses our novel design of covalent inhibitors that targets RET G810C mutation using different Michael receptors. Chapter three concludes our design of unnatural γ-AApeptide to overcome antibiotic resistance due to the abuse of current antibiotics. Chapter four starts with the basic knowledge of solid phase synthesis. After the brief review, our research on the SPPS of BCL-9 sulfono-γ-AApeptide PROTAC linked with VHL and PG E_3 ligase is discussed. Details of sulfono-γ-amino acid building block synthesis, procedure of SPPS, peptide cleavage and purification are also summarized in detail. Chapter five starts with the background unnatural amino acids and foldamers. Then our design based on natural peptide S597 with our sulfono-γ-amino acid to mimic the sequence of site 1 or replacing natural amino acids with our

sulfono-γ-amino acid are discussed. At the end of each chapter, NMR, Q-TOF, ESI-MS, and LC-MS data are attached.

CHAPTER ONE: FIRST RET DEGRADER WITH *IN VIVO* ACTIVITY

1.1 Introduction

The rearranged-during-transfection (*RET*) gene encodes the RET receptor protein tyrosine kinase (PTK)[1-3]. Aberrantly activated RET kinase caused by germline or somatic *RET* mutations is one of the major oncogenic drivers frequently found in medullary thyroid cancer (MTC)[2, 3]. Chromosomal rearrangements that result in aberrant expression and constitutive activation of the fusion RET kinases are associated with ~10% papillary thyroid cancer (PTC) and ~2% non-small cell lung cancer (NSCLC) and are proven driver oncogenes[1, 4]. Furthermore, RET alterations were observed at a low rate in diverse cancer types that contribute to tumorigenesis and maintenance of these RET-positive cancers, which are approved targets for cancer therapy[5-7]. Although more than 100 different RET fusion genes have been detected[3], the most frequently observed RET fusions are CCDC6-RET and KIF5B-RET fusions in PTC and NSCLC.

Two RET-selective protein tyrosine kinase inhibitors (TKIs), selpercatinib (LOXO-292)[8] and pralsetinib (BLU-667)[9], have been approved for treating RET-positive cancers[1, 3]. These are ATP competitive RET inhibitors that inhibit the RET kinase activity[10]. Inhibition of RET kinase activity by these inhibitors does not reduce the RET protein level. Instead, inhibition of the RET kinase activity by selpercatinib or pralsetinib consistently increased the CCDC6-RET fusion protein level in human cancer cells[11] (see also Results below). A higher level of RET fusion oncogene expression has been implicated in the reduced effectiveness of RET kinase inhibitors, such as in the case of RET inhibitor RXDX-105[1, 12]. While the effectiveness of selpercatinib and pralsetinib at their full prescription strength may not be impacted by a higher level of oncogenic

RET expression, dose reduction is required in patients who have treatment-related adverse events. In fact, 30% of thyroid cancer patients and 41% of NSCLC patients treated with selpercatinib had dose reduction[13, 14]. Conceivably, the efficiency of these occupancy-based drugs may be reduced at a lower drug dose. This may contribute to the persistence of residual tumors that exist in over 90% of patients in selpercatinib- or pralsetinib treatment[3]. Thus, depletion of oncogenic RET protein is likely to have an added benefit in addition to inhibition of the oncogenic RET kinase activity in RET-targeted cancer therapy.

Proteolysis targeting chimera (PROTAC) is a developing modality to achieve targeted protein degradation with heterobifunctional small chemical molecules[15, 16]. A PROTAC brings an E3 ligase into close proximity to the target protein of interest to form a ternary complex, resulting in ubiquitination and proteasomal degradation of the target protein. A PROTAC typically consists of three moieties: a ligand that engages the target protein of interest, a ligand of an E3 ubiquitin ligase that recruits a ubiquitin ligase, and a linker that tethers these two ligands[15]. For protein kinases, a kinase inhibitor may be used as the basis for the design of the target-binding ligand[17, 18]. A ligand to the von Hippel-Lindau tumor suppressor (VHL) protein and immunomodulatory imide drugs (IMiDs) that bind cereblon (CRBN) are the most commonly used ligands for E3 ubiquitin ligases in PROTAC design. The VHL ligand recruits the CUL2-RBX1-ElongB/C-VHL (CRL2^{VHL}) ubiquitin ligase[19]. IMiDs, including thalidomide, lenalidomide, and pomalidomide, recruit the ubiquitously expressed cullin ring ligase 4 (CUL4)-RBX1-DDB1-CRBN ($\text{CRL4}^{\text{CRBN}}$) E3 ligase[16, 20]. More recently, phenyl glutarimide (PG) analogues of CRBN binders were used to improve the chemical stability of CRBN ligands[21]. In addition to high-affinity ligands for binding the target protein and the E3 ligase, an appropriate linker that connects the two ligands is critical for the formation of a productive ternary complex to allow efficient degradation of the target protein. An optimal linker is determined by its composition, length, and the position of coupling to the ligands[22, 23].

In this study, we designed, synthesized, and evaluated in cell cultures *in vitro* and in an animal model *in vivo* RET PROTACs based on selpercatinib (LOXO-292) as the RET ligand, IMiDs-Lenalidomide, and PG as the E3 ligase ligand, and various flexible and rigid linkers of different compositions and lengths coupling to different positions of the IMiDs or PG. Our investigation identified YW-N-7 as a RET PROTAC that could fully degrade RET in the cell lines tested and demonstrated potent *in vivo* activity in inhibiting oncogenic RET-driven tumor growth in animals.

1.2 Results

1.2.1 Design of PROTAC

Our design was based on LOXO-292 (selpercatinib), an FDA-approved RET kinase inhibitor to treat lung or thyroid cancer (Figure 1A). We recently published the co-crystal structure of LOXO-292/RET (PDB: 7JU6),[10] which reveals that the terminal hydroxypropyl group of LOXO-292 has minimal impact on its binding to RET (Figure 1B and 1C). Unlike the rest of the structure buried in the RET hydrophobic cleft, this hydroxypropyl group (shaded in light blue) is outside the protein and exposed to the solvent. No interactions are identified between this group and the protein based on the crystal structure. We thereby postulated that this group could be replaced with certain linkers to link an ubiquitin E3 ligase binding ligand to make PROTAC compounds for degrading RET. We decided to choose lenalidomide which is known to target the E3 ligase cereblon (CRBN) (Figure 1C). In parallel, we also attempted to select phenyl glutarimide (PG) moiety as PG is also a CRBN ligand but is believed to have enhanced chemical

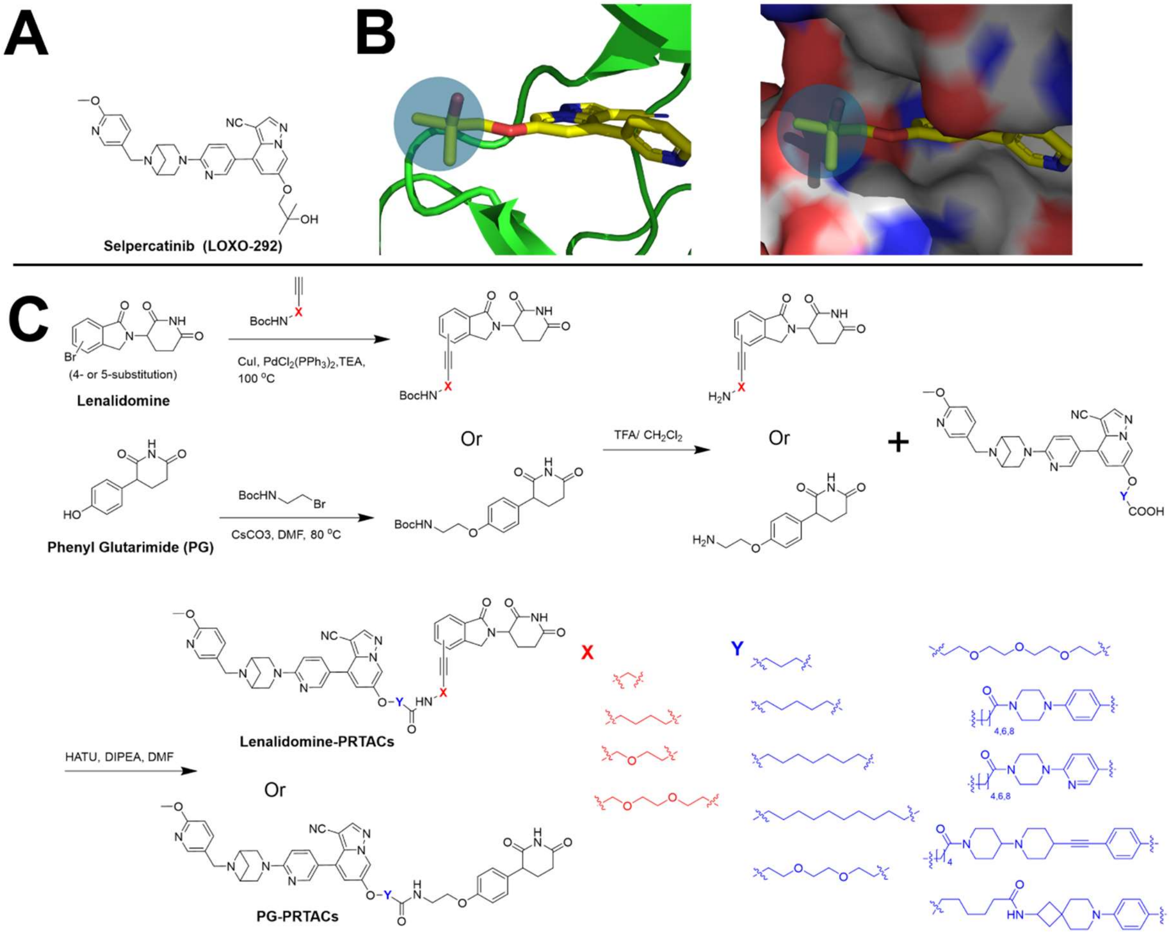
A
B
C
Selpercatinib (LOXO-292)
NC
OH
Br
(4- or 5-substitution)
Lenalidomine
BocHN
X
CuI, PdCl2(PPh3)2,TEA,
100 °C
Or
TFA/ CH2Cl2
+
H2N
Y
COOH
Phenyl Glutarimide (PG)
HO
BocHN
Br
CsCO3, DMF, 80 °C
HATU, DIPEA, DMF
Lenalidomine-PRTACs
PG-PRTACs
HN
4,6,8
4

Figure 1.1. Design of PROTAC. A. The structure of LOXO-292. B. The co-crystal structure of LOXO-292/RET complex (PDB: 7JU6) shown in cartoon and surface representation, respectively. C. The synthetic routes of lenalidomine and phenyl glutarimide (PG) based PROTAC derivatives of LOXO-292.

stability (Figure 1C). To this end, a variety of PROTAC compounds bearing various flexible and rigid linkers of different compositions and lengths were synthesized and studied for their ability to inhibit RET activity and degrade RET protein (Table 1).

1.2.2 SAR study

Table 1.1. PROTAC compounds and their ability to degrade RET at 50 nM; The three most potent lead compounds are shown in red.

<table>
<tr><td colspan="3">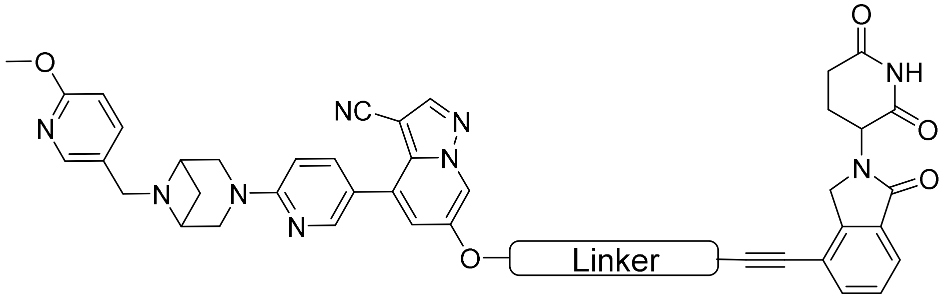 </td></tr>
<tr><th>Manuscript Name</th><th>Linkers</th><th>Degradation rates at 50 nM (%)</th></tr>
<tr><td>YW-L-1</td><td>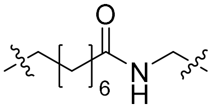</td><td>-73</td></tr>
<tr><td>YW-L-2</td><td>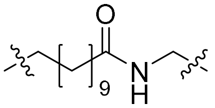</td><td>29.7</td></tr>
<tr><td>YW-L-3</td><td>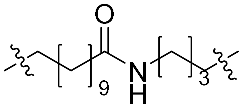</td><td>43.1</td></tr>
<tr><td>YW-L-4</td><td>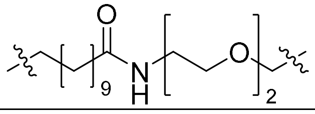</td><td>-4.8</td></tr>
<tr><td>YW-L-5</td><td>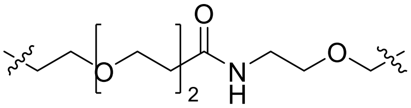</td><td>43.8</td></tr>
<tr><td>YW-L-6</td><td>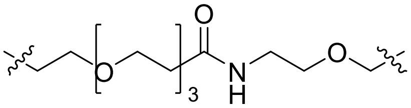</td><td>-38.3</td></tr>
<tr><td>YW-L-7</td><td>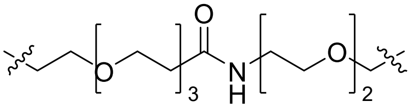</td><td>-20.3</td></tr>
<tr><td>YW-L-8</td><td>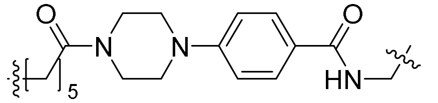</td><td>36</td></tr>
<tr><td>YW-L-9</td><td>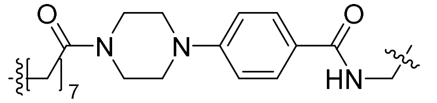</td><td>33</td></tr>
</table>

Table 1 1. Continued

YW-L-10	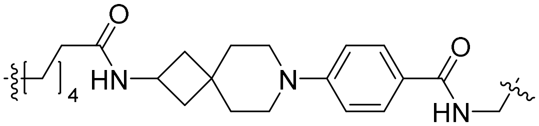	69
YW-L-11	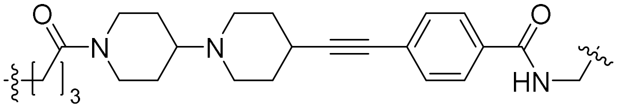	76.2
YW-L-12	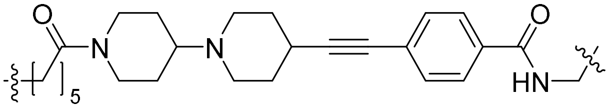	84
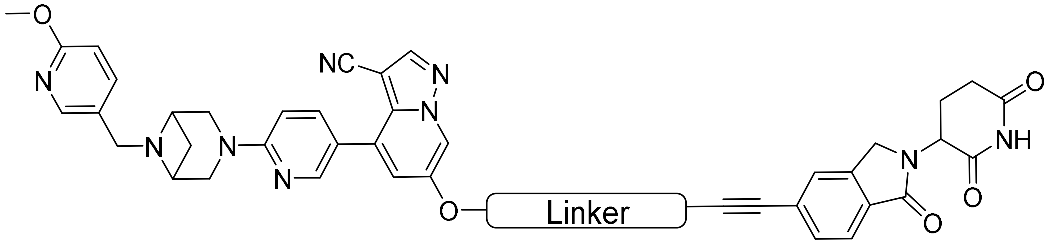		
YW-L-13	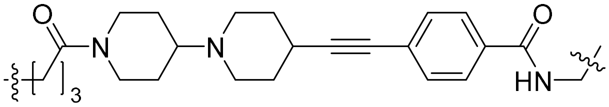	96
	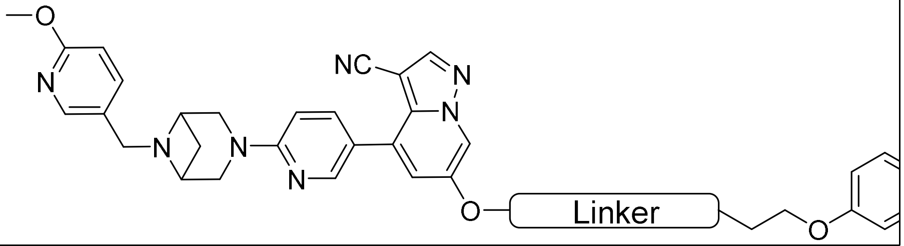	
YW-N-1	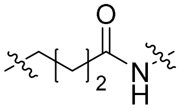	-105
YW-N-2	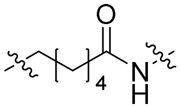	-75
YW-N-3	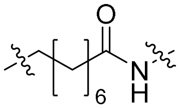	-133
YW-N-4	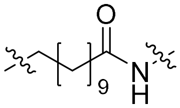	40

Table 1 1. Continued

YW-N-5	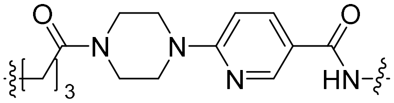	68
YW-N-6	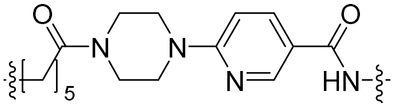	37
YW-N-7	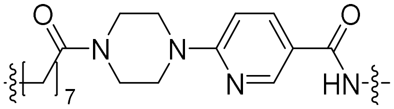	88
YW-N-8	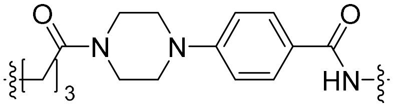	60
YW-N-9	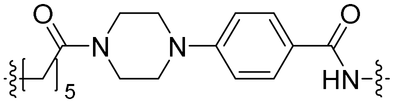	82
YW-N-10	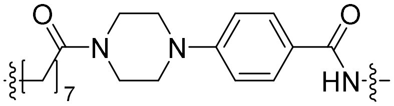	57
YW-N-11	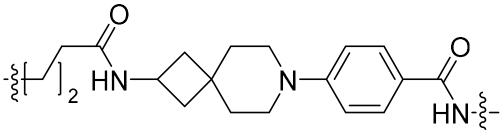	92

1.2.3 LOXO-292 and BLU-667 treatment

To assess the impact of RET kinase inhibitors on the RET protein, we first examined the RET protein level in the presence of two FDA-approved drugs Selpercatinib (LOXO-292) and Pralsetinib (BLU-667). Surprisingly, upon treatment of both compounds, the level of RET protein dramatically increased (Figure 2A and Figure 2B), in contrast to the intuition that LOXO-292 and BLU-667 should change the phosphorylation level but not alter the total RET protein level. This may be owing to the ability of cancer cells to express more RET protein due to the decreased level of RET kinase activity upon the inhibition of LOXO-292 and BLU-667, respectively. This phenomenon has been implicated in the reduced effectiveness of RET kinase inhibitors.

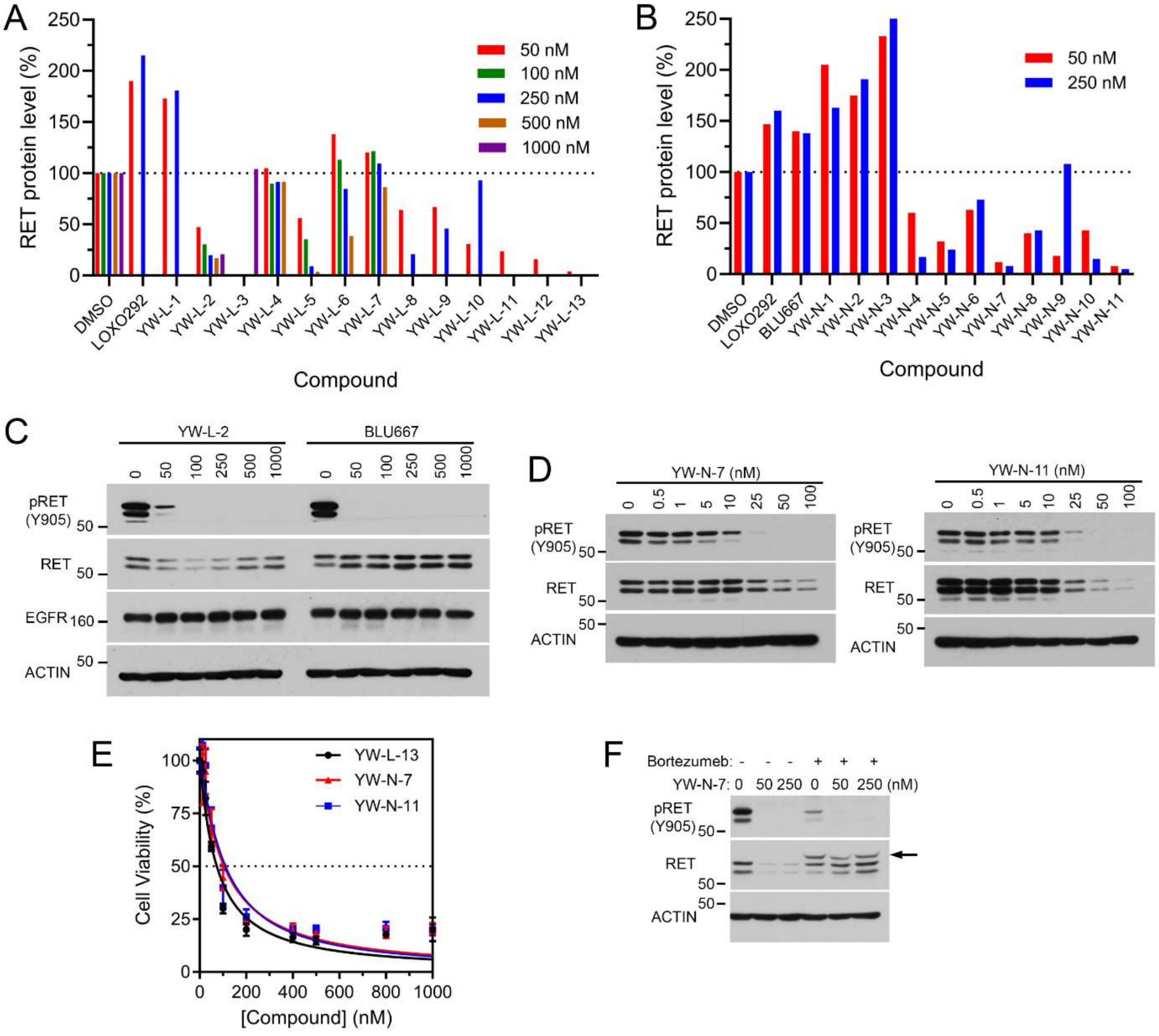

Figure 1.2. Evaluation of RET PROTACs. **A, B:** Degradation of the RET protein. **C:** RET kinase inhibition, RET and EGFR protein degradation by YW-L-2 and Blu 667 **D:** Concentration-dependent inhibition and degradation of RET by YW-N-7 and YW-N-11. **E:** cell cytotoxicity of YW-L-13, YW-N-7 and YW-N-11 **F:** Bortezumeb's effect on YW-N-7-induced CCDC6-RET degradation.

1.2.4 Lenalidomide-based PROTAC degradation result

To assess whether our design strategy could lead to RET protein degradation, we first synthesized a series of conjugates of lenalidomide and LOXO-292 bearing different linkers (Table 1 and Figure 2A). Our first attempt, **YW-L-1**, showed no capability to degrade RET. Instead, it seemed that the compound boosted the RET expression, similar to the effect of LOXO-292 (Figure 2A and 2B) and BLU-667 (Figure 2B). However, elongation of the linkers led to compounds **YW-**

L-2 and **YW-L-3** which started to exhibit activity to degrade RET. This initial success demonstrated the strategy of linking LOXO-29 and lenalidomide for targeted degradation of RET is possible. The distance between RET and the E3 ligase is crucial, as longer linkers seem to have stronger activity in degrading RET. However, none of the compounds were able to completely degrade RET at higher concentrations (Figure 2C). The western blot is consistent with the screening (Figure 2A) that BLU-667 treatment led to elevated expression level of RET (Figure 2C). We next examined whether a hydrophobic or hydrophilic linker was ideal for the degradation of RET. Interestingly, the replacement of hydrophobic linkers with hydrophilic linkers only gave promiscuous SAR. Except for **YW-L-5**, the other three compounds **YW-L-4**, **YW-L-6,** and **YW-L-7** did not exhibit any activity for RET degradation. Since longer hydrophobic linkers were favored, we speculated a rigid hydrophobic linker may lead to more potent RET degraders, as the distance between RET and CRBN would be more defined with the rigid spacer. Indeed, all the compounds from **YW-L-8** to **YW-L-12** showed good activity in degrading RET. In particular, **YW-L-12** could degrade 84% RET at 50 nM. Lastly, we also investigated the impact of the linkage position on the aromatic ring of the lenalidomide. Intriguingly, with the same linker used for **YW-L-11** in which the linkage point is at position 4, the linkage at position 5 led to an even more potent compound **YW-L-13** that could degrade 96% RET protein at 50 nM.

1.2.5 Phenyl glutarimide-based PROTAC for RET protein degradation

Since phenyl glutarimide (PG) is currently recognized as the alternative ligand to target CRBN E3 ligase but with enhanced stability in comparison to lenalidomide, we next studied the conjugates of PG and LOXO-292 for their potential as PROTAC compounds to degrade RET. Similar to lenalidomide-based PROTAC compounds, with shorter linkers **YW-N-1**, **YW-N-2** and **YW-N-3** did not show any inhibitory activity (Table 1), whereas **YW-N-4** bearing a longer linker revealed 40% RET degradation at 50 nM. As anticipated, compounds from **YW-N-5** to **YW-N-11** all show significant degradation of RET protein due to the rigid linkers employed between PG and the parent compound LOXO-292, a trend already observed for lenalidomide PROTAC development. Among them, both **YW-N-7** and **YW-N-11** demonstrated the most potent activity in RET degradation (Table 1) on a dose-dependent manner (Figure 2D). As shown in Figure 2D, both **YW-N-7** and **YW-N-11** virtually completely degraded RET protein at 100 nM.

1.2.6 The cytotoxicity of YW-L-13, YW-N-7 and YW-N-11

Since RET is crucial for cancer cell growth, the inhibition of RET kinase activity or the eradication of RET protein itself are expected to induce cancer cell death. As shown in Figure 2E, the most potent compounds from both lenalidomide- and PG-based PROTACs **YW-L-13**, **YW-N-7** and **YW-N-11** all revealed potent anti-cancer activity by killing cancer cells effectively. The EC_{50} ranged between 50-100 nMs, which are in good agreement with their ability to degrade RET protein.

1.2.7 YW-N-7 RET degradation with proteasome inhibitor

To ensure that our PROTAC compounds exerted their activity through proteasome-mediated protein degradation, we next chose to test the ability of **YW-N-7** to degrade RET in the presence of Bortezomib, an FDA-approved proteasome inhibitor. As shown in Figure 2, in the absence of Bortezomib, **YW-N-7** could completely inhibit RET phosphorylation and eradicate RET protein as low as 50 nM. In the presence of Bortezomib, **YW-N-7** could still function as a kinase inhibitor as LOXO-292 to block the phosphorylation of RET. However, since Bortezomib blocked the proteasomal enzymatic activity, the ability of **YW-N-7** to degrade RET was inhibited on a dose-dependent manner. Overall, this experiment demonstrated that our PROTAC compounds exerted dual functional roles to inhibit RET by suppressing RET kinase activity and degrading RET protein.

1.2.8 Pharmacokinetics (PK) Test

To assess the potential of our PROTAC compounds as a research tool or potential RET-targeted therapy, we set out to carry out in vivo studies. We first evaluated the PK profile of the aforementioned lead compounds. As shown in Figure 3, among three compounds, **YW-L-13**, which exhibited the most potent in vitro activity, revealed a poor PK profile with a short half-life and ultrafast clearance. This is somehow in alignment with the reports that some CRBN-targeting ligands including lenalidomide are not stable. **YW-N-11** showed improved PK properties, whereas YW-N-7 demonstrated the best PK profile with a half-life time of ~16 h. As such, we decided to study the efficacy of YW-N-7 on a B/KR cell-derived xenografted mouse tumor model.

1.2.9 YW-N-7 inhibits B/KR CDX tumor growth in mice

After the pharmacokinetics (PK) test, we did a further *in vivo* cell viability test with the best PK data, **YW-N-7**. From Figure 4A, it was clear that the B/KR cell viability decreased notably after being treated with **YW-N-7** for three days. The IC_{50} of YW-N-7 was 105.2 nM. After being treated with 500 nM for three days, the cell viability dropped to less than 20%. It suggested that **YW-N-7** could effectively inhibit B/KR cell growth by degrading RET protein level and inhibiting RET kinase activity. This could be further confirmed by immunoblotting data. After cells were treated with **YW-N-7** at different concentrations for 15 h, it showed both pRET (Y905) and KIF5B-RET could be degraded at as low as 50 nM (Figure 4B) To determine if the

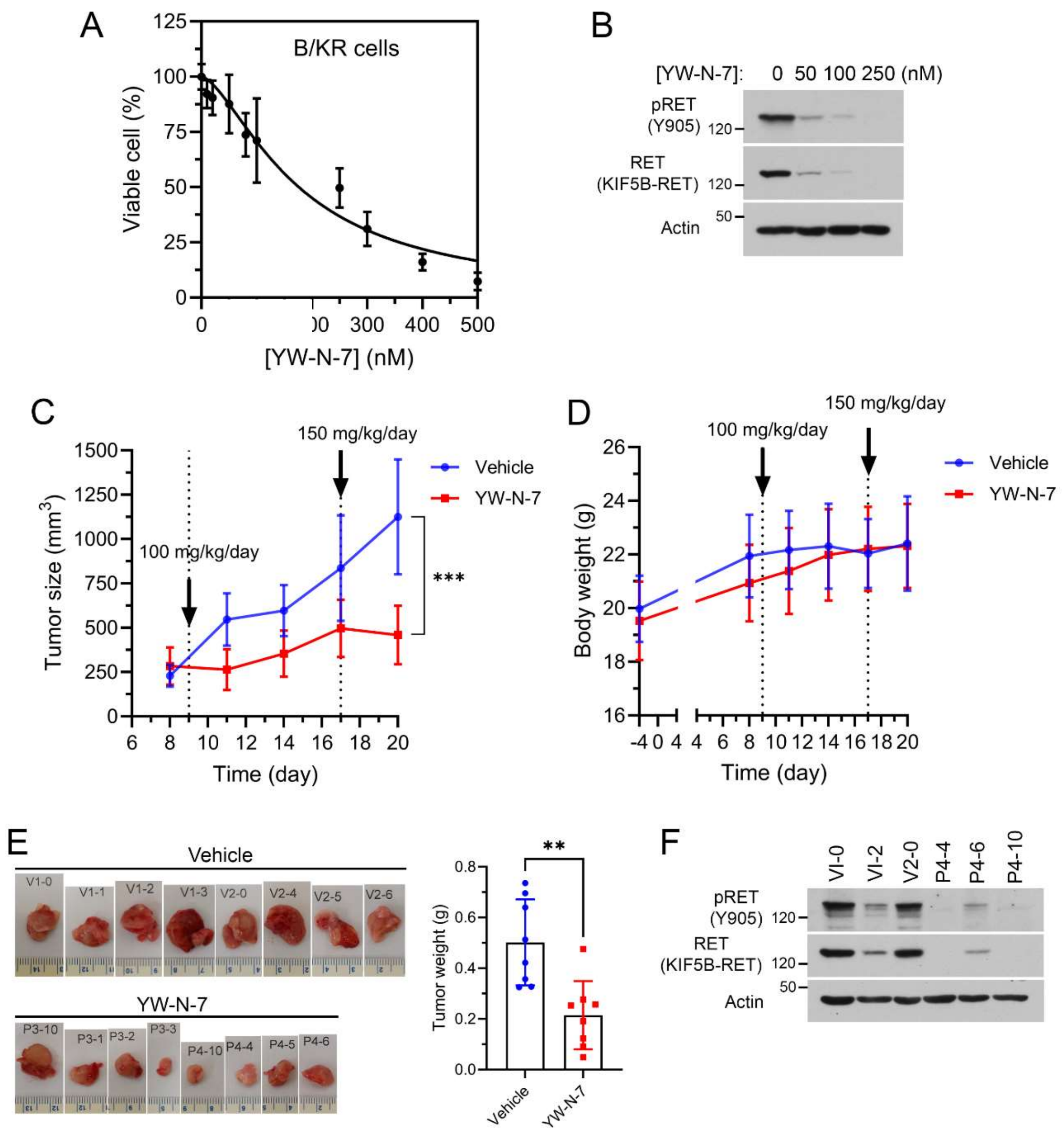

Figure 1.3. YW-N-7 inhibits cell-derived xenograft (CDX) tumors in animals. **A**: Cells treated with various concentrations of YW-N-7. **B**: Cells treated with indicated concentrations of YW-N-7. (**C-D)**: CDX tumors were treated with YW-N-7 or mock-treated with vehicle. **C**: Body weights were measured with a scale. **D**, **E**: Images of tumors collected at the endpoint. **F**: Immunoblots of tumor tissue samples.

RET PROTAC YW-N-7 could inhibit RET oncogene-driven tumors in animals, we tested the effect of YW-N-7 on tumor growth of B/KR CDXs. After measurable s.c. tumors were established, mice bearing a similar size of tumors were treated with **YW-N-7** (100 mg/kg/day) or the solvent (control) by intraperitoneal injection starting on Day 9. Tumors grew rapidly in the solvent-treated group. The **YW-N-7** treatment significantly inhibited tumor growth (Figure 4C). Because the YW-N-7 treatment did not reduce the animal body weight (Figure 4D), the drug dose was increased to 150 mg/kg/day on Day 17, which remained tolerated by the animals (Figure 4D). Figure 4E showed that tumors from **YW-N-7** -treated animals were significantly smaller than tumors from the solvent-treated animals. Immunoblotting analysis of tumor samples showed that the phospho-RET and KIF5B-RET protein were decreased in samples from the **YW-N-7**-treated group (Figure 4F).

1.3 Discussion

The rearranged-during-transfection (RET) protein is an attractive target for cancer therapy. Aberrantly activated RET kinase caused by germline or somatic *RET* mutations is one of the major oncogenic drivers frequently found in medullary thyroid cancer (MTC). However, the current drugs selpercatinib (LOXO-292) and pralsetinib (BLU-667) as RET kinase inhibitors do not reduce RET protein level. Instead, consistently increased the RET fusion protein level in human cancer cells. The overexpression of RET could reduce the effectiveness of the kinase inhibitors and contribute to protein mutation and drug resistance. Thus, depletion of oncogenic RET protein is likely to have an added benefit in addition to inhibition of the oncogenic RET kinase activity.

Proteolysis targeting chimera (PROTAC) is a developing modality to achieve targeted protein degradation with heterobifunctional small chemical molecules. A PROTAC, bearing an E_3 binding ligand, a linker and a ligand that engages the target protein of interest, brings an E_3 ligase into close proximity to the target protein of interest to form a ternary complex, resulting in ubiquitination and proteasomal degradation of the target protein. Immunomodulatory imide drugs (IMiDs), including thalidomide, lenalidomide, and pomalidomide, bind ubiquitously expressed cereblon (CRBN) E_3 ligase, are commonly used ligands for E_3 ubiquitin ligases in PROTAC design. More recently, phenyl glutarimide (PG) analogues of CRBN binders were used to improve the chemical stability of CRBN ligands.

To deplete RET protein, we decided to design PROTAC compounds using LOXO-292 (selpercatinib) as the RET-targeting ligand. This is because the co-crystal structure of LOXO-292/RET (PDB: 7JU6), suggested that the terminal hydroxypropyl group of LOXO-292 has minimal impact on its binding to RET (Figure 1B and 1C). We postulated that this group could be replaced with certain linkers to link an ubiquitin E3 ligase binding ligand to degrade RET. For targeting E3, we chose lenalidomide, a common ligand of the E3 ligase cereblon (CRBN). We also made bifunctional molecules containing LOXO-292 scaffold and PG as a comparison.

Our subsequent SAR studies suggested that a rigid and hydrophobic linker is preferable to join the LOXO-292 moiety and the CRBN binding ligand to make PROTAC compounds that could degrade RET effectively. Indeed, both lenalidomide- and PG-based PROTAC compounds could lead to the depletion of RET. The three lead compounds, lenalidomide-based **YW-L-13**, and PG-based **YW-N-7** and **YW-N-11**, demonstrated remarkable activity that completely depleted RET in cancer cells at a concentration of 100 nM or below. Consistent with their ability to degrade RET, they exhibited potent cytotoxicity toward cancer cells with EC50s less than 100 nM. In contrast, we observed treatment of either selpercatinib (LOXO-292) or pralsetinib (BLU-667) increased RET protein level dramatically, which is consistent with the previous research findings. Also, in the presence of high concentration of the proteosome inhibitor Bortezomib, the ability of **YW-N-**

7 to degrade RET was impaired, however, it still exhibited potent inhibitory activity for RET phosphorylation, suggesting that **YW-N-7** has synergistic dual roles in inhibiting RET function: acting as RET kinase inhibitor as well as RET protein degrader.

To select the lead compound for in vivo animal study, the lead compounds were first evaluated by PK studies. Consistent with the previous reports, lenalidomide-based **YW-L-13** revealed a poor PK profile, whereas **YW-N-7** showed a good half-life time of 15.6 h. Therefore YW-N-7 was selected for further investigation. Next, we demonstrated that YW-N-7 could potently kill RET-positive B/KR cancer cells, by depleting RET protein and inhibiting RET kinase activity (Figure 4A and 4B). To determine if the **YW-N-7** could inhibit RET oncogene-driven tumor growth in animals, we tested the effect of YW-N-7 on tumor growth on a B/KR cell-derived xenograft mouse model. The treatment of YW-N-7 led to significant tumor regression in mice. Immunoblotting analysis of tumor samples showed that the phospho-RET and KIF5B-RET protein were decreased in samples from the **YW-N-7**-treated group, demonstrating the consistent mechanism of in vitro and in vivo. As **YW-N-7** revealed synergistic dual roles of RET inhibition by inhibiting RET kinase activity and degrading RET, it could be used as a powerful research tool to gain insight into RET functional mechanism by selectively depleting RET protein. Its potent activity also enables it a lead compound for development of RET-targeted cancer therapy.

1.4 Conclusion

In summary, we have developed a series of bifunctional molecules as novel PROTAC compounds for the targeted degradation of RET. These molecules are based on a LOXO-292 scaffold, a CRBN E3 ligand using either lenalidomide or phenyl glutarimide (PG), and a linker of varied lengths, flexibility, and hydrophobicity. Among them, **YW-N-7** as our lead tool compound exhibited synergistic dual functional roles by selectively depleting RET while inhibiting the kinase activity of RET simultaneously in vitro and in vivo. The compound demonstrates significant antitumor efficacy on a B/KR cell-derived xenografted mouse model. This study exemplifies the feasibility of **YW-N-7** as both a powerful tool compound to study RET biomechanism and a promising lead compound for RET-targeted cancer therapy.

1.5 Synthesis and biological test

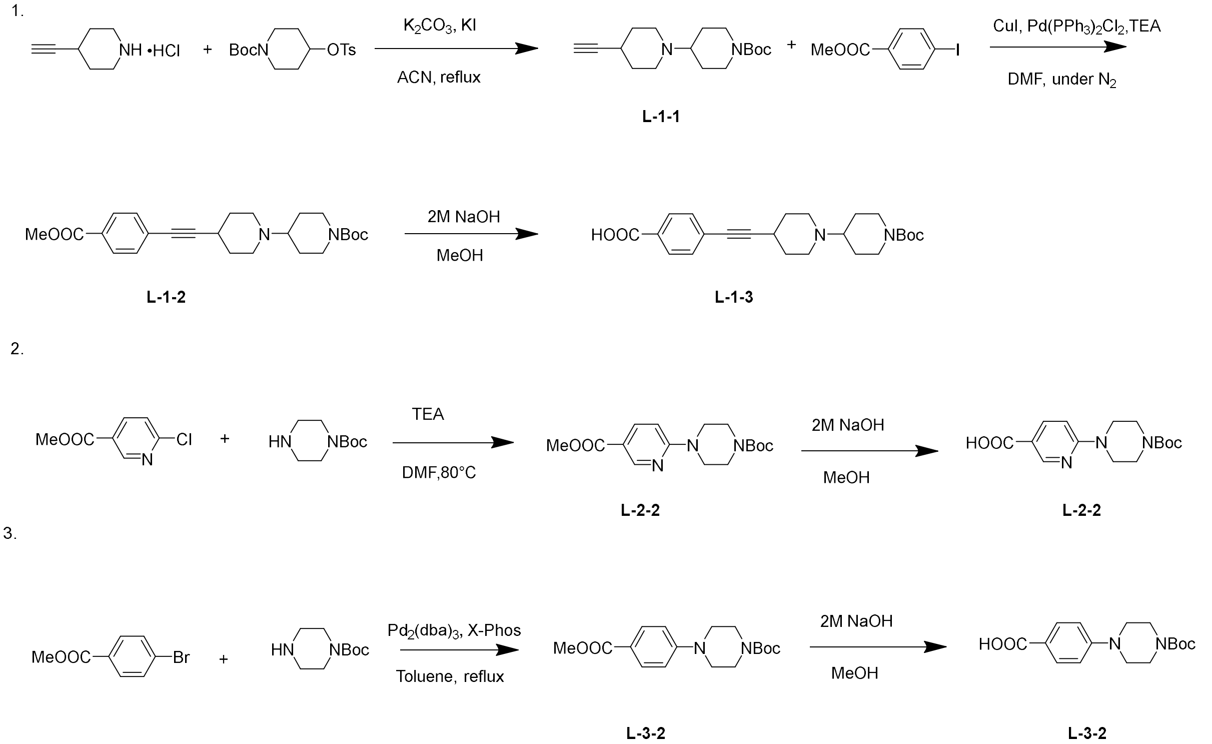
1.
NH •HCl
BocN
OTs
K2CO3, KI
ACN, reflux
N
NBoc
L-1-1
MeOOC
I
CuI, Pd(PPh3)2Cl2,TEA
DMF, under N2
L-1-2
2M NaOH
MeOH
HOOC
L-1-3
2.
Cl
N
HN
TEA
DMF,80°C
L-2-2
L-2-2
3.
Br
Pd2(dba)3, X-Phos
Toluene, reflux
L-3-2
L-3-2

Figure 1.4. Synthesis route of L-1-1, L-2-2, L-3-2.

1.5.1 Synthesis of L-1-3

Step 1: Tert-butyl 4-(Tosyloxy) piperidine-1-carboxylate and 4-ethynylpiperidine HCl salt were dissolved in ACN, then 10eq of K_2CO_3 and 0.2eq of KI were added. The reaction solution was stirred for 48h. The reaction was diluted with water and extracted with EA 3 times. Combine the EA phase, the organic phase was washed with brine, dried with anhydrous Na_2SO_4, then evaporated under reduced pressure. The left residue was purified by column chromatography to get **L-1-1**, using EA to get product. $[M+H^+]$:293.2

Step 2: Methyl 4-iodobenzoate(1eq) and tert-butyl 4-ethynyl-[1,4'-bipiperidine]-1'-carboxylate(1eq) were dissolved in anhydrous DMF, then 0.2eq of CuI and Pd $(PPh_3)_2Cl_2$ were added. The mixture was purged under N_2 for 5min. Then 3eq of TEA was added under N_2 environment. The mixture was stirred under 100°C for 4h. Then the reaction was cooled down to R.T., DMF was evaporated under reduced pressure. The left residue was purified by column chromatography, using EA: MeOH=30:1 to get product, **L-1-2**. $[M+H^+]$:427.6

Step 3: Tert-butyl 4-((4-(methoxycarbonyl) phenyl) ethynyl)-[1,4'-bipiperidine]-1'-carboxylate was dissolved in MeOH, 2eq of 2M NaOH was added. The reaction solution was stirred under 100°C for 2h. Next, MeOH was evaporated under reduced pressure, the left residue was diluted with H_2O and acidified to pH around 4 using 1M HCl. The H_2O solution was extracted by DCM for two times, combine the organic layer, washed by Brine and dried by anhydrous Na_2SO_4. EA was removed under reduced pressure, the left residue was purified by column chromatography, using DCM: MeOH=20:1 to get product, **L-1-3**. $[M+H^+]$:412.5

1.5.2 Synthesis of L-2-2:

Step 1: Methyl 4-bromobenzoate, tert-butyl piperazine-1-carboxylate, $Pd_2(dba)_3$, and X-phos were dissolved in toluene. The reaction solution was purged with nitrogen and sealed. The mixture was refluxED 8 hours. Next, toluene was evaporated under reduced pressure, water was added and extracted with 300ml EA three times. EA was evaporated and the left oil was purified by column to get product tert-butyl 4-(4-(methoxycarbonyl) phenyl) piperazine-1-carboxylate.

Step 2: tert-butyl 4-(4-(methoxycarbonyl) phenyl) piperazine-1-carboxylate was dissolved in MeOH, then 2M NaOH 3eq was added. The resulting mixture was refluxed under 70°C for 8 hours. After the reaction was done, cool down to R.T., followed by evaporating MeOH and acidifying the solution to pH around 4, then extracted by EA 3 times. Combine the EA phase and washed by

Brine, then dried by Na_2SO_4, EA was evaporated under reduced pressure and purified by column to get product 4-(4-(tert-butoxycarbonyl) piperazin-1-yl) benzoic acid, using Hex: EA=3:1 to get product. ^1H NMR (600 MHz, DMSO-d_6) δ 12.42 (s, 1H), 7.77 (s, 2H), 6.96 (s, 2H), 3.45 (s, 4H), 3.29 (s, 4H), 1.42 (s, 9H). ^{13}C NMR (600 MHz, DMSO-d_6) δ 167.69, 157.20, 153.58, 130.92, 121.56, 115.62, 81.28, 48.87, 29.38.

1.5.3 Synthesis of L-3-2:

Methyl 4-bromobenzoate, tert-butyl piperazine-1-carboxylate, $Pd_2(dba)_3$, and X-phos were dissolved in toluene. The reaction solution was purged with nitrogen and sealed. The mixture was refluxed for 8 hours. Next, toluene was evaporated under reduced pressure, water was added and extracted with 300ml EA three times. EA was evaporated and the left oil was purified by column to get product **L-3-1**.

Tert-butyl 4-(4-(methoxycarbonyl) phenyl) piperazine-1-carboxylate was dissolved in MeOH, then 2M NaOH 3eq was added. The resulting mixture was refluxed under 70°C for 8 hours. After the reaction was done, cool down to R.T., followed by evaporating MeOH and acidifying the solution to pH around 4, then extracted by DCM 3 times. Combine the DCM phase and washed by Brine, then dried by Na_2SO_4, DCM was evaporated under reduced pressure and purified by column to get product **L-3-2**. ^1H NMR (600 MHz, DMSO-d_6) δ 12.42 (s, 1H), 7.77 (s, 2H), 6.96 (s, 2H), 3.45 (s, 4H), 3.29 (s, 4H), 1.42 (s, 9H). ^{13}C NMR (151 MHz, DMSO-d_6) δ 167.69, 157.20, 153.58, 130.92, 121.56, 115.62, 81.28, 48.87, 29.38.

1.5.4 Synthesis of W-1-4

Step 1: 5-bromo-2-fluoropyridine and tert-butyl 3,6-diazabicyclo[3.1.1]heptane-6-carboxylate were mixed dissolved in DMSO, then 10 eq K_2CO_3 was added. The solution was stirred under 100°C overnight. On the second day, the reaction solution was diluted water and extracted with

EA, then organic phase was washed with Brine and dried with Na_2SO_4, followed by concentrated under reduced pressure. The residue was purified by chromatography to get **W-1-1**. (Hexane:EA=1:1, get product).

Step 2: **W-1-1** was dissolved in 4 M HCl in dioxane and stirred for 2. Then, the solvent was evaporated under reduced pressure. The left residue, W-1-2, was used for the next step without any further purification.

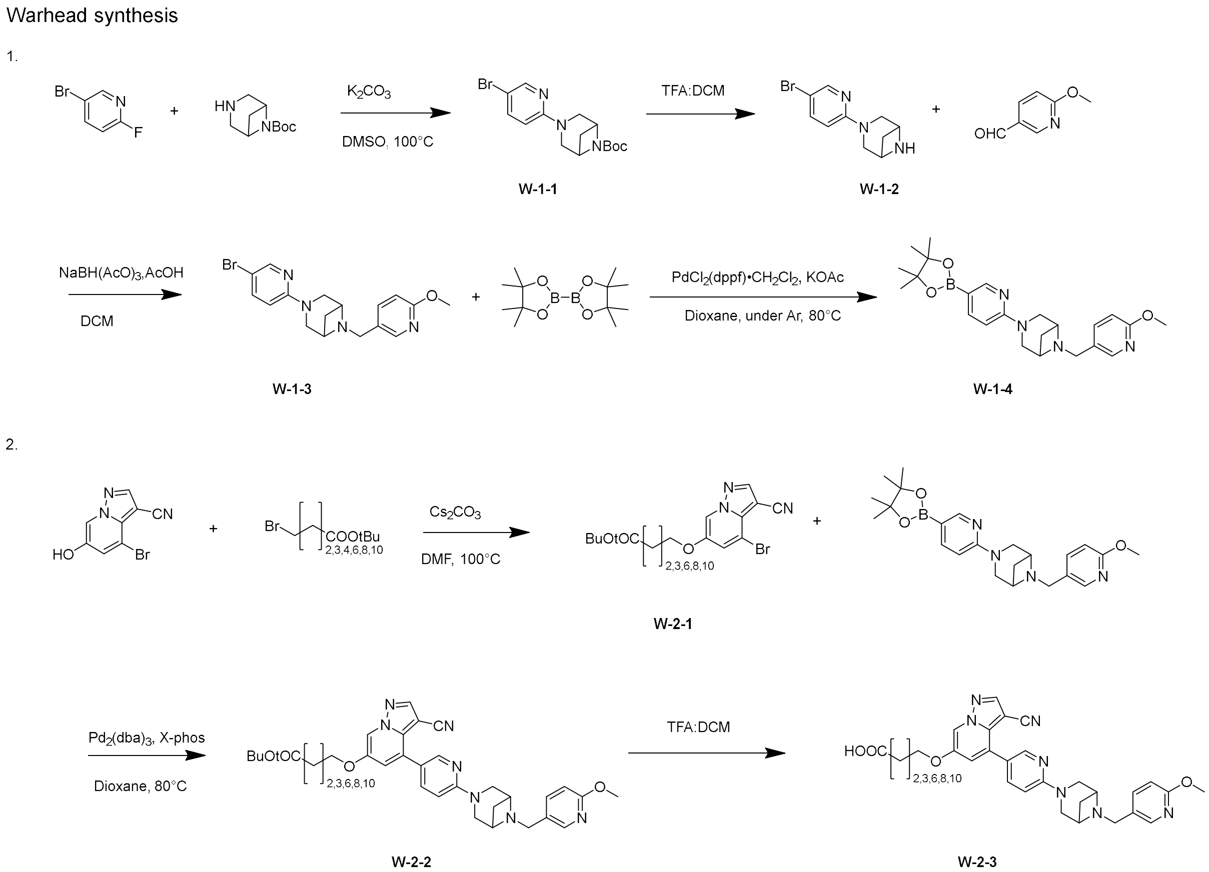
Warhead synthesis
1.
K2CO3
DMSO, 100°C
TFA:DCM
W-1-1
W-1-2
NaBH(AcO)3,AcOH
DCM
PdCl2(dppf)•CH2Cl2, KOAc
Dioxane, under Ar, 80°C
W-1-3
W-1-4
2.
Cs2CO3
DMF, 100°C
2,3,4,6,8,10
2,3,6,8,10
W-2-1
Pd2(dba)3, X-phos
Dioxane, 80°C
TFA:DCM
W-2-2
W-2-3

Figure 1.5. Synthesis of different methylene linkers of W-2-3.

Step 3: **W-1-2** was mixed with 6-methoxynicotinaldehyde in 1,2-Dichloroethane (DCE), then 3 eq of Sodium triacetoxyborohydride [$NaBH(AcO)_3$] and 3 eq of Triethylamine (TEA) were added. The resulting solution was stirred under room temperature (RT) overnight. The second day, the reaction solution was diluted with water and extracted with EA. The organic phase was washed with Brine and dried by Na_2SO_4, then evaporated under reduced pressure. The left residue was purified by chromatography (pure EA get product **W-1-3** with 1% TEA). ^{1}H NMR (600 MHz, Chloroform-*d*) δ 8.25 (d, *J* = 2.5 Hz, 1H), 8.09 – 8.00 (m, 1H), 7.59 (ddd, *J* = 10.1, 8.7, 2.5 Hz, 2H), 6.71 (d, *J* = 8.5 Hz, 1H), 6.45 (d, *J* = 9.0 Hz, 1H), 3.91 (s, 3H), 3.76 – 3.68 (m, 4H), 3.51 (s, 2H), 3.46 (d, *J* = 11.9 Hz, 2H), 2.66 (q, *J* = 6.8 Hz, 1H), 1.60 (d, *J* = 8.6 Hz, 1H).

Step 4: The 3-(5-bromopyridin-2-yl)-6-((6-methoxypyridin-3-yl)methyl)-3,6-diazabicyclo[3.1.1]heptane (1eq), Bis(pinacolato) diboron (2eq), Acetic potassium(3eq) and $PdCl_2(dppf)\cdot CH_2Cl_2$(0.1eq) were mixed together in dioxane and sparged under N_2 for 10min, the reaction solution was sealed and stirred under 90°C overnight. The second day, the reaction solution was filtered through filter paper and evaporated under reduced pressure. The left residue was purified by chromatography (EA:MeOH=10:1, get product).

$[M+H]^+$:341.2 in form of boron acid in LC-MS.

1.5.5 Synthesis of W-2-3

Step 1: 4-bromo-6-hydroxypyrazolo[1,5-a] pyridine-3-carbonitrile (1.0 eq) was stirred with tert-butyl 4-bromobutanoate (1.1eq) in DMF under 70°C for 3h. Three hours later, the reaction solution was diluted with H_2O and extracted with EA, then washed with Brine and concentrated under reduced pressure. The left residue was purified by chromatography to get product **W-2-1**. (Hexane:EA=3:1 get product), $[M+H]^+$:366.0

Step 2: tert-butyl 4-((4-bromo-3-cyanopyrazolo[1,5-a]pyridin-6-yl)oxy)butanoate (1.0 eq), 6-((6-methoxypyridin-3-yl)methyl)-3-(5-(4,4,5,5-tetramethyl-1,3,2-dioxaborolan-2-yl)pyridin-2-yl)-3,6-diazabicyclo[3.1.1]heptane (1.5 eq), X-phos (0.2 eq), $Pd_2(dba)_3$ (0.05eq) and 2M K_3PO_4 were mixed together in dioxane and sparged under N_2 for 10min. The resulting mixture was stirred overnight. Next, the dioxane was evaporated under reduced pressure and the residue was directly purified by column chromatography using EA:MeOH=10:1, product **W-2-2**. $[M+H]^+$:596.6

Step 3: The previous step product was dissolved in DCM:TFA=1:1 to react for 2h. Then, the solution was evaporated under reduced pressure and co-evaporated with hex and DCM to totally remove TFA. The residue was purified by column chromatography, using DCM:MeOH=10:1 to get **W-2-3**. $[M+H]^+$:540.1

The rest of warheads with different length of linkers were synthesized using the same procedure.

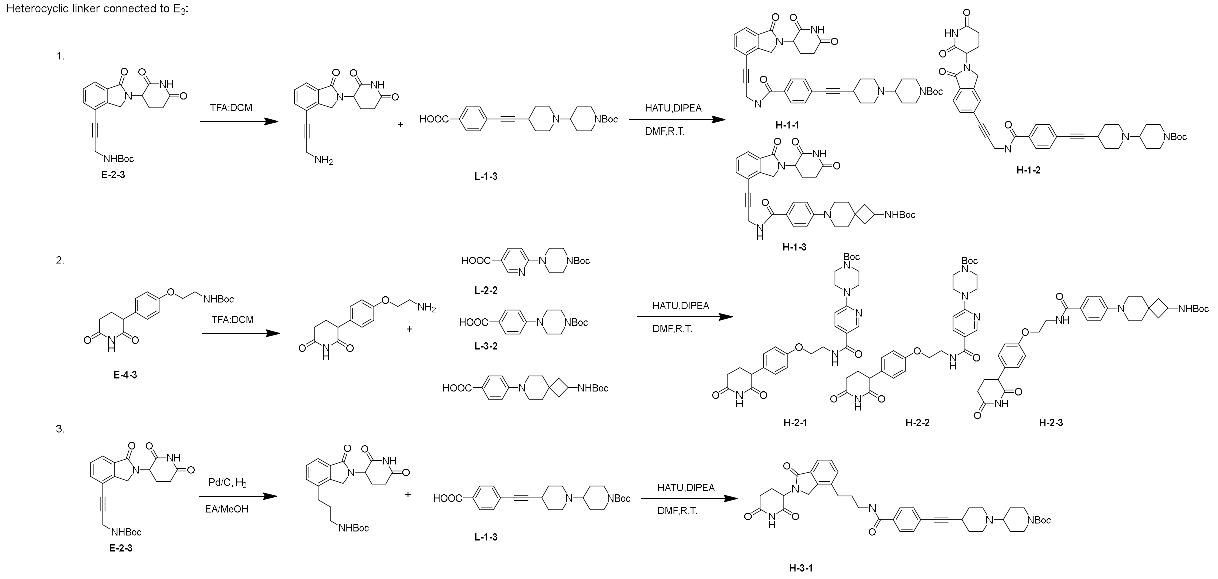
Heterocyclic linker connected to E3:
1.
E-2-3
TFA:DCM
L-1-3
HATU,DIPEA
DMF,R.T.
H-1-1
H-1-2
H-1-3
2.
E-4-3
TFA:DCM
L-2-2
L-3-2
HATU,DIPEA
DMF,R.T.
H-2-1
H-2-2
H-2-3
3.
E-2-3
Pd/C, H2
EA/MeOH
L-1-3
HATU,DIPEA
DMF,R.T.
H-3-1

Figure 1.6. Synthesis of various E_3 ligands with different heterocycle linkers.

1.5.6 Synthesis of H-1-1 to H-1-3

Compound E-2-3 was dissolved in TFA:DCM=1:1 solution and stirred for 2 hours. Then, solvent was removed under reduced pressure, and the left residue was co-evaporated with hexane for 5 times to totally remove TFA. The left oil residue was dissolved with L-1-3 in DMF, 1.2 eq of HATU and 3 eq of DIPEA were added. The reaction solution was stirred under R.T. overnight. Next, DMF was removed under reduced pressure, the left solid was purified by column chromatography to get product, using EA:MeOH=10:1 to get product H-1-1. $[M+H]^+$: 691.8 With the same strategy, H-1-1 to H-3-1 were prepared.

1.6 Cell and animal test material

1.6.1 Antibodies

Antibodies to phospho-RET (Y905) (#3221), RET (#14698), and EGFR (#2232) were from Cell Signaling Technology (Danvers, MA,USA). anti-β-actin antibody (#A5316) was from Sigma Aldrich (St. Louis, MO, USA).

1.6.2 Cell lines and cell culture

The CCDC6-RET fusion-positive human TPC1 thyroid carcinoma cells were from the European Collection of Authenticated Cells Culture (ECACC). Mouse BaF3 cells expressing KIF5B-RET (B/KR) were generated using a lentiviral vector as described previously[4]. Cells were free of mycoplasma. TPC1 cells were cultured in RPMI-1640/5% fetal bovine serum (FBS) plus penicillin-streptomycin (100 U/ml) at 37 ºC/5% CO_2. B/KR cells were cultured in RPMI-1640/10% FBS plus penicillin-streptomycin (100 U/ml) at 37 ºC/5% CO_2.

1.6.3 Cell-based assays and Immunoblotting analysis

Cell viability assay was performed using CellTiter-glo reagent (Promega, Madison, WI, USA) in 96-well plates as described previously. For experiments with TPC1 cells, cell viability was determined after 5 days of drug treatment[4, 24-26]. For experiments with B/KR cells, cell viability was determined after 3 days of drug treatment. For immunoblotting analysis of CCDC6-RET protein degradation, TPC1 cells cultured in 60-mm plates (50% confluent) were either treated with the test compound for 24 h or for the length of time indicated in the Figure x legend. For immunoblotting analysis of KIF5B-RET protein degradation in B/KR cells, $2x10^6$ cells in 6-well plate were treated with the test compound for 15 h.

Cell lysates were prepared by lysis in cold Lysis Buffer A (50 mM Tris-HCl, pH7.5, 150 mM NaCl, 1 mM EDTA, 1 mM EGTA, 25 mM NaF, 5 mM sodium pyrophosphate, 1 mM Na_3VO_4, 2 µg/ml aprotinin, 2 µg/ml leupeptin, 1 mM dithiothreitol, 20 mM p-nitrophenyl phosphate, 1% Triton X-100). Cell lysate supernatants were obtained by microcentrifugation twice at 16000 rpm for 10 min at 4 ºC. Equal amounts of soluble cell lysate proteins were separated on 10% SDS-polyacrylamide gels, transferred to nitrocellulose filters and analyzed by immunoblotting.

1.6.4 PK study

In two separate experiments, the compound YW-N-7 was administered either p.o. or i.p. to mice at the dose of 50 mg/kg (1 mg/20g, volume 150 uL). After administration, 75 uL blood samples are collected at 10 min, 20 min, 30 min, 1h, 2h, 4h, 8h, 16h, 24h, 36h, 48h (n=3 per time point, and each mouse was used for three time points, thus 12 mice were used for either p.o. or i.p. to make a total of 24 mice) after drug administration. Blood samples were collected into 1.5-mL Eppendorf tubes containing 30 µL disodium EDTA (0.5 M, pH 8.0), kept on ice, then centrifuged at 4000 rpm/min for 10 min under 4 °C. The supernatants (serum) were collected and stored under −80 °C for future analysis. 100 uL of the serum samples are added to 9:1 ration of acetonitrile and glacial acetic acid. The samples are cooled in ice for 10 min, followed by centrifuging at 10,000 rpm and 4 °C for 10 min. The clear supernatants are transferred to vials and analyzed by LC/MS/MS.

1.6.5 Cell-derived xenograft (CDX) tumor study

The CDX tumor growth experiment in animals was approved by the IACUC of the University of Oklahoma Health Sciences Center. B/KR cells used for the animal experiment were verified for free of mouse pathogens by IDEXX BioAnalytics. Cells were prepared in serum-free RPMI-1640 medium and inoculated s.c. ($5x10^6$ cells/0.1 ml/each) into the right flanks of 6-week old female

SHO mice (Charles River). After measurable tumors were established, mice were treated either with YW-N-7 at the dose specific in the figure legend or with the same volume of vehicle by i.p. injection. Each group had 8 mice bearing tumors of the similar size. The compound was dissolved in a vehicle that contained 5% 1-methyl-2-pyrrolidinone, 40% polyethylene glycol 400, 5% solutol HS-15, and 49.5% saline. Tumor sizes and animal body weights were measured similar to that described[24]. Statistical analysis was performed using unpaired t-test with Welch's correction. $p < 0.05$ was considered statistically significant.

1.7. Additional Compounds

In addition, we also synthesize VHL, pomalidomide, and thalidomide as E_3 ligands PROTAC molecules with different length of methylene linkers (Figure 1.7.). However, none of them have comparable degradation rate compared with lenalidomide or PG E_3 ligands. We didn't continue to do further research about these three ligands.

Table 1.2. HRMS data

Compound	Degradation rates at 50 nM (%)
YW-V-1	-120.7
YW-V-2	54.4
YW-V-3	15
YW-V-4	-7.8
YW-T-1	4.1
YW-T-2	1.9
YW-T-3	ND
YW-T-4	ND
YW-T-5	25.3
YW-T-6	43.5

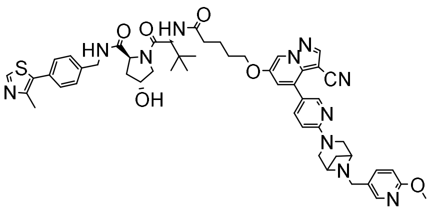

YW-V-1

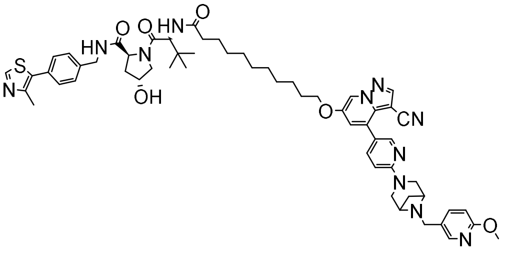

YW-V-2

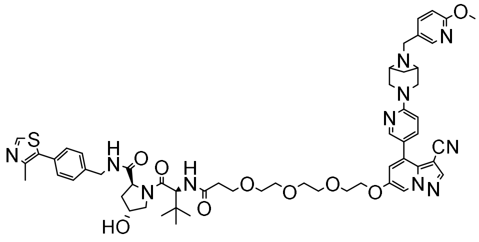

YW-V-3

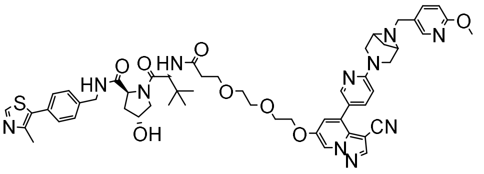

YW-V-4

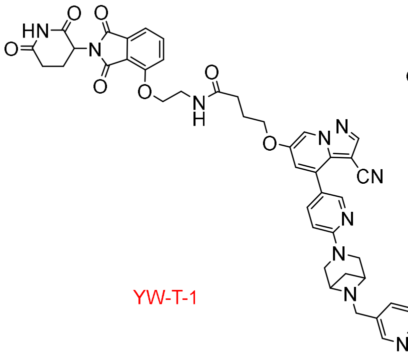

YW-T-1

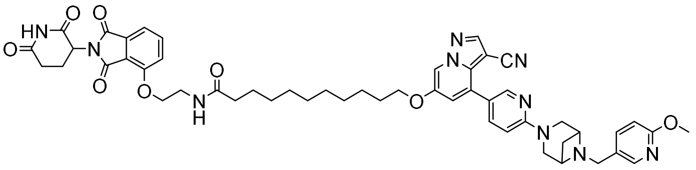

YW-T-2

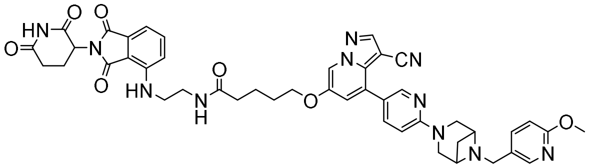

YW-T-3

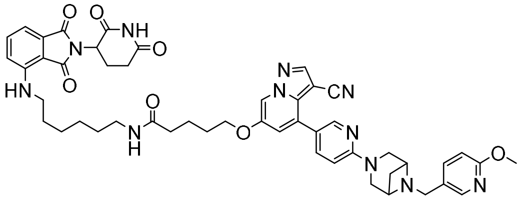

YW-T-4

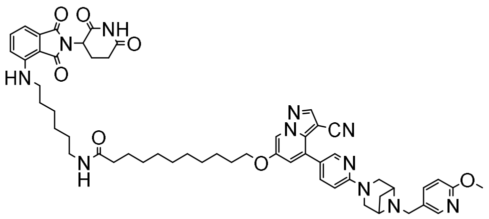

YW-T-5

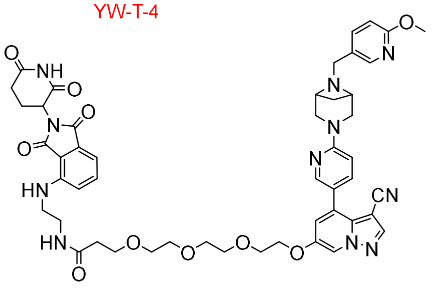

YW-T-6

Figure 1.7. Additional compounds

CHAPTER TWO: COVALENT INHIBITOR TO TARGET RET G810C MUTATION

2.1. Introduction

RET receptor tyrosine kinase is encoded by RET proto-oncogene, and RET tumors are usually caused by chromosome rearrangements or point mutations. About 1%-2% NSCLC originated from RET chimeric proteins, including fusions with KIF5B, CCDC6, NCOA4, and TRIM33. Aberrant RET signaling also can result in thyroid cancer. For example, MTC either arise sporadically (75%) or as a consequence of RET germline mutation.[27] In addition, RET chromosomal rearrangements, such as, CCDC6-RET, PRKAR1A-RET, and TRIM24-RET, are related to PTC.

Previously, first generation inhibitors are multi-kinase inhibitors, Cabozantinib, Vandetanib, and Lenvatinib, which were used to treat RET malignancy. [27] Vandetanib showed a potency with 100nM IC_{50}. It can effectively inhibit the phosphorylation and signaling transduction of RET/PTC3, RET/MEN2B, and EGF/RET chimeric receptor. [28] In clinical trial, it revealed an 11-month prolongation of median progression-free survival (from 19.3 months to an estimated 30.5 months).[29] For Cabozantinib, it inhibited TT cell RET phosphorylation bearing C634W mutation, which is usually related to familial MTC (FMTC) and MEN2A.[30] However, the overall survival (OS) has no big difference between Cabozantinib and Placebo (26.6 months and 21.1 months). In selective phase 3 III trial of Lenvatinib, it showed significantly improved median PFS and ORR, reaching 18.3 months/64.8% compared to 3.6 months/1.5% in 392 patients with differentiated thyroid carcinoma (DTC). [31] Moreover, in a phase II trial against 25 NSCLC patients, it revealed promising clinical activity with an ORR of 16% and a median PFS of 7.3 months.[32]

In 2020, the US Food and Drug administration granted two RET selective inhibitors, Selpercatinib and Pralsetinib. It demonstrated good potency *in vitro* and *in vivo* towards cells harboring RET alternations, especially gatekeeper V804M/L mutants. The crystal structures unveil that they bind to RET kinase domain very different from multi-kinase inhibitors (MKI). They occupy both the front and back pockets of the catalytic cleft, in contrast to MKI, they don't pass through the channel formed by V804 and K758. Instead, they wrap around the lysine, thus avoiding steric hinderance with V804M/L gatekeeper mutations. Especially, Selpercatinib displays exceptional efficacy towards RET wild type (WT) and RET gatekeeper V804M/L mutations with impressive IC_{50} value of 0.4 nM and 0.8/0.4 nM.[33] Among 105 participants clinical trial who has been treated with platinum-based chemotherapy, it achieved 64% ORR with a median PFS of 16.5 months. In the previously untreated 39 patients, the ORR was 85%, with 90% of the response last for 6 months.[34] However, in recent research, solvent front mutations, particularly G810S/C/R, have been identified as the main drivers to long-term administration of acquired resistance to selective RET inhibitors, such as Selpercatinib and Pralsetinib. The first case of solvent front mutations patients was observed in a patient with KIF5B-RET fusion NSCLC which had good clinical result at first, but later developed acquired drug resistance. In circular tumor DNA sequencing test, it turned out to correlate with G810S/C/R mutations. The potency of selpercatinib towards these three mutations decrease several folds compared with WT.[35] Among G810S/C/R mutations, the G810C is the main solvent front mutation. Now, it is urgent to develop next generation RET inhibitor to solve the problem of G810C mutation.

Targeted covalent inhibitors are rationally designed inhibitors that bind to protein first, then react rapidly to a proximate nucleophile, usually cysteine, to form a bond. Compared with conventional inhibitors, it offers several advantages, such as improved potency, selectivity, pharmacodynamics, and efficacy.[36] At the same time, due to its very reactive warheads, it has shortcomings of indiscriminate reactivity that could form covalent adduct with unexpected targets and idiosyncratic toxicities. Even though most pharmaceutical companies don't put that much resource on covalent drug pipelines, still there are several examples of covalent drug that have been approved for therapeutics or at late-stage clinical trials. For example, Afatinib, Mobocertinib, Dacomitinib are approved for EGFR driven lung cancer; Neratinib is used for HR2 positive breast cancer; Ibrutinib is a BTK inhibitor for leukemia, lymphoma; Penicillin has been used as broad-spectrum antibiotics since last century.

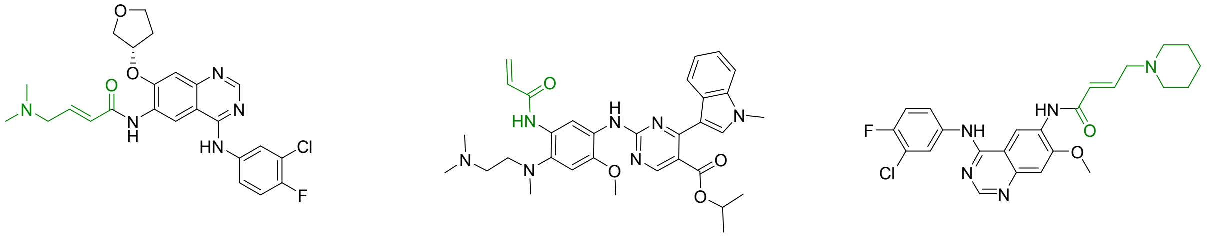

Afatinib

EGFR drived lung cancer

Mobocertinib

EGFR drived lung cancer

Dacomitinib

EGFR drived lung cancer

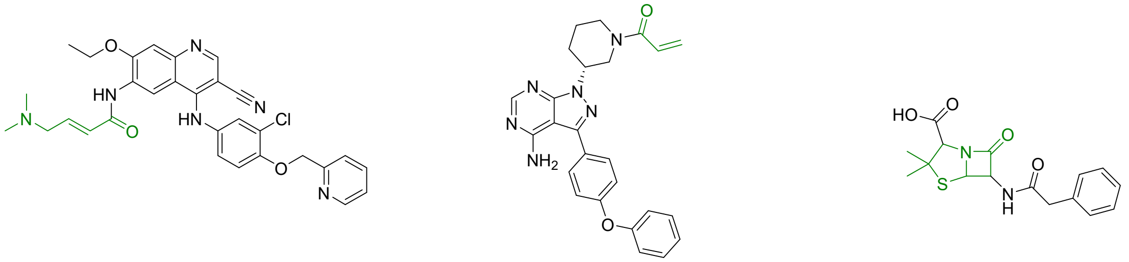

Neratinib

HR2 positive breaset cander.

Ibrutinib

A BTK inhibitor for leukemia, lymphoma

penicillin

β-lactam antibiotics

Figure 2.1. Examples of Covalent Inhibitor.

2.2. Design of RET Covalent inhibitors

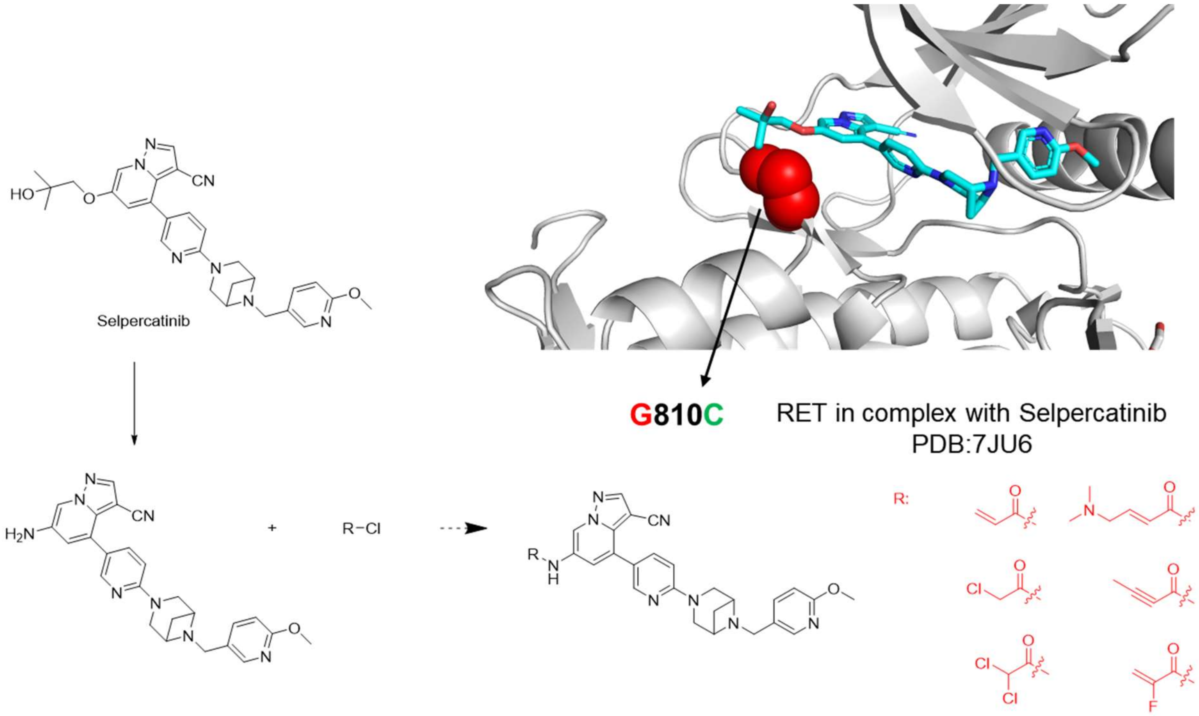

Figure 2.2. Design of RET Covalent inhibitor.

Based on the crystal structure (Figure 2.2.) of Selpercatinib binding with RET tyrosine kinase domain (PDB:7JU6), G810C mutation causes steric clash with the solvent front quaternary hydroxy group resulting in resistance to Selpercatinib. In our design, we replace the solvent front hydroxy group with different Michael receptors. We expect mutated cysteine to form a bond with the active Michael warheads, thus deactivate G810C RET mutant.

2.3. Result

First, we synthesized six different RET covalent inhibitors using different Michael receptors. YW-D-50-2, YW-D-50-6, and YW-D-50-7 showed acceptable IC_{50} against B/KR(G810C). From WB (Figure 2.3.), it showed that YW-D-50-2, YW-D-50-6 can effectively inhibit the phosphorylation of RET(Y905), but it didn’t show a good potency towards WT RET. This represented YW-D-50-2, YW-D-50-6 had good selectivity between WT and G810C RET. Still, we need more characterizations to confirm the binding mechanism and PK/PD data of these two lead compounds.

Table 2.1. SAR of different Michael Receptors.

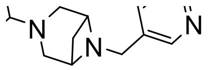		
Compound	R	IC_{50} B/KR(G810C)
YW-D-50-2		26.10
YW-D-50-3		360.5
YW-D-50-4		81.19
YW-D-50-5		93.85
YW-D-50-6		14.19
YW-D-50-7		11.53

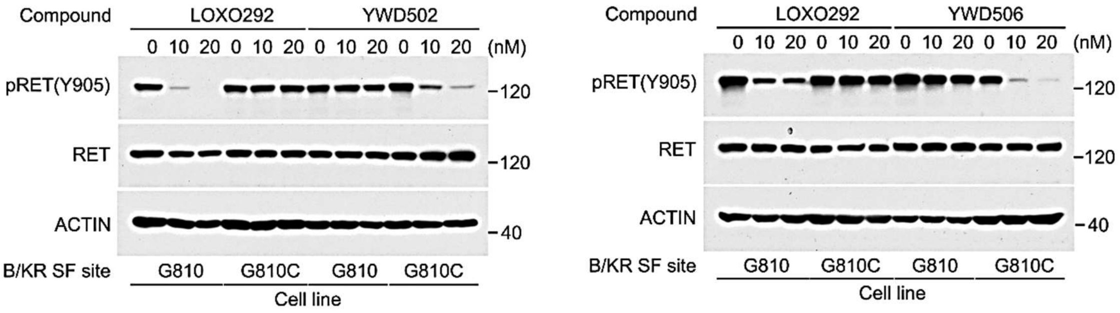
Compound
LOXO292
YWD502
0 10 20 0 10 20 0 10 20 0 10 20 (nM)
pRET(Y905)
-120
RET
-120
ACTIN
-40
B/KR SF site
G810
G810C
G810
G810C
Cell line
Compound
LOXO292
YWD506
0 10 20 0 10 20 0 10 20 0 10 20 (nM)
pRET(Y905)
-120
RET
-120
ACTIN
-40
B/KR SF site
G810
G810C
G810
G810C
Cell line

Figure 2.3. WB data of YW-D-50-2, YW-D-50-6.

2.4. Chemistry Synthesis

Synthesis route:

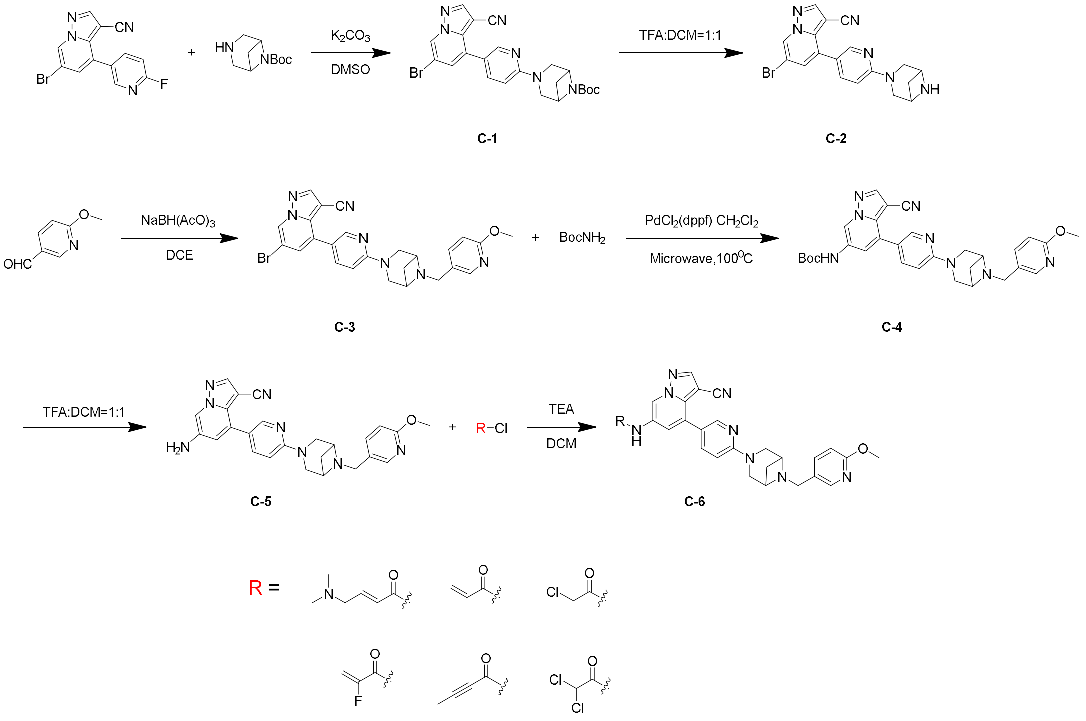
K$_2$CO$_3$
DMSO
C-1
TFA:DCM=1:1
C-2
NaBH(AcO)$_3$
DCE
C-3
BocNH$_2$
PdCl$_2$(dppf) CH$_2$Cl$_2$
Microwave,100^{0}C
C-4
TFA:DCM=1:1
C-5
R-Cl
TEA
DCM
C-6
R =

Figure 2.4. Covalent Inhibitor Synthesis Route.

C-1

6-bromo-4-(6-fluoropyridin-3-yl) pyrazolo[1,5-a] pyridine-3-carbonitrile(1eq) and tert-butyl 3,6-diazabicyclo [3.1.1] heptane-6-carboxylate (1.1eq) were dissolved in DMSO with 5eq of K_2CO_3. The reaction solution was stirred for 3 days under 110°C. After, the reaction solution was cooled down to R.T, extracted with EA for 3 times. Combine the organic layers, washed with Brine, dried by anhydrous Na_2SO_4. Then, EA was removed under reduced pressure, the left oil run column chromatography using Hex:EA=1:1 to get product, Rf=0.54.

C-2

C-1 was dissolved in a mixture of DCM:TFA=1:1 for 2h, then acid was removed under reduced pressure. The left oil was purified by column chromatography, using DCM:MEOH=10:1 to get product, Rf=0.4.

C-3

Compound C-2 (1eq) was dissolved in DCM under R.T.. Then, 2eq of 6-methoxynicotinaldehyde was added, followed by 1.5eq of sodium triacetoxyhydride and 1eq of AcOH. The reaction mixture was stirred overnight. Next day, reaction was quenched with $NaHCO_3$ and extracted with DCM for two times. Combine the organic layers, washed with Brine, and dried with anhydrous Na_2SO_4. DCM was removed under reduced pressure, the left residue was purified by column chromatography, using DCM:MeOH=10:1 to get product, Rf=0.2

C-4

A mixture of compound C-3 (1eq) and tert-butyl carbamate (1.1eq) were dissolved in toluene, then 0.05 eq of $Pd_2(dba)_3$, 4eq of Cs_2CO_3, and 0.05 eq of Xantphos were added. This Hartwig-Buchwald reaction runs under microwave at 110ºC for 2h. Then, the solvent was removed under reduced pressure. The left residue was dissolved in acetonitrile and water, filtered, and purified by HPLC.

C-6

Compound C-4 was dissolved in TFA: DCM=1:1 and stirred for 2 h. After, solvent was removed under reduced pressure, the left oil was co-evaporated with hex for 5 times to totally removed TFA to get C-5. C-5 was used for the next step without any further purification. C-5 was dissolved in DCM in ice bath, then 2 eq of TEA was added, followed by 2 eq of different Michael receptor warheads. The reaction solution was stirred overnight. Next, DCM was removed, the left residue was dissolved in ACN and water, filtered, purified by HPLC at last.

CHAPTER THREE: DENDRIMERIC PEPTIDOMIMETIC AS ANTIMICROBIAL

3.1. Introduction

It is estimated that 700,000 to several million deaths result from bacterial infections per year, and 2.8 million people are infected by bacteria resistant to current antibiotics in the USA, with at least 35,000 people dying from that. Due to the scarcity of new antibiotics to combat antibacterial resistance (AMR), over 50 million people could die by 2050, with the yearly death toll being 10 million under the current predicted model.[37] As a result, it is extremely urgent to develop new antibacterial agents that can mitigate emerging antibiotic resistance.

Host defense peptides (HDP), which are produced by organisms as the first-line agents to defend against a wide range of bacteria, have gained much attention from scientists.[38] Usually, HDPs share two common features: one is the cationic charges, and the other one is a proper ratio of hydrophobic residues, which enable HDPs to adopt amphipathic structures and exhibit significant selectivity toward bacteria over mammalian cells. This is because the outer leaflet of the mammalian cell membrane is composed of zwitterionic lipids, while the outer leaflet of the bacteria membrane mainly consists of negatively charged phospholipids. As a result, the negatively charged bacterial membrane tends to interact with cationic HDPs preferentially, leading to bacterial cell death while maintaining low hemolysis risks and cytotoxicity.[39] In human, the two main classes of HDP are defensin and cathelicidin. Defensins usually have a β-sheet core and it can be subdivided into α, β, and θ defensins.[40] Cathelicidins are produced as prepropeptides that commonly have cathelin-like domain before cleavage by serine proteases. A majority of cathelicidins have secondary helical structure. One side of the helix is hydrophilic cationic charged amino acids, the other side is hydrophobic. Thus, cathelicidins can interact and perturb with anionic surface of bacteria.[40] Nevertheless, there are still drawbacks associated with HDPs, such as proteolytic degradation susceptibility, poor selectivity, and moderate activity. To address these problems, several classes of peptidomimetics have been developed to overcome the drawbacks of HDP, including peptoids,[41] β-peptides,[42] γ-AApeptides,[43] and oligourea (Figure 3.1.).[44] These new unnatural peptidomimetic sequences can mimic HDP function against pathogens and retain resistance to proteolytic hydrolysis (Figure 3.2.).[45]

Lipidated peptides have been presented as antibiotics for years. For instance, polymyxin B[46] and daptomycin[47] are two FDA-approved lipo-cyclic peptides. While daptomycin only displays activity against Gram-positive bacteria, polymyxin B is only active for Gram-negative bacteria. Despite distinct antibacterial mechanisms, it has been shown that lipid tails are critical for their activity, which facilitate bacterial membrane interaction.[48] Recently, our group designed a new class of antimicrobial peptidomimetic compounds composed of γ-AA amino acid (Figure 1) .To further explore the antimicrobial potential of γ-AApeptides, we herein report a new class of short, lipidated dendrimeric γ-AApeptides as potential antibacterial agents.

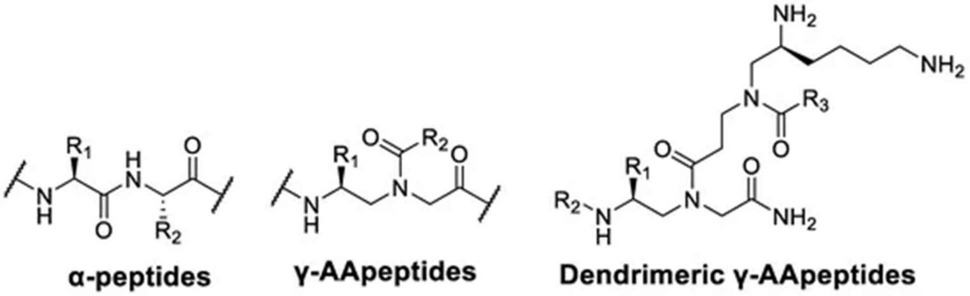

Figure 3.1. Structure of α-peptides, γ-AA peptides, and dendrimeric γ-AA peptides.

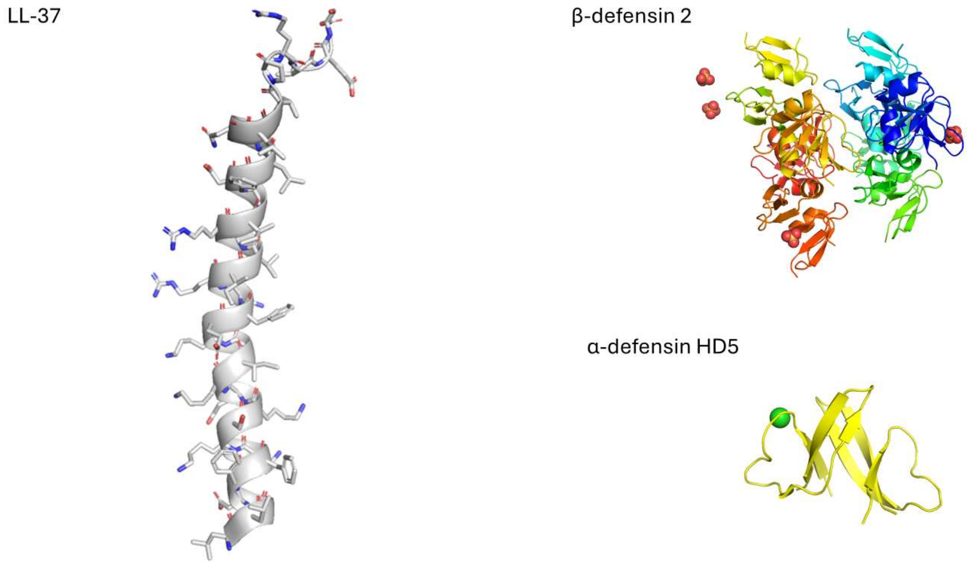

Figure 3.2. Examples of HDPS

3.2. Examples of HDP and mimics

In recent years, our group developed several γ-AA peptides and lipidated γ-AA peptides,such as compounds, **26, 29,** and **31**, based on the structure of HDP. For the lipidated γ-AA peptides, the lipidated tail would be inserted into bacterial membrane, while the positive lysine's function as positive charged group to attach to the surface of the bacterial membrane. However, lipidated peptides don't guarantee good selectivity. The cytotoxicity and *in vivo* activity were not evaluated.

To achieve the goal of developing small-molecule antimicrobial peptide derivatives with drug-like properties, a new series of compounds with admantaneacetyl groups was developed, they showed broad-spectrum activities.Moreover, the lead compound **28** didn't show significant activity loss even under Na^+, K^+, and Ca^{2+} cations. But we didn't run extensive structure activity relationships research about compound **28**. In the future, more research can be done with **28** to explore more enhanced activities and therapeutic index (Figure 3.3). [49]

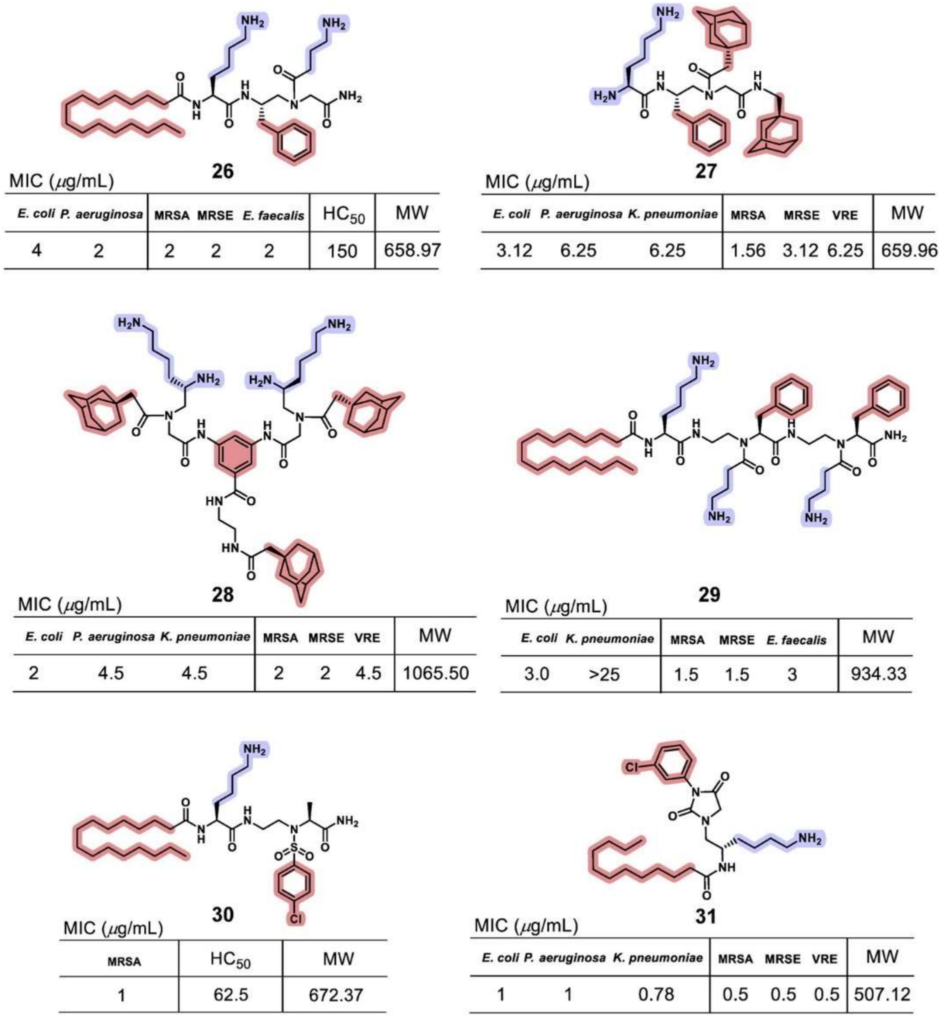

26

MIC (μg/mL)

E. coli	*P. aeruginosa*	MRSA	MRSE	*E. faecalis*	HC_{50}	MW
4	2	2	2	2	150	658.97

27

MIC (μg/mL)

E. coli	*P. aeruginosa*	*K. pneumoniae*	MRSA	MRSE	VRE	MW
3.12	6.25	6.25	1.56	3.12	6.25	659.96

28

MIC (μg/mL)

E. coli	*P. aeruginosa*	*K. pneumoniae*	MRSA	MRSE	VRE	MW
2	4.5	4.5	2	2	4.5	1065.50

29

MIC (μg/mL)

E. coli	*K. pneumoniae*	MRSA	MRSE	*E. faecalis*	MW
3.0	>25	1.5	1.5	3	934.33

30

MIC (μg/mL)

MRSA	HC_{50}	MW
1	62.5	672.37

31

MIC (μg/mL)

E. coli	*P. aeruginosa*	*K. pneumoniae*	MRSA	MRSE	VRE	MW
1	1	0.78	0.5	0.5	0.5	507.12

Figure 3.3. Examples of recently developed γ-AA peptides and lipidated γ-AA peptides to mimic HDPs in our group.

3.3. Results and Discussion

In our current design, a positively charged γ-AApeptide building block was attached to the secondary amine of another γ-AApeptide building block, to which different lengths of lipid tails were introduced to make a series of miniature lipo-dendrimeric γ-AApeptides (Figure 1). As such, these amphipathic structures were expected to mimic the antibacterial function of HDPs. The positively charged side chains would form electrostatic attraction with bacterial membranes, whereas the lipid tail would facilitate the insertion of the compounds into bacterial membranes, leading to membrane disruption. To this end, the compounds were tested for the ability to kill a panel of Gram-positive and Gram-negative bacteria (Table 1). For the building blocks conjugating to the C16 lipid tail, such as Leu (YW-1), Phe (YW-2), Ala (YW-3), Tyr (YW-4), Ser (YW-5), Lys (YW-6), and Arg (YW-7), different γ-AA amino acids were synthesized and solid phase was used to do final synthesis, the structure of newly synthesized compounds listed in Scheme 1. It shows these compounds generally exhibited effective antimicrobial activity and did not show hemolytic activity up to 125 μg/mL. While YW-1 displayed the most broad-spectrum antimicrobial activity against a panel of Gram-positive and Gram-negative bacteria, certain compounds, such as YW-3, 4, 6, and 7, demonstrated highly selective activity toward MRSA (MIC: 0.75–1.5 μg/mL) (Table 3.1.). The findings suggested that functional groups on the building blocks conjugated to the C16 lipid tail could play an important role in antibacterial activity and selectivity, which could direct the future design and optimization of this class of compounds (Figure 3.4).

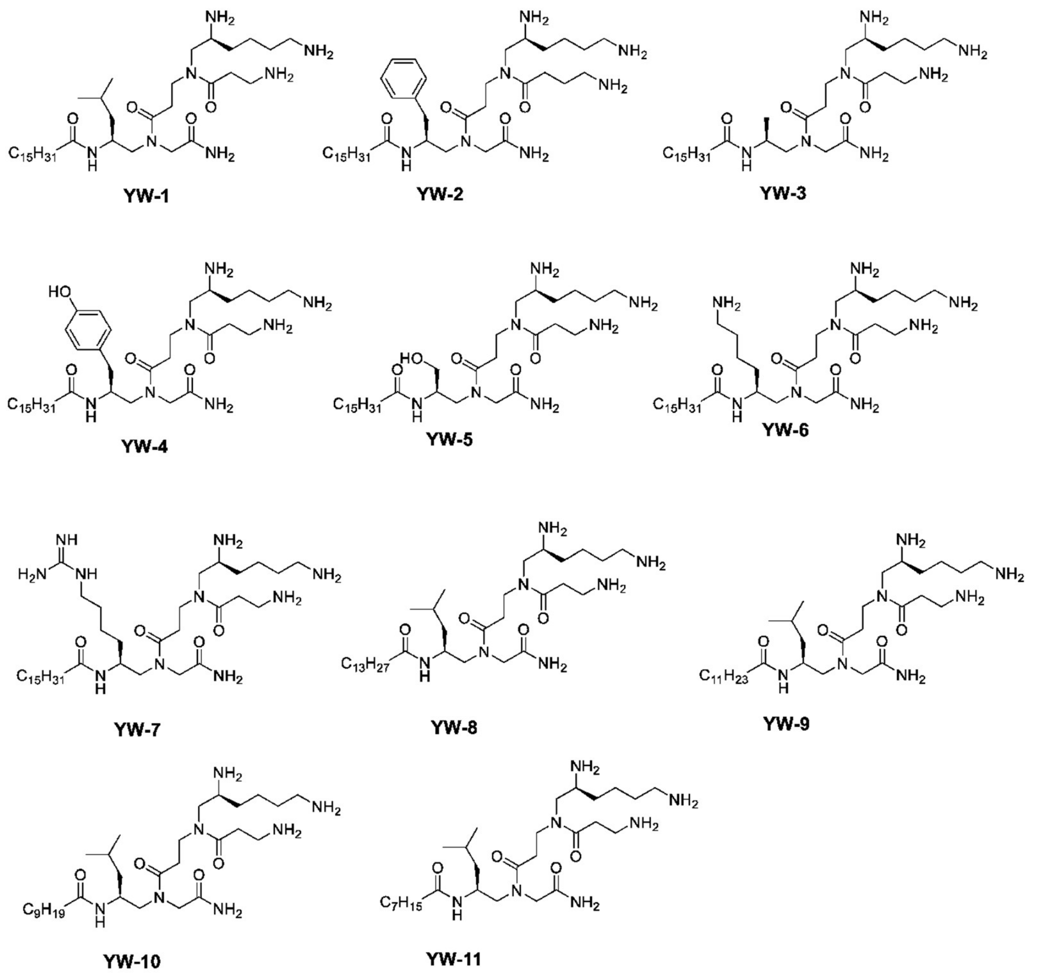

YW-1 **YW-2** **YW-3**

YW-4 **YW-5** **YW-6**

YW-7 **YW-8** **YW-9**

YW-10 **YW-11**

Figure 3.4. The structures of lipidated dendrimeric γ-AApeptides.

Table 3.1. Antibacterial activity, hemolytic activity, and selectivity of dendrimeric γ-Aapeptides. "---" means not tested.

	MIC (μg/mL)						HC$_{50}$ (μg/mL)	Selectivity Index (HC$_{50}$/MICMRSA)
	Gram-Positive (+)			**Gram-Negative (−)**				
	MRSA	**E.F.**	**MRSE**	**P.A.**	**K.P.**	**E. *coli***		
YW-1	1.5-3	1.5-3	1.5-3	6-12.5	12.5-25	3-6	>125	>41.7
YW-2	1.5-3	1.5-3	1.5-3	12.5-25	6-12.5	3-6	>125	>41.7
YW-3	0.75-1.5	3-6	6-12.5	6-12.5	>25	3-6	>125	>83.3
YW-4	0.75-1.5	3-6	3-6	>25	>25	3-6	>125	>83.3
YW-5	1.5-3					6-12.5	>125	>41.7
YW-6	1.5-3					6-12.5	>125	>83.3
YW-7	0.75–1.5	3–6	3–6	12.5–25	>25	3–6	>125	>83.3
YW-8	12.5–25					>25		
YW-9	>25					>25		
YW-10	>25					>25		
YW-11	>25					>25		

3.4. Materials and Methods

3.4.1. Membrane Depolarization Study

To probe the mechanism of antibacterial activity, we first carried out a membrane depolarization study with the membrane potential-sensitive dye 3,3′-dipropylthiadicarbocyanine iodide (diSC35) (Figure 2A,B).[50] DiSC35 usually accumulates in living bacterial membranes, and due to self-quenching, it shows low fluorescence intensity. However, if the membrane is disrupted, and the fluorophore is released from the membrane, fluorescence will improve dramatically. As shown in Figure 2, when the bacteria were treated with different concentrations of the lead compound YW-1, both E. coli and MRSA exhibited dose-dependent increases in fluorescence intensity. It was intriguing that YW-1, at a two-fold of MIC or above, caused even more intensive fluorescence than the positive control Triton, which is well known for causing membrane damage. This experiment result demonstrated that the bacterial membranes were disrupted by YW-1, indicating a potential mechanism similar to that of HDPs (Figure 3.5.).

coli.

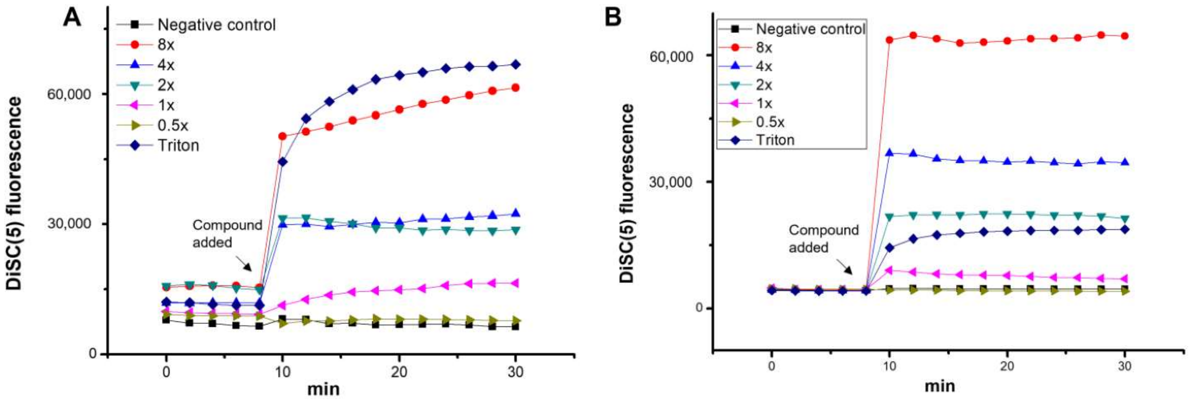

Figure 3.5. Membrane depolarization study of YW-1 against Gram-negative bacteria E. coli (A) and Gram-positive bacteria MRSA (B). Triton x-100 as a positive control.

3.4.2 Outer Membrane (OM) Permeabilization

Next, using E. coli as a microorganism, we evaluated the OM permeabilization of YW-1. In aqueous conditions, 1-N-Phenylnaphthylamine (NPN) is blocked by the cell wall. However, if the OM is permeabilized, and NPN is taken up as a result, the fluorescence intensity will increase, compared to non-treated OM.[51] As shown in Figure 3A, with 1% Triton as a control, the permeabilization capability of the OM was determined by the absorbance of NPN in a concentration-dependent manner. YW-1 exhibited a good potency in outer membrane permeability with 1 × MIC of 98%, compared with that of 1% Triton (Figure 3.6.).

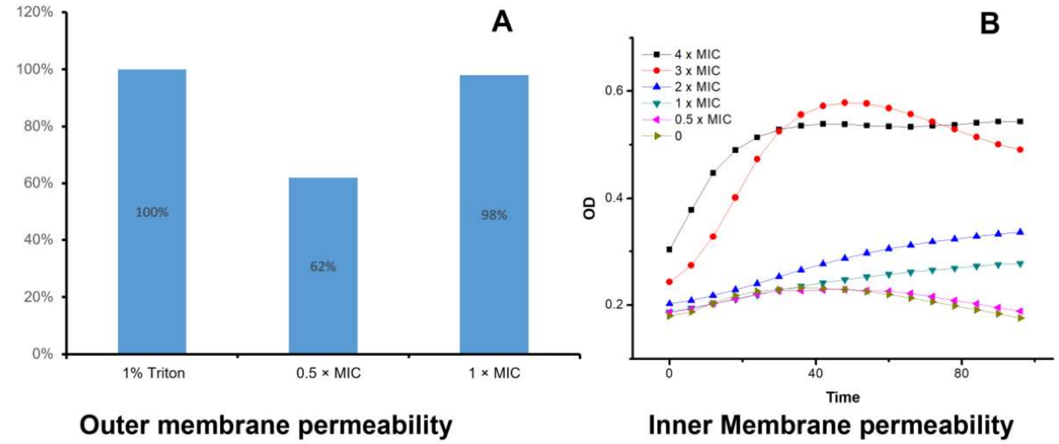

Figure 3.6. Outer membrane (OM) permeabilization (A) and inner membrane permeabilization (B) against E. coli.

3.4.3. Inner Membrane (IM) Permeabilization

We next used the o-nitrophenyl-β-d-galactopyranoside (ONPG) hydrolysis assay to test the ability of the lead compound YW-1 to permeabilize the inner membrane of Gram-negative bacteria (Figure 3B). If the lead compound YW-1 compromised the bacterial inner membrane, ONPG would interact with the cytoplasmic enzyme β-galactosidase to form o-nitrophenol, which can be measured under OD 420 nm.[52] As shown in Figure 3B, when E. coli were treated with YW-1 with 8 × MIC, 4 × MIC, 2 × MIC, and 1 × MIC, the OD 420 nm intensity was enhanced to a great extent.

3.4.4. Fluorescence Microscopy

To further assess that the bacteria were killed with YW-1 by comprising the cell membrane, we conducted a fluorescence microscopy experiment (Figure 3.7). Two dyes, 4′,6-diamidino-2-phenylindole (DAPI) and propidium iodide (PI), were employed in this experiment. PI can only stain dead or injured cells since it does not have cell membrane permeability. Instead, DAPI can be used to stain both dead and live cells because it is cell permeable. After MRSA and E. coli were treated with YW-1, red fluorescence was observed under the PI channel (Figure 3.7.), suggesting that bacterial membranes were compromised by YW-1.

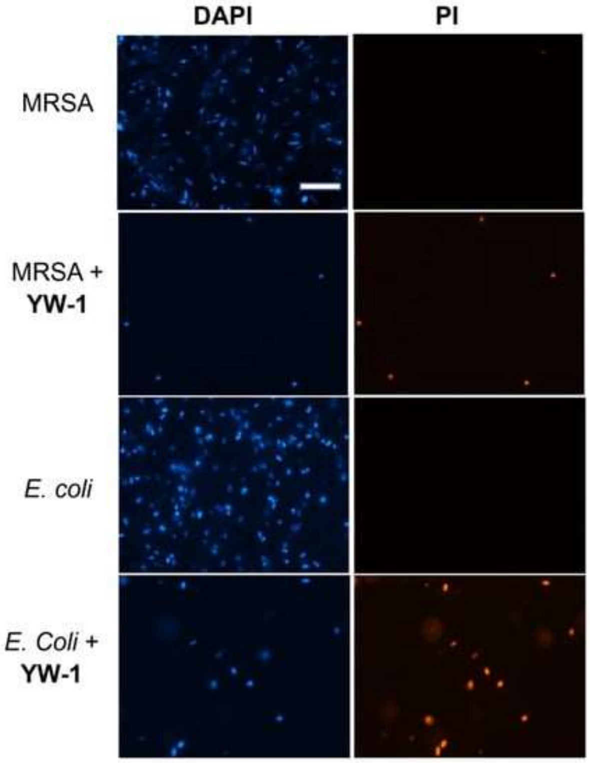

Figure 3.7. Fluorescence microscopy of the bacteria MRSA and E. coli treated with 2 × MIC of YW-1, scale bar 10 μm.

3.4.5. Transmission Electron Microscopy (TEM)

TEM microscopy offers convenient access to check the intactness of cell membranes. The cell membranes of MRSA and E. coli were intact. However, after treatment with YW-1, the membranes clearly demonstrated damages, and bacterial cells lost their spherical (MRSA) or rod (E. coli) shapes (Figure 5), indicating that the membranes of these bacteria were disrupted (Figure 3.8).

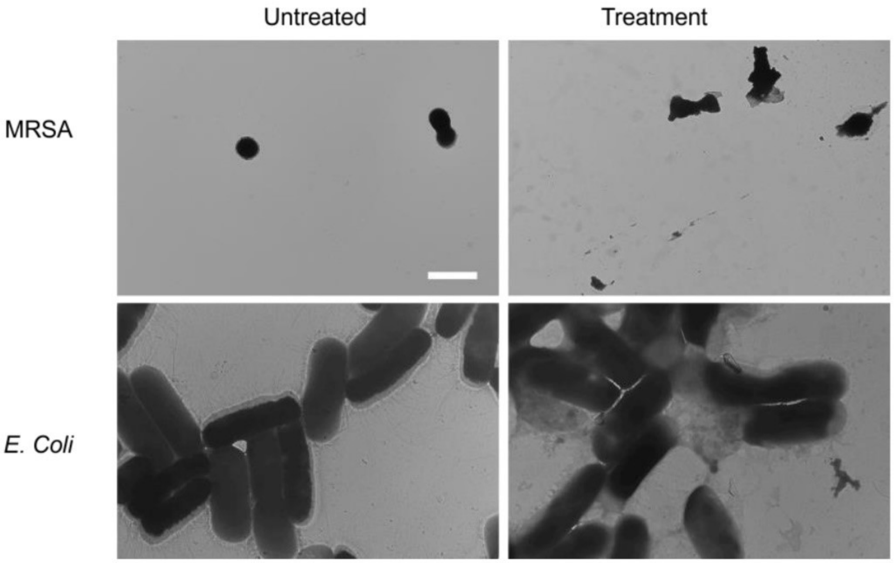

Figure 3.8. TEM graphs of MRSA and E. coli in the presence and absence of YW-1 at 2 × MIC, scale bar 2 μm.

3.4.6. Bacterial Killing Efficiency

3.4.6.1. Time-Kill Kinetics Study

To evaluate how rapidly bacteria could be eradicated (Figure 3.9), the lead compound YW-1 was examined for its ability to eradicate MRSA and E. coli by studying the time-kill kinetics. As shown in Figure 6, YW-1 could remove MRSA and E. coli thoroughly with 4 × MIC and 8 × MIC within 2 h.

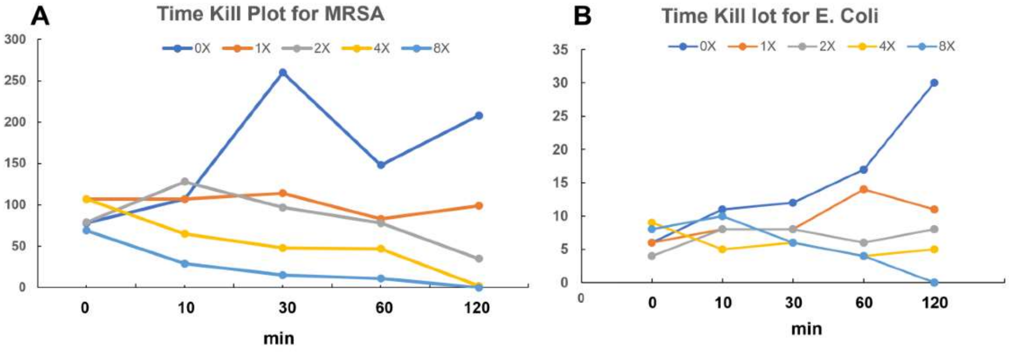

Figure 3.9. Time-kill kinetics of YW-1 toward MRSA (A) and E. coli (B).

3.4.6.2. Drug Resistance Test

Since the abuse of antibiotics, antibacterial drug resistance has become an increasingly serious threat. Thus, it is of great importance to assess the drug resistance of newly developed lead compounds. As shown in figure 3.10, the control, ciprofloxacin, developed drug resistance after 14 generations, since the MIC increased about 100-fold. In comparison, YW-1 did not have an obvious change in MIC, which suggests that YW-1 has a low probability of developing antibiotic resistance. Our compound had a lower probability of developing drug resistance.

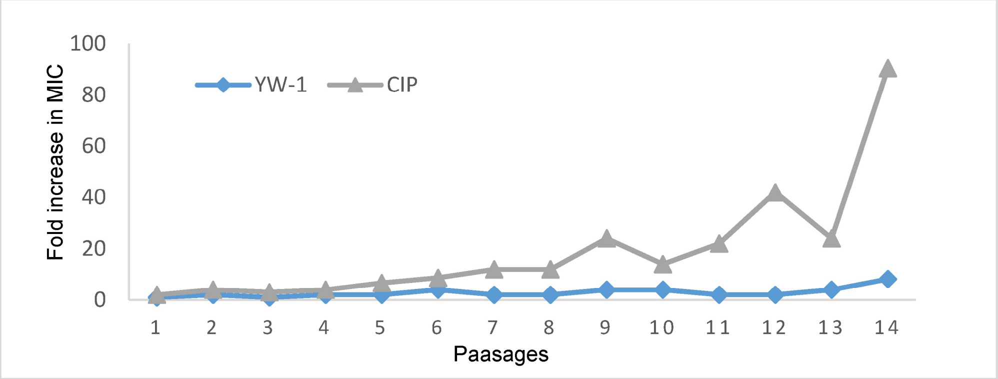

Figure 3.10. Drug resistance study of YW-1 toward MRSA.

3.5. Experiment Procedure

3.5.1. General Experiment Methods

Chemical reagents and solvents were bought from Sigma Aldrich, Oakwood, TCI, and Chem-Impex. Final products were purified with Waters Breeze 2 HPLC and lyophilized using Labconco lyophilizer. HPLC traces of the final product were collected using 5–95% acetonitrile in water with 0.1% HPLC-grade TFA for at least 40 min. The nuclear magnetic resonance (NMR) data were collected using the Agilent 600 MHz NEO instrument. High-resolution mass spectra of compounds (Table S1) were collected using an Agilent Technologies 6540 UHD accurate-mass Q-TOF LC/MS spectrometer. Antibacterial assays and mechanism of action studies were performed using a Biotec multimode microplate reader synergy H4. Six different species of bacteria were used for bacteria assay tests, such as MRSA (ATCC 33591), MRSE (RP62A), VREF (ATCC 700802), E. coli (ATCC 25922), K. pneumoniae (ATCC 13383), and P. aeruginosa (ATCC 27853).

3.5.2. MIC (Minimum Inhibitory Concentration)

Concisely, E. coli, K. pneumoniae, P. aeruginosa, MRSA, MRSE, and VREF were cultivated in 37 °C TSB medium for 16 h. Subsequently, 4 ml of new TSB medium was added to 100 μL of cultivated bacterial solution and incubated for another 6 h to reach the mid-log phase. Next, 96-well plates were injected with 50 μL of bacterial solution that reached mid-log phase and 50 μL of compounds with different concentrations, which ranged from 0.75–25 μg/mL. Then, the 96-wells plates were incubated for another 16 h at 37 °C. After 16 h, MICs were determined by a multimode microplate reader.

3.5.3. Hemolytic Activity

Human red blood cells were washed with 1 × PBS buffer, then centrifuged at 700 g for 10 min. After discarding the top clear solution, the bottom cells were diluted to obtain 5% solution using 1 × PBS buffer.

Then, 50 μL of cell solution was injected into 96-well plates. Following this, 50 μL of synthesized compounds with different concentrations from 250 to 1.95 μg/mL were added into 96-well plates. Then, the mixture was incubated for 1 h at 37 °C. After centrifuging at 3500× g rpm for 10 min, 30 μL of the supernatant was transferred into a new 96-well plate with 100 μL of 1 × PBS buffer. With the same microplate reader, the data of absorbance at 540 nm were compared. Positive control: 2% Triton-100. Calculation formula: percentage of hemolysis = [(Absorbance of sample-Absorbance of PBS)/(Absorbance of Triton-Absorbance of PBS)] × 100.

3.5.4. Drug Resistance Study

The first generation of MIC data of YW-1 against MRSA and E. coli was already obtained in an MIC study. Then, the MRSA of the first generation in the well next to the last clear well was diluted to the mid-log phase, and MICs were tested at 37 °C. This step was repeated for 14 passages. The data of drug resistance for E. coli were obtained using the same method with bacterial E. coli.

3.5.5. TEM

An amount of 30 μL of mid-log phase MRSA and E. coli was diluted to 3 mL in TSB medium with 2 × MIC of YW-1, and the mixture was incubated for 2 h. The bacterial pellets were centrifuged at 3000× g rpm for 10 min. For the next step, PBS buffer was used to wash three times. Then, the suspended bacterial samples were dropped on grids and dried in a vacuum oven at 45 °C. TEM images were obtained using a FEI Morgagni 268D TEM, with an Olympus MegaView III CAMERA on the microscope, at 60 kV.

3.5.6. Inner Membrane Permeability

Mid-log phase E. coli was obtained in Mueller Hinton Broth with 2% lactose at 37 °C; then, it was centrifuged at 3000× g rpm for 10 min at 4 °C and washed with 20 mM glucose and 1.5 mM ONPG in 5 nM HEPES buffer one time. Next, the bacterial solution was diluted until OD600 = 0.1 using the same buffer. Following this, 50 μL of diluted bacterial solution was injected into a 96-well plate, and 50 μL of YW-1 in different concentrations and melittin were injected into the bacterial solution, respectively. The OD420 was read at 37 °C every 6 min until the fluorescence reached the highest plateau.

3.5.7. Fluorescence Microscopy

A total of 30 μL of mid-log phase bacterial solution was diluted to 3 mL in TSB medium with 2 × MIC of YW-1. The mixture was incubated for 2 h at 37 °C. Following this, the bacterial solution was centrifuged at 3000 rpm for 10 min. The top solution was thrown away, the bottom bacterial pellets were washed with PBS buffer, and PI (5 μg/mL) and DAPI (10 μg/mL) were added sequentially on ice under a dark environment. After dyeing with PI and DAPI, the bacterial cells were washed with PBS buffer. Immediately after 100 μL of PBS was added to suspend the bacterial cell, 10 μL of the suspended solution was dropped onto the slide, and data were obtained using a Zeiss Axiovert 200 inverted microscope.

3.5.8. Time-Kill Kinetics Study

Different concentrations of YW-1 and ciprofloxacin were mixed with 300 μL of mid-log phase bacterial solution in TSB medium. The mixture was incubated for 0, 10, and 30 min and 1 and 2 h, respectively. At the time, E. coli were diluted 100-fold, and the MRSA was diluted 100-fold. A total of 100 μL of each was transferred on TSB agar plates. After 16 h at 37 °C, CFUs were read using the Biotec multimode microplate reader.

3.6. Conclusions

In summary, we developed a new series of antibacterial compounds. The lead compound, YW-1, showed potency towards both Gram-positive and Gram-negative bacteria. Further, YW-1 killed bacteria by disrupting cell membranes, confirmed with TEM, OM permeabilization, and membrane depolarization though without apparent drug-developed resistance. Meanwhile, it displayed good selectivity with low hemolytic toxicity. Taken together, YW-1 showed good therapeutic potential, and it could be a candidate to solve the problem of AMR.

3.7. General Synthesis of Compound

The Fmoc protected amino acids were bought from Chemimpex, reagents used in reaction are bought from Fisher Scientific and Sigma Aldrich. The building blocks were synthesized following previously published paper from our group. Next, the building block was loaded on Rink-Amide beads with DIC and HOBt in DMF reacting for 4 hours. After deprotecting Fmoc protecting, palmitic acid was coupled DIC and HOBt. The Alloc protecting group of the secondary amine was removed with Dimethylamine Boron ((CH3)2NH.BH3) and Tetrakis(triphenylphosphine) Palladium, the second building was coupled like the first building block. Deprotect the alloc protecting group again, then couple Fmoc protected beta alaine. Subsequently, the Fmoc was removed, and the beads were cleaved with 50% TFA in DCM. The solvent was removed and solid was precipitated with cold ether. Finally, the oil was purified by HPLC and got the last product.

Table 3.2. HRMS data

Peptide	HRMS (ESI) [Exact Mass+H^+] calculated	HRMS (ESI) [Exact Mass+H^+] found
YW-1	667.5742	668.5747
YW-2	701.5568	702.5604
YW-3	625.5255	626.5286
YW-4	717.5517	718.5532
YW-5	641.5204	642.5214
YW-6	682.5833	683.5852
YW-7	724.6051	725.6050
YW-8	673.5255	674.5298
YW-9	645.4942	646.4979
YW-10	617.4629	618.4668
YW-11	589.4316	590.4355

CHAPTER FOUR: BCL-9 P-PROTAC TO DEGRADE B-CATENIN

4.1. Fmoc SPPS

4.1.1. Background of Fmoc SPPS

Pioneered by Robert Bruce Merrifield, the well-established peptide synthesis in lab is known as solid phase peptide synthesis. On a solid-support resin, it allows scientists to synthesize peptide chain via successive coupling AA.[53] In contrast to solution phase synthesis that time-consuming isolation of product from reaction solution, the nascent peptide chain attached covalently to the solid supportive resin that functionalized with different reactive groups, such as hydroxy or amine groups. Usually, vessels for SPPS have silica pads that help researchers remove excessive starting material and side products easily. Depending on the side chain and protecting strategy, nowadays, the most often used two SPPS are Fmoc-SPPS and Boc-SPPS. The general procedure of Fmoc-SPPS is to repeat several cycles of coupling N-terminal Fmoc protected AA. This cycle is repeated until the desired peptide sequence is done. During coupling steps, capping methods, such as a mixture of pyridine and acetic anhydride, are often used to block the unreacted amine to reduce side products. Compared with Boc/Bzl SPPS using HF as N-terminal deprotecting strategy, Fmoc-SPPS deprotection method is much more milder using 20-50% piperidine in DMF (Figure 4.1).[54] Moreover, the new free amine is neutral, not like Boc SPPS that free amine is pronated under strong acidic condition, that is directly used for next step coupling reaction without any neutralization. It is also easy to confirm whether the deprotection is done since chromophores are produced. Because chromophores show strong color under UV, it is very convenient to check the reaction. Usually, after two times deprotection with 20% piperidine for 10 min, the deprotection is done.

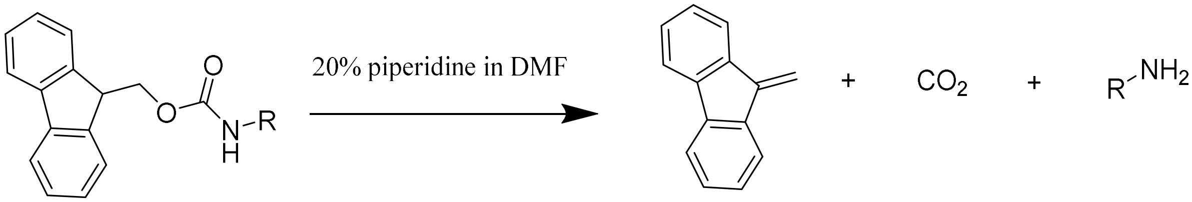

Figure 4.1. Deprotection Mechanism of Fmoc-SPPS.

On Fmoc SPPS, the side chains of AA are usually acid sensitive protecting groups, such as Boc used for Lys, tBu used for Glu and Asp, Trt used for Gln and Asn. The cleavage cocktails can remove all the acid sensitive protecting groups at cleavage step. Scavengers including triisopropylsilane (TIPS) and water are most added with a small ratio during cleavage step to prevent side reactions. Nevertheless, some other scavenger reagents could also be use.[55, 56]

4.1.2. Coupling Reagents and Limitations for Fmoc SPPS

For the coupling reagent, diisopropylcarbodiimide (DIC) is frequently used SPPS since it is liquid, and the urea byproduct is easily washed away by DMF. Another carbodiimide coupling reagent, 1-Ethyl-3-(3-dimethylaminopropyl)carbodiimide (EDC), is usually used for solution phase coupling as it has a tertiary amine, as a result, the byproduct is easily washed away during aqueous work-up. To circumvent racemization problem, different "racemization suppressing" chemicals are added to reaction, such as the triazoles 1-hydroxy-benzotriazole (HOBt), and 1-hydroxy-7-aza-benzotriazole (HOAt). After carboxylic acid forms O-acylisourea intermediate with carbodiimide, these two chemicals will attack O-acylisourea to form an active ester, which will react with a free amine to form an amide bond.[57]

The other two often used coupling reagents are aminium/uronium and phosphonium salts (Figure 4.2). This type coupling reagent completely omit carbodiimide. Instead, it incorporates

HOAt/HOBt moiety as an amimium/uronium or phosphonium as an anion (tetrafluoroborate or hexafluorophosphate). Aminium/uronium coupling reagents include HATU (HOAt), HBTU/TBTU (HOBt), HCTU (6-Cl HOBt). The only difference between HBTU and TBTU is the choice of anion. Phosphonium coupling reagents include PyBOP (HOBt) and PyAOP (HOAt) .[58]

However, this step-by-step coupling SPPS has limitations. Even though it is ideal for small peptides containing AA from 2 to 100, it is difficult to synthesize even longer peptide sequence. For longer peptide sequences, the methods developed are chemical ligations, such as native chemical ligation (NCL), Ser/Thr ligation (STL), α-Ketoacid-Hydroxylamine (KAHA) Amide-Forming Ligation. In solution phase, unprotected peptide chain reacts chemo selectively with each other. For example, in NCL, a peptide thioester would selectively react with an N-terminal cysteine peptide sequence.

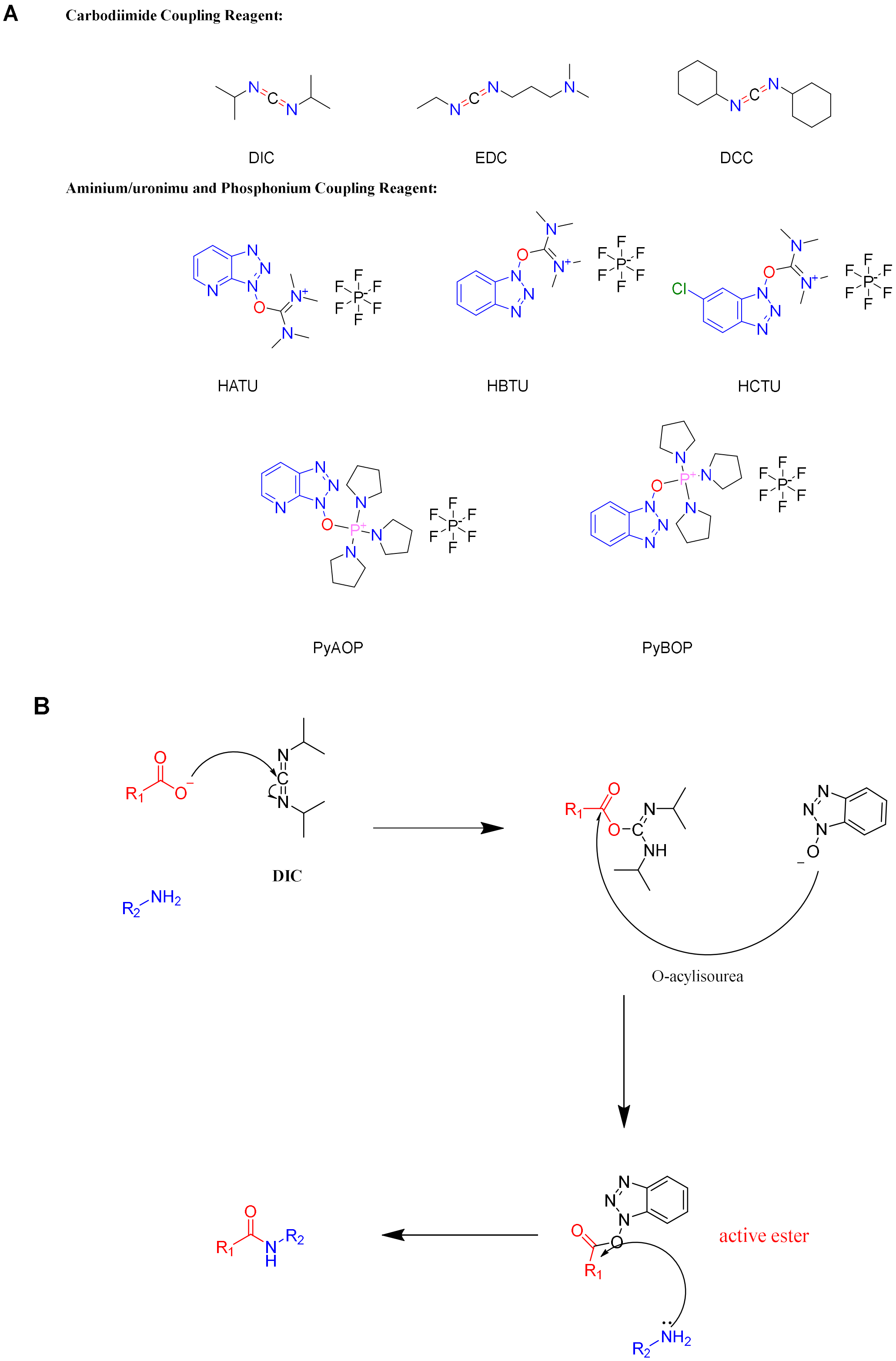
A
Carbodiimide Coupling Reagent:
DIC
EDC
DCC
Aminium/uronimu and Phosphonium Coupling Reagent:
HATU
HBTU
HCTU
PyAOP
PyBOP
B
DIC
O-acylisourea
active ester

Figure 4.2. Coupling reagents and mechanism. A: Different Types of Coupling Reagents. B: Carbodiimide Reagent Coupling Mechanism.

Bases for SPPS:

DIPEA

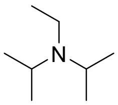

Pyridine

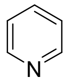

NMM

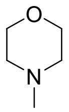

DMAP

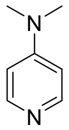

TEA

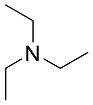

TMP

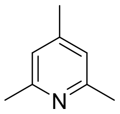

2,3,5,6-tetramethyl pyridine

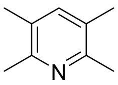

DB(DMAP)

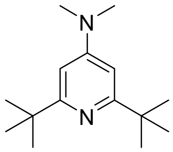

Additives for Coupling

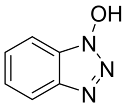

HOBt

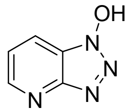

HOAt

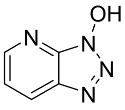

4-HOAt

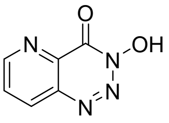

HOOBt

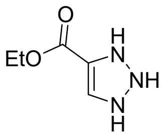

HOCt

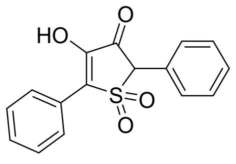

TDO

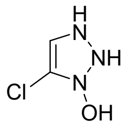

5-Chloro-1-hydroxtriazole

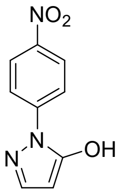

HOHpp

Figure 4.3. Base and additives for coupling.

4.1.3. Resins in Fmoc-SPPS

Resin Core: Polystyrene is most often used resin core in SPPS, but other core matrices are also used in special synthesis, including polyacrylate, polyacrylamide, polyethylene glycol.[59] These other core resins are utilized in some special peptide synthesis, such as preparing some peptides that are prone to aggregate.

Linear polystyrene tends to dissolve in hydrophobic solvents, but precipitate in protic solvents. Usually, polystyrene supports used in SPPS contain 1-2% DVB as crosslinking agent. Crosslinked polystyrene is insoluble in common solvents; thus, it is normally prepared and used as small, spherical beads.

Polystyrene

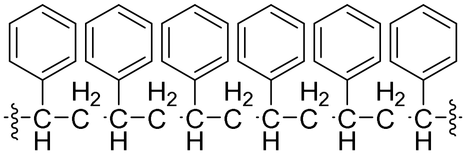

Figure 4.4. Structure of Polystyrene

Amino Core Resins: Aminomethyl (AM) has long been used as core resin in SPPS.[60] At first, 4-Methylbenzhydryl amine resins (MBHA) were developed for the formation of peptide bond in Boc-N protection/TFA deprotection. Generally, carboxylic acids and electrophilic alkyl substrates would form very stable amide or amine bonds. To cleave product, strong acid is required, such as high concentration of TFA. At the same time, it can also be used as base resin to anchor acid labile linkers such as Rink Amide linker.[61] These resins are generated via electrophilic aromatic substitution (EAS), and the efficiency of EAS is hard to control. Consequently, despite optimized protocols, the qualities of AM resins vary in different batches.

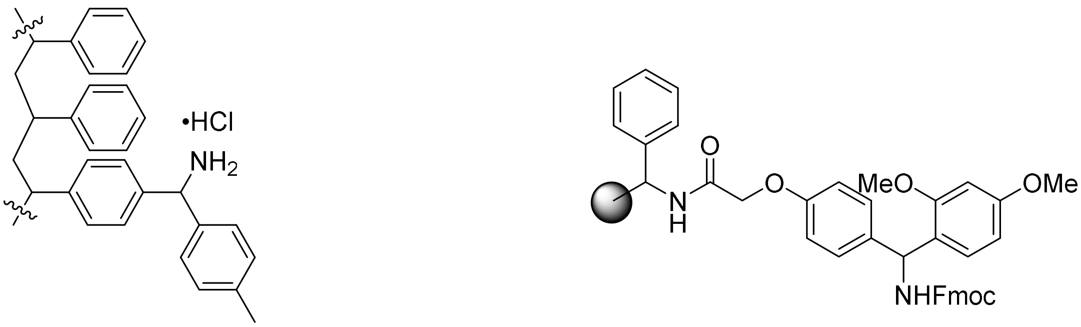

MBHA resin HCl

Fmoc-Rink Amide MBHA Resin

Figure 4.5. Structure of AM resin

Merrifield Resin: Merrifield resin was named after the Noble Laureate who first used it in peptide synthesis, the structure is chloromethyl polystyrene.[53] Linkers are attached to Merrifield Resin by nucleophilic attack replacing the original chloride. The resulting new bond is usually acid stable and requires strong acid for cleavage. However, carboxylic acid is not easily freed from Merrifield resin using acid cleavage cocktail. Instead, other cleavage methods including saponification, transesterification, and cyclization-release have proven effective.[62-65] Merrifield resin is usually generated by two methods: direct incorporation via EAS or substituted monomer co-polymerized with styrene. Overall, substituted resins are generated by substrate direct incorporation which leads to isomers. For instance, 70% of Merrifield resin are para-chloromethyl substituted, the other 30% resin are meta-substituted. Conversely, by using pure monomer, co-polymerization can prepare 98% para substituted resin. In addition, it can control the degree of resin substitution by changing the ratio of styrene and substituted monomer (Figure 4.6).

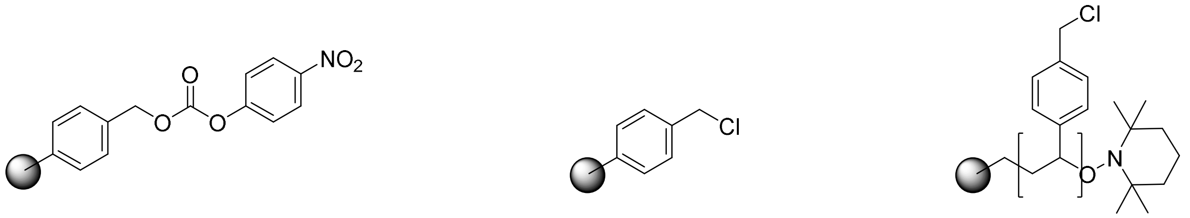

p-Nitrophenyl carbonate Merrifield resin   Merrifield resin HL   Merrifield's peptide resin

Figure 4.6. Different kinds of Merrifield resin

Swelling Factor of Resin: Even though resins are insoluble in organic solvents, they can be swollen by aprotic solvents such as toluene, dimethylformamide (DMF), and dichloromethane (DCM) (Table 4.1.). For example, one gram of 1% of divinylbenzene (DVB) cross-linked resin swells 4-6 times as its original volume in DCM. In comparison, one gram of 2% DVB cross-linked resin swells 2-4 times in DCM. Since the reaction kinetics depends on diffusion, the swelling factor matters in SPPS. Consequently, well-swollen beads have a shorter reaction time and better product conversion since it has a higher rate of reagents diffusing into the core part of matrix.

Table 4.1. Swelling factor of 1% cross-linked polystyrene resins in different solvents.

THF	5.5	Acetonitrile	3.5
Toluene	5.3	Et_2O	3.2
DCM	5.2	EtOH	2.0
Dioxane	4.9	MeOH	1.8
DMF	4.7	H_2O	1.0 (no swelling)

4.1.4. Cleavage Cocktails

The linker is where the C-terminal amino acid attaches, and there is a wide range of commercially available linkers for different polymeric supports. Actually, the selected cleavage cocktail depends on the linker.

Low concentrations of TFA: With a XAL ("Seiber") or HAL linkers, synthesized peptides are cleaved in low concentration of TFA to get fully protected peptide amides or peptide acid respectively.

High concentration of TFA: With a PAC ("Wang"), PAL, AM ("Rink Amide"), or BAL linker, synthesized peptides are cleaved in high concentration of TFA to get fully-deprotected product (Table 4.2.).

Table 4.2. High Concentration of TFA Fmoc-SPPS Cleavage Cocktail.

	Recipe	Time (h)	Comments
B	TFA/water/phenol/TIPS (88/5/5/2)	1-4	All peptides
K	TFA/phenol/water/thioanisole/EDC (82.5/5/5/5/2.5)	1-4	All peptides
K'	TFA/phenol/water/thioanisole/ 1-dodecanethiol (82.5/5/5/5/2.5)	1-4	All peptides
L	TFA/DTT/Water/TIPS (88/5/5/2)	1-4	All peptides
P	TFA/phenol (95/5)	1-4	tBu group. Do not use with Trp, Met or Cys.
P'	TFA/phenol/Methanesulfonic acis (95/2.5/2.5)	15 min	All peptides
R	TFA/thioanisole/EDT/Anisole (90/5/3/2)	1-8	All peptides
T	TFA/TES (95/5)	1-4	Boc, tBu, Trt. Do not used with Arg or Trp
	TFA/water (95/5)	1-4	Boc, tBu, Trt, Pbf. Do not used with Trp, Met or Cys
	TFA/DCM/indole (70/28/2)	1-4	Do not use with Arg.

Both cleavage cocktails should be prepared fresh before using. Scavengers should also be fresh. Try to buy TFA, and scavengers in small quantities, and discard any long unused scavengers.

4.1.5. HPLC Analysis and Purification

HPLC is the most powerful and convenient tool to analyze and purify peptides. Following is the suggested guidelines:

1. With an unknown peptide, usually, a C-18 reversed phase column is recommended for medium-sized peptides that are moderately hydrophilic.

   Use the following protocol for a standard analytical column:

   Buffer A: 0.1% TFA in H_2O.

   Buffer B: 0.1% TFA in ACN.

   Flow rate: 1-1.5ml/min

   Gradient: 0-90% B in 90min.

2. For peptides with 20-40 amino acids, medium-sized peptides, C-8, C-4 or a polymeric reversed phase column are recommended. These peptides are expected to elute at a high percentage of CAN, and it is safe to start with a high percentage of 10-20% B.
3. Long peptides, or those having many similarly charged groups, may best be purified by either polymeric reversed phase or aqueous ion exchange columns.
4. Peptides containing aromatic side chain, such as Tyr, Phe, or Trp, can be monitored at 240-260 nm, due to characteristic absorbance of aromatic ring. Otherwise, monitor at 210-214 nm, this is close to the wavelength of peptide bond.
5. If DMF is used to help dissolve the peptide, you will see a large peak at the beginning. If peptide is small and eluted early, use low percentage of B to separate peptide from DMF.

4.2. Introduction

With Wnt ligand, the canonical Wnt pathway causes accumulation of β-catenin in cell cytoplasm, next, it is translocated to nucleus and form a complex with BCL 9, PYGO, TCF/LEF to activate Wnt target gene transcription. Previous research demonstrated that BCL 9 amplification was related to several human cancers and other diseases, such as breast cancer, prostate cancer, type 2 diabetes and others.[66] It is also associated with tumor progression, low survival rate and not ideal clinical outcomes. Furthermore, an enhanced level of β catenin can increase cell proliferation, migration invasion, and tumor metastasis.[67] Without Wnt ligand binding, adenomatous polyposis coli (APC) and glycogen synthase kinase 3β (GSK3β) bind to β-catenin, after several cycles of phosphorylation and ubiquitination, it is degraded by proteasome.[68]

Proteolysis Targeting Chimera is a strong modality tool to degrade intracellular or nuclear protein of interest. It provides a new way to solve the drug resistance problem of small molecular inhibitors. The PROTAC molecules consists of three parts: E_3 ligand, linker, and targeting protein bind ligand. After recruiting E_3 ligase to targeting protein, they form a tertiary complex and E_3 ligase ubiquitinates the target protein several times, then recognized and degraded by proteosome.[69] PROTAC molecules can be used to target undruggable protein, as only a tight binder is required for the target protein.[70] Furthermore, PROTAC molecules is also a great tool to validate the targets and gather more information about protein functions and signaling pathways. Compared with nucleotide-based methods like oligonucleotides, RNAi or genome editing methods that have limited applications due to their stability *in vivo* and *in vitro*. Most PROTAC molecules are developed from small molecule bind ligand, usually their molecular weights are not more than 1500 Da. As a result, they possess the advantages of small molecules, such as, good membrane permeability, *in vivo* stability, target specific and economic synthesis.[71] These make PROTAC molecules can enter cell and rapidly delete target proteins efficiently. It has been 20 years since the first research paper about PROTAC molecule been published. Now, this technology is translocated from academic to industry. As a new area of drug discovery, PROTAC strategies are successfully applied to degrade different proteins *in vitro* and *in vivo,* including estrogen receptor (ER),[72] androgen receptor (AR), Kirsten rat sarcoma virus (KRAS) G12C mutation,[73] Bromodomain-containing protein 9 (BRD 9),[74] Signal transducer and activator of transcription 5 (STAT5),[75] Cyclin-dependent kinase 9 (CDK 9)[76], etc. Many biotech startups and companies build their own PROTAC pipelines and several PROTAC molecules have entered clinical trials. For example, ARV-110 and ARV-471 entered clinical trials in 2019, they provided the first clinical proof-of-concept for well-established tumor modality with PROTAC molecules. [77] In contrast to small molecule PROTAC, there are not so researches about peptidyl PROTAC (p-PROTAC) (Table 4.3.). The main challenges p-PROTAC face are poor cell permeability and low stability. However, p-PROTAC also has several advantages. First, it can be used to target some undruggable proteins with large shallow surfaces. Second, it has fewer side effects and is safer. [78] For instance, previously published protein binding ligand and E_3 recruiting ligand were endogenous peptides with high specificity and affinity. Those endogenous ligands compared with exogenous small molecular inhibitors and antibodies are ideal choices for drug development.[78]

Table 4.3. Comparison of p-PROTAC and small molecule PROTAC.

	Peptide-PROTAC	**Small molecule PROTAC**
Targeting warhead	Peptides	Small molecules
Advantages	Specific targeting “undruggable” POI with specificity Resistance to target mutation Not labor intensive Low toxicity and high safety *in vivo*	Higher cellular permeability Better stability Cost effective
Disadvantages	Poor cell membrane permeability Lower stability Few research on their efficacy	Limitation of degradation of “undruggable” protein Inability to target “undruggable” shallow surface protein Toxic side effects
Clinical trials	NA	ARV-110, ARV-471, NX-2127

In 2019, Dr. Cai’s lab reported several sulfonyl γ-AA peptides that could effectively inhibit the protein-protein interaction (PPI) between BCL 9 and β-catenin.[79] Sulfonyl γ-AA peptides can mimic the secondary structure of natural helix. Owing to its unnatural amino acids and secondary helix structure, it shows better cell permeability and is resistant to enzyme degradation. We had a question: Can we degrade β-catenin using our sulfonyl γ-AA peptides?

4.3. Design

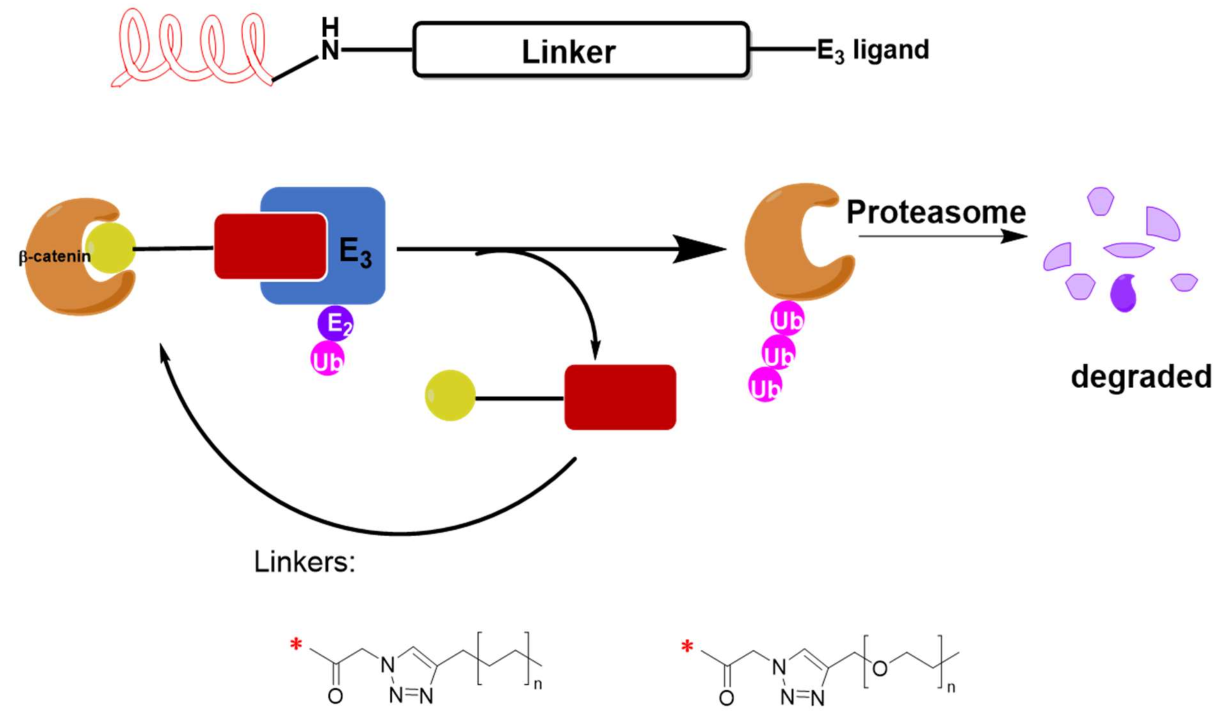
H
N
Linker
E_3 ligand
β-catenin
E_3
E_2
Ub
Proteasome
Ub
Ub
Ub
degraded
Linkers:
*
N
N=N
O
n
*
N
N=N
O
O
n

Figure 4.7. Design of Sulfono-γ-AApeptide PROTAC.

For our sulfonyl γ-AA p-PROTAC design, at one end, we put our sulfonyl γ-AA peptide helix and at the other end, put E_3 ligand linked by click reaction. At first, we chose sequence 2 from the paper since it showed a good binding affinity. For E_3 ligands, we tried VHL and phenyl glutarimide (PG).

4.4. Synthesis

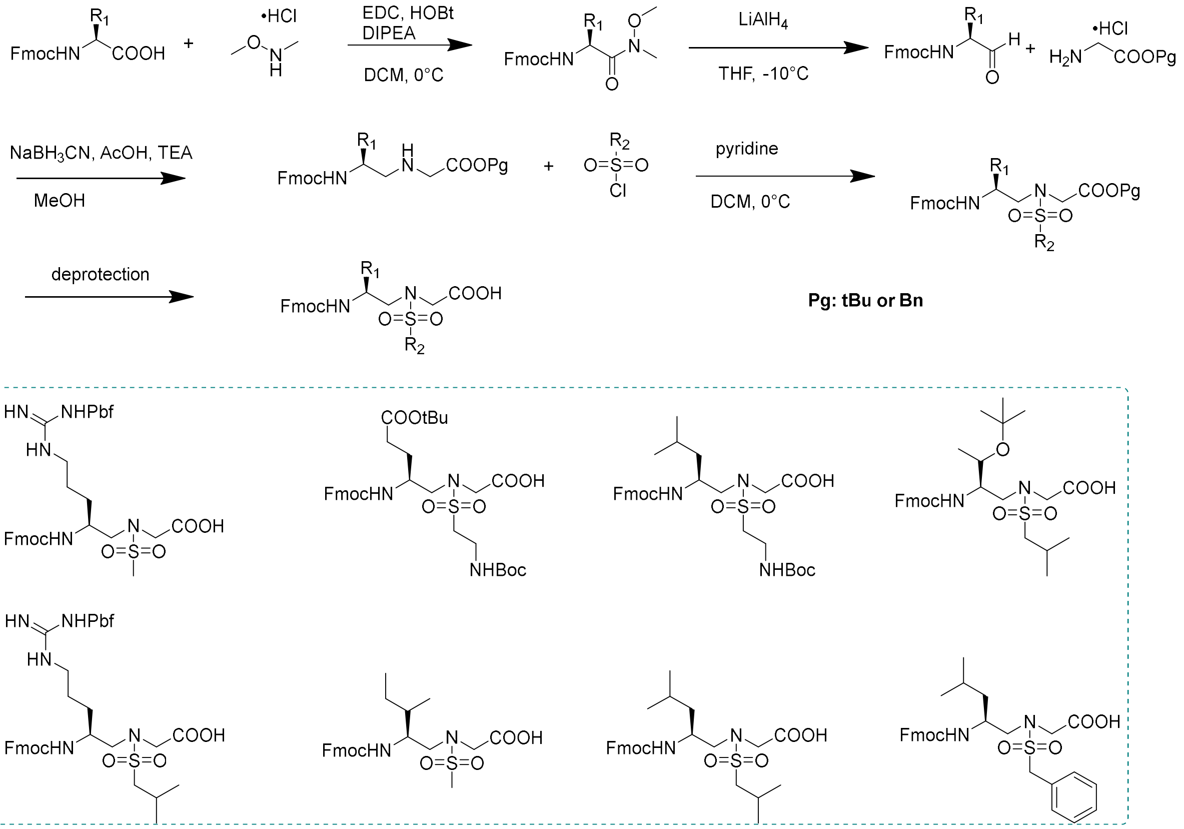
EDC, HOBt
DIPEA
DCM, 0°C
LiAlH4
THF, -10°C
NaBH3CN, AcOH, TEA
MeOH
pyridine
DCM, 0°C
deprotection
Pg: tBu or Bn

Figure 4.8. Building preparation.

4.4.1. Building Preparation

BB$_1$ Preparation:

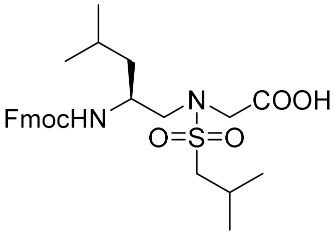

Step 1:

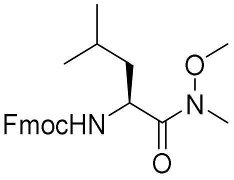

10g Fmoc-Leu-OH (28.3 mmol, 1eq), EDC (34.0 mmol, 1.2eq), HOBt (34.0 mmol, 1.2eq) and N, N-diisopropylethylamine (DIPEA, 62.3 mmol, 2.2eq) were dissolved in DCM under 0°C. After 5 min, 3.3g of N, O-dimethlyhydroxyamine (34.0 mmol, 1.2eq) was added. The reaction solution was stirred for 2 h.

Work-up: After 2 h, DCM was removed under reduced pressure. Then 1M HCl solution was added to remove unreacted starting material and excessive EDC. The aqueous was extracted with EA two times, combined organic layers and washed with Brine, dried with Na_2SO_4. Then, EA was filtered with cotton, and removed under reduced pressure. The left oil is used for the next step without any further purification.

Step 2:

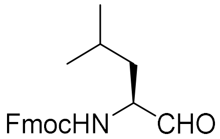

The first step product was dissolved in THF under sodium chloride and ice mixture (temperature between -15°C - -10°C). After cooling down for 10 min, 1.3g of Lithiumaluminumhydride (34 mmol, 1.2eq) was added in three portions. Then, the reaction was stirred for 30 min.

Work-up: Excessive 1M HCl was poured to quench reaction. Next, the aqueous layer was extracted with EA times. Combine organic layer and washed with Brine, then dried by Na_2SO_4. Then, EA was evaporated under reduced pressure. The left residue is used for the next step without any further purification.

Step 3:

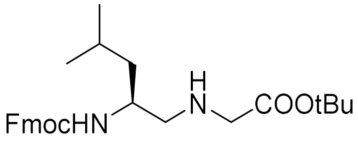

The previous step product was dissolved in MeOH under 0°C, then 5.1g of tert-butyl glycinate (28.3 mmol, 1eq) was added, followed by 2.8g of TEA (28.3 mmol, 1eq). The reaction mixture was stirred for 10 min. Next, 3.5g of $NaBH_3CN$ (56.3 mmol, 2eq) and 1.7g of AcOH (28.3 mmol, 1eq) were added. The reaction was stirred for 2 h.

Work-up: MeOH was evaporated under reduced pressure, then saturated $NaHCO_3$ was poured into the left solid to quench the reaction. The aqueous layer was extracted with EA times, combine organic layer and washed with brine, dried with Na_2SO_4. The EA layer was filtered through cotton to remove Na_2SO_4, then EA was removed under reduced pressure. The left residue was purified by column chromatography, using HEX: EA=2:1 to get final product.

Step 4:

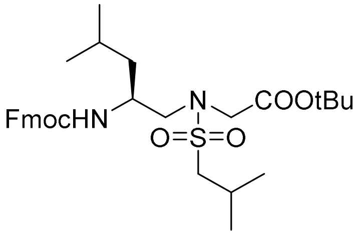

The step 3 product was dissolved in DCM under 0°C, then 1.2eq of 2-methylpropanesulfonyl chloride and 10 eq of pyridine were added. The reaction mixture was stirred overnight.

Work-up: DCM was evaporated under reduced pressure, followed by adding excessive 1M HCl. The aqueous layer was extracted with EA two times, combine EA, washed by Brine, and dried by anhydrous Na_2SO_4. The EA was filtered through cotton, then evaporated under reduced pressure. The left oil was purified by column chromatography, using HEX: EA=4:1 to get product.

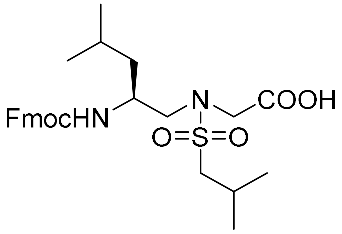

The step 4 product was dissolved in DCM: TFA=1:1 and stirred for 2h under R.T..

Work-up: The reaction solvent was evaporated under reduced pressure, then co-evaporated with hex 4 times to totally remove TFA. The left oil was purified by column chromatography, using HEX: EA=1:1 to get final product.

BB_2 Preparation:

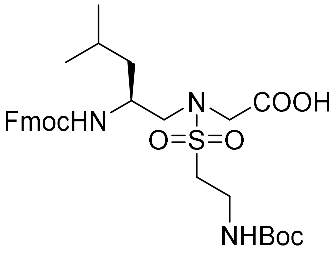

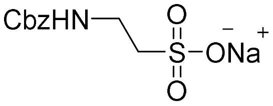

Taurine (1eq) was dissolved in a mixture of dioxane and H_2O, followed by 1 eq of CbzCl and 2 eq of NaOH. The reaction mixture was stirred overnight.

Work-up: Dioxane was evaporated under reduced pressure, then the aqueous layer was extracted with EA two times to remove unreacted CbzCl. Keep the aqueous layer, and co-evaporated with toluene to remove water several times. When the white solid precipitated, it can be used for the next step without any further purification, sodium 2-((benzyloxy)carbonyl) amino) ethane-1-sulfonate.

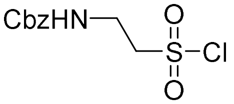

The previous step product, sodium 2-(benzyloxy)carbonyl) amino) ethane-1-sulfonate, was added with SO_2Cl_2 slowly. Then the reaction mixture was refluxed under 85°C for 4 h.

Work-up: The reaction mixture was cooled down to R.T., then SO_2Cl_2 was removed under reduced pressure. The left residue was co-evaporated with DCM for 4 time to totally remove SO_2Cl_2, then purified by column chromatography, using HEX: EA=2:1 to get product, benzyl (2-(chlorosulfonyl)ethyl) carbamate.

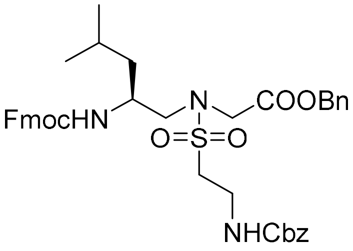

Benzyl (S)-(2-((((9H-fluoren-9-yl) methoxy) carbonyl) amino)-4-methylpentyl) glycinate was prepared using the same method as BB_1, then it was dissolved in DCM and cooled down to 0°C. Next, 10 eq of pyridine and 1.2 eq of benzyl (2-(chlorosulfonyl)ethyl) carbamate to reaction solution. The reaction mixture was stirred under R.T. overnight.

Work-up: DCM was removed under reduced pressure, then EA and 1M HCl were added. Then, the aqueous layer was extracted with EA for another time. Combine EA, washed with Brine and dried with Na_2SO_4. Next, EA was removed under reduced pressure. The left residue was purified by column chromatography, using HEX: EA=4:1 to get product, benzyl (S)-N-(2-((((9H-fluoren-9-yl) methoxy) carbonyl)amino)-4-methylpentyl)-N-((2-(((benzyloxy)carbonyl)amino)ethyl)sulfonyl)glycinate.

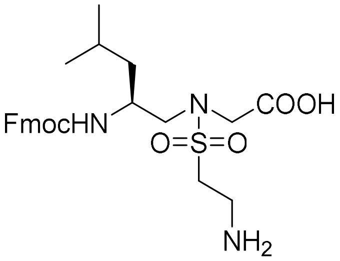

The previous step product was dissolved in a mixture of EA: MeOH=1:1, then catalytic amount (5%-10%) of Pd/C was added. The reaction ran under H_2 environment overnight. Next, the reaction was monitored by TCL. Usually, it takes three times for the reaction to be completely done.

Work-up: The reaction solution was filtered through celite, evaporated under reduced pressure. The left oil is used for the next step without any further purification, (S)-N-(2-(((9H-fluoren-9-yl) methoxy) carbonyl) amino)-4-methylpentyl)-N-((2-aminoethyl) sulfonyl) glycine.

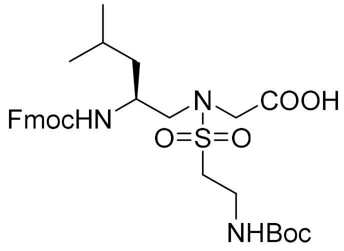

The previous step product, (S)-N-(2-((9H-fluoren-9-yl) methoxy) carbonyl) amino)-4-methylpentyl)-N-((2-aminoethyl) sulfonyl) glycine, was dissolved in THF and H_2O. Then, 3 eq of $NaHCO_3$ was added to adjust pH to basic, checked by pH paper around 9, followed by adding 1.5 eq of $(Boc)_2O$. The reaction mixture was stirred under 0°C overnight. Next day, the reaction was monitored by TLC, if the reaction is not done, add another 1 eq of $(Boc)_2O$ and 1 eq of $NaHCO_3$. Work-up: THF was removed under reduced pressure, then 1M HCl was added to turn the pH of the aqueous to acidic. Then, the aqueous was extracted with EA for two times. Combine the EA, washed with Brine, and dried with Na_2SO_4. Next, EA was removed under reduced pressure. The left residue was purified by column chromatography, using HEX: EA=1:1 to get final BB_2.

BB_3 Preparation:

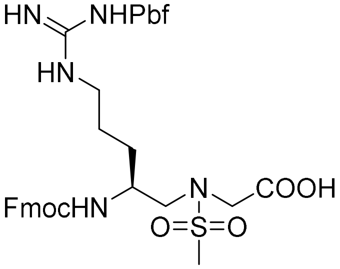

The preparation of BB_3 uses the same strategy as previous BB_1 and BB_2 preparation. However, we need to pay attention to the second step. For other natural AA, it is fine under $LiAlH_4$, arginine was easy to be reduced under this strong reducing reagent. In arginine BB preparation, the $LiAlH_4$ reduction step should be less than 12min, if exceeding 20min, the final yield is very low.

4.4.2. Fmoc-SPPS synthesis

The Rink amide beads were sink in DCM to swell for 10 min. Then, 20% percent of piperidine in DMF was used to deprotect Fmoc protecting group. Next, the first building block was coupled with HOBt (4eq), DIC (2eq) in DMF for 4 h. Check reaction by ninhydrin test. When the reaction is done, continue coupling the next one building block until the sequence is finished. Lastly, couple the azidoacetic acid for a later click reaction or put a different length of linkers, then couple the PG E_3 ligand. After finishing all the coupling reaction, a cleavage cocktail containing 88% TFA, 5% phenol, 5% water, and 2% TIPS was used to cleave the product. Precipitated by cold ether, centrifuged, then purified by HPLC (Figure 4.9).

Sulfonyl p-PROTAC Synthesis

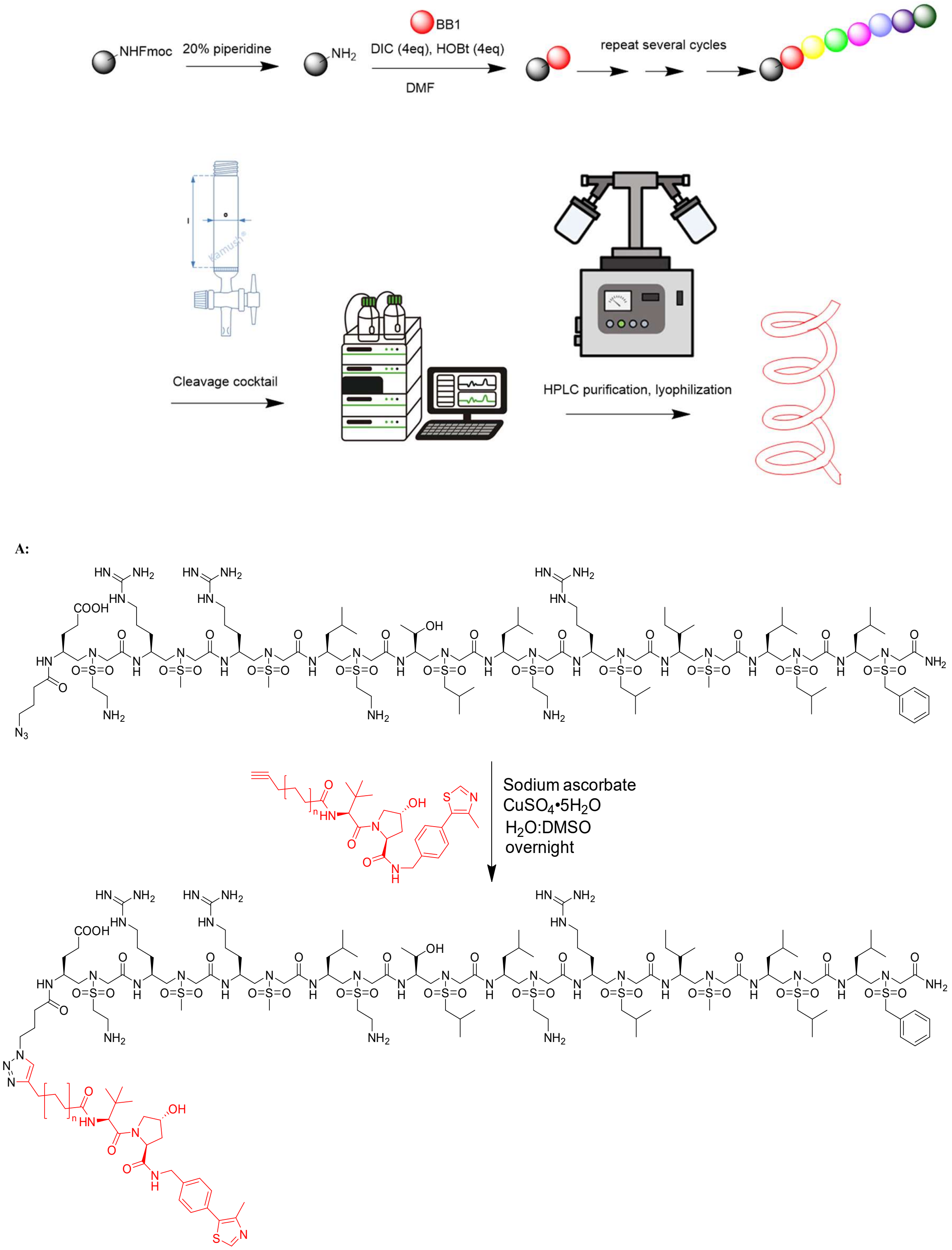
NHFmoc
20% piperidine
NH2
BB1
DIC (4eq), HOBt (4eq)
DMF
repeat several cycles
Cleavage cocktail
HPLC purification, lyophilization
A:
Sodium ascorbate
CuSO4•5H2O
H2O:DMSO
overnight

Figure 4.9. Synthesis procedure of Sulfono-γ-AApeptide PROTAC

B:

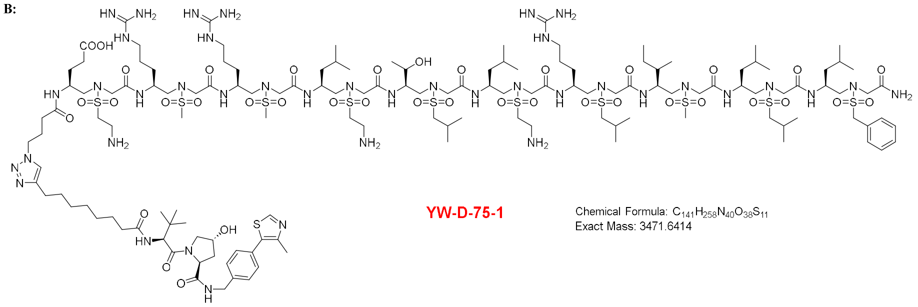

YW-D-75-1

Chemical Formula: $C_{141}H_{258}N_{40}O_{38}S_{11}$
Exact Mass: 3471.6414

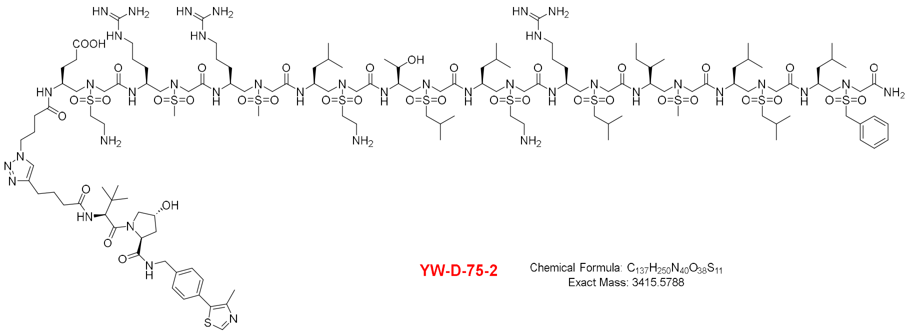

YW-D-75-2

Chemical Formula: $C_{137}H_{250}N_{40}O_{38}S_{11}$
Exact Mass: 3415.5788

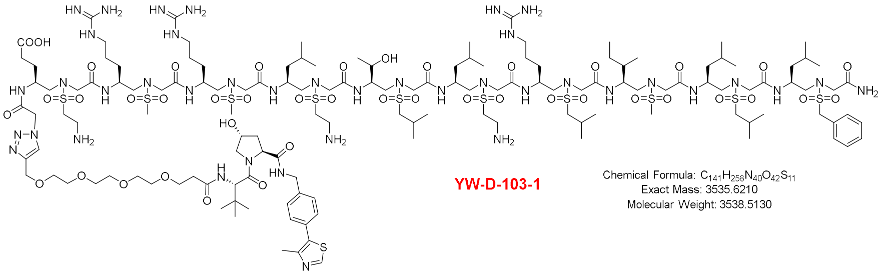

YW-D-103-1

Chemical Formula: $C_{141}H_{258}N_{40}O_{42}S_{11}$
Exact Mass: 3535.6210
Molecular Weight: 3538.5130

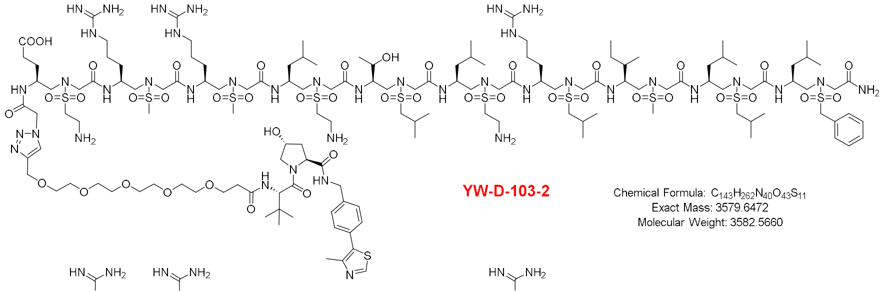

YW-D-103-2

Chemical Formula: $C_{143}H_{262}N_{40}O_{43}S_{11}$
Exact Mass: 3579.6472
Molecular Weight: 3582.5660

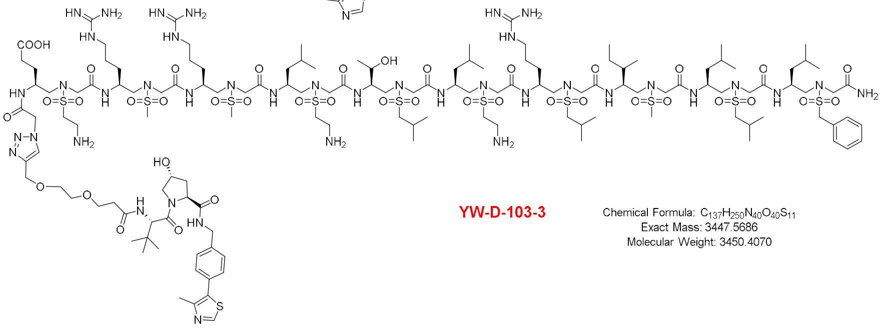

YW-D-103-3

Chemical Formula: $C_{137}H_{250}N_{40}O_{40}S_{11}$
Exact Mass: 3447.5686
Molecular Weight: 3450.4070

Figure 4.10. Synthesis design. A: Solution phase click reaction. B: Synthesis of different lengths of p-PROTAC.

Until now, five VHL sulfonyl p-PROTAC sequences are synthesized, our collaborator Dr. Chen at Moffit Cancer Center test their abilities to degrade β-catenin against U2OS and SW480 cells (Figure 4.11.).

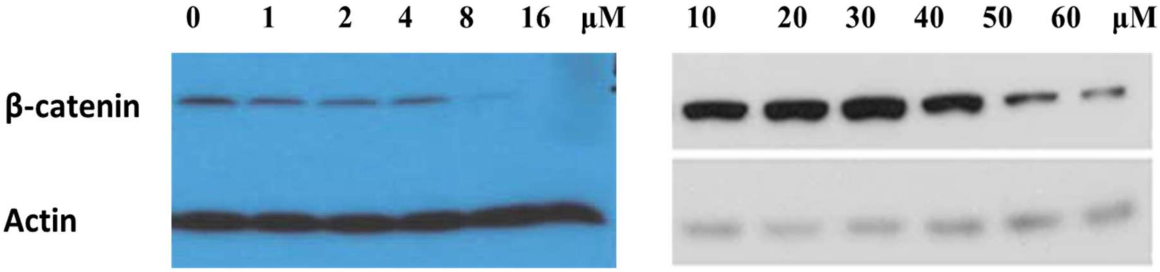

YW-D-103-2 xStAx-VHLL

Figure 4.11. WB data of YW-D-103-2 and previously reported xStAx-VHLL

At the first western blot experiment, we found that YW-D-103-2 could effectively degrade β-catenin at 8 uM (Figure). However, the repeat experiment was not consistent with the first time. Moreover, we found that p-PROTAC with VHL ligand showed cell toxicity, it not only degraded β-catenin but also degraded actin. As a result, we are trying to replace VHL with PG E_3 ligand since they recruit different E_3 Ligase.[77] By changing the E_3 ligand, we want to know whether the cell toxicity would disappear. The p-PROTAC with PG plan is undergoing, we finished the synthesis, and are waiting for our collaborator to test.

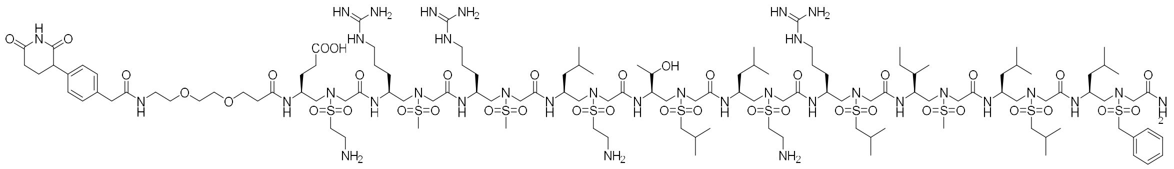

YW-D-117-1

Chemical Formula: $C_{125}H_{233}N_{35}O_{39}S_{10}$
Exact Mass: 3168.4532
Molecular Weight: 3171.0450

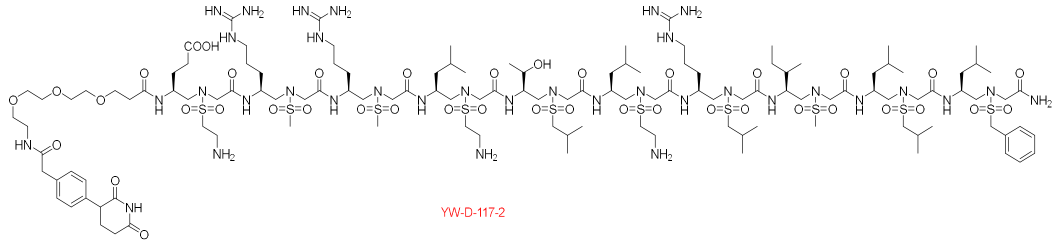

YW-D-117-2

Chemical Formula: $C_{127}H_{237}N_{35}O_{40}S_{10}$
Exact Mass: 3212.4794
Molecular Weight: 3215.0980

Figure 4.12. Structure of PG Sulfono-γ-AApeptide PROTAC.

CHAPTER FIVE: S597 PEPTIDOMIMETIC TO ACTIVATE INSULIN RECEPTOR

5.1. Background

Peptides are short sequences of amino acids linked by peptide bond. A polypeptide is a longer, continuous, unbranched peptide chain. Peptide sequences of not more than twenty amino acids are called oligopeptides, such as dipeptides, tripeptides, and tetrapeptides.[80] If the molecular weight of polypeptides exceeds 10000, they are called proteins. Proteins consist of one or more polypeptides, in biological functional pathway, they are bound to ligands such as coenzymes or cofactors. For example, proteins bind to DNA, RNA or another protein to form complex functional macromolecular assemblies.

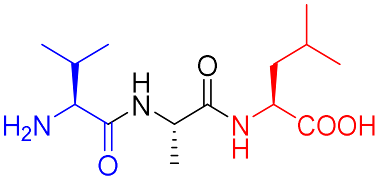

Figure 5.1. A tripeptide consists of Val, Ala, and Leu AA

Among proteins, an alpha helix is a sequence of amino acid in protein that twists into a helix. It is the most common secondary structure in proteins. It is also the most often appeared secondary structure in proteins that can be easily predicted with a sequence of amino acids. Naturally, the alpha helix has a right-handed conformation in which the N-H group of one amino acid in backbone forms a hydrogen bond to the C=O group that is four residues earlier, (*i+4-i*). Amino-acid propensities:Different amino acids have different propensities to form an α-helical structure. Alanine, leucine, methionine, lysine, and glutamic acid all have especially high helix-forming propensities; however, proline and glycine have poor helix-forming propensities. Proline either breaks or kinks a helix since it has tertiary amine instead of the N-H bond as a hydrogen bond acceptor. Furthermore, its side chain interfere sterically with the preceding backbone-inside a helix, this forces a 30° bend of the backbone. [81] For glycine, it has high conformation flexibility that entropy cost would be expensive to form α-helix structure.

Table 5.1. Table of L amino acids propensities to form α-helix: Difference in free energy change each amino acid.[82]

Amino acid	1-letter	Helical penalty	
		Kcal/mol	kJ/mol
Alanine	A	0.00	0.00
Arginine	R	0.21	0.88
Asparagine	N	0.65	2.72
Aspartate	D	0.69	2.89
Cysteine	C	0.68	2.85
Glutamate	E	0.40	1.67
Glutamine	Q	0.39	1.63
Glycine	G	1.00	4.18
Histidine	H	0.61	2.55
Isoleucine	I	0.41	1.72
Leucine	L	0.21	0.88
Lysine	K	0.26	1.09
Methionine	M	0.24	1.00
Phenylalanine	F	0.54	2.26
Proline	P	3.16	13.22
Serine	S	0.50	2.09
Threonine	T	0.66	2.76
Tryptophan	W	0.49	2.05
Tyrosine	Y	0.53	2.22
Valine	V	0.61	2.55

Estimated free energy change in kcal/mol within an α helical conformation. Relative to alanine set as zero. More positive numbers are not favored, it means more free energy changes. Depending on the detailed chemical environment, significant deviations from these standard numbers may happen.

5.2. Functional roles of α-helix

5.2.1. DNA binding

α-helices have particular importance in DNA binding motifs, including zinc-finger, leucine zipper, and helix-turn-helix motifs. Since the conventional structure diameter of an α-helix is about 12 Å (1.2nm), including the average length of AA side chains, about the same width of the major in B-form DNA. Furthermore, the coil-coil dimers of helices can position internation surfaces to the symmetrical repeat double-helical DNA.[83] For example, the double-helical DNA of transcription factor Max use a helical coil-coil to dimerize, position both helices to interact with two successive turns of DNA grove, (PDB: 1HLO).

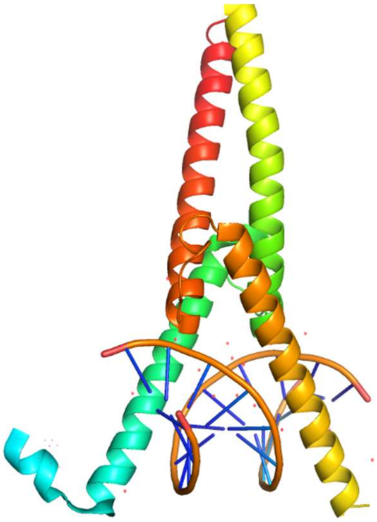

Figure 5.2. Transcriptional factor Max DNA binding with leucine zipper coil-coil(PDB:1HLO).

5.2.2. Membrane spanning

For transmembrane proteins, α-helices are the most common structures. Researchers presume that the helical structure can hide all hydrogen bonds internally, leaving no polar groups to membrane if the side chains of AA are nonpolar. Proteins are anchored to membrane by single transmembrane helix, sometimes by coil-coil helices, or by a helix bundle, in most occasions containing seven helices arranged in a ring, such as rhodopsins, (PDB: 1GZM).[83]

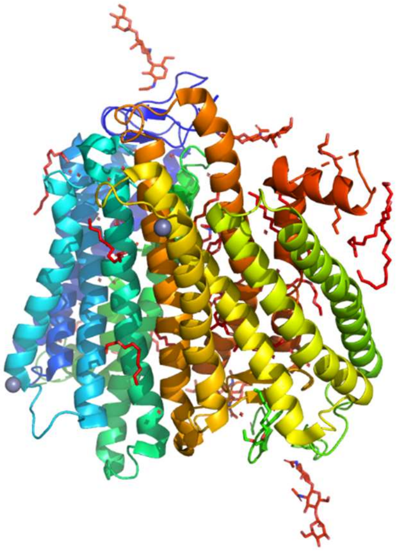

Figure 5.3. Structure of Bovine Rhodopsin in a Trigonal Crystal Form.

5.3. Unnatural helical peptide foldamers

Compared with unconventional peptide helical foldamers, conventional peptide helical foldamers have the disadvantages of easy loss of secondary helical structure, susceptibility to proteolytic degradation, and cell membrane penetration problem.[81, 82, 84] Since Seebach and Gellman independently reported helical structure of β-peptides, several classes of foldamers have been developed.[84-86] The advantages of unnatural peptide helical foldamers are that it can mimic the functions of natural peptide helices at same time overcome its limitations.

Recently, researchers developed several new types of helical peptide foldamers, such as β-peptides,[87] azapeptides,[88, 89] oligourea, peptoids,[89] α-aminoxy-peptides,[90] γ-peptides,[91] and sulfono-γ-AApeptides.[84] Since the unnatural peptide helical foldamers are composed of unnatural AA, thus, they have unique advantages over natural α-peptide helices, such as good *in-vivo* stability and bioavailability, improved selectivity and diversity.

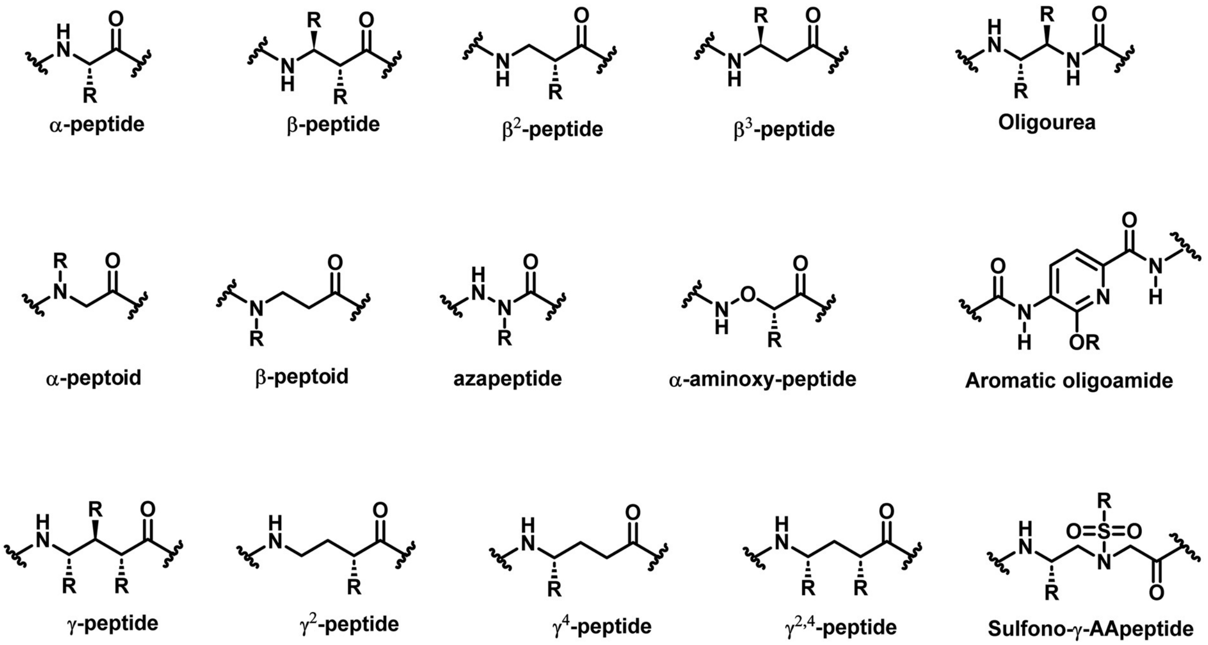
α-peptide
β-peptide
β^{2}-peptide
β^{3}-peptide
Oligourea
α-peptoid
β-peptoid
azapeptide
α-aminoxy-peptide
Aromatic oligoamide
γ-peptide
γ^{2}-peptide
γ^{4}-peptide
γ^{2,4}-peptide
Sulfono-γ-AApeptide

Figure 5.4. structure of α-peptide helical foldamer residues and unnatural helical foldamer residues.

5.4. Sulfono-γ-AApeptide

In 2015, our group developed a new type of helix using sulfono-γ-AA.[84] Sulfono-γ-AA are derivatives of natural AA, it is comparable to two natural AA in length, and have two side chains as dipeptide, one is from the side chain of canonical twenty natural amino acids, another is from the introduced natural or unnatural side chain of sulfonyl chloride. As a result, it provides great diversities of side chain since different sulfonyl chlorides are commercially available. Recently, we solved the crystal structure of homogeneous L-sulfono-γ-AApeptide foldamers (Figure 5.5.), it turned to be an unexpected left-handed 14-helix hydrogen bond pattern; furthermore, it has a helical pitch of 5.1 Å (versus 5.4 Å of α-helix), and the side chain aligned perfectly from top to bottom along the helical backbone. It showed both the intramolecular hydrogen bond and the curvature of sulfono-γ-AA helped stabilize the helical backbone.

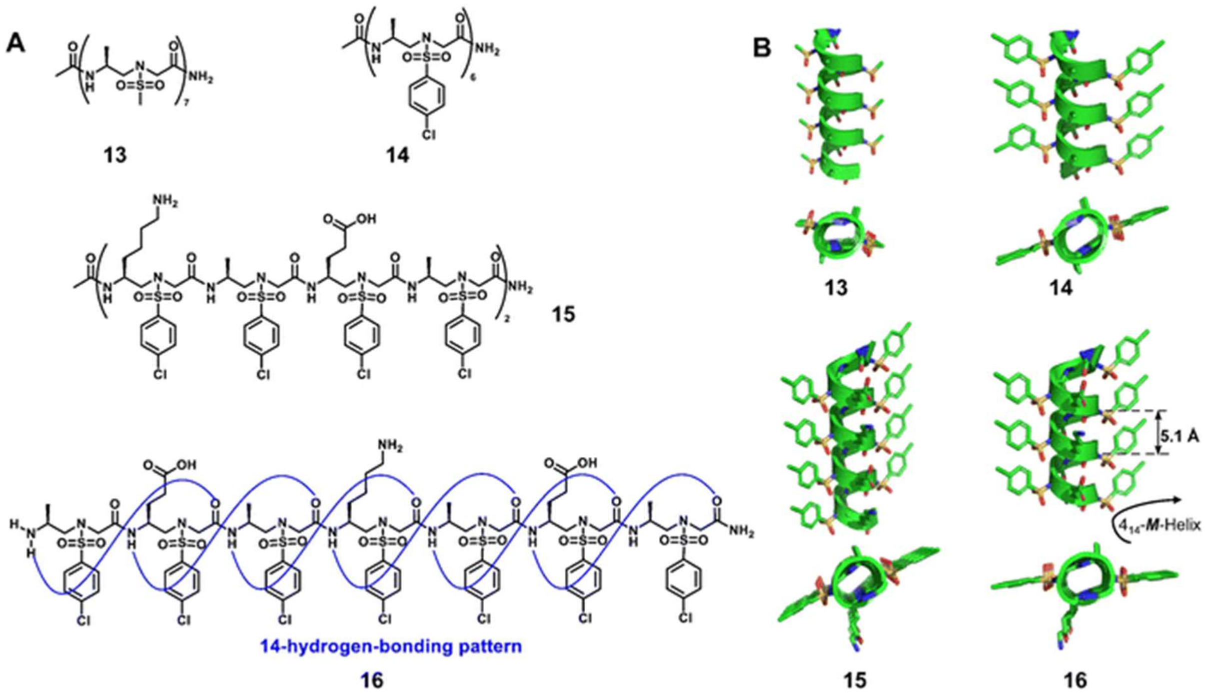

Figure: 5.5. Chemical structure of 13, 14, 15, 16. B: Crystal structure of 13, 14, 15, 16.

5.5. S597 insulin peptidomimetic

In 2007, Maja Jensen reported that S597 peptide leads to comparable level activation of protein kinase B (PKB) and glycogen synthesis to activation by insulin, even though the phosphorylation level in lower. However, Src homology 2/α collagen-related (Shc) and extracellular signal-regulated kinase (ERK) 2 were absent from activation by S597. It resulted in cell proliferation is only slightly stimulated by S597. It is the first time to possible design insulin receptor binding mimetics with metabolic equipotency but low mitogenicity.[92] In 2022, Junhee solved the crystal structure of S597 binding with insulin receptor.[93] Even though S597 activate insulin receptor (IR) and has comparable potency on glycemic control,, however, the binding mechanisms are different. IR is fully activated by four insulins to two distinct sites forming a compact T-shape, in contrast, two S597 molecules bind and form an extended T-shaped IR by simultaneously binding to both the L1 domain of one protomer and the FnIII-1 domain of another.

Moreover, S597 could activate IR mutants that were resistant to insulin and elicit insulin-like signaling.

S597 Peptide sequence:

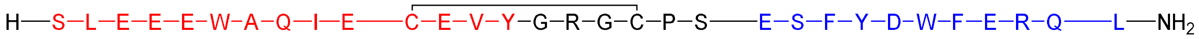
H—S—L—E—E—E—W—A—Q—I—E—C—E—V—Y—G—R—G—C—P—S—E—S—F—Y—D—W—F—E—R—Q—L—NH2

Figure 5.6. Sequence of S597.

In the future, researchers are going to evaluate whether insulin in combination with S597 could lower the insulin requirements in diabetes patients.

5.5.1. Design of S597 Sulfono-γ-AApeptide

In our first design (Figure 5.8.), we tried to replace the two helices of S597 with our sulfono-γ-AA peptide. Our sulfono-γ-AA are unnatural AA while main the same length of dipeptides, it is resistant to proteolytic degradation at same time show better cell permeability. By introducing a part of unnatural helix or replacing natural AA with unnatural AA, we guessed that it would improve analogues' stability and cell permeability, thus, might improve its potency and pharmacokinetics.

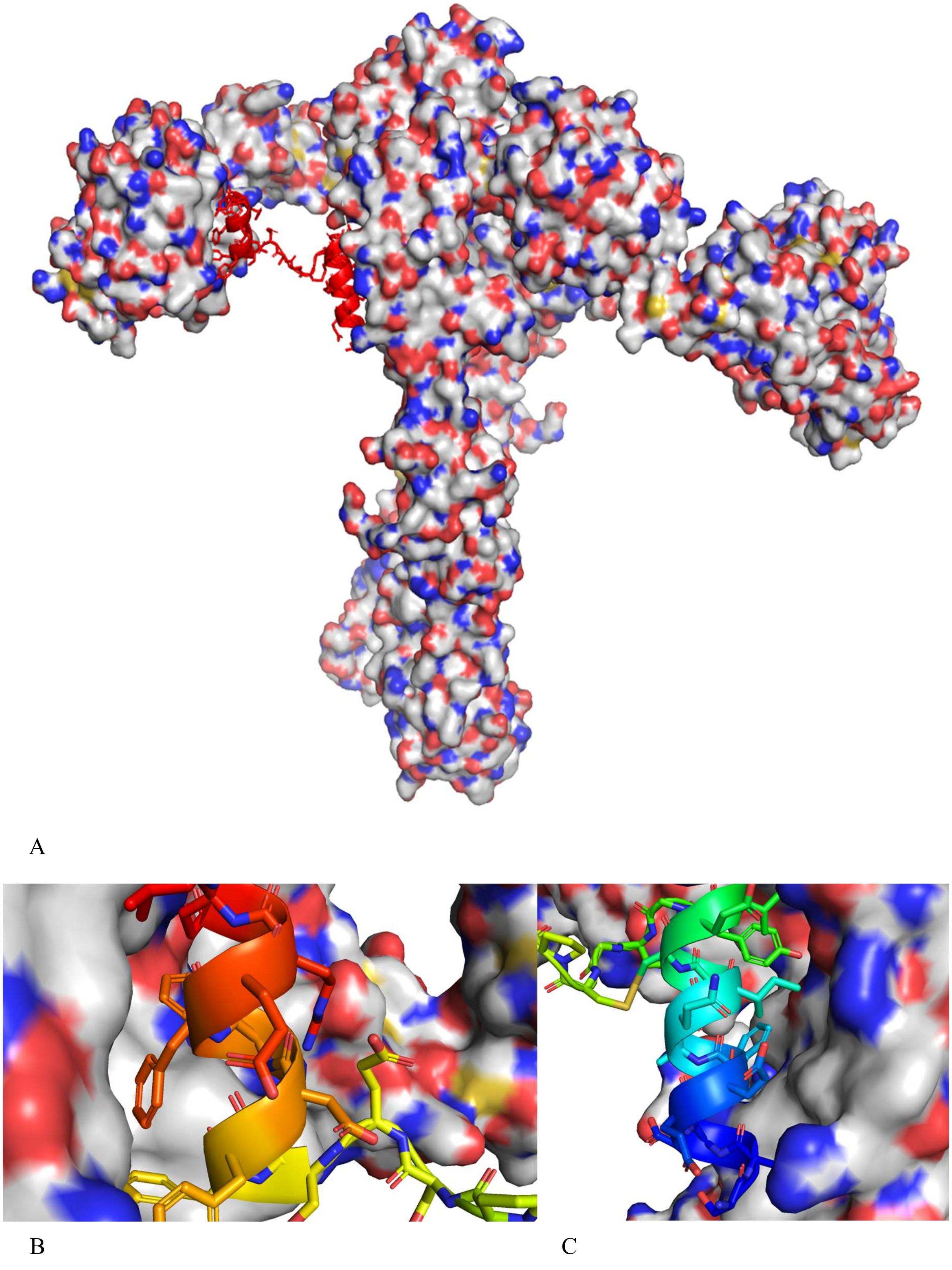

Figure 5.7. Crystal structure of S597 bind with IR (A), (PDB:8DTL), site 1(B) binding and site 2(C) binding.

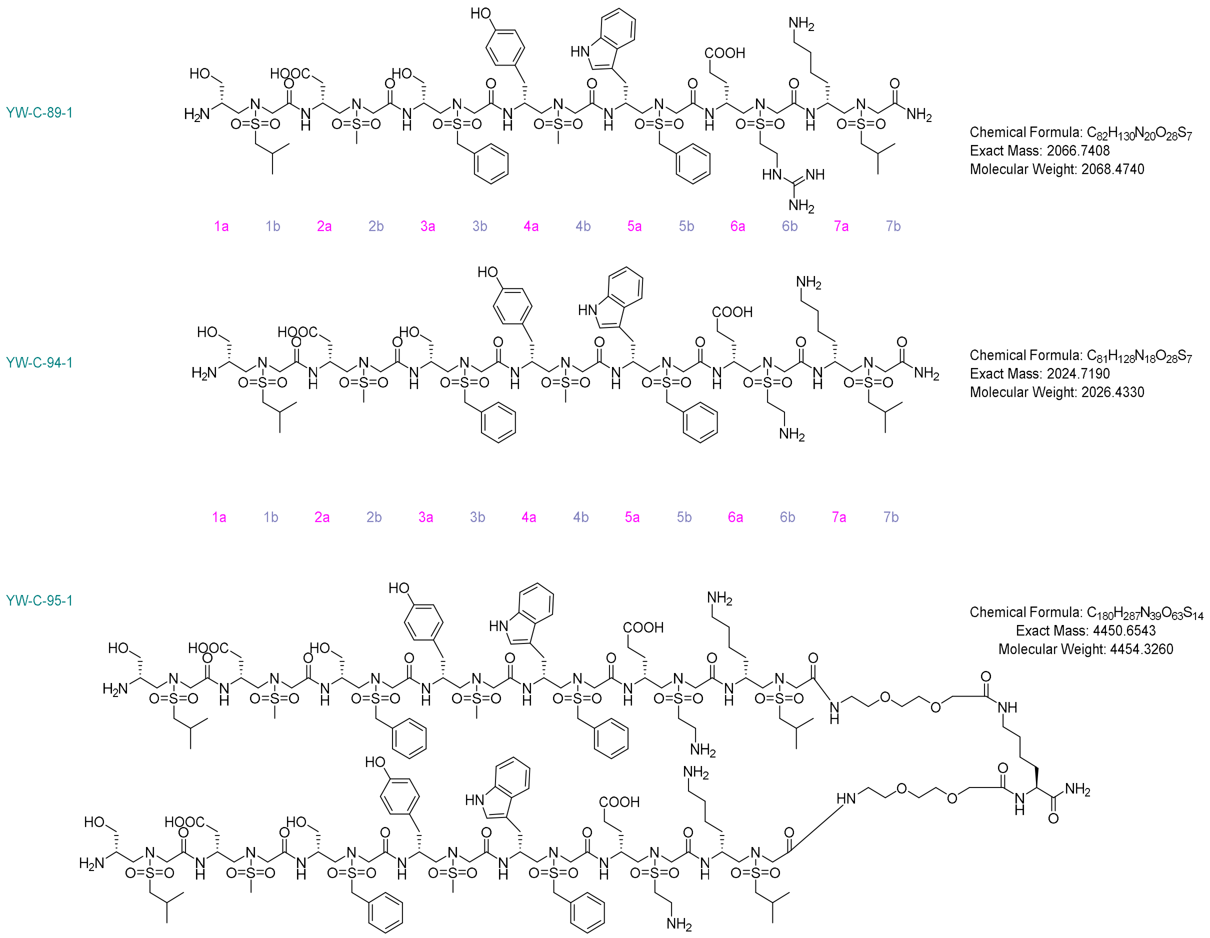
YW-C-89-1
Chemical Formula: $C_{82}H_{130}N_{20}O_{28}S_7$
Exact Mass: 2066.7408
Molecular Weight: 2068.4740
1a
1b
2a
2b
3a
3b
4a
4b
5a
5b
6a
6b
7a
7b
YW-C-94-1
Chemical Formula: $C_{81}H_{128}N_{18}O_{28}S_7$
Exact Mass: 2024.7190
Molecular Weight: 2026.4330
1a
1b
2a
2b
3a
3b
4a
4b
5a
5b
6a
6b
7a
7b
YW-C-95-1
Chemical Formula: $C_{180}H_{287}N_{39}O_{63}S_{14}$
Exact Mass: 4450.6543
Molecular Weight: 4454.3260

Figure 5.8. Structure of Site 1 sulfono-γ-AApeptide mimic, monomer and dimer.

First, we prepare several S597 sufono-γ-AApeptides. YW-C-89-1 and YW-C-94-1 are the site 1 mimetic of S597 peptide, YW-C-95-1 is the dimer of site 1 mimetic. Our collaborator tested whether it could activate insulin receptor, and the result was negative. Then, we proposed another strategy. Now, we are trying to replace several AA of S597 that don't show apparent interaction with insulin receptor. Using this strategy (Figure 5.9.), we got YW-D-109-1 and YW-D-109-2.

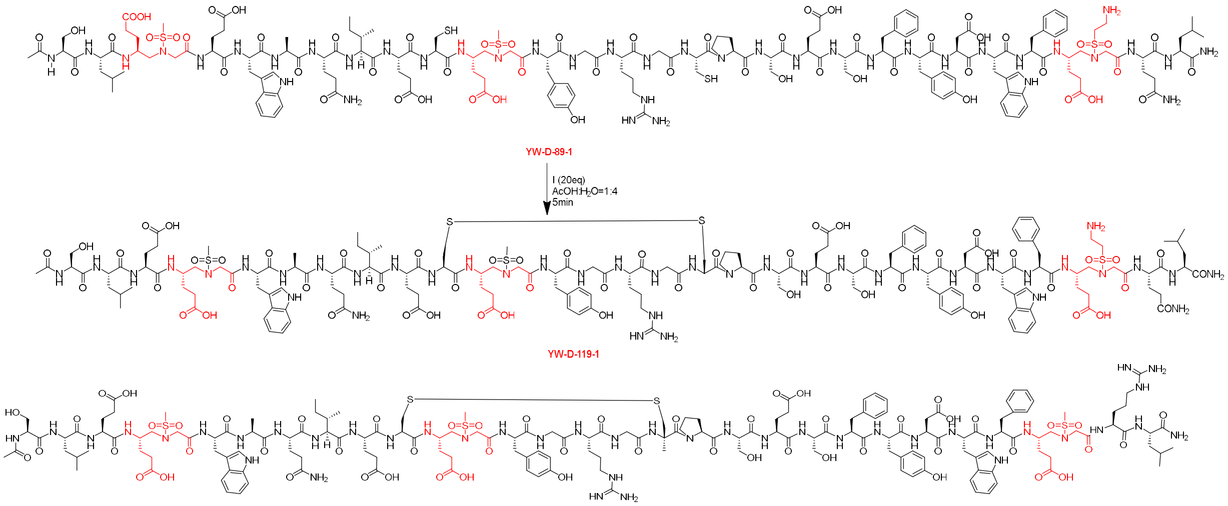
YW-D-89-1
I (20eq)
AcOH:H2O=1:4
5min
YW-D-119-1

Figure 5.9. Structure of site modification with Sulfono-γ-AA.

REFERENCES

(1) Thein, K. Z.; Velcheti, V.; Mooers, B. H. M.; Wu, J.; Subbiah, V. Precision therapy for RET-altered cancers with RET inhibitors. *Trends Cancer* 2021, *7* (12), 1074-1088. DOI: 10.1016/j.trecan.2021.07.003.

(2) Drilon, A.; Hu, Z. I.; Lai, G. G. Y.; Tan, D. S. W. Targeting RET-driven cancers: lessons from evolving preclinical and clinical landscapes. *Nat Rev Clin Oncol* 2018, *15* (3), 151-167. DOI: 10.1038/nrclinonc.2017.175.

(3) Hu, X.; Khatri, U.; Shen, T.; Wu, J. Progress and challenges in RET-targeted cancer therapy. *Front Med* 2023, *17* (2), 207-219. DOI: 10.1007/s11684-023-0985-y From NLM Medline.

(4) Huang, Q.; Schneeberger, V. E.; Luetteke, N.; Jin, C.; Afzal, R.; Budzevich, M. M.; Makanji, R. J.; Martinez, G. V.; Shen, T.; Zhao, L.; et al. Preclinical Modeling of KIF5B-RET Fusion Lung Adenocarcinoma. *Molecular cancer therapeutics* 2016, *15* (10), 2521-2529. DOI: 10.1158/1535-7163.MCT-16-0258.

(5) Subbiah, V.; Cassier, P. A.; Siena, S.; Garralda, E.; Paz-Ares, L.; Garrido, P.; Nadal, E.; Vuky, J.; Lopes, G.; Kalemkerian, G. P.; et al. Pan-cancer efficacy of pralsetinib in patients with RET fusion-positive solid tumors from the phase 1/2 ARROW trial. *Nat Med* 2022, *28* (8), 1640-1645. DOI: 10.1038/s41591-022-01931-y.

(6) Subbiah, V.; Wolf, J.; Konda, B.; Kang, H.; Spira, A.; Weiss, J.; Takeda, M.; Ohe, Y.; Khan, S.; Ohashi, K.; et al. Tumour-agnostic efficacy and safety of selpercatinib in patients with RET fusion-positive solid tumours other than lung or thyroid tumours (LIBRETTO-001): a phase 1/2, open-label, basket trial. *Lancet Oncol* 2022, *23* (10), 1261-1273. DOI: 10.1016/S1470-2045(22)00541-1.

(7) Liu, X.; Hu, X.; Shen, T.; LI, Q.; Mooers, B. H. M.; Wu, J. RET kinase alterations in targeted cancer therapy. *Cancer Drug Resist* 2020, *3*, 472-481, Review. DOI: http://dx.doi.org/10.20517/cdr.2020.15.

(8) Drilon, A.; Subbiah, V.; Gautschi, O.; Tomasini, P.; de Braud, F.; Solomon, B. J.; Shao-Weng Tan, D.; Alonso, G.; Wolf, J.; Park, K.; et al. Selpercatinib in Patients With RET Fusion-Positive Non-Small-Cell Lung Cancer: Updated Safety and Efficacy From the Registrational LIBRETTO-001 Phase I/II Trial. *Journal of clinical oncology : official journal of the American Society of Clinical Oncology* 2023, *41* (2), 385-394. DOI: 10.1200/JCO.22.00393.

(9) Gainor, J. F.; Curigliano, G.; Kim, D. W.; Lee, D. H.; Besse, B.; Baik, C. S.; Doebele, R. C.; Cassier, P. A.; Lopes, G.; Tan, D. S. W.; et al. Pralsetinib for RET fusion-positive non-small-cell lung cancer (ARROW): a multi-cohort, open-label, phase 1/2 study. Lancet Oncol 2021, 22 (7), 959-969. DOI: 10.1016/S1470-2045(21)00247-3.

(10) Subbiah, V.; Shen, T.; Terzyan, S. S.; Liu, X.; Hu, X.; Patel, K. P.; Hu, M.; Cabanillas, M.; Behrang, A.; Meric-Bernstam, F.; et al. Structural basis of acquired resistance to selpercatinib and pralsetinib mediated by non-gatekeeper RET mutations. *Ann Oncol* 2021, *32* (2), 261-268. DOI: 10.1016/j.annonc.2020.10.599.
(11) Hu, X.; Liu, X.; Khatri, U.; Wu, J. The heterogeneous transition state of resistance to RET kinase inhibitors converges on ERK1/2-driven Aurora A/B kinases. *Drug Resist Updat* 2023, *68*, 100958. DOI: 10.1016/j.drup.2023.100958.
(12) Li, G. G.; Somwar, R.; Joseph, J.; Smith, R. S.; Hayashi, T.; Martin, L.; Franovic, A.; Schairer, A.; Martin, E.; Riely, G. J.; et al. Antitumor Activity of RXDX-105 in Multiple Cancer Types with RET Rearrangements or Mutations. *Clinical cancer research : an official journal of the American Association for Cancer Research* 2017, *23* (12), 2981-2990. DOI: 10.1158/1078-0432.CCR-16-1887.
(13) Drilon, A.; Subbiah, V.; Gautschi, O.; Tomasini, P.; de Braud, F.; Solomon, B. J.; Shao-Weng Tan, D.; Alonso, G.; Wolf, J.; Park, K.; et al. Selpercatinib in Patients With RET Fusion-Positive Non-Small-Cell Lung Cancer: Updated Safety and Efficacy From the Registrational LIBRETTO-001 Phase I/II Trial. *Journal of clinical oncology : official journal of the American Society of Clinical Oncology* 2022, JCO2200393. DOI: 10.1200/JCO.22.00393.
(14) Wirth, L. J.; Sherman, E.; Robinson, B.; Solomon, B.; Kang, H.; Lorch, J.; Worden, F.; Brose, M.; Patel, J.; Leboulleux, S.; et al. Efficacy of Selpercatinib in RET-Altered Thyroid Cancers. *The New England journal of medicine* 2020, *383* (9), 825-835. DOI: 10.1056/NEJMoa2005651.
(15) Pettersson, M.; Crews, C. M. PROteolysis TArgeting Chimeras (PROTACs) - Past, present and future. *Drug Discov Today Technol* 2019, *31*, 15-27. DOI: 10.1016/j.ddtec.2019.01.002 From NLM Medline.
(16) Hanzl, A.; Winter, G. E. Targeted protein degradation: current and future challenges. *Curr Opin Chem Biol* 2020, *56*, 35-41. DOI: 10.1016/j.cbpa.2019.11.012 From NLM Medline.
(17) Powell, C. E.; Gao, Y.; Tan, L.; Donovan, K. A.; Nowak, R. P.; Loehr, A.; Bahcall, M.; Fischer, E. S.; Janne, P. A.; George, R. E.; et al. Chemically Induced Degradation of Anaplastic Lymphoma Kinase (ALK). *J Med Chem* 2018, *61* (9), 4249-4255. DOI: 10.1021/acs.jmedchem.7b01655 From NLM Medline.
(18) Donovan, K. A.; Ferguson, F. M.; Bushman, J. W.; Eleuteri, N. A.; Bhunia, D.; Ryu, S.; Tan, L.; Shi, K.; Yue, H.; Liu, X.; et al. Mapping the Degradable Kinome Provides a Resource for Expedited Degrader Development. *Cell* 2020, *183* (6), 1714-1731 e1710. DOI: 10.1016/j.cell.2020.10.038 From NLM Medline.
(19) Bondeson, D. P.; Mares, A.; Smith, I. E.; Ko, E.; Campos, S.; Miah, A. H.; Mulholland, K. E.; Routly, N.; Buckley, D. L.; Gustafson, J. L.; et al. Catalytic in vivo protein knockdown by small-molecule PROTACs. *Nature chemical biology* 2015, *11* (8), 611-617. DOI: 10.1038/nchembio.1858 From NLM Medline.
(20) Winter, G. E.; Buckley, D. L.; Paulk, J.; Roberts, J. M.; Souza, A.; Dhe-Paganon, S.; Bradner, J. E. DRUG DEVELOPMENT. Phthalimide conjugation as a strategy for in vivo target protein degradation. *Science* 2015, *348* (6241), 1376-1381. DOI: 10.1126/science.aab1433 From NLM Medline.

(21) Min, J.; Mayasundari, A.; Keramatnia, F.; Jonchere, B.; Yang, S. W.; Jarusiewicz, J.; Actis, M.; Das, S.; Young, B.; Slavish, J.; et al. Phenyl-Glutarimides: Alternative Cereblon Binders for the Design of PROTACs. *Angew Chem Int Ed Engl* 2021, *60* (51), 26663-26670. DOI: 10.1002/anie.202108848 From NLM Medline.

(22) Han, X.; Wang, C.; Qin, C.; Xiang, W.; Fernandez-Salas, E.; Yang, C. Y.; Wang, M.; Zhao, L.; Xu, T.; Chinnaswamy, K.; et al. Discovery of ARD-69 as a Highly Potent Proteolysis Targeting Chimera (PROTAC) Degrader of Androgen Receptor (AR) for the Treatment of Prostate Cancer. *J Med Chem* 2019, *62* (2), 941-964. DOI: 10.1021/acs.jmedchem.8b01631 From NLM Medline.

(23) Xiang, W.; Zhao, L.; Han, X.; Qin, C.; Miao, B.; McEachern, D.; Wang, Y.; Metwally, H.; Kirchhoff, P. D.; Wang, L.; et al. Discovery of ARD-2585 as an Exceptionally Potent and Orally Active PROTAC Degrader of Androgen Receptor for the Treatment of Advanced Prostate Cancer. *J Med Chem* 2021, *64* (18), 13487-13509. DOI: 10.1021/acs.jmedchem.1c00900 From NLM Medline.

(24) Shen, T.; Hu, X. Q.; Liu, X.; Subbiah, V.; Mooers, B. H. M.; Wu, J. The L730V/I RET roof mutations display different activities toward pralsetinib and selpercatinib. *Npj Precision Oncology* 2021, *5* (1). DOI: ARTN 48
10.1038/s41698-021-00188-x.

(25) Liu, X.; Shen, T.; Mooers, B. H. M.; Hilberg, F.; Wu, J. Drug resistance profiles of mutations in the RET kinase domain. *Br J Pharmacol* 2018, *175* (17), 3504-3515. DOI: 10.1111/bph.14395.

(26) Subbiah, V.; Gouda, M. A.; Iorgulescu, J. B.; Dadu, R.; Patel, K.; Sherman, S.; Cabanillas, M.; Hu, M.; Castellanos, L. E.; Amini, B.; et al. Adaptive Darwinian off-target resistance mechanisms to selective RET inhibition in RET driven cancer. *NPJ Precis Oncol* 2024, *8* (1), 62. DOI: 10.1038/s41698-024-00563-4 From NLM PubMed-not-MEDLINE.

(27) Cascetta, P.; Sforza, V.; Manzo, A.; Carillio, G.; Palumbo, G.; Esposito, G.; Montanino, A.; Costanzo, R.; Sandomenico, C.; De Cecio, R. RET inhibitors in non-small-cell lung cancer. *Cancers* 2021, *13* (17), 4415.

(28) Carlomagno, F.; Vitagliano, D.; Guida, T.; Ciardiello, F.; Tortora, G.; Vecchio, G.; Ryan, A. J.; Fontanini, G.; Fusco, A.; Santoro, M. ZD6474, an orally available inhibitor of KDR tyrosine kinase activity, efficiently blocks oncogenic RET kinases. *Cancer research* 2002, *62* (24), 7284-7290.

(29) Wells Jr, S. A.; Robinson, B. G.; Gagel, R. F.; Dralle, H.; Fagin, J. A.; Santoro, M.; Baudin, E.; Elisei, R.; Jarzab, B.; Vasselli, J. R. Vandetanib in patients with locally advanced or metastatic medullary thyroid cancer: a randomized, double-blind phase III trial. *Journal of clinical oncology* 2012, *30* (2), 134.

(30) Cuccuru, G.; Lanzi, C.; Cassinelli, G.; Pratesi, G.; Tortoreto, M.; Petrangolini, G.; Seregni, E.; Martinetti, A.; Laccabue, D.; Zanchi, C. Cellular effects and antitumor activity of RET inhibitor RPI-1 on MEN2A-associated medullary thyroid carcinoma. *Journal of the National Cancer Institute* 2004, *96* (13), 1006-1014.

(31) Schlumberger, M.; Tahara, M.; Wirth, L. J.; Robinson, B.; Brose, M. S.; Elisei, R.; Habra, M. A.; Newbold, K.; Shah, M. H.; Hoff, A. O. Lenvatinib versus placebo in radioiodine-refractory thyroid cancer. *New England Journal of Medicine* 2015, *372* (7), 621-630.

(32) Velcheti, V.; Hida, T.; Reckamp, K.; Yang, J.; Nokihara, H.; Sachdev, P.; Feit, K.; Kubota, T.; Nakada, T.; Dutcus, C. Phase 2 study of lenvatinib (LN) in patients (Pts) with RET fusion-positive adenocarcinoma of the lung. *Annals of Oncology* 2016, *27*, vi417.

(33) Subbiah, V.; Velcheti, V.; Tuch, B.; Ebata, K.; Busaidy, N.; Cabanillas, M.; Wirth, L.; Stock, S.; Smith, S.; Lauriault, V. Selective RET kinase inhibition for patients with RET-altered cancers. *Annals of Oncology* 2018, *29* (8), 1869-1876.

(34) Wirth, L. J.; Sherman, E.; Robinson, B.; Solomon, B.; Kang, H.; Lorch, J.; Worden, F.; Brose, M.; Patel, J.; Leboulleux, S. Efficacy of selpercatinib in RET-altered thyroid cancers. *New England Journal of Medicine* 2020, *383* (9), 825-835.

(35) Solomon, B. J.; Tan, L.; Lin, J. J.; Wong, S. Q.; Hollizeck, S.; Ebata, K.; Tuch, B. B.; Yoda, S.; Gainor, J. F.; Sequist, L. V. RET solvent front mutations mediate acquired resistance to selective RET inhibition in RET-driven malignancies. *Journal of Thoracic Oncology* 2020, *15* (4), 541-549.

(36) Ferguson, F. M.; Gray, N. S. Kinase inhibitors: the road ahead. *Nature reviews Drug discovery* 2018, *17* (5), 353-377.

(37) Health, U. D. o.; Services, H. Antibiotic resistance threats in the United States, 2019. *(No Title)* 2019.

(38) Hancock, R. E.; Sahl, H.-G. Antimicrobial and host-defense peptides as new anti-infective therapeutic strategies. *Nature biotechnology* 2006, *24* (12), 1551-1557.

(39) Mercer, D. K.; O'Neil, D. A. Peptides as the next generation of anti-infectives. *Future medicinal chemistry* 2013, *5* (3), 315-337.

(40) Mookherjee, N.; Anderson, M. A.; Haagsman, H. P.; Davidson, D. J. Antimicrobial host defence peptides: functions and clinical potential. *Nature reviews Drug discovery* 2020, *19* (5), 311-332.

(41) Chongsiriwatana, N. P.; Patch, J. A.; Czyzewski, A. M.; Dohm, M. T.; Ivankin, A.; Gidalevitz, D.; Zuckermann, R. N.; Barron, A. E. Peptoids that mimic the structure, function, and mechanism of helical antimicrobial peptides. *Proceedings of the National Academy of Sciences* 2008, *105* (8), 2794-2799.

(42) Porter, E. A.; Weisblum, B.; Gellman, S. H. Mimicry of host-defense peptides by unnatural oligomers: antimicrobial β-peptides. *Journal of the American Chemical Society* 2002, *124* (25), 7324-7330.

(43) Niu, Y.; Padhee, S.; Wu, H.; Bai, G.; Qiao, Q.; Hu, Y.; Harrington, L.; Burda, W. N.; Shaw, L. N.; Cao, C. Lipo-γ-AApeptides as a new class of potent and broad-spectrum antimicrobial agents. *Journal of medicinal chemistry* 2012, *55* (8), 4003-4009.

(44) Claudon, P.; Violette, A.; Lamour, K.; Decossas, M.; Fournel, S.; Heurtault, B.; Godet, J.; Mély, Y.; Jamart-Grégoire, B.; Averlant-Petit, M. C. Consequences of isostructural main-chain modifications for the design of antimicrobial foldamers: Helical mimics of host-defense peptides based on a heterogeneous amide/urea backbone. *Angewandte Chemie International Edition* 2010, *49* (2), 333-336.

(45) Violette, A.; Fournel, S.; Lamour, K.; Chaloin, O.; Frisch, B.; Briand, J.-P.; Monteil, H.; Guichard, G. Mimicking helical antibacterial peptides with nonpeptidic folding oligomers. *Chemistry & biology* 2006, *13* (5), 531-538.

(46) Tsubery, H.; Ofek, I.; Cohen, S.; Fridkin, M. N-terminal modifications of polymyxin B nonapeptide and their effect on antibacterial activity. *Peptides* 2001, *22* (10), 1675-1681.

(47) Steenbergen, J. N.; Alder, J.; Thorne, G. M.; Tally, F. P. Daptomycin: a lipopeptide antibiotic for the treatment of serious Gram-positive infections. *Journal of antimicrobial Chemotherapy* 2005, *55* (3), 283-288.

(48) Lockwood, N. A.; Haseman, J. R.; Tirrell, M. V.; Mayo, K. H. Acylation of SC4 dodecapeptide increases bactericidal potency against Gram-positive bacteria, including drug-resistant strains. *Biochemical journal* 2004, *378* (1), 93-103.

(49) Wang, M.; Feng, X.; Gao, R.; Sang, P.; Pan, X.; Wei, L.; Lu, C.; Wu, C.; Cai, J. Modular design of membrane-active antibiotics: from macromolecular antimicrobials to small scorpionlike peptidomimetics. *Journal of medicinal chemistry* 2021, *64* (14), 9894-9905.

(50) Hu, Y.; Amin, M. N.; Padhee, S.; Wang, R. E.; Qiao, Q.; Bai, G.; Li, Y.; Mathew, A.; Cao, C.; Cai, J. Lipidated peptidomimetics with improved antimicrobial activity. *ACS medicinal chemistry letters* 2012, *3* (8), 683-686.

(51) Yang, Z.; He, S.; Wang, J.; Yang, Y.; Zhang, L.; Li, Y.; Shan, A. Rational design of short peptide variants by using Kunitzin-RE, an amphibian-derived bioactivity peptide, for acquired potent broad-spectrum antimicrobial and improved therapeutic potential of commensalism coinfection of pathogens. *Journal of medicinal chemistry* 2019, *62* (9), 4586-4605.

(52) Wang, M.; Gao, R.; Zheng, M.; Sang, P.; Li, C.; Zhang, E.; Li, Q.; Cai, J. Development of bis-cyclic imidazolidine-4-one derivatives as potent antibacterial agents. *Journal of medicinal chemistry* 2020, *63* (24), 15591-15602.

(53) Merrifield, R. B. Solid phase peptide synthesis. I. The synthesis of a tetrapeptide. *Journal of the American Chemical Society* 1963, *85* (14), 2149-2154.

(54) Albericio, F. *Solid-phase synthesis: a practical guide*; CRC Press, 2000.

(55) Huang, H.; Rabenstein, D. A cleavage cocktail for methionine-containing peptides. *The Journal of peptide research* 1999, *53* (5), 548-553.

(56) Dick, F. Acid cleavage/deprotection in Fmoc/tBiu solid-phase peptide synthesis. *Peptide Synthesis Protocols* 1995, 63-72.

(57) Joullié, M. M.; Lassen, K. M. Evolution of amide bond formation. *Arkivoc* 2010, *8* (189-250), 75.

(58) El-Faham, A.; Albericio, F. Peptide coupling reagents, more than a letter soup. *Chemical reviews* 2011, *111* (11), 6557-6602.

(59) García-Martín, F.; Quintanar-Audelo, M.; García-Ramos, Y.; Cruz, L. J.; Gravel, C.; Furic, R.; Côté, S.; Tulla-Puche, J.; Albericio, F. ChemMatrix, a poly (ethylene glycol)-based support for the solid-phase synthesis of complex peptides. *Journal of combinatorial chemistry* 2006, *8* (2), 213-220.

(60) Mitchell, A.; Erickson, B.; Ryabtsev, M.; Hodges, R.; Merrifield, R. tert-Butoxycarbonylaminoacyl-4-(oxymethyl) phenylacetamidomethyl-resin, a more acid-resistant support for solid-phase peptide synthesis. *Journal of the American Chemical Society* 1976, *98* (23), 7357-7362.

(61) Hutchins, S. M.; Chapman, K. T. A strategy for urea linked diamine libraries. *Tetrahedron letters* 1995, *36* (15), 2583-2586.

(62) Chamoin, S.; Houldsworth, S.; Kruse, C.; Bakker, W. I.; Snieckus, V. The Suzuki-Miyaura cross coupling reactions on solid support. Link to solution phase directed ortho metalation. The Leznoff acetal linker approach to biaryl and heterobiaryl aldehydes. *Tetrahedron letters* 1998, *39* (24), 4179-4182.

(63) Marquais, S.; Arlt, M. Aryl-aryl cross coupling on a solid support using zinc organic reagents and palladium catalysis. *Tetrahedron letters* 1996, *37* (31), 5491-5494.

(64) Hanessian, S.; Yang, R.-Y. Solution and solid phase synthesis of 5-alkoxyhydantoin libraries with a three-fold functional diversity. *Tetrahedron letters* 1996, *37* (33), 5835-5838.

(65) Park, K.-H.; Ehrler, J.; Spoerri, H.; Kurth, M. J. Preparation of a 990-member chemical compound library of hydantoin-and isoxazoline-containing heterocycles using multipin technology. *Journal of Combinatorial Chemistry* 2001, *3* (2), 171-176.

(66) Logan, C. Y.; Nusse, R. The Wnt signaling pathway in development and disease. *Annu. Rev. Cell Dev. Biol.* 2004, *20*, 781-810.

(67) Groenewald, W.; Lund, A. H.; Gay, D. M. The Role of WNT Pathway Mutations in Cancer Development and an Overview of Therapeutic Options. *Cells* 2023, *12* (7), 990.

(68) Klaus, A.; Birchmeier, W. Wnt signalling and its impact on development and cancer. *Nature Reviews Cancer* 2008, *8* (5), 387-398.

(69) Luh, L. M.; Scheib, U.; Juenemann, K.; Wortmann, L.; Brands, M.; Cromm, P. M. Prey for the proteasome: targeted protein degradation—a medicinal chemist's perspective. *Angewandte Chemie International Edition* 2020, *59* (36), 15448-15466.

(70) Cromm, P. M.; Crews, C. M. Targeted protein degradation: from chemical biology to drug discovery. *Cell chemical biology* 2017, *24* (9), 1181-1190.

(71) Burslem, G. M.; Crews, C. M. Proteolysis-targeting chimeras as therapeutics and tools for biological discovery. *Cell* 2020, *181* (1), 102-114.

(72) Hu, J.; Hu, B.; Wang, M.; Xu, F.; Miao, B.; Yang, C.-Y.; Wang, M.; Liu, Z.; Hayes, D. F.; Chinnaswamy, K. Discovery of ERD-308 as a highly potent proteolysis targeting chimera (PROTAC) degrader of estrogen receptor (ER). *Journal of medicinal chemistry* 2019, *62* (3), 1420-1442.

(73) Bond, M. J.; Chu, L.; Nalawansha, D. A.; Li, K.; Crews, C. M. Targeted degradation of oncogenic KRASG12C by VHL-recruiting PROTACs. *ACS central science* 2020, *6* (8), 1367-1375.

(74) Zoppi, V.; Hughes, S. J.; Maniaci, C.; Testa, A.; Gmaschitz, T.; Wieshofer, C.; Koegl, M.; Riching, K. M.; Daniels, D. L.; Spallarossa, A. Iterative design and optimization of initially inactive proteolysis targeting chimeras (PROTACs) identify VZ185 as a potent, fast, and selective von Hippel–Lindau (VHL) based dual degrader probe of BRD9 and BRD7. *Journal of medicinal chemistry* 2018, *62* (2), 699-726.

(75) Kaneshige, A.; Bai, L.; Wang, M.; McEachern, D.; Meagher, J. L.; Xu, R.; Wang, Y.; Jiang, W.; Metwally, H.; Kirchhoff, P. D. A selective small-molecule STAT5 PROTAC degrader capable of achieving tumor regression in vivo. *Nature Chemical Biology* 2023, *19* (6), 703-711.

(76) Olson, C. M.; Jiang, B.; Erb, M. A.; Liang, Y.; Doctor, Z. M.; Zhang, Z.; Zhang, T.; Kwiatkowski, N.; Boukhali, M.; Green, J. L. Pharmacological perturbation of CDK9 using selective CDK9 inhibition or degradation. *Nature chemical biology* 2018, *14* (2), 163-170.

(77) Chirnomas, D.; Hornberger, K. R.; Crews, C. M. Protein degraders enter the clinic—a new approach to cancer therapy. *Nature Reviews Clinical Oncology* 2023, *20* (4), 265-278.

(78) Kaspar, A. A.; Reichert, J. M. Future directions for peptide therapeutics development. *Drug discovery today* 2013, *18* (17-18), 807-817.

(79) Sang, P.; Zhang, M.; Shi, Y.; Li, C.; Abdulkadir, S.; Li, Q.; Ji, H.; Cai, J. Inhibition of β-catenin/B cell lymphoma 9 protein− protein interaction using α-helix–mimicking sulfono-γ-AApeptide inhibitors. *Proceedings of the National Academy of Sciences* 2019, *116* (22), 10757-10762.

(80) Lehninger, A. L.; Nelson, D. L.; Cox, M. M. *Lehninger principles of biochemistry*; Macmillan, 2005.

(81) Richardson, J. S. The anatomy and taxonomy of protein structure. *Advances in protein chemistry* 1981, *34*, 167-339.

(82) Pace, C. N.; Scholtz, J. M. A helix propensity scale based on experimental studies of peptides and proteins. *Biophysical journal* 1998, *75* (1), 422-427.

(83) Branden, C. I.; Tooze, J. *Introduction to protein structure*; Garland Science, 2012.

(84) Sang, P.; Shi, Y.; Huang, B.; Xue, S.; Odom, T.; Cai, J. Sulfono-γ-AApeptides as helical mimetics: Crystal structures and applications. *Accounts of chemical research* 2020, *53* (10), 2425-2442.

(85) Seebach, D.; Overhand, M.; Kühnle, F. N.; Martinoni, B.; Oberer, L.; Hommel, U.; Widmer, H. β-Peptides: Synthesis by Arndt-Eistert homologation with concomitant peptide coupling. Structure determination by NMR and CD spectroscopy and by X-ray crystallography. Helical secondary structure of a β-hexapeptide in solution and its stability towards pepsin. *Helvetica Chimica Acta* 1996, *79* (4), 913-941.

(86) Appella, D. H.; Christianson, L. A.; Karle, I. L.; Powell, D. R.; Gellman, S. H. β-Peptide foldamers: robust helix formation in a new family of β-amino acid oligomers. *Journal of the American Chemical Society* 1996, *118* (51), 13071-13072.

(87) Cheng, R. P.; Gellman, S. H.; DeGrado, W. F. β-Peptides: from structure to function. *Chemical reviews* 2001, *101* (10), 3219-3232.

(88) Proulx, C.; Sabatino, D.; Hopewell, R.; Spiegel, J.; García Ramos, Y.; Lubell, W. D. Azapeptides and their therapeutic potential. *Future medicinal chemistry* 2011, *3* (9), 1139-1164.

(89) Fischer, L.; Claudon, P.; Pendem, N.; Miclet, E.; Didierjean, C.; Ennifar, E.; Guichard, G. The Canonical Helix of Urea Oligomers at Atomic Resolution: Insights Into Folding-Induced Axial Organization. *Angewandte Chemie International Edition* 2010, *6* (49), 1067-1070.

(90) Jones, J. E.; Diemer, V.; Adam, C.; Raftery, J.; Ruscoe, R. E.; Sengel, J. T.; Wallace, M. I.; Bader, A.; Cockroft, S. L.; Clayden, J. Length-dependent formation of transmembrane pores by 310-helical α-aminoisobutyric acid foldamers. *Journal of the American Chemical Society* 2016, *138* (2), 688-695.

(91) Legrand, B.; Maillard, L. T. α, β-Unsaturated γ-Peptide Foldamers. *ChemPlusChem* 2021, *86* (4), 629-645.

(92) Jensen, M.; Hansen, B.; De Meyts, P.; Schäffer, L.; Ursø, B. Activation of the Insulin Receptor by Insulin and a Synthetic Peptide Leads to Divergent Metabolic and Mitogenic Signaling and Responses. *Journal of Biological Chemistry* 2007, *282* (48), 35179-35186. DOI: 10.1074/jbc.m704599200 (acccessed 2023-05-12T00:05:29).

(93) Park, J.; Li, J.; Mayer, J. P.; Ball, K. A.; Wu, J.; Hall, C.; Accili, D.; Stowell, M. H. B.; Bai, X.-C.; Choi, E. Activation of the insulin receptor by an insulin mimetic peptide. *Nature Communications* 2022, *13* (1). DOI: 10.1038/s41467-022-33274-0 (acccessed 2023-05-12T00:23:52).

APPENDICES

Appendix A: S1 ^{1}H-NMR, ^{13}C-NMR, and HRMS

YW-L-1

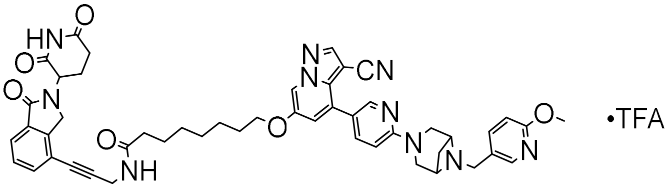

^{1}H NMR (400 MHz, DMSO-d_6) δ 11.05 (s, 1H), 9.39 (q, *J* = 5.6 Hz, 1H), 8.73 – 8.69 (m, 1H), 8.68 (d, *J* = 2.1 Hz, 1H), 8.59 (d, *J* = 0.9 Hz, 1H), 8.42 (t, *J* = 2.7 Hz, 1H), 8.41 – 8.36 (m, 2H), 7.93 – 7.86 (m, 2H), 7.84 (dd, *J* = 8.6, 2.5 Hz, 1H), 7.76 – 7.62 (m, 2H), 7.53 (t, *J* = 7.6 Hz, 1H), 7.28 (dd, *J* = 3.2, 2.1 Hz, 1H), 7.26 (d, *J* = 2.1 Hz, 1H), 6.94 (d, *J* = 8.6 Hz, 2H), 6.82 (dd, *J* = 9.0, 1.6 Hz, 1H), 5.16 (ddd, *J* = 13.3, 5.1, 1.9 Hz, 3H), 4.63 (t, *J* = 6.3 Hz, 5H), 4.47 (d, *J* = 6.1 Hz, 4H), 4.16 (d, *J* = 5.4 Hz, 3H), 4.13 – 4.01 (m, 8H), 3.88 (d, *J* = 6.6 Hz, 8H), 3.52 (dt, *J* = 11.9, 6.5 Hz, 2H), 2.97 – 2.88 (m, 1H), 2.88 – 2.83 (m, 1H), 2.61 (d, *J* = 1.7 Hz, 1H), 2.41 – 2.36 (m, 2H), 2.21 (td, *J* = 7.3, 2.2 Hz, 2H), 2.13 (td, *J* = 7.4, 2.1 Hz, 3H), 2.10 – 1.98 (m, 4H), 1.75 (tq, *J* = 13.7, 6.7 Hz, 4H), 1.52 (ttd, *J* = 14.6, 7.6, 2.7 Hz, 4H), 1.42 (h, *J* = 7.1 Hz, 4H), 1.37 – 1.22 (m, 8H).

^{13}C NMR (400 MHz, DMSO-d_6) δ 173.69, 172.51, 171.37, 168.22, 167.80, 158.17, 157.72, 150.06, 149.15, 147.67, 146.41, 141.87, 141.55, 138.59, 136.04 129.50, 123.68, 123.03, 115.37, 111.24, 105.23, 93.08, 81.33, 69.58, 62.74, 53.89, 52.03, 49.99, 48.70, 47.30, 43.70, 35.52, 34.09, 31.64, 29.06, 28.87, 26.58, 25.77, 25.55, 24.89, 22.92.

YW-L-2

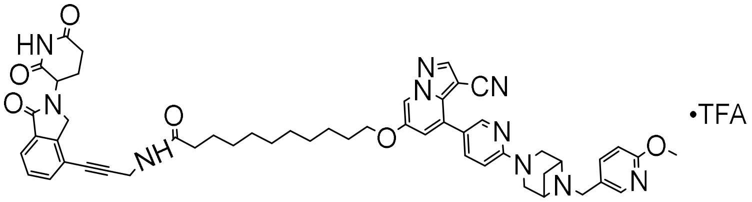

^{1}H NMR (400 MHz, DMSO-d_6) δ 10.40 (s, 1H), 9.31 (q, *J* = 5.9, 5.4 Hz, 1H), 8.61 (dd, *J* = 6.3, 2.1 Hz, 1H), 8.51 (s, 1H), 8.33 (dd, *J* = 13.6, 2.4 Hz, 1H), 8.28 (t, *J* = 5.5 Hz, 1H), 7.93 – 7.72 (m, 2H), 7.67 (d, *J* = 7.5 Hz, 1H), 7.58 (d, *J* = 7.6 Hz, 1H), 7.47 (t, *J* = 7.6 Hz, 1H), 7.19 (d, *J* = 2.0 Hz, 1H), 6.86 (d, *J* = 8.3 Hz, 1H), 6.74 (d, *J* = 8.8 Hz, 1H), 5.09 (dd, *J* = 13.3, 5.1 Hz, 1H), 4.57 (d, *J* = 5.7 Hz, 4H), 4.40 (t, *J* = 3.7 Hz, 3H), 4.36 (s, 1H), 4.26 (s, 1H), 4.22 (s, 1H), 4.14 (s, 1H), 4.08 (d, *J* = 5.3 Hz, 2H), 4.06 – 3.94 (m, 5H), 3.84 (s, 1H), 3.80 (s, 1H), 3.45 (dt, *J* = 12.1, 6.5 Hz, 1H), 2.85 (ddd, *J* = 18.2, 13.6, 5.4 Hz, 1H), 2.55 (s, 2H), 2.04 (t, *J* = 7.4 Hz, 2H), 2.00 – 1.90 (m, 2H), 1.66 (p, *J* = 6.6 Hz, 2H), 1.44 (q, *J* = 7.0 Hz, 2H), 1.33 (t, *J* = 7.5 Hz, 2H), 1.18 (s, 10H).

^{13}C NMR (400 MHz, DMSO-d_6) δ 173.29, 172.52, 171.44, 150.06, 149.76, 147.99, 147.04, 144.44, 141.84, 138.76, 134.60, 129.16, 123.68, 123.01, 113.13, 111.23, 105.22, 93.18, 81.34, 77.75, 69.62, 62.79, 53.89, 52.06, 50.03, 48.71, 47.34, 43.70, 35.57, 31.66, 29.37, 29.16, 29.06, 26.60, 25.88, 25.63, 22.93.

YW-L-3

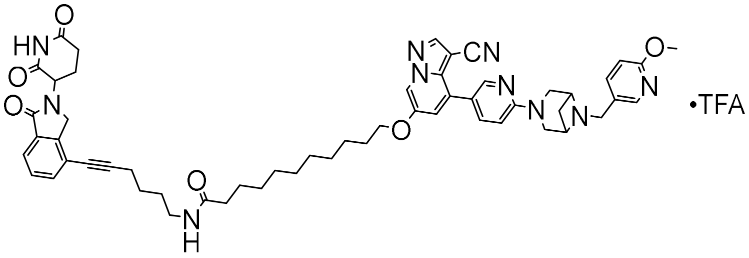

^{1}H NMR (400 MHz, DMSO-d_6) δ 9.37 (q, *J* = 5.5 Hz, 1H), 8.68 (d, *J* = 6.2 Hz, 1H), 8.59 (d, *J* = 10.6 Hz, 1H), 8.52 – 8.24 (m, 2H), 7.88 (dd, *J* = 8.6, 2.4 Hz, 1H), 7.81 (q, *J* = 5.7, 4.3 Hz, 1H), 7.73 (dd, *J* = 21.0, 7.6 Hz, 2H), 7.55 (t, *J* = 7.6 Hz, 1H), 7.31 – 7.22 (m, 1H), 6.93 (d, *J* = 8.2 Hz, 1H), 6.81 (d, *J* = 8.8 Hz, 1H), 5.15 (dd, *J* = 13.3, 5.0 Hz, 1H), 4.63 (d, *J* = 5.9 Hz, 3H), 4.46 (d, *J* = 4.7 Hz, 5H), 4.37 (s, 2H), 4.32 (s, 1H), 3.91 (s, 1H), 3.88 (d, *J* = 4.1 Hz, 4H), 3.65 (t, *J* = 4.5 Hz, 3H), 3.54 (dt, *J* = 19.3, 5.0 Hz, 3H), 3.41 (t, *J* = 5.9 Hz, 2H), 3.18 (q, *J* = 5.9 Hz, 2H), 2.91 (ddd, *J* = 18.1, 13.6, 5.5 Hz, 2H), 2.04 (h, *J* = 8.0, 6.7 Hz, 4H), 1.74 (p, *J* = 6.8, 6.1 Hz, 2H), 1.43 (dp, *J* = 15.3, 7.2 Hz, 4H), 1.35 – 1.10 (m, 11H).

^{13}C NMR (101 MHz, DMSO-d_6) δ 173.31, 172.69, 171.42, 167.95, 164.62, 157.75, 150.06, 149.75, 147.15, 144.43, 141.84, 141.35, 138.76, 136.21, 134.85, 132.57, 129.51, 129.18, 123.97, 123.00, 120.59, 120.37, 117.97, 114.93, 113.12, 111.23, 105.22, 91.79, 81.78, 81.34, 69.83, 69.63, 69.20, 62.79, 58.59, 53.89, 52.12, 50.04, 48.71, 47.40, 38.89, 35.78, 31.66, 29.70 – 28.60 (m), 25.90, 25.72, 22.83.

YW-L-4

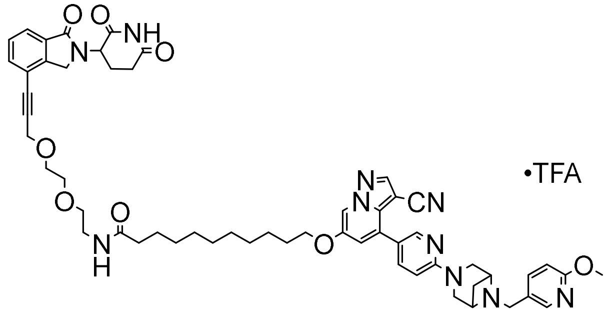

^{1}H NMR (400 MHz, DMSO-d_6) δ 9.37 (q, *J* = 5.5, 5.0 Hz, 1H), 8.68 (t, *J* = 3.7 Hz, 1H), 8.59 (d, *J* = 10.5 Hz, 1H), 8.40 (dd, *J* = 13.1, 2.4 Hz, 1H), 7.88 (dd, *J* = 8.8, 2.4 Hz, 1H), 7.77 (t, *J* = 5.7 Hz, 1H), 7.70 (d, *J* = 7.5 Hz, 1H), 7.61 (d, *J* = 7.5 Hz, 1H), 7.50 (t, *J* = 7.6 Hz, 1H), 7.27 (t, *J* = 4.3 Hz, 1H), 6.92 (t, *J* = 7.2 Hz, 1H), 6.81 (d, *J* = 8.8 Hz, 1H), 5.14 (dd, *J* = 13.2, 5.1 Hz, 1H), 4.63 (d, *J* = 5.7 Hz, 2H), 4.47 (d, *J* = 5.7 Hz, 2H), 4.42 (s, 1H), 4.33 (s, 1H), 4.28 (s, 1H), 4.21 (s, 1H), 4.10 (d, *J* = 5.8 Hz, 4H), 4.07 (d, *J* = 5.6 Hz, 4H), 4.04 (s, 3H), 3.52 (dt, *J* = 12.1, 6.6 Hz, 1H), 3.07 (q, *J* = 6.2 Hz, 2H), 2.91 (ddd, *J* = 17.9, 13.4, 5.5 Hz, 2H), 2.61 (s, 2H), 2.03 (h, *J* = 6.1 Hz, 4H), 1.73 (p, *J* = 6.8, 6.4 Hz, 2H), 1.56 (q, *J* = 3.4 Hz, 4H), 1.43 (dp, *J* = 21.3, 7.4 Hz, 4H), 1.24 (d, *J* = 13.0 Hz, 11H).

^{13}C NMR (101 MHz, DMSO-d_6) δ 173.30, 172.46, 171.44, 168.13, 164.62, 157.77, 149.76, 148.01, 147.04, 144.20, 141.84, 141.35, 138.74, 136.21, 134.51, 132.45, 129.28, 120.38, 119.28, 113.12, 111.23, 105.20, 96.61, 81.34, 76.98, 69.62, 62.80, 53.89, 52.11, 50.04, 48.71, 43.69, 38.27, 35.92, 31.69, 29.38, 28.87, 25.94, 25.90, 22.80, 18.92.

YW-L-5

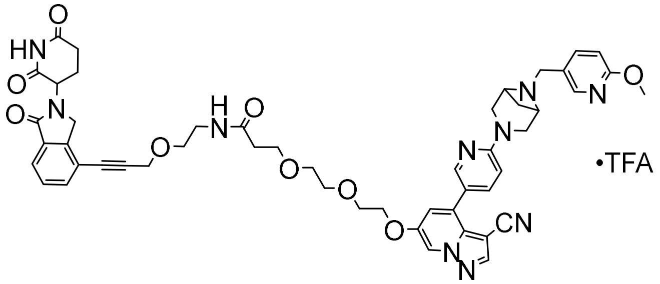

^{1}H NMR (400 MHz, DMSO-d_6) δ 9.38 (q, *J* = 5.7, 4.7 Hz, 1H), 8.71 (d, *J* = 6.5 Hz, 1H), 8.58 (s, 1H), 8.40 (dd, *J* = 12.7, 2.4 Hz, 1H), 7.97 (q, *J* = 5.7 Hz, 1H), 7.92 – 7.86 (m, 1H), 7.72 (dd, *J* = 26.5, 7.6 Hz, 2H), 7.54 (t, *J* = 7.6 Hz, 1H), 7.31 (d, *J* = 7.5 Hz, 1H), 6.93 (t, *J* = 7.4 Hz, 1H), 6.81 (d, *J* = 8.8 Hz, 1H), 5.15 (dd, *J* = 13.3, 5.1 Hz, 1H), 4.64 (d, *J* = 5.8 Hz, 3H), 4.52 – 4.42 (m, 8H), 4.36 (s, 2H), 4.23 (q, *J* = 4.9, 3.9 Hz, 4H), 4.14 – 4.01 (m, 3H), 3.94 – 3.84 (m, 4H), 3.77 (q, *J* = 4.3 Hz, 2H), 3.57 (dt, *J* = 16.3, 6.4 Hz, 6H), 3.52 – 3.45 (m, 2H), 3.26 (q, *J* = 5.7 Hz, 2H), 2.94 – 2.84 (m, 1H), 2.31 (d, *J* = 6.4 Hz, 2H), 2.05 (ddd, *J* = 21.8, 11.2, 4.9 Hz, 2H).

^{13}C NMR (101 MHz, DMSO-d_6) δ 173.33, 171.42, 170.70, 167.94, 164.62, 158.44, 149.90, 149.75, 147.98, 147.08, 144.44, 141.84, 138.75, 134.76, 132.56, 129.53, 129.16, 123.95, 122.96, 120.37, 117.92, 114.91, 113.28, 111.22, 105.22, 91.72, 81.89, 69.99, 69.12, 68.62, 62.78, 58.42, 53.88, 52.11, 50.03, 48.71, 47.39, 43.69, 38.86, 36.49, 31.67, 26.59, 22.79.

YW-L-6

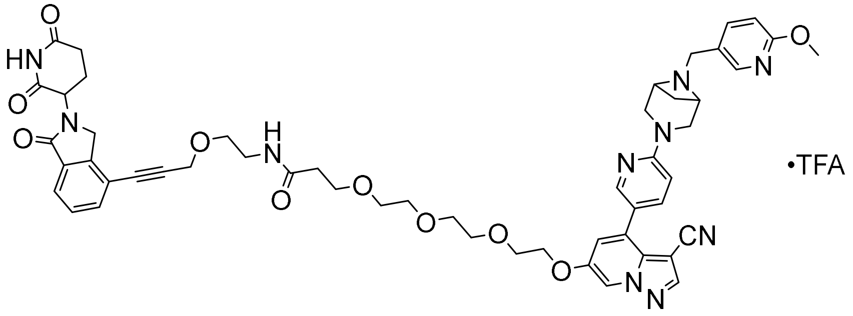

^{1}H NMR (400 MHz, DMSO-d_6) δ 9.43 (s, 1H), 8.73 (d, J = 6.6 Hz, 1H), 8.64 – 8.55 (m, 1H), 8.41 (d, J = 12.8 Hz, 1H), 7.97 (t, J = 5.5 Hz, 1H), 7.88 (t, J = 12.0 Hz, 2H), 7.74 (dd, J = 24.9, 7.6 Hz, 2H), 7.56 (t, J = 7.8 Hz, 1H), 7.32 (d, J = 7.5 Hz, 1H), 6.94 (d, J = 8.3 Hz, 1H), 6.83 (d, J = 8.7 Hz, 1H), 5.16 (dd, J = 13.4, 5.0 Hz, 1H), 4.65 (d, J = 5.6 Hz, 4H), 4.47 (d, J = 8.9 Hz, 5H), 4.25 (d, J = 5.8 Hz, 3H), 4.15 – 4.01 (m, 3H), 3.97 – 3.85 (m, 4H), 3.80 (t, J = 4.3 Hz, 2H), 3.65 – 3.39 (m, 15H), 3.27 (d, J = 6.4 Hz, 2H), 2.93 (td, J = 16.1, 14.6, 5.2 Hz, 1H), 2.61 (d, J = 17.3 Hz, 1H), 2.31 (t, J = 6.4 Hz, 2H), 2.14 – 1.94 (m, 2H).

^{13}C NMR (101 MHz, DMSO-d_6) δ 173.33, 171.43, 170.71, 167.96, 164.63, 157.76, 149.77, 147.97, 149.06, 147.10, 144.46, 141.86, 141.37, 138.77, 136.29, 134.79, 132.58, 129.54, 123.98, 122.99, 120.57, 120.39, 117.95, 114.92, 113.35, 111.23, 105.71, 105.25, 91.75, 81.90, 81.40, 70.37, 70.26, 70.12, 69.97, 69.29, 69.16, 68.63, 67.25, 62.78, 58.43, 53.89, 52.13, 50.03, 48.71, 47.40, 43.71, 38.86, 36.50, 31.68, 26.61, 22.81.

YW-L-7

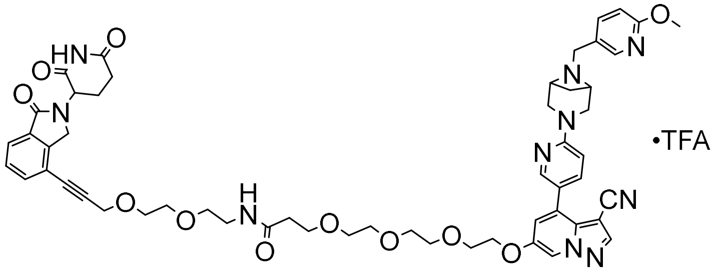

^{1}H NMR (400 MHz, DMSO-d_6) δ 9.37 (q, *J* = 5.4 Hz, 1H), 8.72 (dd, *J* = 6.2, 2.1 Hz, 1H), 8.60 (d, *J* = 10.4 Hz, 1H), 8.53 – 8.24 (m, 2H), 8.00 – 7.80 (m, 3H), 7.74 (dd, *J* = 21.5, 7.6 Hz, 2H), 7.56 (t, *J* = 7.6 Hz, 1H), 7.31 (dd, *J* = 7.5, 2.1 Hz, 1H), 6.93 (dd, *J* = 10.2, 4.2 Hz, 1H), 6.82 (d, *J* = 8.8 Hz, 1H), 5.15 (dd, *J* = 13.3, 5.1 Hz, 1H), 4.64 (d, *J* = 5.6 Hz, 2H), 4.29 – 4.18 (m, 3H), 4.16 – 3.99 (m, 3H), 3.88 (d, *J* = 4.3 Hz, 3H), 3.79 (dd, *J* = 5.6, 3.3 Hz, 4H), 3.49 (p, *J* = 2.7, 2.3 Hz, 5H), 3.46 (q, *J* = 3.7, 3.1 Hz, 4H), 3.41 (t, *J* = 5.9 Hz, 3H), 3.20 (q, *J* = 5.8 Hz, 3H), 2.90 (dtd, *J* = 16.3, 12.2, 10.9, 5.7 Hz, 2H), 2.60 (dt, *J* = 15.1, 3.0 Hz, 2H), 2.42 (dd, *J* = 13.3, 4.5 Hz, 1H), 2.30 (t, *J* = 6.4 Hz, 2H), 2.16 – 1.91 (m, 2H).

^{13}C NMR (101 MHz, DMSO-d_6) δ 173.32, 171.42, 170.61, 167.94, 164.62, 157.79, 149.91, 149.75, 148.03, 147.09, 144.43, 141.84, 141.33, 138.71, 134.86, 132.56, 129.19, 123.97, 122.97, 120.56, 120.37, 117.95, 114.91, 113.33, 111.22, 105.19, 91.79, 81.78, 81.39, 70.36, 70.26, 70.12, 69.97, 69.84, 69.58, 69.20, 67.24, 62.79, 58.58, 53.88, 52.12, 50.03, 48.71, 47.39, 38.97, 36.48, 31.66, 26.60, 22.82.

YW-L-8

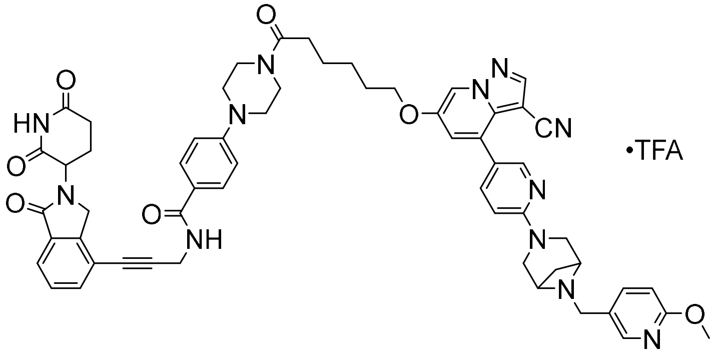

^{1}H NMR (400 MHz, DMSO-d_6) δ 9.37 (q, *J* = 5.4 Hz, 1H), 8.77 (t, *J* = 5.5 Hz, 1H), 8.69 (dd, *J* = 6.4, 2.1 Hz, 1H), 8.59 (d, *J* = 10.6 Hz, 1H), 8.40 (dd, *J* = 14.4, 2.5 Hz, 1H), 7.88 (dt, *J* = 8.7, 2.1 Hz, 1H), 7.81 – 7.71 (m, 3H), 7.67 (d, *J* = 7.6 Hz, 1H), 7.54 (t, *J* = 7.6 Hz, 1H), 7.28 (dd, *J* = 7.3, 2.1 Hz, 1H), 6.94 (ddd, *J* = 17.1, 9.0, 4.2 Hz, 3H), 6.81 (d, *J* = 8.8 Hz, 1H), 5.14 (dd, *J* = 13.3, 5.1 Hz, 1H), 4.63 (d, *J* = 5.8 Hz, 3H), 4.47 (d, *J* = 6.6 Hz, 2H), 4.36 – 4.31 (m, 2H), 4.11 (d, *J* = 5.3 Hz, 2H), 3.89 (d, *J* = 15.2 Hz, 5H), 3.59 (t, *J* = 5.1 Hz, 3H), 3.27 (dt, *J* = 21.3, 5.1 Hz, 3H), 2.34 (q, *J* = 12.9, 10.1 Hz, 4H), 2.11 – 1.92 (m, 4H), 1.76 (h, *J* = 6.1 Hz, 2H), 1.61 – 1.11 (m, 12H).

^{13}C NMR (101 MHz, DMSO-d_6) δ 173.30, 171.45, 171.24, 168.03, 168.03, 166.14, 164.62, 157.77, 150.07, 149.76, 149.05, 148.01, 147.05, 144.57, 141.85, 141.36, 138.76, 134.47, 132.49, 131.34, 129.54, 129.17, 123.63, 120.33, 118.49, 114.94, 114.17, 113.13, 111.23, 105.21, 93.75, 77.71, 69.62, 62.79, 53.89, 52.03, 50.03, 48.71, 47.75, 47.32, 44.89, 43.69, 41.04, 32.66, 31.65, 29.73, 29.49, 29.17, 28.99, 28.84, 25.79, 25.14, 22.89.

YW-L-9

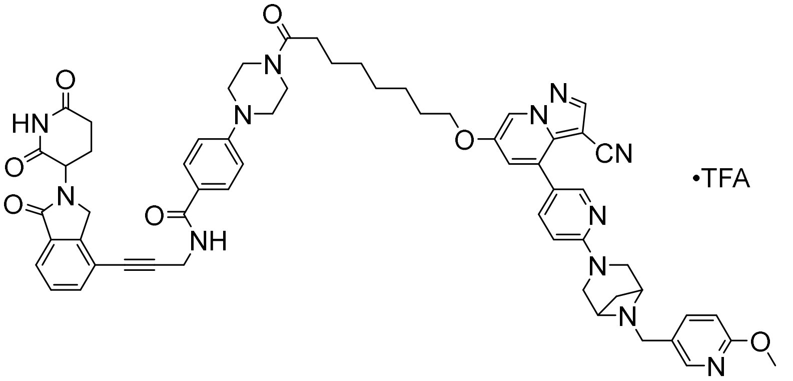

^{1}H NMR (400 MHz, DMSO-d_6) δ 9.39 (q, *J* = 5.4 Hz, 1H), 8.77 (t, *J* = 5.4 Hz, 1H), 8.69 (dd, *J* = 6.6, 2.1 Hz, 1H), 8.59 (d, *J* = 10.7 Hz, 1H), 8.40 (dd, *J* = 14.6, 2.4 Hz, 2H), 7.89 (dt, *J* = 8.6, 2.8 Hz, 2H), 7.79 (d, *J* = 8.5 Hz, 2H), 7.74 (d, *J* = 7.5 Hz, 1H), 7.67 (d, *J* = 7.6 Hz, 1H), 7.54 (t, *J* = 7.6 Hz, 1H), 7.28 (dd, *J* = 7.5, 2.1 Hz, 1H), 7.03 – 6.87 (m, 4H), 6.82 (d, *J* = 8.8 Hz, 1H), 5.15 (dd, *J* = 13.3, 5.1 Hz, 1H), 4.64 (d, *J* = 5.6 Hz, 3H), 4.42 (s, 1H), 4.35 (s, 1H), 4.33 (d, *J* = 3.1 Hz, 1H), 4.25 (d, *J* = 26.4 Hz, 1H), 4.11 (d, *J* = 5.2 Hz, 3H), 4.08 (d, *J* = 4.3 Hz, 1H), 4.04 (s, 1H), 3.96 – 3.82 (m, 5H), 3.59 (t, *J* = 4.9 Hz, 4H), 3.51 (q, *J* = 6.6, 6.2 Hz, 1H), 3.27 (dt, *J* = 21.9, 5.2 Hz, 4H), 2.93 – 2.82 (m, 1H), 2.63 – 2.54 (m, 1H), 2.42 – 2.26 (m, 3H), 2.11 – 2.04 (m, 1H), 2.04 – 1.94 (m, 1H), 1.76 (dq, *J* = 10.9, 6.5, 5.5 Hz, 2H), 1.62 – 1.19 (m, 10H).

^{13}C NMR (101 MHz, DMSO-d_6) δ 173.30, 171.44, 171.24, 168.03, 166.14, 164.62, 158.88, 158.52, 157.71, 153.07, 150.07, 149.75, 149.04, 147.91, 147.04, 144.57, 141.84, 141.34, 138.81, 136.21, 134.46, 132.48, 129.16, 123.62, 123.02, 120.59, 120.37, 118.49, 114.17, 113.14, 111.22, 105.26, 93.75, 81.35, 77.71, 69.62, 62.78, 53.88, 52.03, 50.03, 48.72, 47.76, 47.32, 44.90, 43.72, 32.66, 31.65, 29.73, 29.17, 28.99, 26.60, 25.79, 25.14, 22.89.

YW-L-11

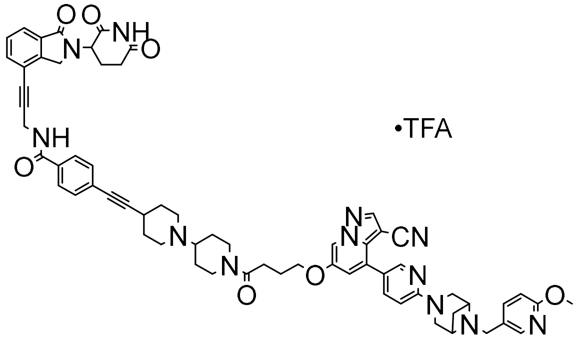

^{1}H NMR (400 MHz, DMSO-d_6) δ 9.62 (s, 1H), 9.42 (s, 1H), 9.15 (q, *J* = 5.4 Hz, 1H), 8.79 – 8.67 (m, 1H), 8.60 (dd, *J* = 10.6, 3.4 Hz, 1H), 8.40 (dd, *J* = 15.0, 2.4 Hz, 1H), 7.89 (dd, *J* = 8.4, 6.2 Hz, 3H), 7.75 (d, *J* = 7.5 Hz, 1H), 7.68 (dd, *J* = 7.5, 2.3 Hz, 1H), 7.54 (dt, *J* = 22.9, 8.3 Hz, 3H), 7.28 (d, *J* = 2.0 Hz, 1H), 6.93 (dd, *J* = 9.2, 3.0 Hz, 1H), 6.82 (dd, *J* = 8.9, 2.7 Hz, 1H), 5.16 (dd, *J* = 13.3, 5.1 Hz, 2H), 4.63 (t, *J* = 5.3 Hz, 2H), 4.57 (d, *J* = 12.9 Hz, 1H), 4.47 (d, *J* = 5.9 Hz, 2H), 4.38 (td, *J* = 19.5, 18.8, 5.9 Hz, 4H), 4.21 (s, 1H), 4.18 – 3.99 (m, 6H), 3.96 – 3.81 (m, 4H), 3.63 – 3.36 (m, 4H), 3.35 – 3.14 (m, 1H), 3.04 (t, *J* = 11.0 Hz, 2H), 2.91 (tq, *J* = 14.4, 8.7, 7.0 Hz, 2H), 2.64 – 2.53 (m, 4H), 2.43 – 2.25 (m, 1H), 2.20 (d, *J* = 13.6 Hz, 1H), 2.16 – 2.10 (m, 1H), 2.10 – 1.93 (m, 7H), 1.86 (q, *J* = 12.5 Hz, 1H), 1.73 – 1.36 (m, 2H), 1.24 (d, *J* = 3.3 Hz, 1H).

^{13}C NMR (101 MHz, DMSO-d_6) δ 173.30, 171.46, 170.39, 168.00, 165.73, 158.83, 158349, 157.79, 149.75, 149.02, 147.99, 147.09, 144.56, 141.84, 141.32, 138.74, 136.26, 134.59, 133.67, 132.50, 132.01, 131.84, 129.59, 129.20, 128.10, 125.98, 123.74, 122.99, 120.71, 120.56, 120.38, 118.35, 114.91, 113.24, 111.22, 105.65, 105.21, 94.25, 93.01, 83.19, 81.41, 77.96, 69.10, 62.78, 53.89, 52.04, 50.03, 48.70, 47.34, 46.15, 43.72, 31.64, 29.95, 29.60, 28.79, 27.81, 26.82, 26.61, 26.00, 24.55, 24.11, 22.91.

YW-L-12

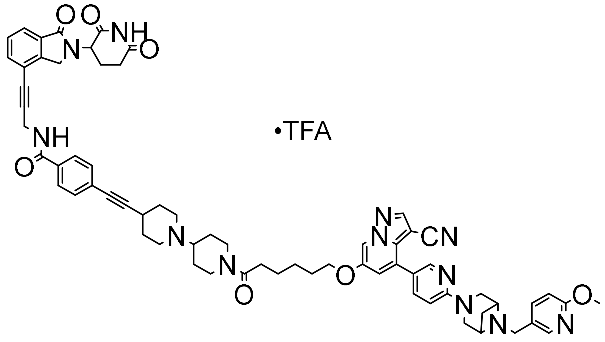

^{1}H NMR (400 MHz, DMSO-d_6) δ 9.91 – 9.58 (m, 1H), 9.44 (q, *J* = 5.9, 4.6 Hz, 1H), 9.16 (q, *J* = 5.8 Hz, 1H), 8.70 (dt, *J* = 5.1, 2.5 Hz, 1H), 8.59 (d, *J* = 2.0 Hz, 1H), 8.43 (d, *J* = 2.3 Hz, 1H), 8.39 (d, *J* = 2.4 Hz, 1H), 8.01 – 7.80 (m, 4H), 7.75 (d, *J* = 7.5 Hz, 1H), 7.68 (dd, *J* = 7.5, 2.7 Hz, 1H), 7.61 – 7.54 (m, 2H), 7.54 – 7.47 (m, 1H), 7.28 (dt, *J* = 8.3, 2.2 Hz, 1H), 6.92 (t, *J* = 7.9 Hz, 2H), 6.82 (d, *J* = 9.0 Hz, 1H), 5.16 (dd, *J* = 13.3, 5.1 Hz, 1H), 4.64 (t, *J* = 5.4 Hz, 2H), 4.55 (d, *J* = 12.8 Hz, 1H), 4.48 (d, *J* = 6.0 Hz, 2H), 4.38 (td, *J* = 19.5, 18.9, 6.5 Hz, 3H), 4.22 (s, 1H), 4.17 – 3.98 (m, 6H), 3.96 – 3.84 (m, 4H), 3.50 (dd, *J* = 23.9, 8.7 Hz, 4H), 3.34 – 3.14 (m, 1H), 3.03 (dt, *J* = 17.2, 8.0 Hz, 2H), 2.91 (dp, *J* = 20.4, 6.8, 6.1 Hz, 2H), 2.61 (d, *J* = 3.6 Hz, 1H), 2.44 – 2.28 (m, 3H), 2.25 – 2.16 (m, 1H), 2.16 – 1.94 (m, 6H), 1.88 (t, *J* = 13.4 Hz, 1H), 1.80 (q, *J* = 7.1, 6.5 Hz, 2H), 1.54 (ddt, *J* = 40.0, 15.6, 9.6 Hz, 6H).

^{13}C NMR (101 MHz, DMSO-d_6) δ 173.30, 171.46, 170.94, 168.01, 165.74, 164.37, 158.93, 157.75, 157.49, 150.05, 149.75, 149.02, 147.94, 147.06, 144.56, 141.84, 141.32, 138.78, 136.22, 134.60, 133.66, 132.50, 132.01, 131.84, 129.54, 129.19, 128.10, 125.99, 123.73, 122.96, 120.57, 120.38, 118.36, 117.94, 115.03, 114.92, 113.17, 111.22, 105.24, 94.27, 93.01, 92.83, 81.38, 81.06, 77.95, 69.61, 62.87, 62.77, 53.88, 52.05, 50.03, 48.70, 48.49, 48.31, 47.34, 46.13, 44.61, 43.82, 43.72, 32.56, 31.64, 29.95, 29.58, 28.79, 27.80, 26.94, 26.60, 26.14, 26.01, 25.72, 24.93, 24.11, 22.91.

YW-N-1

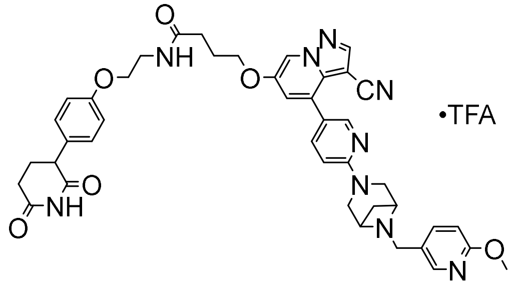

^{1}H NMR (400 MHz, DMSO-d_6) δ 10.79 (s, 1H), 9.39 (s, 1H), 8.67 (d, J = 7.3 Hz, 1H), 8.59 (d, J = 10.4 Hz, 1H), 8.41 (d, J = 12.4 Hz, 1H), 8.07 (q, J = 8.7, 7.4 Hz, 1H), 7.89 (d, J = 8.7 Hz, 1H), 7.28 (d, J = 7.7 Hz, 1H), 7.11 (d, J = 8.5 Hz, 2H), 6.97 – 6.86 (m, 3H), 6.83 (d, J = 9.0 Hz, 1H), 4.64 (d, J = 6.0 Hz, 2H), 4.48 (d, J = 6.3 Hz, 1H), 4.08 (dd, J = 15.9, 10.4 Hz, 4H), 3.97 (s, 2H), 3.89 (s, 4H), 3.41 (s, 4H), 2.70 (s, 1H), 2.23 – 1.93 (m, 5H), 1.76 (t, J = 7.2 Hz, 2H), 1.59 (t, J = 7.7 Hz, 2H), 1.43 (q, J = 7.7 Hz, 2H), 1.24 (dd, J = 17.0, 8.1 Hz, 1H).

^{13}C NMR (101 MHz, DMSO-d_6) δ 174.93, 173.96, 172.95, 164.63, 158.56, 157.80, 150.05, 149.74, 147.86, 147.04, 141.85, 138.82, 136.21, 131.66, 130.03, 123.01, 120.58, 120.34, 114.78, 113.14, 111.23, 105.31, 81.34, 69.57, 66.78, 62.79, 53.90, 50.04, 48.71, 46.95, 43.72, 38.63, 35.63, 31.81, 28.65, 26.45, 25.52, 25.38.

YW-N-2

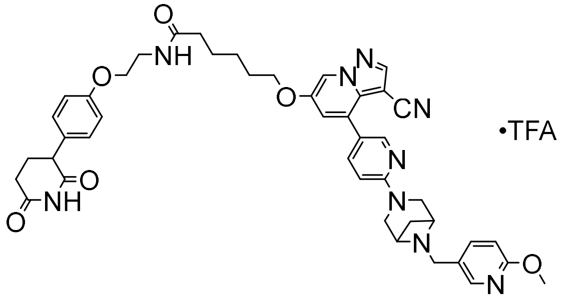

^{1}H NMR (600 MHz, DMSO-d_6) δ 10.32 (s, 1H), 9.30 (d, *J* = 5.1 Hz, 1H), 8.63 (d, *J* = 2.1 Hz, 1H), 8.53 (s, 1H), 8.33 (dd, *J* = 18.0, 2.5 Hz, 2H), 8.16 – 8.05 (m, 1H), 7.81 (dd, *J* = 8.6, 2.5 Hz, 1H), 7.20 (d, *J* = 2.1 Hz, 1H), 7.03 (d, *J* = 8.5 Hz, 2H), 6.86 (dd, *J* = 8.7, 2.9 Hz, 1H), 6.83 – 6.78 (m, 2H), 6.75 (d, *J* = 8.8 Hz, 1H), 4.56 (t, *J* = 6.4 Hz, 3H), 4.40 (d, *J* = 6.5 Hz, 2H), 4.15 (d, *J* = 3.7 Hz, 1H), 4.08 – 4.00 (m, 3H), 3.98 (d, *J* = 12.7 Hz, 2H), 3.90 (td, *J* = 5.7, 2.8 Hz, 2H), 3.70 (dd, *J* = 11.5, 4.9 Hz, 1H), 3.45 (dt, *J* = 12.3, 6.6 Hz, 1H), 3.40 – 3.30 (m, 2H), 2.61 – 2.56 (m, 1H), 2.33 (s, 1H), 2.24 (td, *J* = 7.4, 4.6 Hz, 2H), 2.07 (dtd, *J* = 13.0, 11.7, 4.4 Hz, 1H), 2.02 – 1.96 (m, 1H), 1.96 – 1.87 (m, 3H).

^{13}C NMR (151 MHz, DMSO-d_6) δ 178.31, 174.95, 173.98, 172.04, 164.66, 158.76, 158.51, 157.57, 149.96, 147.05, 141.90, 138.92, 136.01, 132.06, 130.06, 129.51, 123.03, 117.14, 114.74, 111.24, 105.23, 81.64, 69.09, 66.77, 62.75, 53.90, 50.06, 49.99, 48.71, 46.94, 43.74, 38.70, 31.83, 26.43, 24.92.

YW-N-3

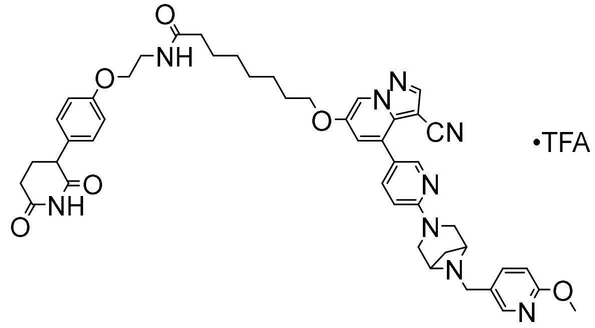

^{1}H NMR (600 MHz, DMSO-d_6) δ 9.32 (q, *J* = 5.4 Hz, 1H), 8.63 (dd, *J* = 10.2, 2.1 Hz, 1H), 8.53 (d, *J* = 16.4 Hz, 1H), 8.33 (dd, *J* = 20.3, 2.5 Hz, 1H), 7.99 (dd, *J* = 6.5, 4.8 Hz, 1H), 7.82 (ddd, *J* = 8.7, 4.9, 2.5 Hz, 1H), 7.21 (dd, *J* = 11.0, 2.1 Hz, 1H), 7.09 – 7.01 (m, 2H), 6.87 (d, *J* = 8.5 Hz, 1H), 6.83 – 6.79 (m, 2H), 6.75 (d, *J* = 8.8 Hz, 1H), 4.56 (t, *J* = 6.6 Hz, 3H), 4.40 (d, *J* = 6.5 Hz, 2H), 4.15 (s, 1H), 4.08 – 3.94 (m, 5H), 3.88 (t, *J* = 5.7 Hz, 2H), 3.81 (d, *J* = 6.4 Hz, 4H), 3.70 (dd, *J* = 11.5, 4.9 Hz, 1H), 3.45 (dt, *J* = 12.1, 6.7 Hz, 1H), 3.33 (q, *J* = 5.7 Hz, 2H), 2.61 – 2.53 (m, 2H), 2.42 – 2.29 (m, 1H), 2.12 – 1.96 (m, 4H), 1.91 (dq, *J* = 13.6, 4.8 Hz, 1H), 1.72 – 1.62 (m, 2H), 1.48 – 1.40 (m, 2H), 1.34 (qd, *J* = 9.2, 7.9, 4.6 Hz, 2H), 1.26 (dtt, *J* = 13.9, 9.7, 5.5 Hz, 2H), 1.22 – 1.14 (m, 2H).

^{13}C NMR (151 MHz, DMSO-d_6) δ 174.94, 173.93, 172.93, 164.60, 158.77, 158.53, 157.80, 148.87, 147.76, 141.87, 138.80, 136.19, 131.68, 130.05, 129.50, 123.02, 117.27, 115.33, 114.74, 113.16, 111.24, 105.23, 81.33, 69.60, 67.26, 62.74, 53.89, 49.67, 48.71, 46.95, 38.59, 35.68, 31.83, 28.98, 28.88, 28.82, 26.45, 25.77, 25.63.

YW-N-4

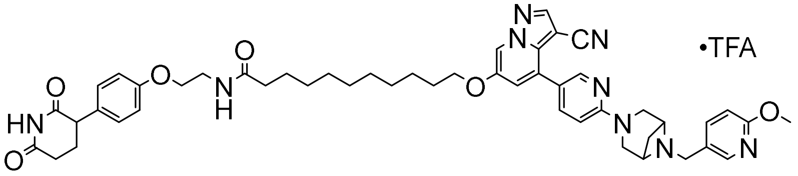

^{1}H NMR (400 MHz, DMSO-d_6) δ 9.37 (s, 1H), 8.69 (d, *J* = 7.3 Hz, 1H), 8.60 (d, *J* = 10.2 Hz, 1H), 8.41 (d, *J* = 13.8 Hz, 1H), 8.02 (d, *J* = 5.8 Hz, 1H), 7.89 (d, *J* = 8.7 Hz, 1H), 7.28 (d, *J* = 8.2 Hz, 1H), 7.13 (d, *J* = 8.1 Hz, 1H), 6.97 – 6.86 (m, 2H), 6.83 (d, *J* = 8.9 Hz, 1H), 4.64 (d, *J* = 6.0 Hz, 1H), 4.47 (s, 1H), 4.12 (s, 3H), 3.89 (s, 2H), 3.77 (s, 2H), 2.95 (s, 1H), 2.80 (s, 1H), 2.69 (s, 1H), 2.35 (s, 1H), 2.08 (t, *J* = 7.5 Hz, 3H), 1.76 (t, *J* = 6.8 Hz, 1H), 1.46 (dt, *J* = 22.3, 7.5 Hz, 3H), 1.38 – 1.08 (m, 8H).

^{13}C NMR (101 MHz, DMSO-d_6) δ 174.94, 173.96, 173.05, 164.79, 157.81, 150.08, 149.39, 147.99, 147.04, 141.86, 138.73, 131.67, 130.04, 114.79, 111.23, 81.33, 69.65, 66.80, 62.81, 53.90, 46.95, 38.62, 35.75, 31.80, 29.40, 29.23, 29.14, 29.07, 28.89, 26.47, 25.89, 25.69.

YW-N-5

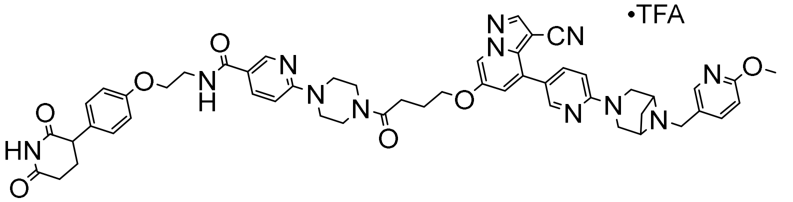

^{1}H NMR (400 MHz, DMSO-d_6) δ 9.44 (q, *J* = 5.2 Hz, 1H), 8.75 (dd, *J* = 7.8, 2.0 Hz, 1H), 8.68 – 8.54 (m, 3H), 8.50 (d, *J* = 2.4 Hz, 1H), 8.41 (dd, *J* = 14.6, 2.4 Hz, 2H), 8.29 (d, *J* = 2.4 Hz, 1H), 8.04 (dd, *J* = 9.0, 2.4 Hz, 1H), 7.98 (dd, *J* = 8.7, 2.5 Hz, 1H), 7.90 (ddd, *J* = 8.0, 4.8, 2.5 Hz, 2H), 7.85 (dd, *J* = 8.6, 2.5 Hz, 1H), 7.32 (dd, *J* = 8.0, 2.0 Hz, 1H), 7.13 (d, *J* = 8.3 Hz, 2H), 6.93 (dd, *J* = 8.6, 4.4 Hz, 4H), 6.83 (d, *J* = 8.9 Hz, 1H), 4.64 (t, *J* = 5.4 Hz, 2H), 4.48 (d, *J* = 6.4 Hz, 1H), 4.23 (s, 1H), 4.11 (ddd, *J* = 27.3, 14.7, 8.9 Hz, 7H), 3.92 (s, 1H), 3.88 (d, *J* = 4.6 Hz, 4H), 3.79 (dd, *J* =

11.5, 4.9 Hz, 1H), 3.73 – 3.65 (m, 2H), 3.55 – 3.46 (m, 1H), 2.71 – 2.60 (m, 1H), 2.57 (t, *J* = 6.9 Hz, 2H), 2.45 (t, *J* = 4.2 Hz, 1H), 2.16 (qd, *J* = 12.1, 4.3 Hz, 1H), 2.02 (tp, *J* = 13.6, 5.1, 4.1 Hz, 4H).

^{13}C NMR (101 MHz, DMSO-*d*$_6$) δ 175.00, 173.99, 170.74, 165.35, 159.24, 157.78, 149.91, 149.76, 147.80, 147.36, 147.10, 141.89, 138.89, 137.48, 131.73, 130.11, 129.46, 123.06, 120.55, 120.40, 119.02, 114.75, 113.22, 111.24, 106.77, 105.33, 81.34, 69.06, 66.52, 62.68, 53.89, 49.97, 48.72, 46.96, 44.64, 41.02, 31.86, 28.90, 26.47, 24.46.

YW-N-6

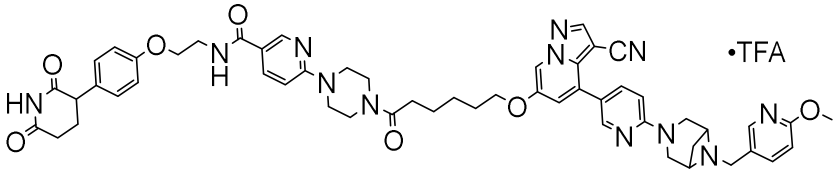

^{1}H NMR (400 MHz, DMSO-*d*$_6$) δ 10.83 (s, 1H), 9.40 (q, *J* = 5.2 Hz, 1H), 8.77 – 8.67 (m, 2H), 8.66 – 8.53 (m, 4H), 8.49 (d, *J* = 2.3 Hz, 1H), 8.46 – 8.36 (m, 3H), 8.29 (d, *J* = 2.4 Hz, 1H), 8.02 (dd, *J* = 9.0, 2.5 Hz, 1H), 7.97 (dt, *J* = 8.8, 3.1 Hz, 1H), 7.89 (dt, *J* = 8.7, 3.0 Hz, 3H), 7.84 (dd, *J* = 8.6, 2.5 Hz, 1H), 7.28 (dt, *J* = 7.1, 2.5 Hz, 2H), 7.13 (d, *J* = 8.4 Hz, 3H), 6.93 (dd, *J* = 8.5, 5.0 Hz, 5H), 6.82 (dd, *J* = 8.9, 2.8 Hz, 2H), 4.63 (t, *J* = 5.4 Hz, 4H), 4.47 (d, *J* = 6.4 Hz, 3H), 4.22 (s, 1H), 4.18 – 4.00 (m, 11H), 3.87 (s, 8H), 3.78 (dd, *J* = 11.5, 4.9 Hz, 1H), 3.72 – 3.46 (m, 11H), 2.69 (s, 1H), 2.63 (dd, *J* = 11.7, 5.3 Hz, 1H), 2.25 (td, *J* = 7.2, 2.2 Hz, 2H), 2.16 (dd, *J* = 12.7, 4.2 Hz, 1H), 2.12 – 2.03 (m, 2H), 2.03 – 1.93 (m, 2H), 1.78 (q, *J* = 8.4 Hz, 4H), 1.58 (p, *J* = 7.7 Hz, 4H), 1.53 – 1.38 (m, 4H), 1.36 – 1.15 (m, 4H).

YW-N-7

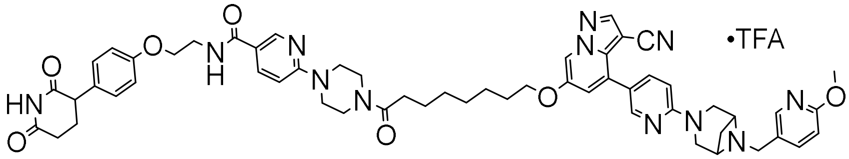

^{1}H NMR (400 MHz, DMSO-d_6) δ 9.35 (q, *J* = 5.4 Hz, 1H), 8.62 (t, *J* = 4.0 Hz, 1H), 8.57 – 8.45 (m, 2H), 8.34 (dd, *J* = 14.5, 2.4 Hz, 1H), 7.97 (dd, *J* = 9.0, 2.4 Hz, 1H), 7.82 (ddd, *J* = 7.8, 4.5, 2.3 Hz, 1H), 7.77 (dd, *J* = 8.6, 2.4 Hz, 1H), 7.22 (d, *J* = 7.9 Hz, 2H), 7.06 (d, *J* = 8.2 Hz, 2H), 6.86 (d, *J* = 8.2 Hz, 3H), 6.76 (d, *J* = 8.8 Hz, 1H), 4.57 (d, *J* = 5.5 Hz, 2H), 4.41 (d, *J* = 6.3 Hz, 1H), 4.15 (s, 1H), 4.10 – 3.91 (m, 5H), 3.85 (s, 1H), 3.82 (s, 2H), 3.80 (s, 1H), 3.71 (dd, *J* = 11.3, 4.9 Hz, 1H), 3.65 – 3.35 (m, 8H), 2.65 – 2.51 (m, 1H), 2.38 (s, 1H), 2.29 (t, *J* = 7.5 Hz, 2H), 2.15 – 1.87 (m, 3H), 1.70 (p, *J* = 6.2 Hz, 2H), 1.46 (p, *J* = 7.3 Hz, 2H), 1.38 (d, *J* = 9.2 Hz, 2H), 1.26 (dd, *J* = 10.3, 4.9 Hz, 2H).

^{13}C NMR (101 MHz, DMSO-d_6) δ 174.92, 173.91, 171.39, 165.33, 164.62, 157.81, 150.06, 149.75, 147.76, 147.15, 141.84, 138.90, 137.55, 131.71, 130.07, 123.03, 119.08, 114.81, 111.22, 111.22, 106.87, 81.34, 69.62, 66.57, 62.76, 53.87, 50.03, 48.73, 46.96, 44.95, 44.71, 43.75, 32.69, 31.81, 29.16, 28.99, 28.84, 26.47, 25.79, 25.10.

YW-N-8

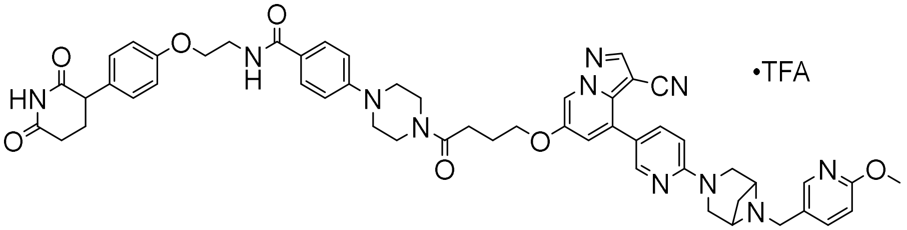

^{1}H NMR (400 MHz, DMSO-d_6) δ 9.43 (q, *J* = 5.1 Hz, 1H), 8.73 (dd, *J* = 7.5, 2.1 Hz, 1H), 8.59 (d, *J* = 10.8 Hz, 1H), 8.47 – 8.34 (m, 3H), 8.29 (d, *J* = 2.5 Hz, 1H), 7.89 (dd, *J* = 8.7, 2.5 Hz, 1H), 7.77 (d, *J* = 8.6 Hz, 2H), 7.31 (dd, *J* = 8.4, 2.1 Hz, 1H), 7.13 (d, *J* = 8.4 Hz, 2H), 7.04 – 6.87 (m, 5H), 6.83 (d, *J* = 8.9 Hz, 1H), 4.64 (t, *J* = 5.1 Hz, 2H), 4.48 (d, *J* = 6.4 Hz, 1H), 4.23 (s, 1H), 4.11 (ddd, *J* = 26.8, 13.2, 7.1 Hz, 6H), 3.90 (d, *J* = 19.9 Hz, 4H), 3.79 (dd, *J* = 11.3, 4.9 Hz, 1H), 3.61 (q, *J* = 6.0 Hz, 6H), 3.52 (q, *J* = 6.4, 6.0 Hz, 1H), 3.28 (dt, *J* = 20.3, 5.0 Hz, 4H), 2.71 – 2.54 (m, 3H), 2.24 – 1.91 (m, 5H).

^{13}C NMR (101 MHz, DMSO-d_6) δ 174.92, 173.91, 170.60, 166.61, 164.62, 158.97, 158.61, 157.83, 152.90, 149.92, 149.75, 149.03, 147.79, 147.06, 141.84, 138.86, 136.25, 131.67, 130.06, 129.47, 129.02, 124.27, 123.05, 120.58, 120.37, 119.82, 114.79, 114.24, 113.30, 111.22, 105.86, 105.34, 81.37, 69.13, 66.59, 62.76, 53.87, 50.03, 48.72, 47.79, 47.50, 46.96, 44.83, 43.75, 31.81, 28.84, 26.47, 24.52.

YW-N-9

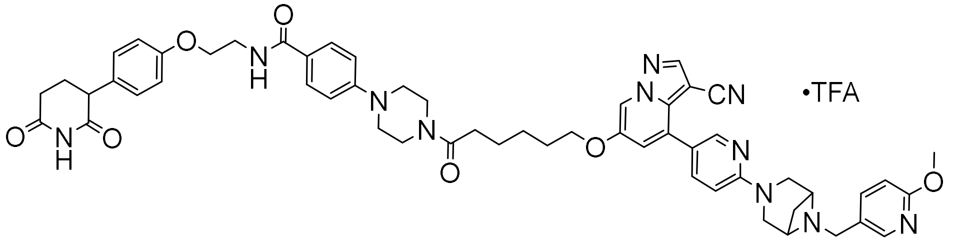

^{1}H NMR (400 MHz, DMSO-d_6) δ 9.42 (q, *J* = 5.7, 4.7 Hz, 1H), 8.70 (dd, *J* = 6.1, 2.1 Hz, 1H), 8.59 (d, *J* = 10.5 Hz, 1H), 8.51 – 8.24 (m, 3H), 8.00 – 7.81 (m, 2H), 7.76 (d, *J* = 8.4 Hz, 2H), 7.27 (dd, *J* = 6.9, 2.0 Hz, 1H), 7.13 (d, *J* = 8.3 Hz, 2H), 7.01 – 6.87 (m, 5H), 6.81 (d, *J* = 8.9 Hz, 1H), 4.64 (d, *J* = 5.8 Hz, 2H), 4.47 (d, *J* = 6.3 Hz, 2H), 4.26 – 3.99 (m, 7H), 3.90 (d, *J* = 17.5 Hz, 4H), 3.78 (dd, *J* = 11.3, 4.9 Hz, 1H), 3.69 – 3.45 (m, 6H), 3.26 (dt, *J* = 22.3, 5.2 Hz, 4H), 2.65 (ddd, *J* = 17.0, 11.5, 5.4 Hz, 1H), 2.39 (t, *J* = 7.2 Hz, 2H), 2.08 (dddd, *J* = 43.0, 18.0, 9.2, 6.0 Hz, 3H), 1.79 (p, *J* = 6.2 Hz, 2H), 1.60 (p, *J* = 7.4 Hz, 2H), 1.48 (tt, *J* = 9.0, 5.8 Hz, 2H), 1.24 (d, *J* = 3.5 Hz, 1H).

^{13}C NMR (101 MHz, DMSO-d_6) δ 174.92, 173.91, 171.13, 166.60, 164.61, 158.79, 157.83, 152.92, 150.05, 149.75, 149.03, 147.97, 147.05, 141.84, 141.32, 138.75, 136.21, 131.67, 130.06, 129.53, 129.00, 124.26, 122.98, 120.57, 120.38, 114.79, 114.24, 113.18, 111.22, 105.67, 105.22, 81.36, 69.60, 66.59, 62.78, 53.88, 50.03, 48.70, 47.91, 47.55, 46.96, 44.93, 43.70, 32.61, 31.81, 28.76, 26.47, 25.71, 24.88.

YW-N-10

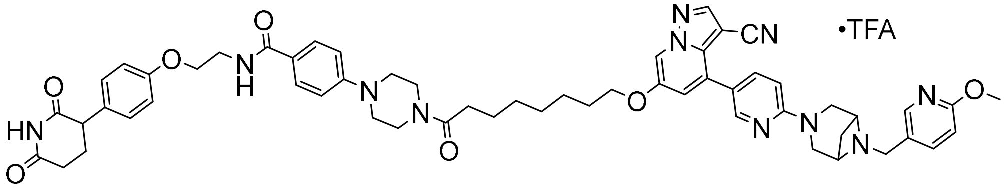

^{1}H NMR (400 MHz, DMSO-d_6) δ 9.37 (q, J = 5.3 Hz, 1H), 8.69 (dd, J = 6.2, 2.1 Hz, 1H), 8.58 (s, 1H), 8.46 – 8.33 (m, 2H), 7.88 (dd, J = 8.7, 2.5 Hz, 1H), 7.76 (d, J = 8.5 Hz, 2H), 7.28 (dd, J = 7.2, 2.1 Hz, 1H), 7.12 (d, J = 8.4 Hz, 2H), 6.99 – 6.87 (m, 5H), 6.81 (d, J = 8.8 Hz, 1H), 4.62 (t, J = 6.2 Hz, 2H), 4.47 (d, J = 6.3 Hz, 2H), 4.21 (s, 1H), 4.07 (dd, J = 15.4, 9.6 Hz, 6H), 3.88 (d, J = 4.4 Hz, 4H), 3.78 (dd, J = 11.3, 4.9 Hz, 2H), 3.25 (dt, J = 22.2, 5.2 Hz, 4H), 2.92 – 2.80 (m, 1H), 2.72 – 2.58 (m, 1H), 2.35 (t, J = 7.4 Hz, 2H), 2.23 – 2.10 (m, 1H), 2.03 (ddt, J = 22.3, 8.7, 4.2 Hz, 2H), 1.76 (p, J = 6.5 Hz, 2H), 1.53 (p, J = 7.4 Hz, 2H), 1.48 – 1.40 (m, 2H), 1.40 – 1.28 (m, 4H), 1.25 (d, J = 9.4 Hz, 1H).

^{13}C NMR (101 MHz, DMSO-d_6) δ 174.92, 173.92, 171.22, 166.60, 157.83, 152.93, 150.07, 149.75, 148.04, 147.04, 141.84, 138.73, 131.67, 130.07, 129.01, 124.25, 123.00, 120.58, 114.79, 114.25, 111.23, 105.18, 81.35, 69.62, 66.60, 62.79, 53.89, 50.03, 48.70, 47.91, 47.54, 46.96, 44.92, 32.65, 31.82, 29.16, 28.98, 28.84, 26.47, 25.79, 25.14.

YW-N-11

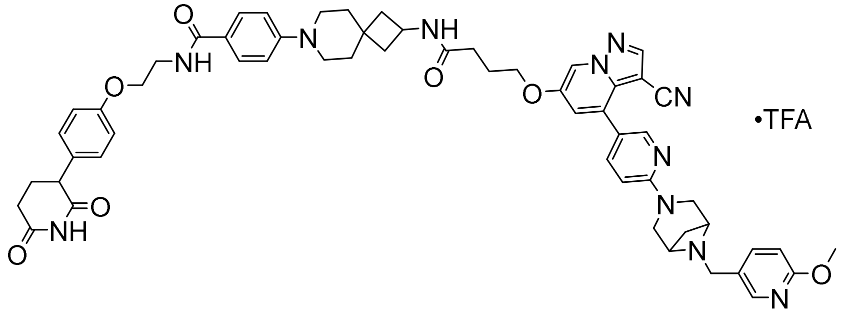

^{1}H NMR (400 MHz, DMSO-d_6) δ 9.38 (q, *J* = 5.3 Hz, 1H), 8.71 (dd, *J* = 6.8, 2.1 Hz, 1H), 8.60 (d, *J* = 10.9 Hz, 1H), 8.52 – 8.24 (m, 3H), 8.12 (dd, *J* = 7.7, 2.9 Hz, 1H), 8.01 – 7.79 (m, 2H), 7.73 (d, *J* = 8.5 Hz, 2H), 7.27 (dd, *J* = 9.4, 2.1 Hz, 1H), 7.19 – 7.11 (m, 2H), 6.93 (td, *J* = 7.1, 3.7 Hz, 5H), 6.81 (d, *J* = 8.8 Hz, 1H), 4.63 (d, *J* = 5.8 Hz, 2H), 4.46 (d, *J* = 6.3 Hz, 2H), 4.22 (h, *J* = 7.7 Hz, 2H), 4.16 – 3.96 (m, 6H), 3.88 (d, *J* = 4.4 Hz, 4H), 3.78 (dd, *J* = 11.3, 4.9 Hz, 1H), 3.54 (dq, *J* = 34.8, 6.1 Hz, 3H), 3.19 (dt, *J* = 39.5, 5.3 Hz, 4H), 2.62 (dd, *J* = 11.6, 5.4 Hz, 1H), 2.45 (t, *J* = 4.3 Hz, 1H), 2.30 – 2.21 (m, 2H), 2.20 – 2.09 (m, 3H), 2.01 (ddt, *J* = 14.9, 11.9, 8.0 Hz, 4H), 1.69 – 1.57 (m, 4H), 1.57 – 1.47 (m, 2H), 1.34 – 1.06 (m, 1H).

^{13}C NMR (101 MHz, DMSO-d_6) δ 174.92, 173.91, 170.94, 166.65, 157.83, 152.98, 149.75, 149.04, 147.93, 147.08, 141.84, 138.76, 136.25, 131.66, 130.06, 129.02, 114.78, 114.29, 111.22, 105.25, 81.37, 69.24, 66.61, 62.77, 53.89, 50.03, 48.70, 46.96, 45.05, 43.70, 35.35, 31.82, 26.47, 24.89.

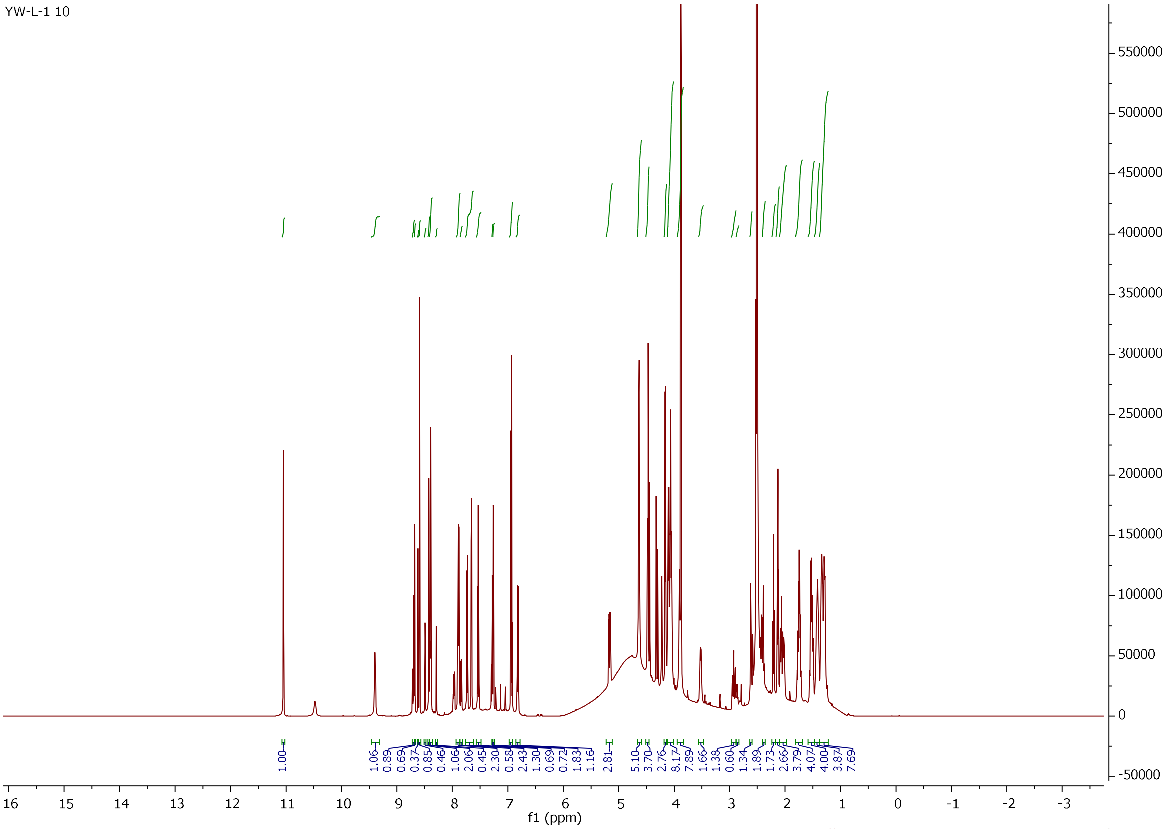
YW-L-1 10
1.00
1.06
0.89
0.69
0.37
0.85
0.46
1.06
2.06
0.45
2.30
0.58
2.43
1.30
0.69
0.72
1.83
1.16
2.81
5.10
3.70
2.76
8.17
7.89
1.66
1.38
0.60
1.34
1.89
1.73
2.66
3.79
4.07
4.00
3.87
7.69
f1 (ppm)
16 15 14 13 12 11 10 9 8 7 6 5 4 3 2 1 0 -1 -2 -3
550000 500000 450000 400000 350000 300000 250000 200000 150000 100000 50000 0 -50000

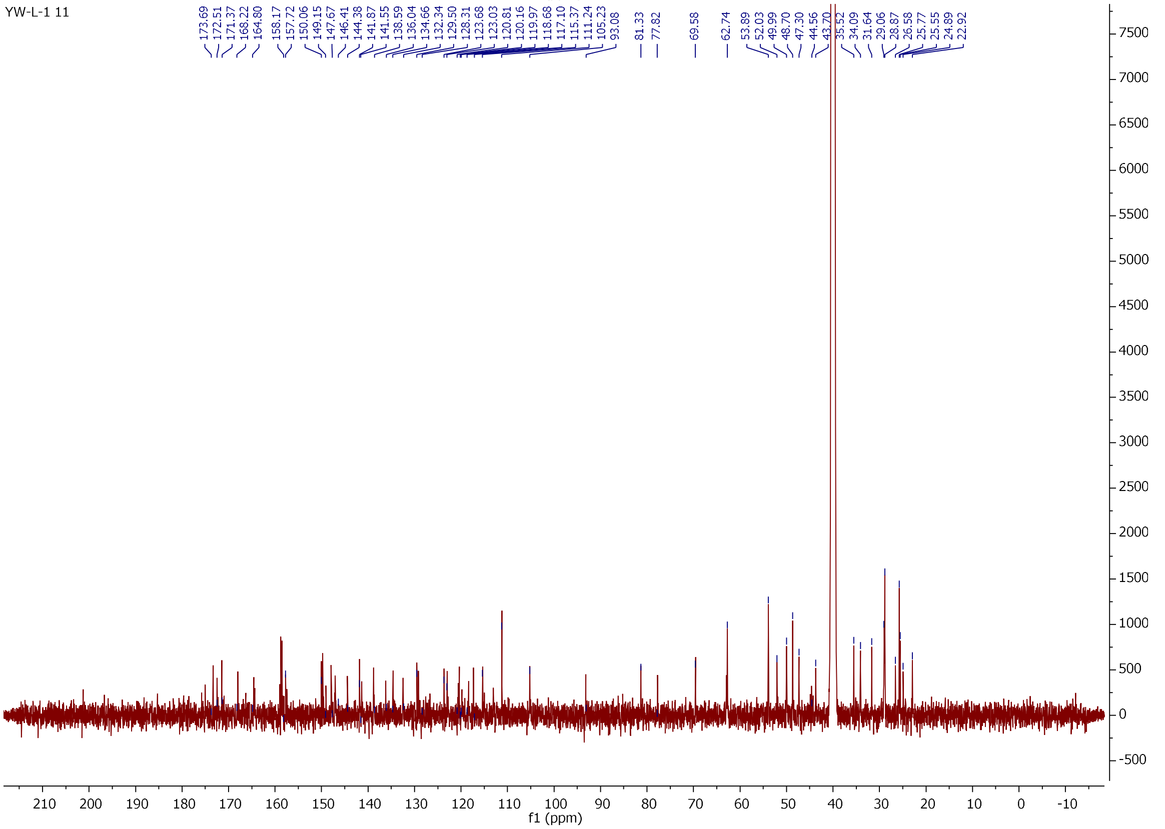
YW-L-1 11
173.69
172.51
171.37
168.22
164.80
158.17
157.72
150.06
149.15
147.67
146.41
144.38
141.87
141.55
138.59
136.04
134.66
132.34
129.50
128.31
123.68
123.03
120.81
120.16
119.97
118.68
117.10
115.37
111.24
105.23
93.08
81.33
77.82
69.58
62.74
53.89
52.03
49.99
48.70
47.30
44.56
43.70
35.62
34.09
31.64
29.06
28.87
26.58
25.77
25.55
24.89
22.92
f1 (ppm)
210 200 190 180 170 160 150 140 130 120 110 100 90 80 70 60 50 40 30 20 10 0 -10
7500 7000 6500 6000 5500 5000 4500 4000 3500 3000 2500 2000 1500 1000 500 0 -500

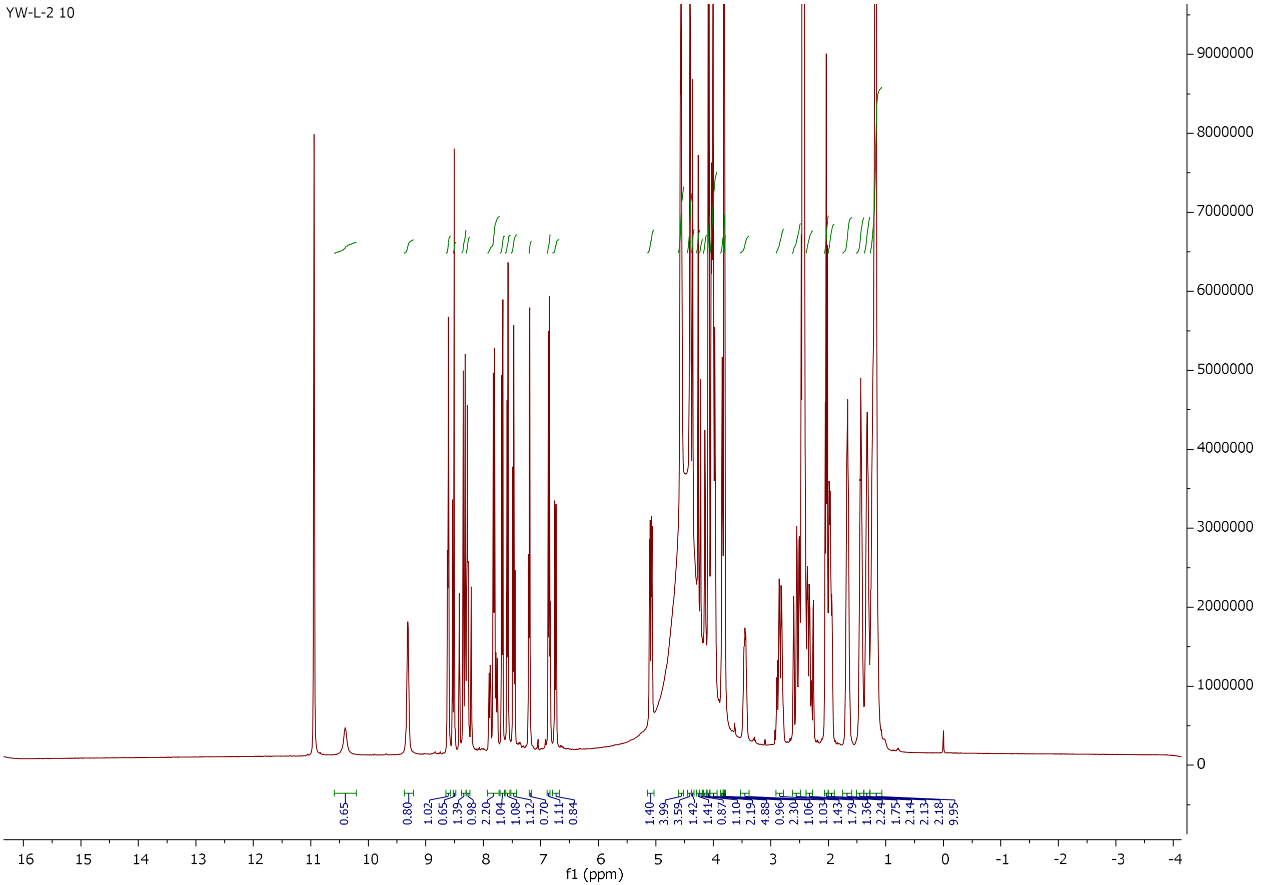
YW-L-2 10
0.65
0.80
1.02
0.65
1.39
0.98
2.20
1.04
1.08
1.12
0.70
1.11
0.84
1.40
3.99
3.59
1.42
1.41
0.87
1.10
2.19
4.88
0.96
2.30
1.06
1.03
1.43
1.79
1.36
2.24
1.75
2.14
2.13
2.18
9.95
16
15
14
13
12
11
10
9
8
7
6
5
4
3
2
1
0
-1
-2
-3
-4
f1 (ppm)
9000000
8000000
7000000
6000000
5000000
4000000
3000000
2000000
1000000
0

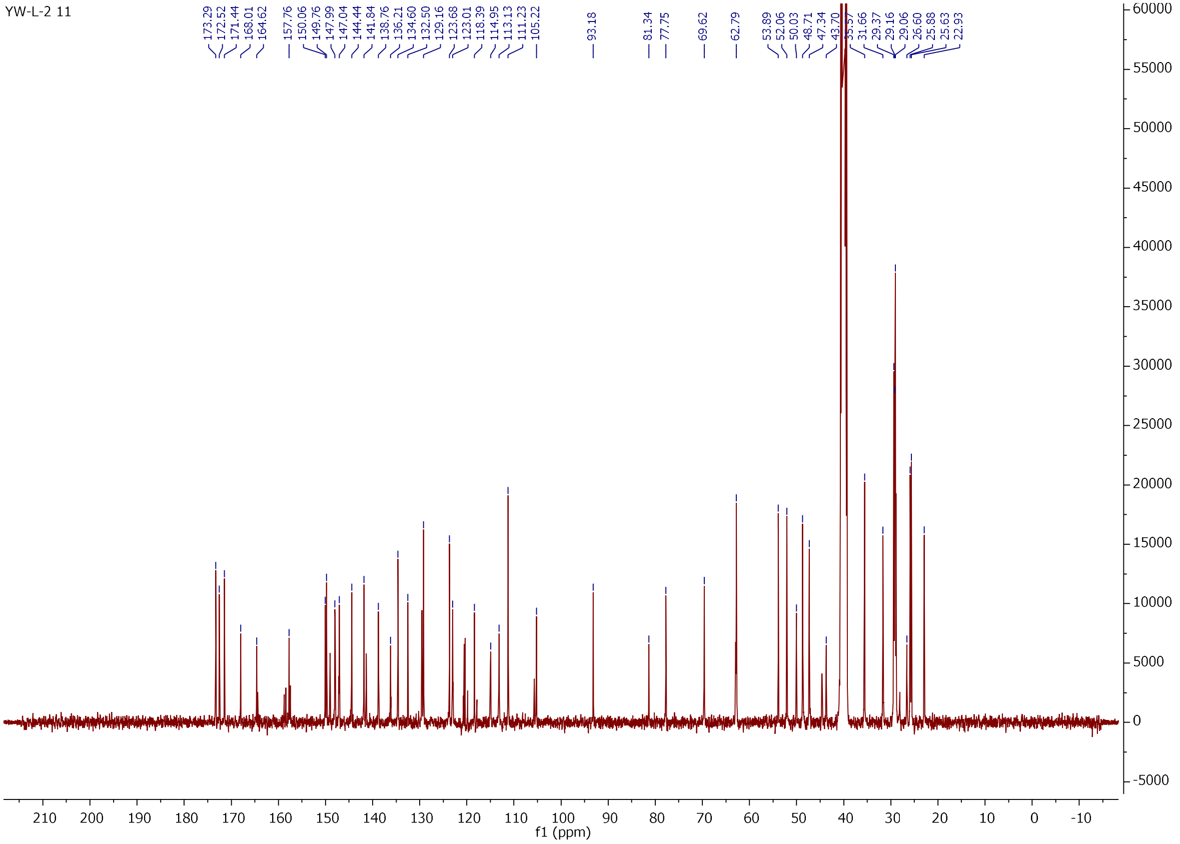
YW-L-2 11
173.29
172.52
171.44
168.01
164.62
157.76
150.06
149.76
147.99
147.04
144.44
141.84
138.76
136.21
134.60
132.50
129.16
123.68
123.01
118.39
114.95
113.13
111.23
105.22
93.18
81.34
77.75
69.62
62.79
53.89
52.06
50.03
48.71
47.34
43.70
35.57
31.66
29.37
29.16
29.06
26.60
25.88
25.63
22.93
210
200
190
180
170
160
150
140
130
120
110
100
90
80
70
60
50
40
30
20
10
0
-10
f1 (ppm)
60000
55000
50000
45000
40000
35000
30000
25000
20000
15000
10000
5000
0
-5000

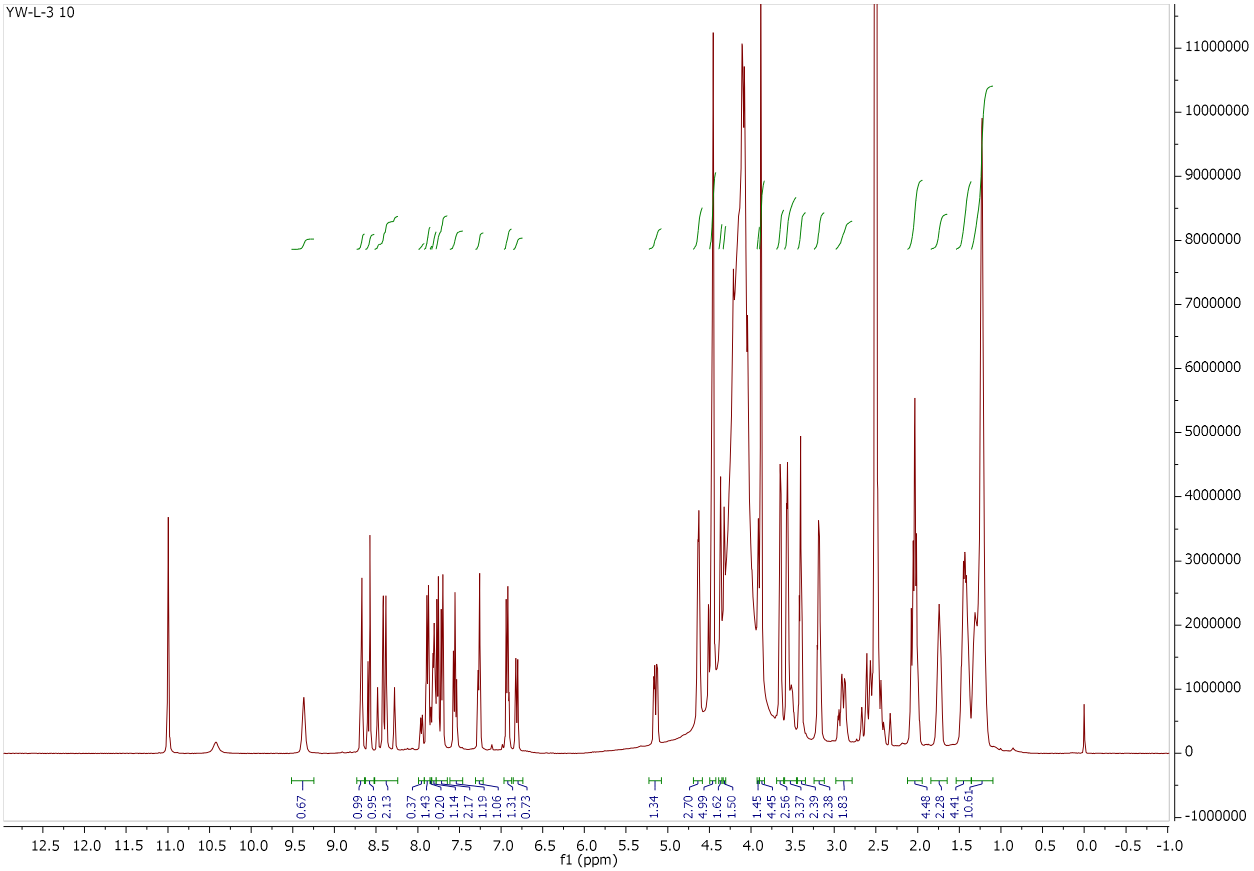
YW-L-3 10
0.67
0.99
0.95
2.13
0.37
1.43
0.20
1.14
2.17
1.19
1.06
1.31
0.73
1.34
2.70
4.99
1.62
1.50
1.45
4.45
2.56
3.37
2.39
2.38
1.83
4.48
2.28
4.41
10.61
12.5 12.0 11.5 11.0 10.5 10.0 9.5 9.0 8.5 8.0 7.5 7.0 6.5 6.0 5.5 5.0 4.5 4.0 3.5 3.0 2.5 2.0 1.5 1.0 0.5 0.0 -0.5 -1.0
f1 (ppm)
11000000
10000000
9000000
8000000
7000000
6000000
5000000
4000000
3000000
2000000
1000000
0
-1000000

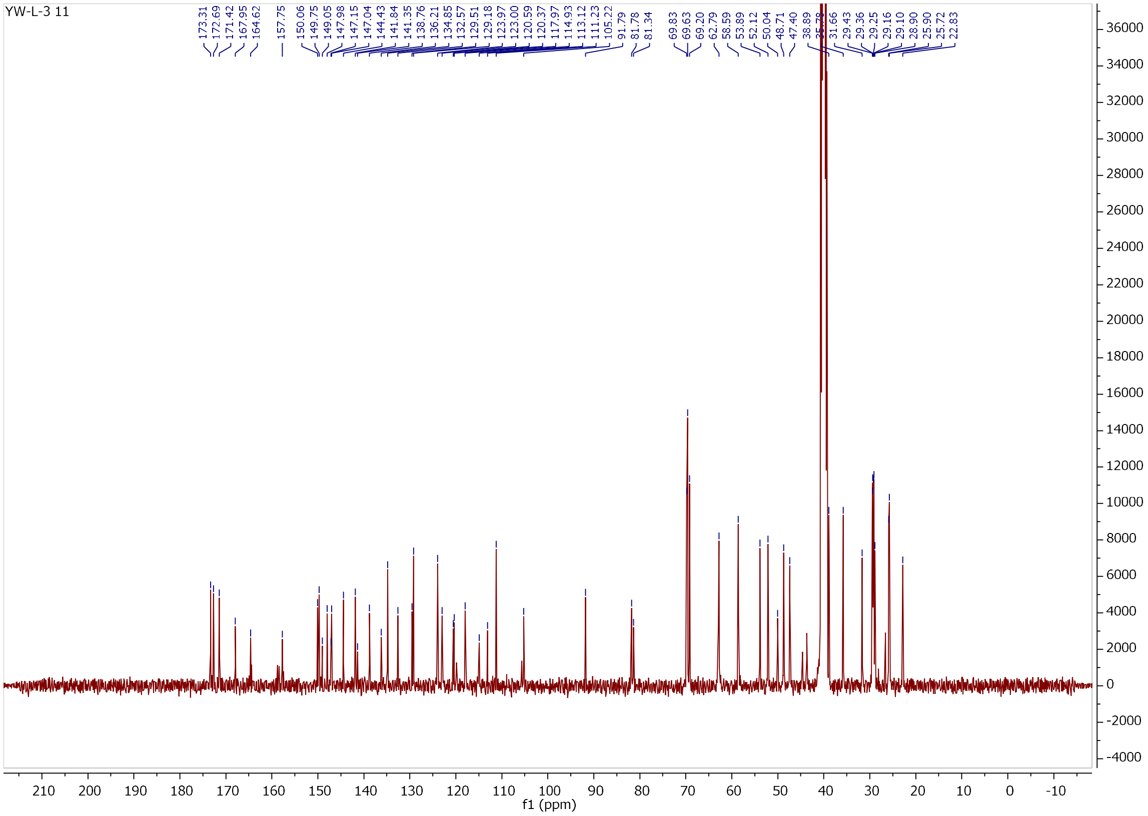
YW-L-3 11
173.31
172.69
171.42
167.95
164.62
157.75
150.06
149.75
149.05
147.98
147.15
147.04
144.43
141.84
141.35
138.76
136.21
134.85
132.57
129.51
129.18
123.97
123.00
120.59
120.37
117.97
114.93
113.12
111.23
105.22
91.79
81.78
81.34
69.83
69.63
69.20
62.79
58.59
53.89
52.12
50.04
48.71
47.40
38.89
35.78
31.66
29.43
29.36
29.25
29.16
29.10
28.90
25.90
25.72
22.83
210 200 190 180 170 160 150 140 130 120 110 100 90 80 70 60 50 40 30 20 10 0 -10
f1 (ppm)
36000
34000
32000
30000
28000
26000
24000
22000
20000
18000
16000
14000
12000
10000
8000
6000
4000
2000
0
-2000
-4000

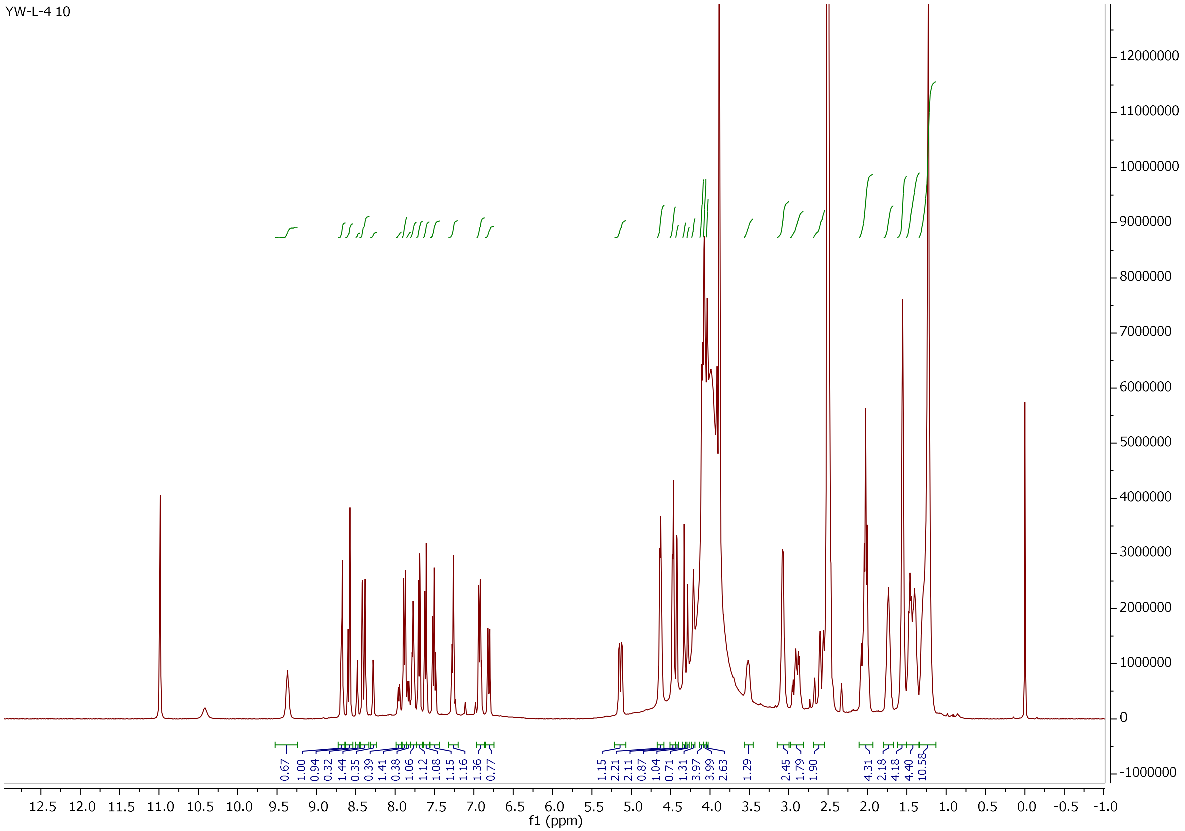
YW-L-4 10
0.67
1.00
0.94
0.32
1.44
0.35
0.39
1.41
0.38
1.06
1.12
1.08
1.15
1.16
1.36
0.77
1.15
2.21
2.11
0.87
1.04
0.71
1.31
3.97
3.99
2.63
1.29
2.45
1.79
1.90
4.31
2.18
4.18
4.40
10.58
f1 (ppm)

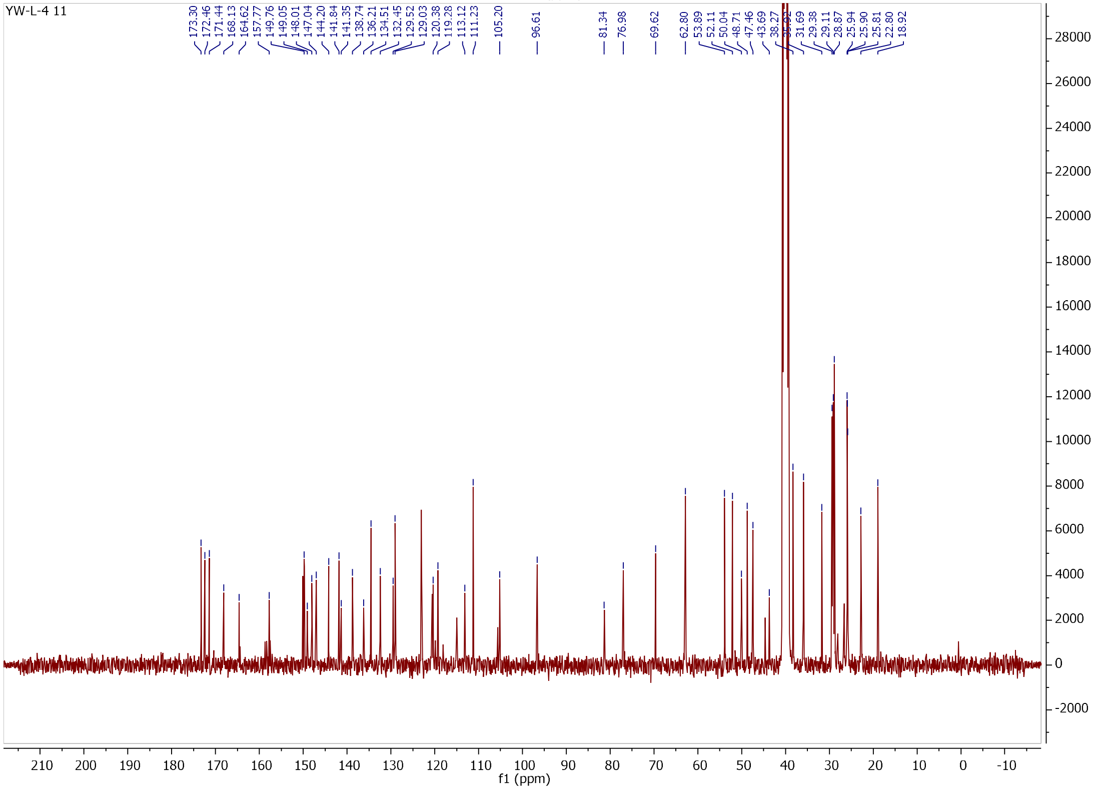
YW-L-4 11
173.30
172.46
171.44
168.13
164.62
157.77
149.76
149.05
148.01
147.04
144.20
141.84
141.35
138.74
136.21
134.51
132.45
129.52
129.03
120.38
119.28
113.12
111.23
105.20
96.61
81.34
76.98
69.62
62.80
53.89
52.11
50.04
48.71
47.46
43.69
38.27
31.69
29.38
29.11
28.87
25.94
25.90
25.81
22.80
18.92
f1 (ppm)

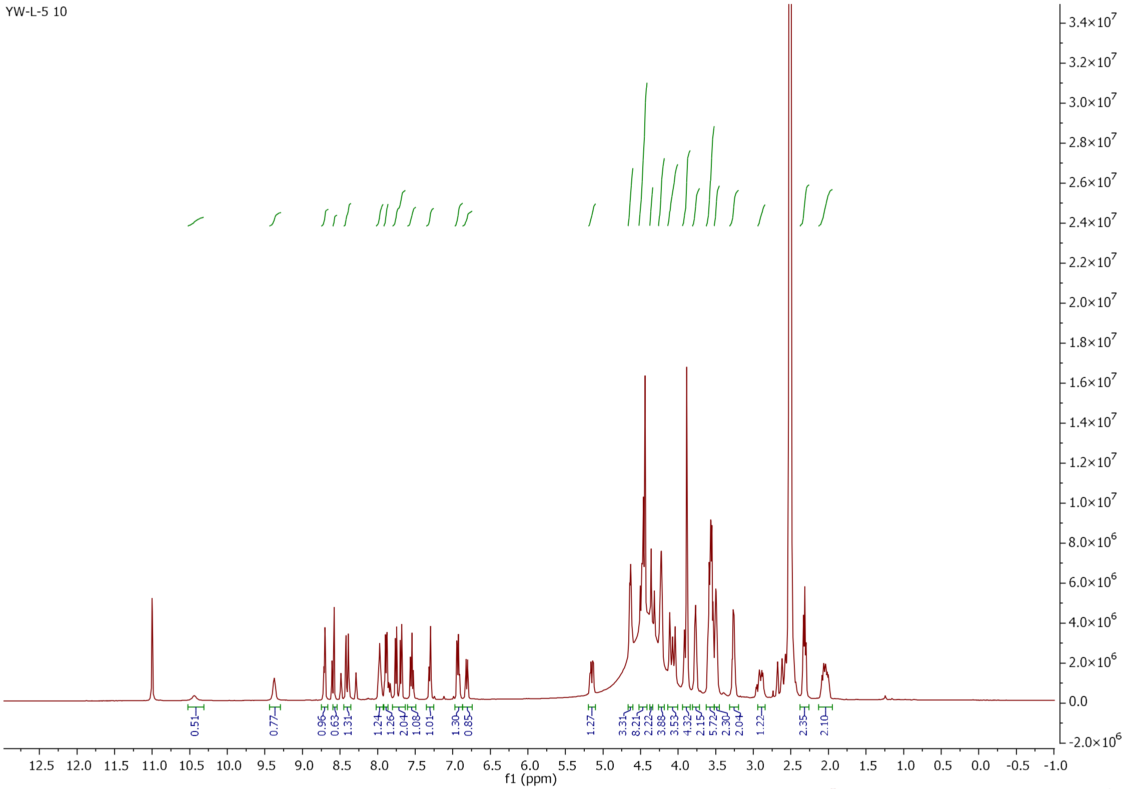
YW-L-5 10
0.51
0.77
0.96
0.63
1.31
1.24
1.26
2.04
1.08
1.01
1.30
0.85
1.27
3.31
8.21
2.22
3.88
3.53
4.32
2.15
5.72
2.30
2.04
1.22
2.35
2.10
3.4×10^7
3.2×10^7
3.0×10^7
2.8×10^7
2.6×10^7
2.4×10^7
2.2×10^7
2.0×10^7
1.8×10^7
1.6×10^7
1.4×10^7
1.2×10^7
1.0×10^7
8.0×10^6
6.0×10^6
4.0×10^6
2.0×10^6
0.0
-2.0×10^6
12.5 12.0 11.5 11.0 10.5 10.0 9.5 9.0 8.5 8.0 7.5 7.0 6.5 6.0 5.5 5.0 4.5 4.0 3.5 3.0 2.5 2.0 1.5 1.0 0.5 0.0 -0.5 -1.0
f1 (ppm)

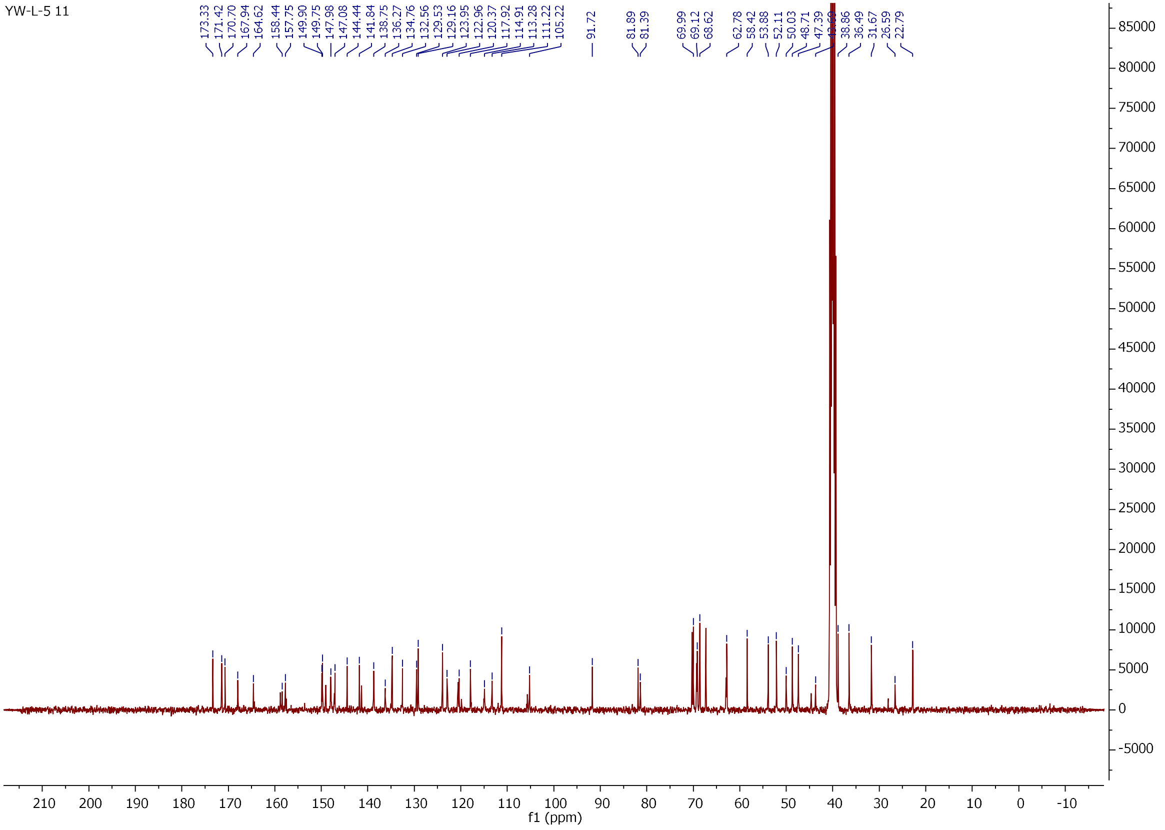
YW-L-5 11
173.33
171.42
170.70
167.94
164.62
158.44
157.75
149.90
149.75
147.98
147.08
144.44
141.84
138.75
136.27
134.76
132.56
129.53
129.16
123.95
122.96
120.37
117.92
114.91
113.28
111.22
105.22
91.72
81.89
81.39
69.99
69.12
68.62
62.78
58.42
53.88
52.11
50.03
48.71
47.39
38.86
36.49
31.67
26.59
22.79
85000
80000
75000
70000
65000
60000
55000
50000
45000
40000
35000
30000
25000
20000
15000
10000
5000
0
-5000
210 200 190 180 170 160 150 140 130 120 110 100 90 80 70 60 50 40 30 20 10 0 -10
f1 (ppm)

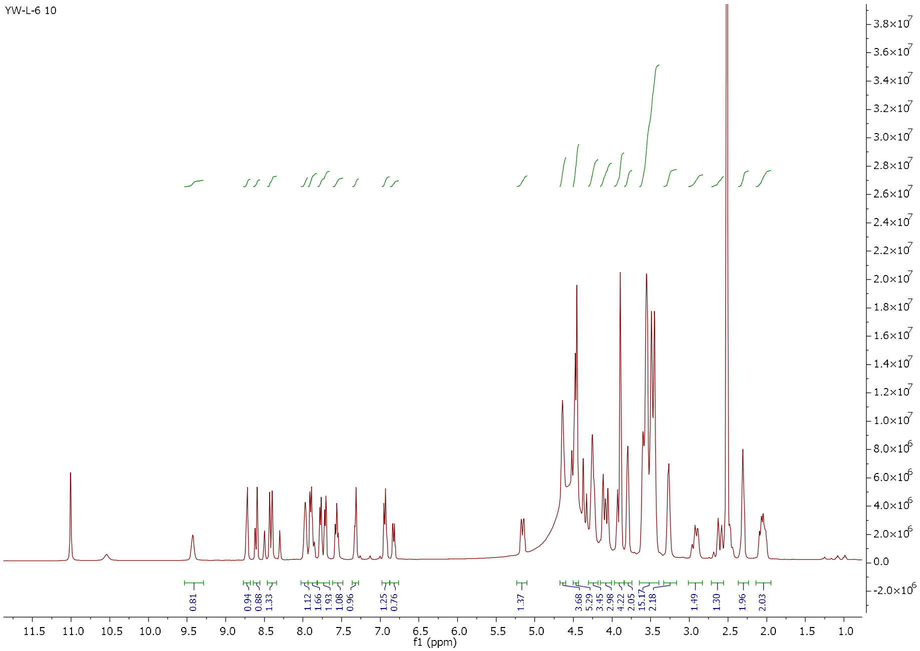
YW-L-6 10
0.81
0.94
0.88
1.33
1.12
1.66
1.93
1.08
0.96
1.25
0.76
1.37
3.68
5.29
3.45
2.98
4.22
2.05
15.17
2.18
1.49
1.30
1.96
2.03
f1 (ppm)
11.5 11.0 10.5 10.0 9.5 9.0 8.5 8.0 7.5 7.0 6.5 6.0 5.5 5.0 4.5 4.0 3.5 3.0 2.5 2.0 1.5 1.0
3.8×10^7 3.6×10^7 3.4×10^7 3.2×10^7 3.0×10^7 2.8×10^7 2.6×10^7 2.4×10^7 2.2×10^7 2.0×10^7 1.8×10^7 1.6×10^7 1.4×10^7 1.2×10^7 1.0×10^7 8.0×10^6 6.0×10^6 4.0×10^6 2.0×10^6 0.0 -2.0×10^6

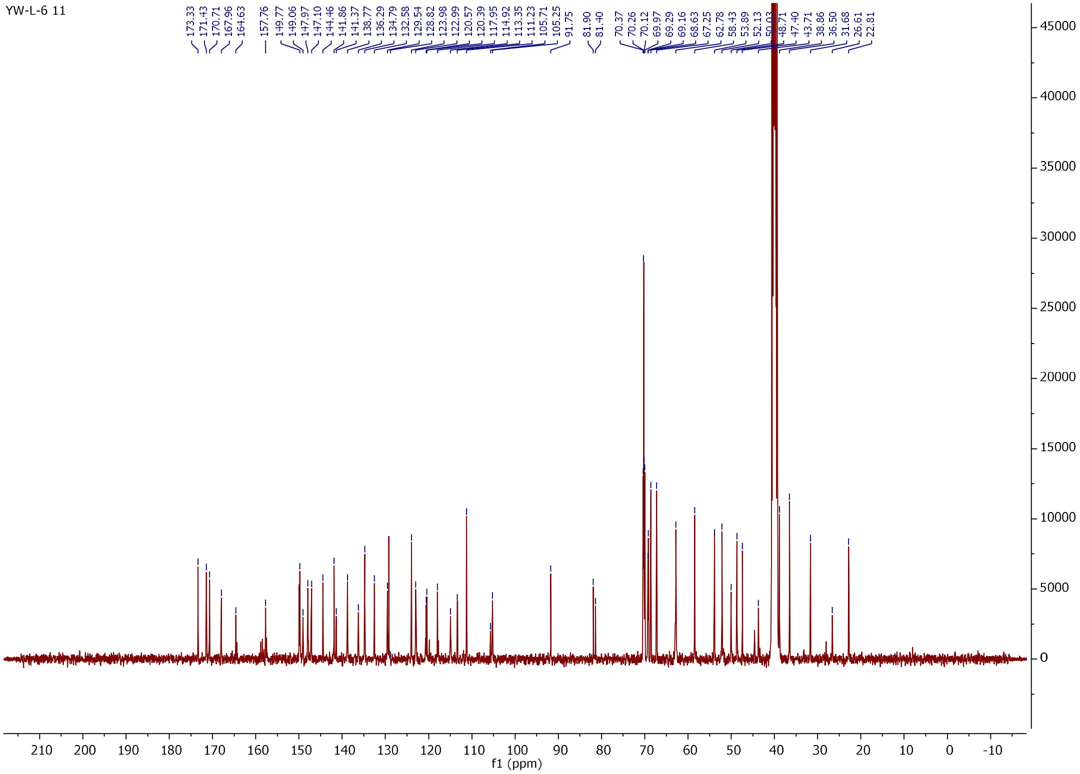
YW-L-6 11
173.33
171.43
170.71
167.96
164.63
157.76
149.77
149.06
147.97
147.10
144.46
141.86
141.37
138.77
136.29
134.79
132.58
129.54
128.82
123.98
122.99
120.57
120.39
117.95
114.92
113.35
111.23
105.71
105.25
91.75
81.90
81.40
70.37
70.26
70.12
69.97
69.29
69.16
68.63
67.25
62.78
58.43
53.89
52.13
50.03
48.71
47.40
43.71
38.86
36.50
31.68
26.61
22.81
f1 (ppm)
210 200 190 180 170 160 150 140 130 120 110 100 90 80 70 60 50 40 30 20 10 0 -10
45000 40000 35000 30000 25000 20000 15000 10000 5000 0

YW-L-7 10

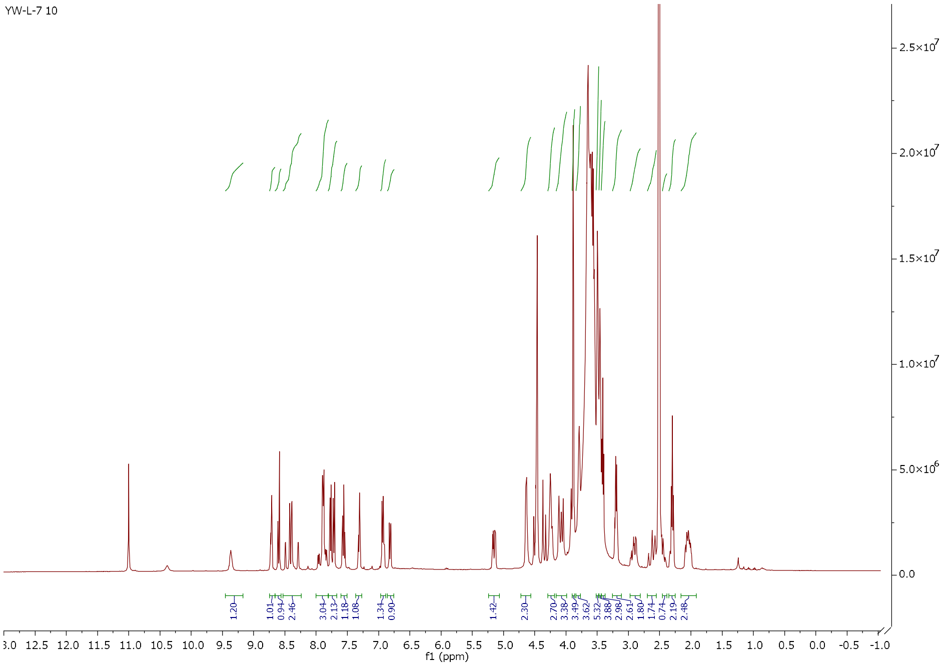

YW-L-7 11

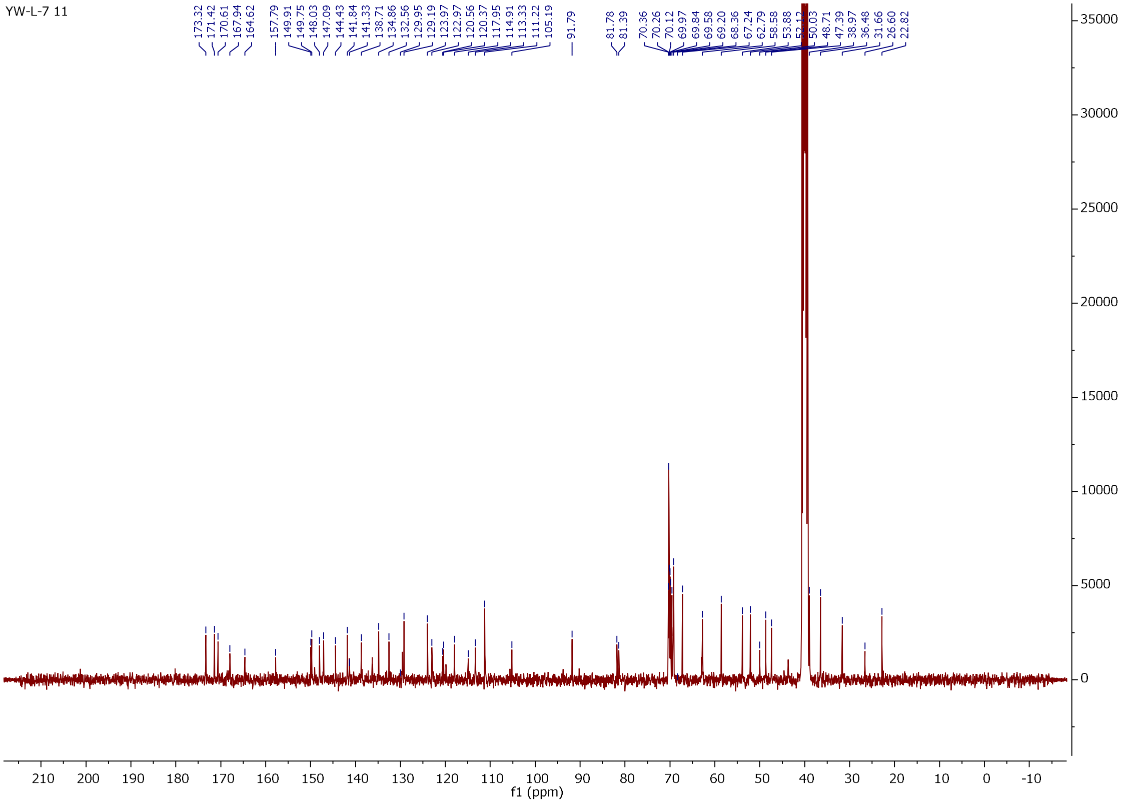

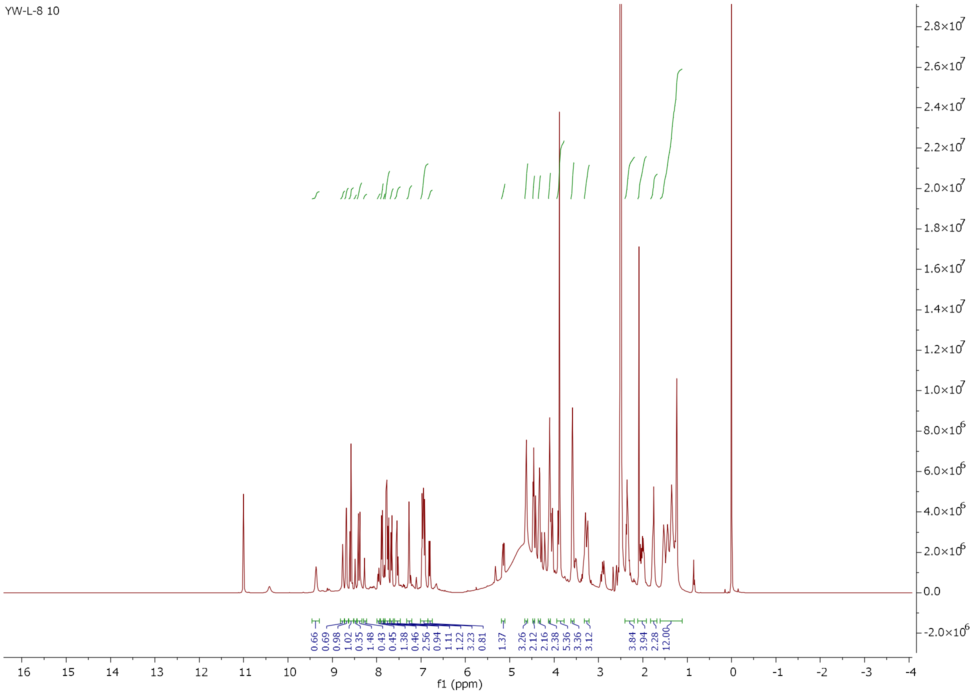
YW-L-8 10
0.66
0.69
0.98
1.02
0.35
1.48
0.43
0.45
1.38
0.46
2.56
0.94
1.11
1.22
3.23
0.81
1.37
3.26
2.12
2.16
2.38
5.36
3.36
3.12
3.84
3.94
2.28
12.00
16 15 14 13 12 11 10 9 8 7 6 5 4 3 2 1 0 -1 -2 -3 -4
f1 (ppm)
2.8×10^7
2.6×10^7
2.4×10^7
2.2×10^7
2.0×10^7
1.8×10^7
1.6×10^7
1.4×10^7
1.2×10^7
1.0×10^7
8.0×10^6
6.0×10^6
4.0×10^6
2.0×10^6
0.0
-2.0×10^6

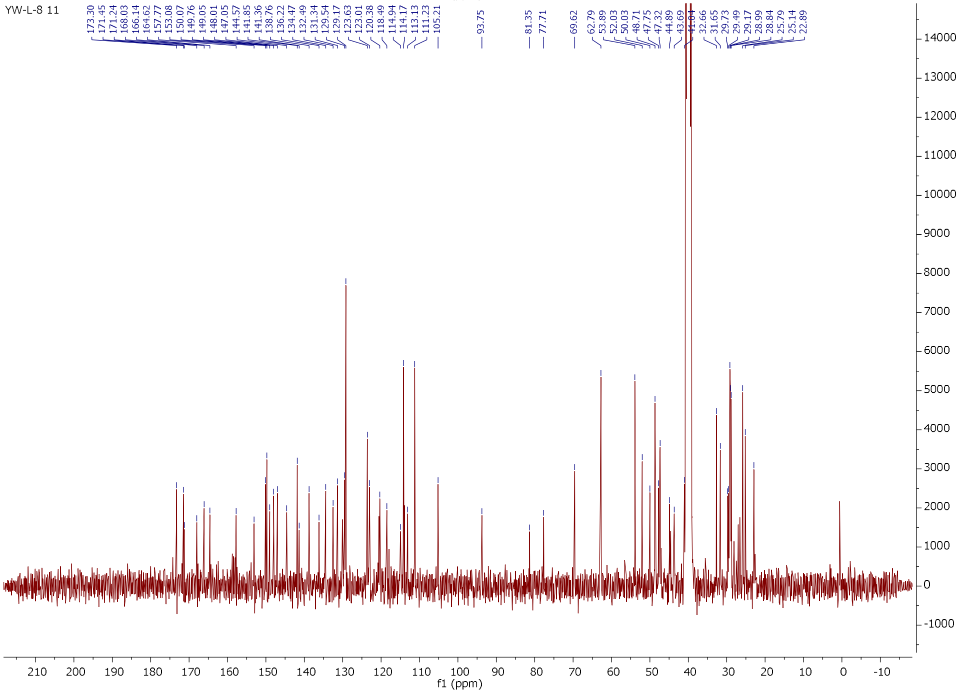
YW-L-8 11
173.30
171.45
171.24
168.03
166.14
164.62
157.77
153.08
150.07
149.76
149.05
148.01
147.05
144.57
141.85
141.36
138.76
136.22
134.47
132.49
131.34
129.54
129.17
123.63
123.01
120.38
118.49
114.94
114.17
113.13
111.23
105.21
93.75
81.35
77.71
69.62
62.79
53.89
52.03
50.03
48.71
47.75
47.32
44.89
43.69
41.04
32.66
31.65
29.73
29.49
29.17
28.99
28.84
25.79
25.14
22.89
210 200 190 180 170 160 150 140 130 120 110 100 90 80 70 60 50 40 30 20 10 0 -10
f1 (ppm)
14000
13000
12000
11000
10000
9000
8000
7000
6000
5000
4000
3000
2000
1000
0
-1000

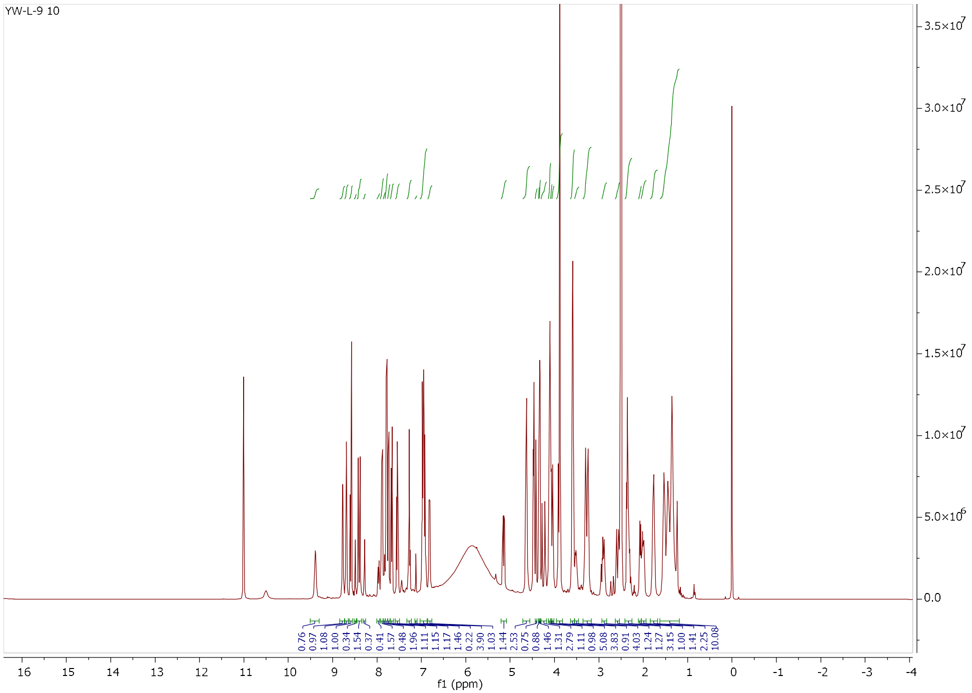
YW-L-9 10
3.5×10⁷
3.0×10⁷
2.5×10⁷
2.0×10⁷
1.5×10⁷
1.0×10⁷
5.0×10⁶
0.0
0.76 0.97 1.08 1.00 0.34 1.54 0.37 0.41 1.57 0.48 1.96 1.11 1.15 1.17 1.46 0.22 3.90 1.03 1.44 2.53 0.75 0.88 1.46 1.31 2.79 1.11 0.98 5.08 3.83 0.91 4.03 1.24 1.27 3.15 1.00 1.41 2.25 10.08
16 15 14 13 12 11 10 9 8 7 6 5 4 3 2 1 0 -1 -2 -3 -4
f1 (ppm)

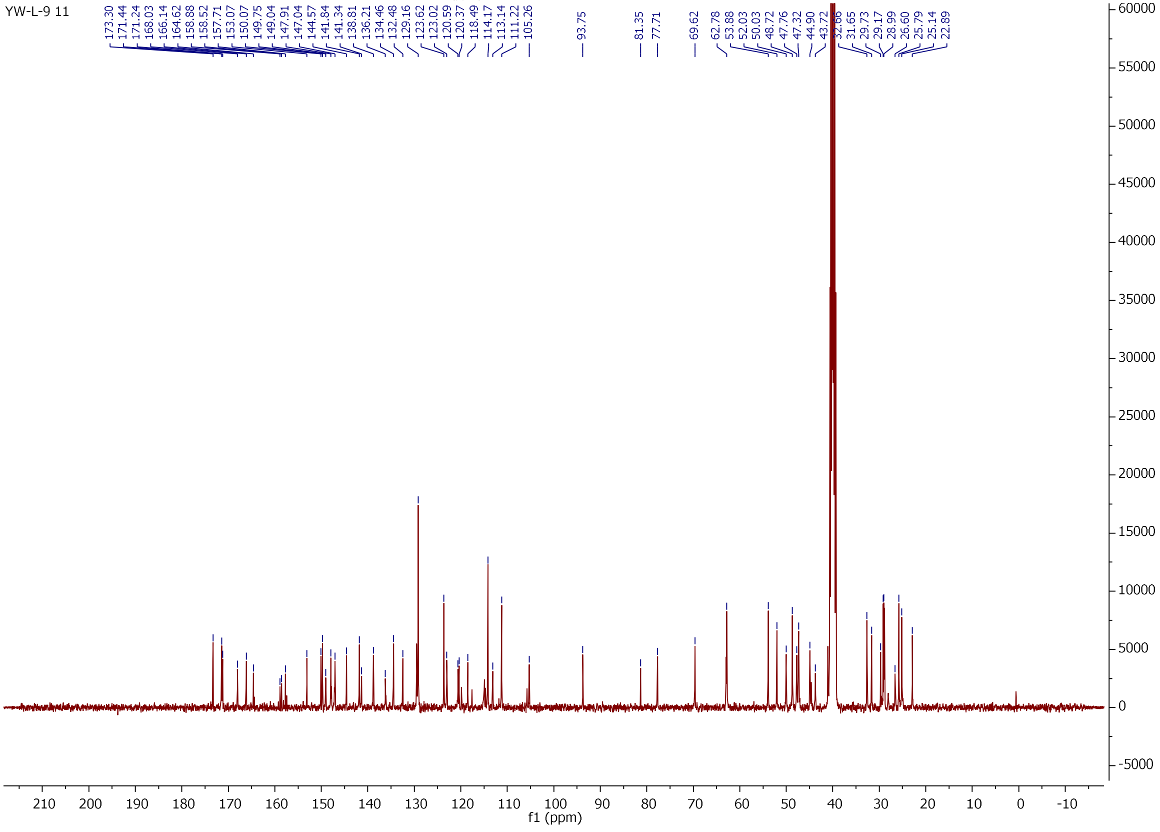
YW-L-9 11
173.30 171.44 171.24 168.03 166.14 164.62 158.88 158.52 157.71 153.07 150.07 149.75 149.04 147.91 147.04 144.57 141.84 141.34 138.81 136.21 134.46 132.48 129.16 123.62 123.02 120.59 120.37 118.49 114.17 113.14 111.22 105.26
93.75
81.35 77.71
69.62
62.78 53.88 52.03 50.03 48.72 47.76 47.32 44.90 43.72 32.66 31.65 29.73 29.17 28.99 26.60 25.79 25.14 22.89
60000
55000
50000
45000
40000
35000
30000
25000
20000
15000
10000
5000
0
-5000
210 200 190 180 170 160 150 140 130 120 110 100 90 80 70 60 50 40 30 20 10 0 -10
f1 (ppm)

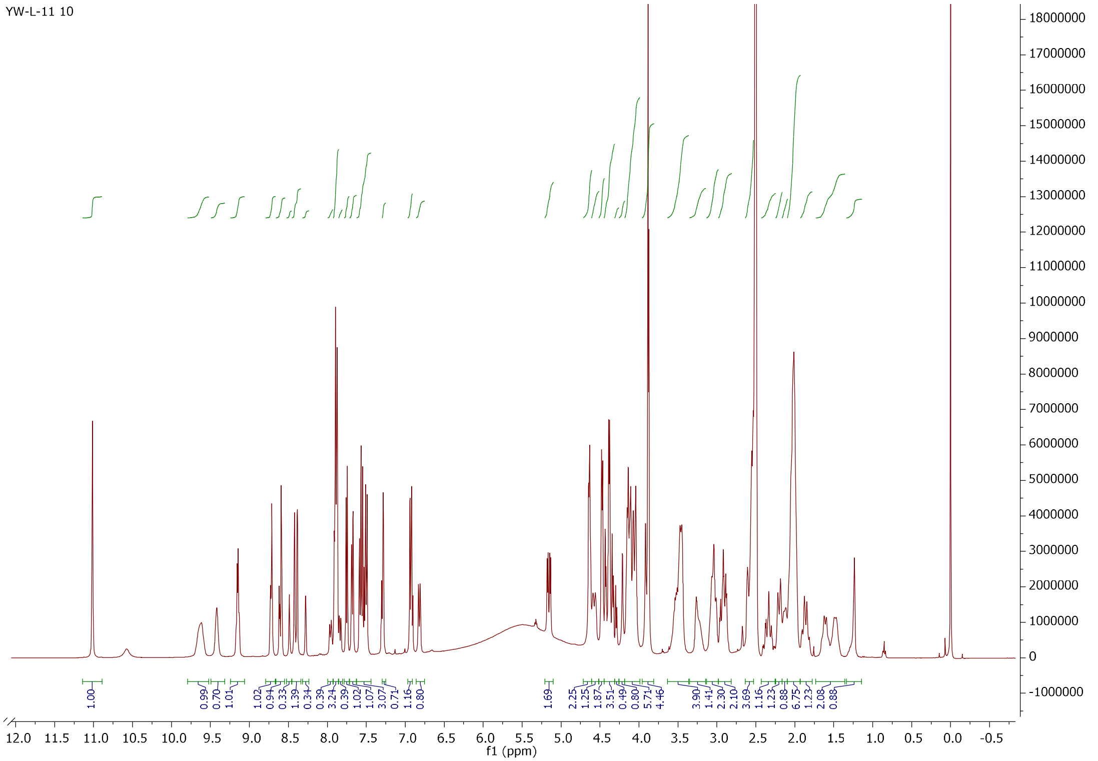
YW-L-11 10
1.00
0.99
0.70
1.01
1.02
0.94
0.33
1.39
0.34
0.39
3.24
0.39
1.02
1.07
3.07
0.71
1.16
0.80
1.69
2.25
1.25
1.87
3.51
0.49
0.80
5.71
4.46
3.90
1.41
2.30
2.10
3.69
1.16
1.23
0.88
6.75
1.23
2.08
0.88
f1 (ppm)

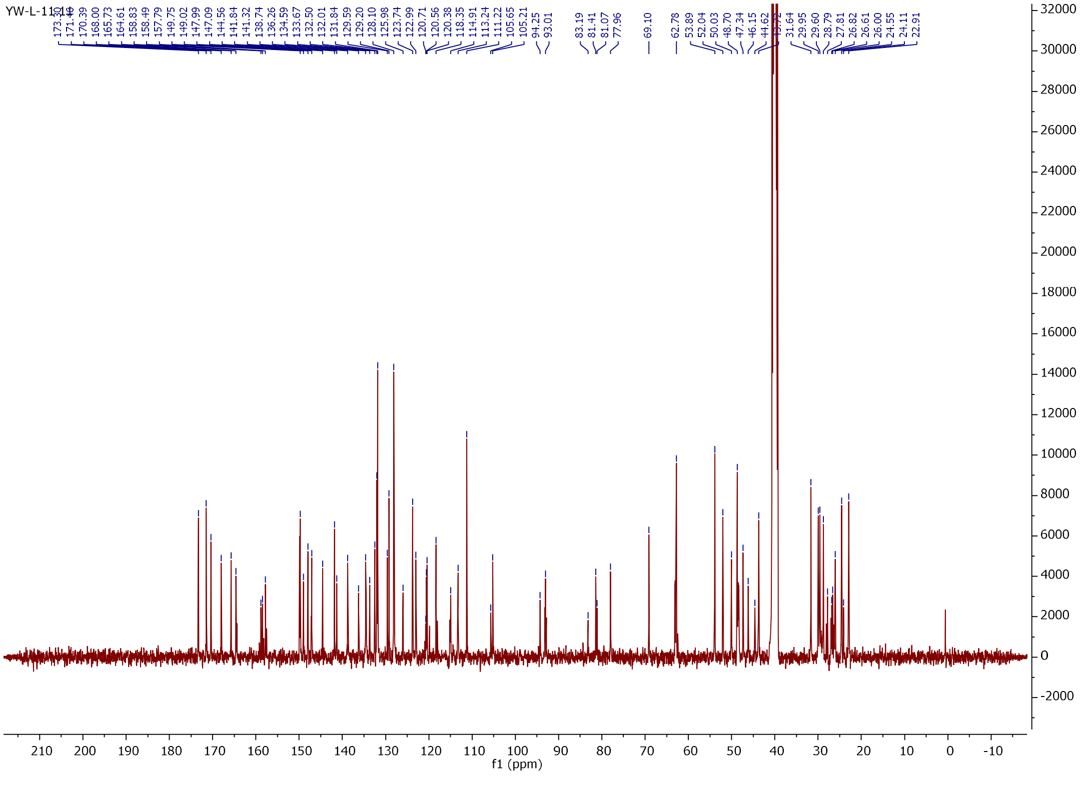
YW-L-11 11
173.30
171.46
170.39
168.00
165.73
164.61
158.83
158.49
157.79
149.75
149.02
147.99
147.09
144.56
141.84
141.32
138.74
136.26
134.59
133.67
132.50
132.01
131.84
129.59
129.20
128.10
125.98
123.74
122.99
120.71
120.56
120.38
118.35
114.91
113.24
111.22
105.65
105.21
94.25
93.01
83.19
81.41
81.07
77.96
69.10
62.78
53.89
52.04
50.03
48.70
47.34
46.15
44.62
43.72
31.64
29.95
29.60
28.79
27.81
26.82
26.61
26.00
24.55
24.11
22.91
f1 (ppm)

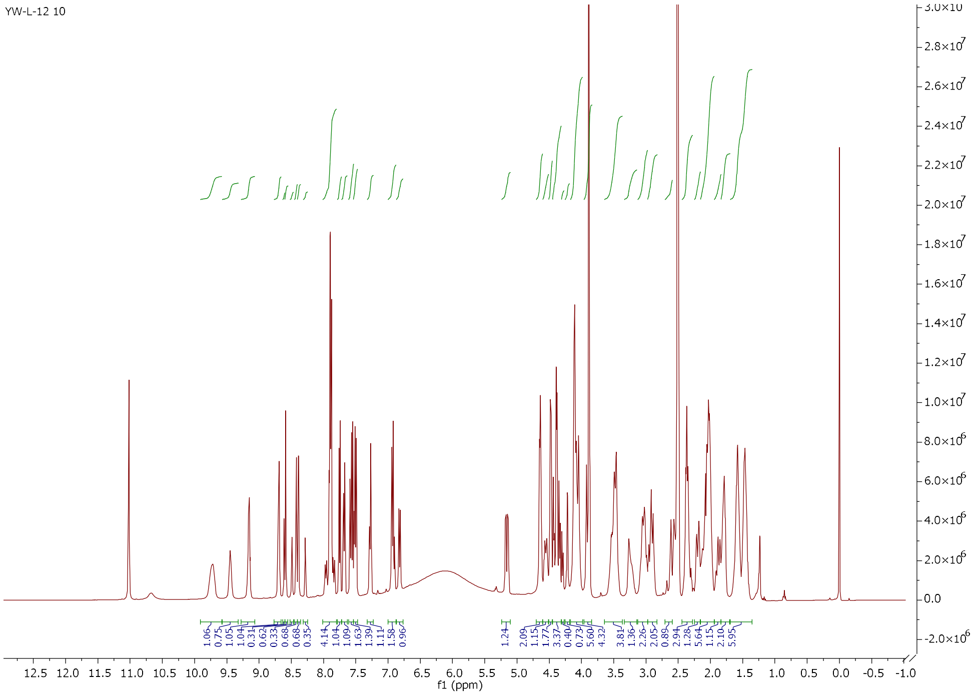
YW-L-12 10
1.06 0.75 1.05 1.04 0.31 0.62 0.33 0.68 0.68 0.35 4.14 1.04 1.09 1.63 1.39 1.11 1.58 0.96 1.24 2.09 1.15 1.77 3.37 0.40 0.73 5.60 4.32 3.81 1.36 2.26 2.05 0.89 2.94 1.28 5.64 1.15 2.10 5.95
12.5 12.0 11.5 11.0 10.5 10.0 9.5 9.0 8.5 8.0 7.5 7.0 6.5 6.0 5.5 5.0 4.5 4.0 3.5 3.0 2.5 2.0 1.5 1.0 0.5 0.0 -0.5 -1.0
f1 (ppm)
3.0×10⁷ 2.8×10⁷ 2.6×10⁷ 2.4×10⁷ 2.2×10⁷ 2.0×10⁷ 1.8×10⁷ 1.6×10⁷ 1.4×10⁷ 1.2×10⁷ 1.0×10⁷ 8.0×10⁶ 6.0×10⁶ 4.0×10⁶ 2.0×10⁶ 0.0 -2.0×10⁶

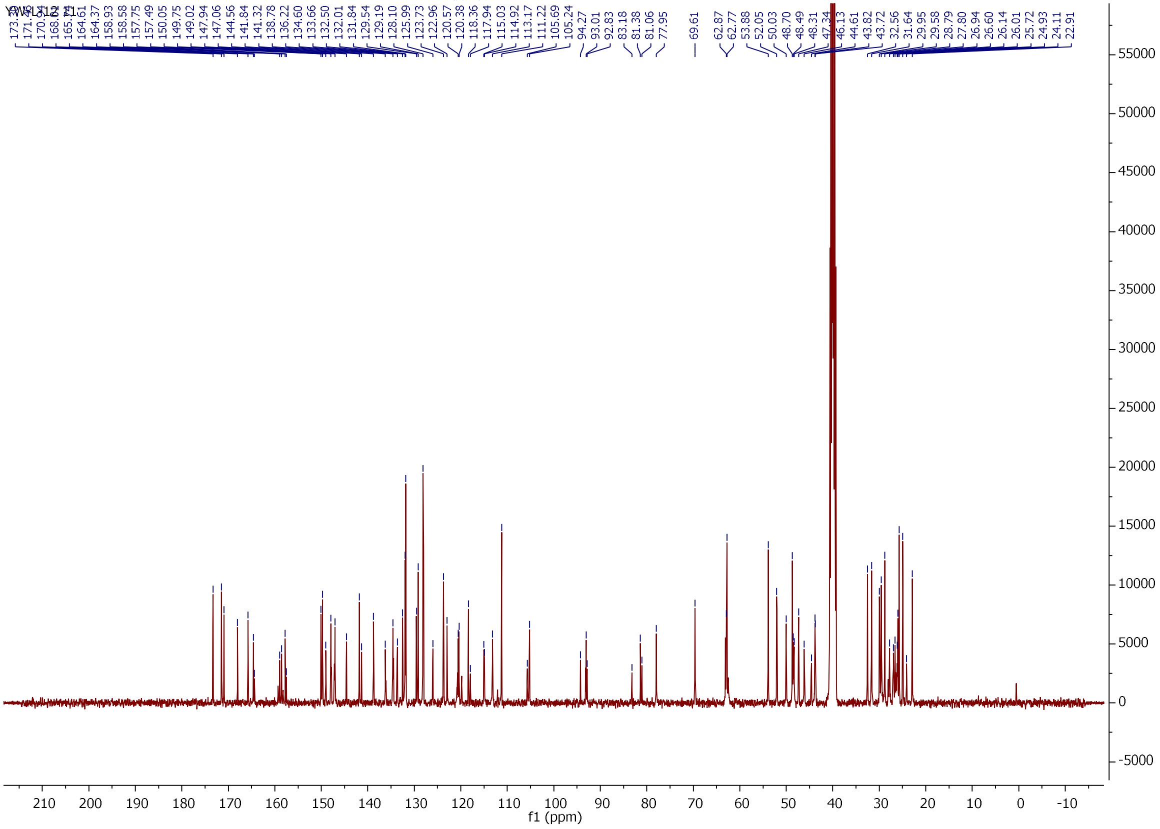
YW-L-12 11
173.30 171.46 170.94 168.02 165.74 164.61 164.37 158.93 158.58 157.75 157.49 150.05 149.75 149.02 147.94 147.06 144.56 141.84 141.32 138.78 136.22 134.60 133.66 132.50 132.01 131.84 129.54 129.19 128.10 125.99 123.73 122.96 120.57 120.38 118.36 117.94 115.03 114.92 113.17 111.22 105.69 105.24 94.27 93.01 92.83 83.18 81.38 81.06 77.95 69.61 62.87 62.77 53.88 52.05 50.03 48.70 48.49 48.31 47.34 46.13 44.61 43.82 43.72 32.56 31.64 29.95 29.58 28.79 27.80 26.94 26.60 26.14 26.01 25.72 24.93 24.11 22.91
210 200 190 180 170 160 150 140 130 120 110 100 90 80 70 60 50 40 30 20 10 0 -10
f1 (ppm)
55000 50000 45000 40000 35000 30000 25000 20000 15000 10000 5000 0 -5000

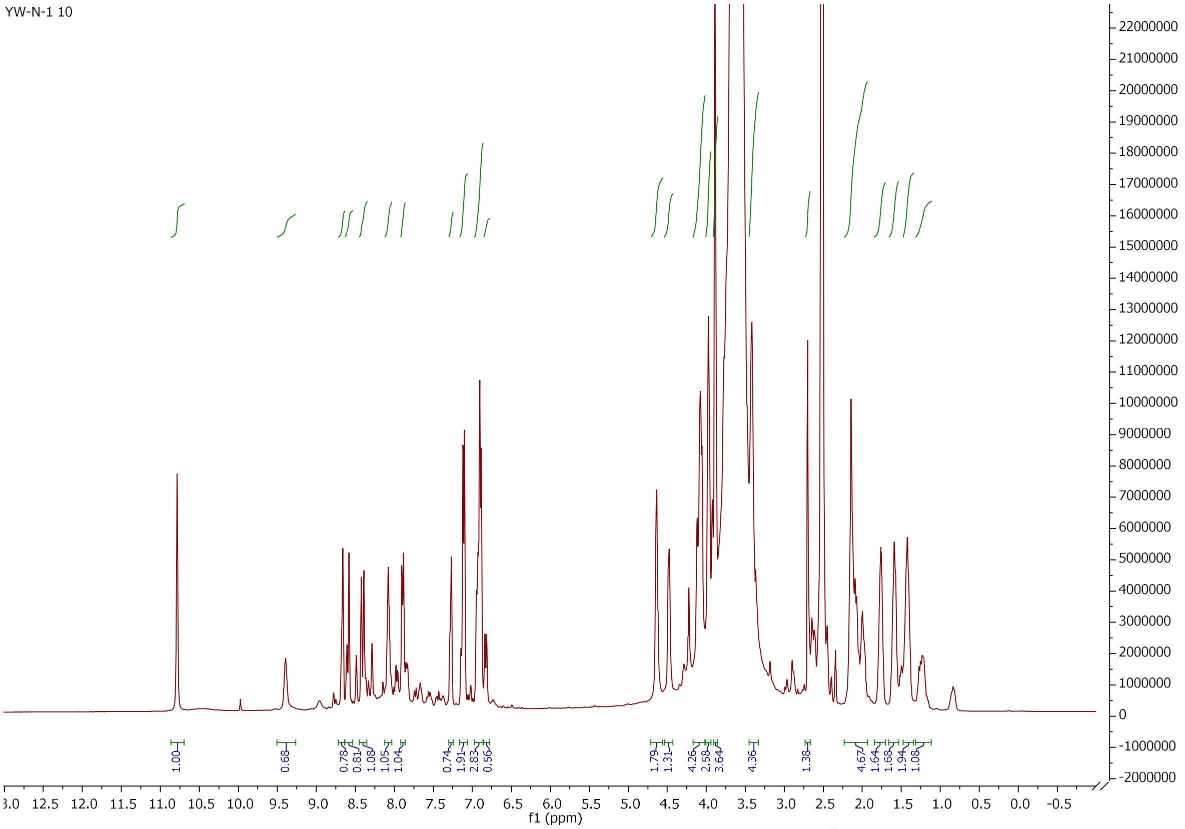
YW-N-1 10
1.00
0.68
0.78
0.81
1.08
1.05
1.04
0.74
1.91
2.83
0.56
1.79
1.31
4.26
2.58
3.64
4.36
1.38
4.67
1.64
1.68
1.94
1.08
13.0 12.5 12.0 11.5 11.0 10.5 10.0 9.5 9.0 8.5 8.0 7.5 7.0 6.5 6.0 5.5 5.0 4.5 4.0 3.5 3.0 2.5 2.0 1.5 1.0 0.5 0.0 -0.5
f1 (ppm)
22000000
21000000
20000000
19000000
18000000
17000000
16000000
15000000
14000000
13000000
12000000
11000000
10000000
9000000
8000000
7000000
6000000
5000000
4000000
3000000
2000000
1000000
0
-1000000
-2000000

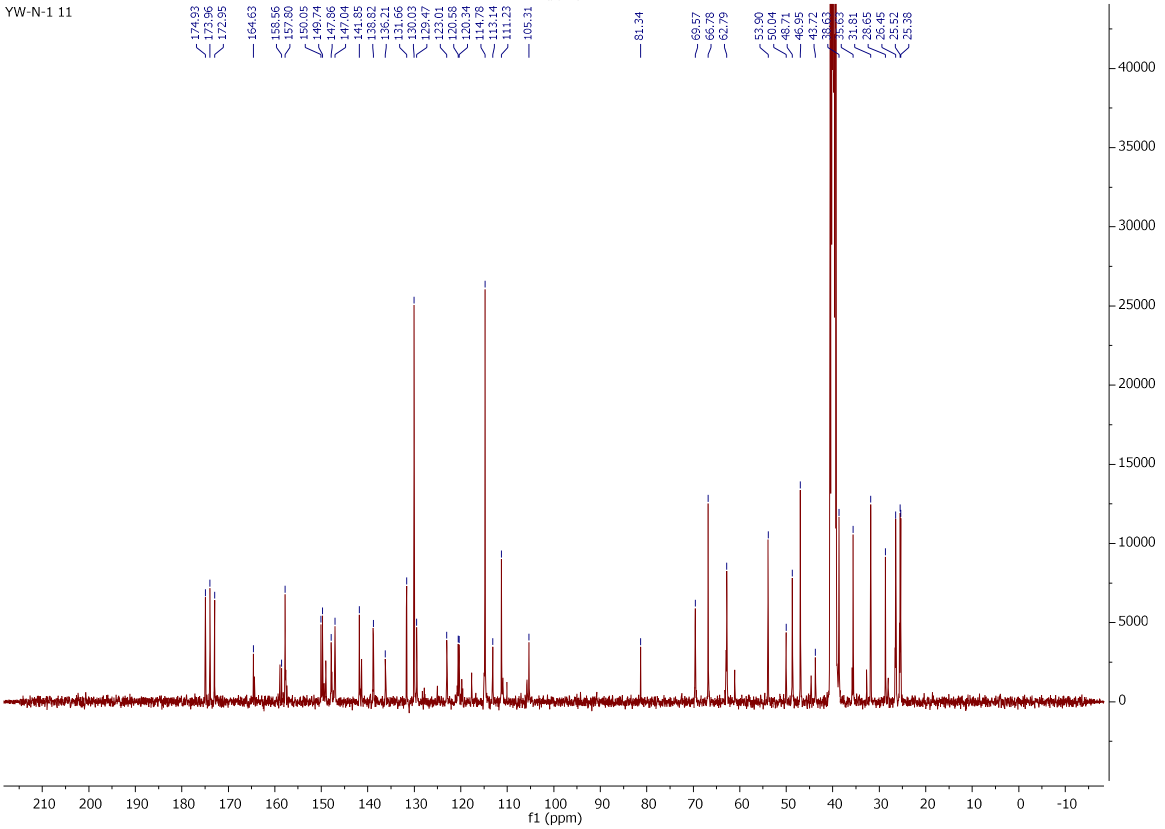
YW-N-1 11
174.93
173.96
172.95
164.63
158.56
157.80
150.05
149.74
147.86
147.04
141.85
138.82
136.21
131.66
130.03
129.47
123.01
120.58
120.34
114.78
113.14
111.23
105.31
81.34
69.57
66.78
62.79
53.90
50.04
48.71
46.95
43.72
38.63
35.63
31.81
28.65
26.45
25.52
25.38
210 200 190 180 170 160 150 140 130 120 110 100 90 80 70 60 50 40 30 20 10 0 -10
f1 (ppm)
40000
35000
30000
25000
20000
15000
10000
5000
0

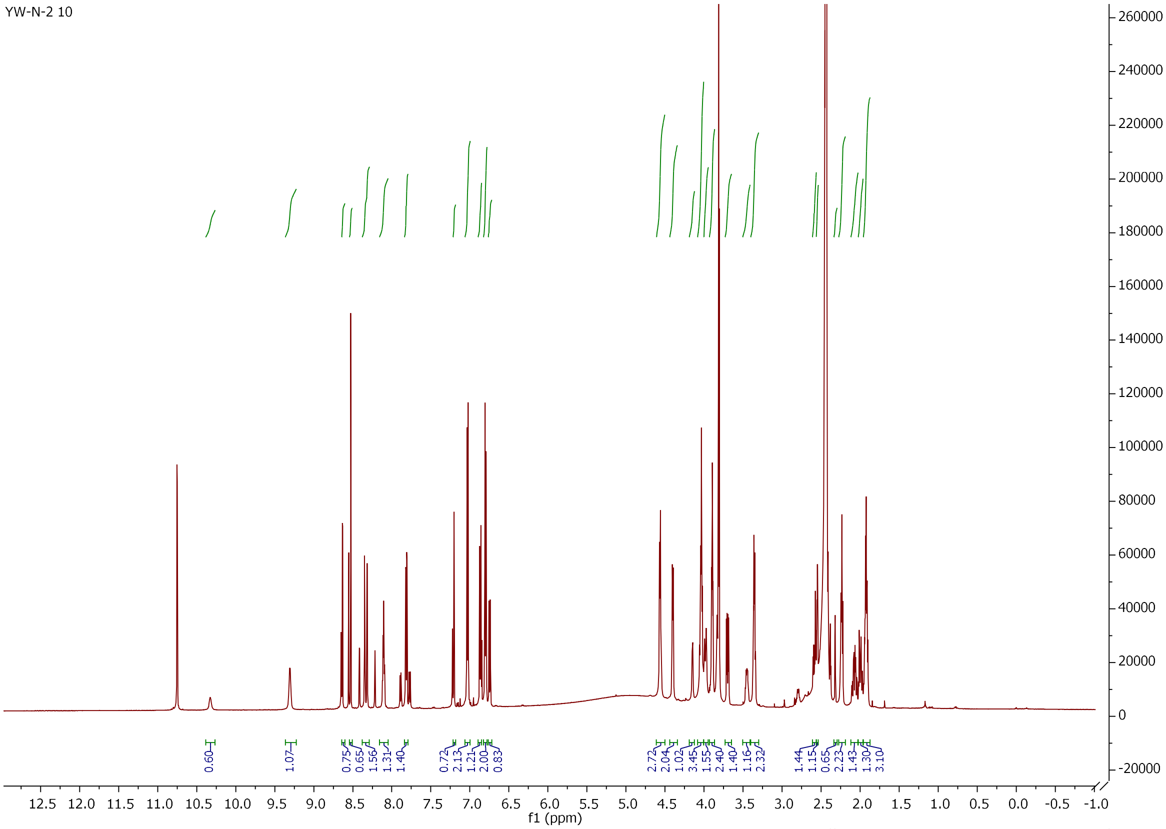
YW-N-2 10
0.60
1.07
0.75
0.65
1.56
1.31
1.40
0.72
2.13
1.21
2.00
0.83
2.72
2.04
1.02
3.45
1.55
2.40
1.40
1.16
2.32
1.44
1.15
0.65
2.23
1.43
1.30
3.10
12.5 12.0 11.5 11.0 10.5 10.0 9.5 9.0 8.5 8.0 7.5 7.0 6.5 6.0 5.5 5.0 4.5 4.0 3.5 3.0 2.5 2.0 1.5 1.0 0.5 0.0 -0.5 -1.0
f1 (ppm)
260000
240000
220000
200000
180000
160000
140000
120000
100000
80000
60000
40000
20000
0
-20000

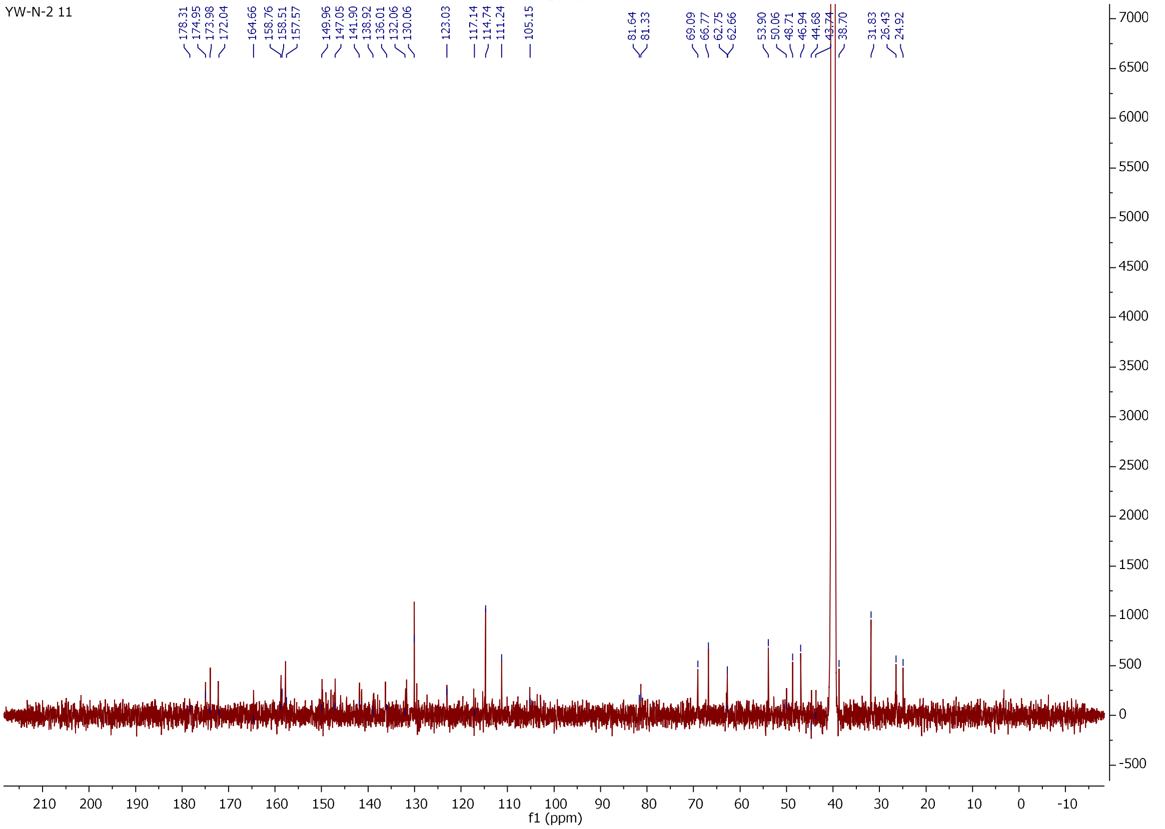
YW-N-2 11
178.31
174.95
173.98
172.04
164.66
158.76
158.51
157.57
149.96
147.05
141.90
138.92
136.01
132.06
130.06
123.03
117.14
114.74
111.24
105.15
81.64
81.33
69.09
66.77
62.75
62.66
53.90
50.06
48.71
46.94
44.68
43.74
38.70
31.83
26.43
24.92
210 200 190 180 170 160 150 140 130 120 110 100 90 80 70 60 50 40 30 20 10 0 -10
f1 (ppm)
7000
6500
6000
5500
5000
4500
4000
3500
3000
2500
2000
1500
1000
500
0
-500

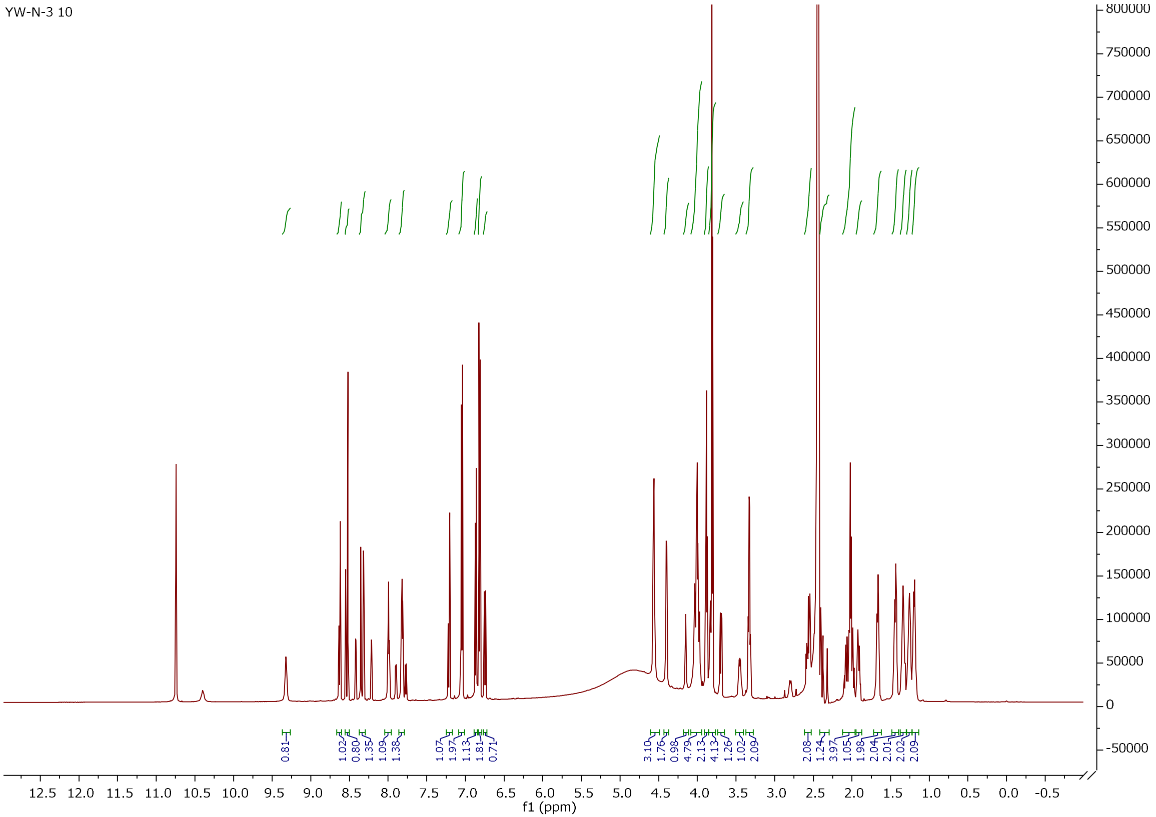
YW-N-3 10
0.81
1.02
0.80
1.35
1.09
1.38
1.07
1.97
1.13
1.81
0.71
3.10
1.76
0.98
4.79
2.13
4.13
1.26
1.02
2.09
2.08
1.24
3.97
1.05
1.98
2.04
2.01
2.02
2.09
f1 (ppm)

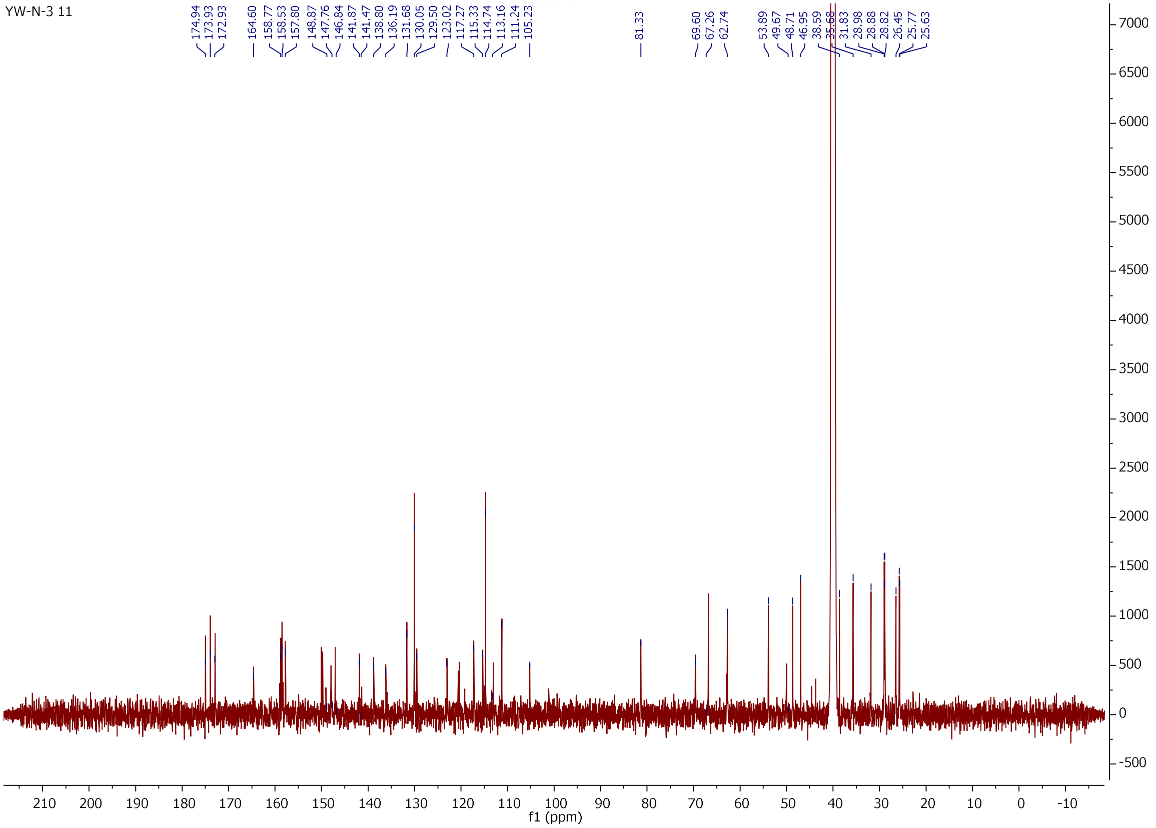
YW-N-3 11
174.94
173.93
172.93
164.60
158.77
158.53
157.80
148.87
147.76
146.84
141.87
141.47
138.80
136.19
131.68
130.05
129.50
123.02
117.27
115.33
114.74
113.16
111.24
105.23
81.33
69.60
67.26
62.74
53.89
49.67
48.71
46.95
38.59
35.68
31.83
28.98
28.88
28.82
26.45
25.77
25.63
f1 (ppm)

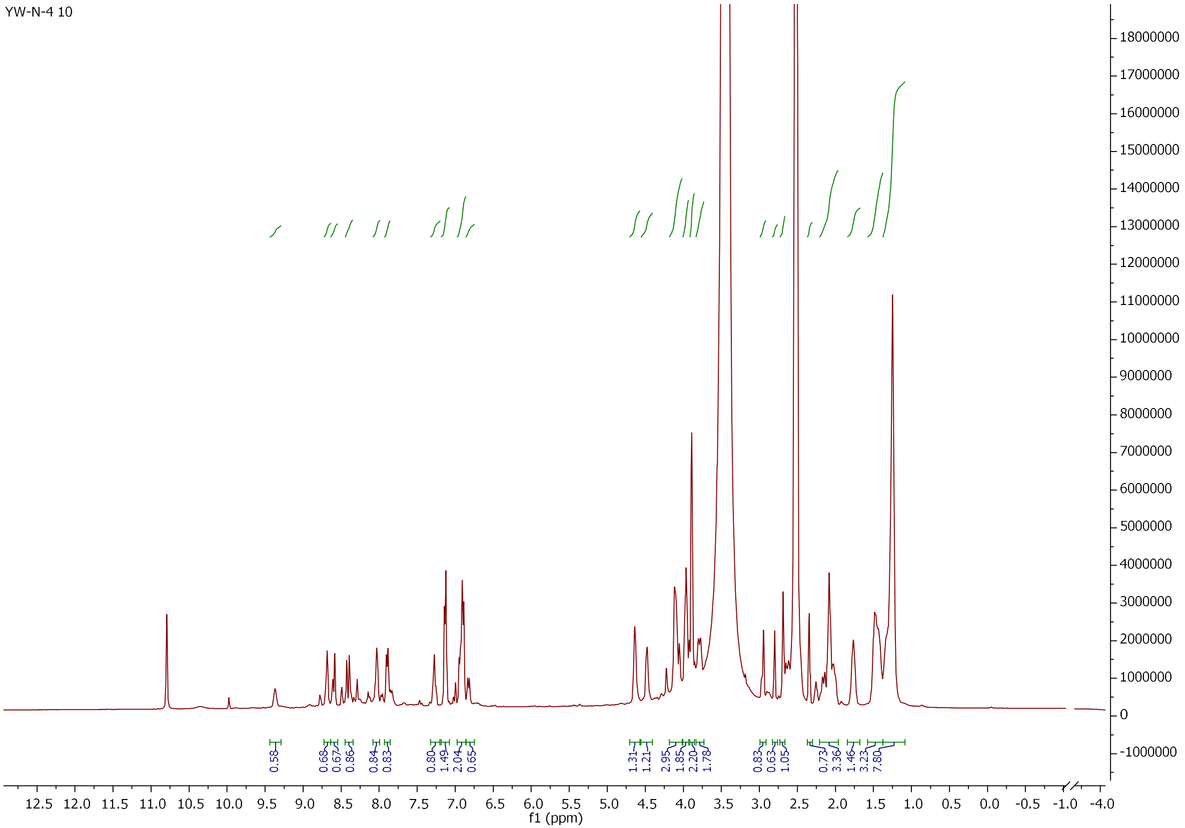
YW-N-4 10
0.58
0.68
0.67
0.86
0.84
0.83
0.80
1.49
2.04
0.65
1.31
1.21
2.95
1.85
2.20
1.78
0.83
0.63
1.05
0.73
3.36
1.46
3.23
7.80
12.5 12.0 11.5 11.0 10.5 10.0 9.5 9.0 8.5 8.0 7.5 7.0 6.5 6.0 5.5 5.0 4.5 4.0 3.5 3.0 2.5 2.0 1.5 1.0 0.5 0.0 -0.5 -1.0 -4.0
f1 (ppm)
18000000
17000000
16000000
15000000
14000000
13000000
12000000
11000000
10000000
9000000
8000000
7000000
6000000
5000000
4000000
3000000
2000000
1000000
0
-1000000

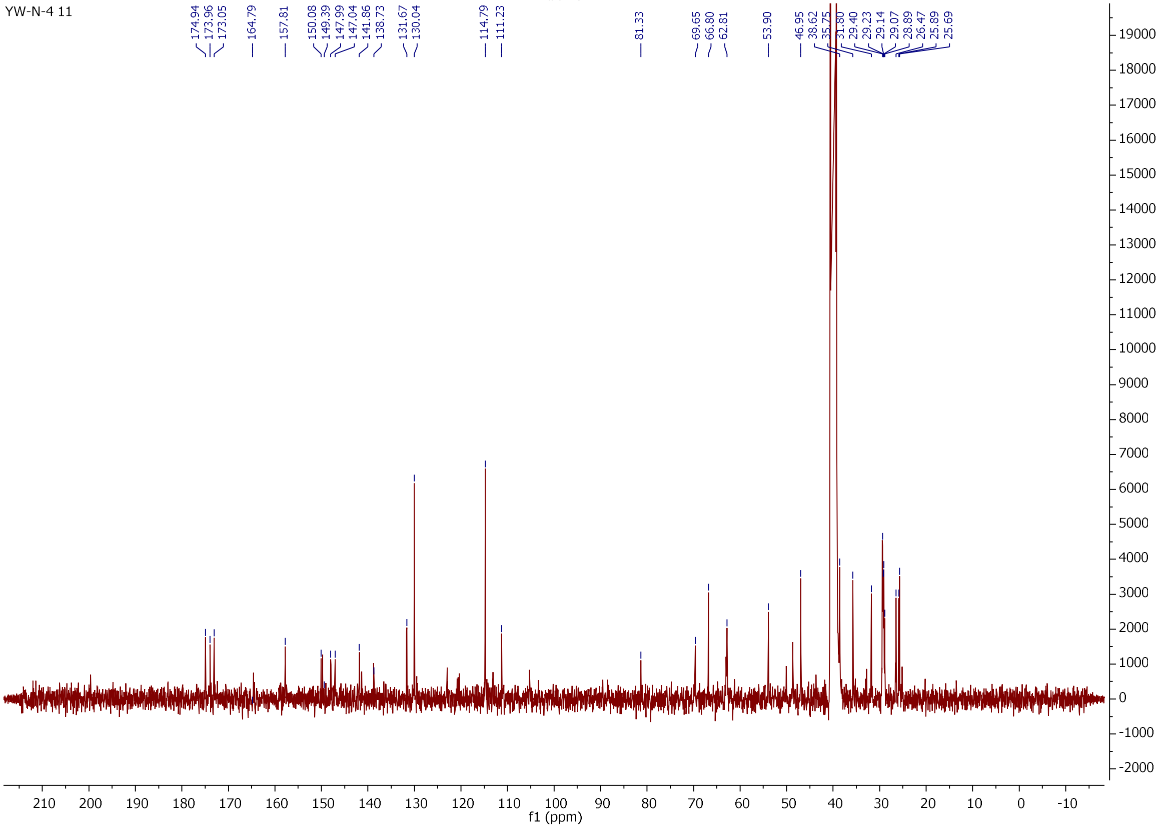
YW-N-4 11
174.94
173.96
173.05
164.79
157.81
150.08
149.39
147.99
147.04
141.86
138.73
131.67
130.04
114.79
111.23
81.33
69.65
66.80
62.81
53.90
46.95
38.62
35.75
31.80
29.40
29.23
29.14
29.07
28.89
26.47
25.89
25.69
210 200 190 180 170 160 150 140 130 120 110 100 90 80 70 60 50 40 30 20 10 0 -10
f1 (ppm)
19000
18000
17000
16000
15000
14000
13000
12000
11000
10000
9000
8000
7000
6000
5000
4000
3000
2000
1000
0
-1000
-2000

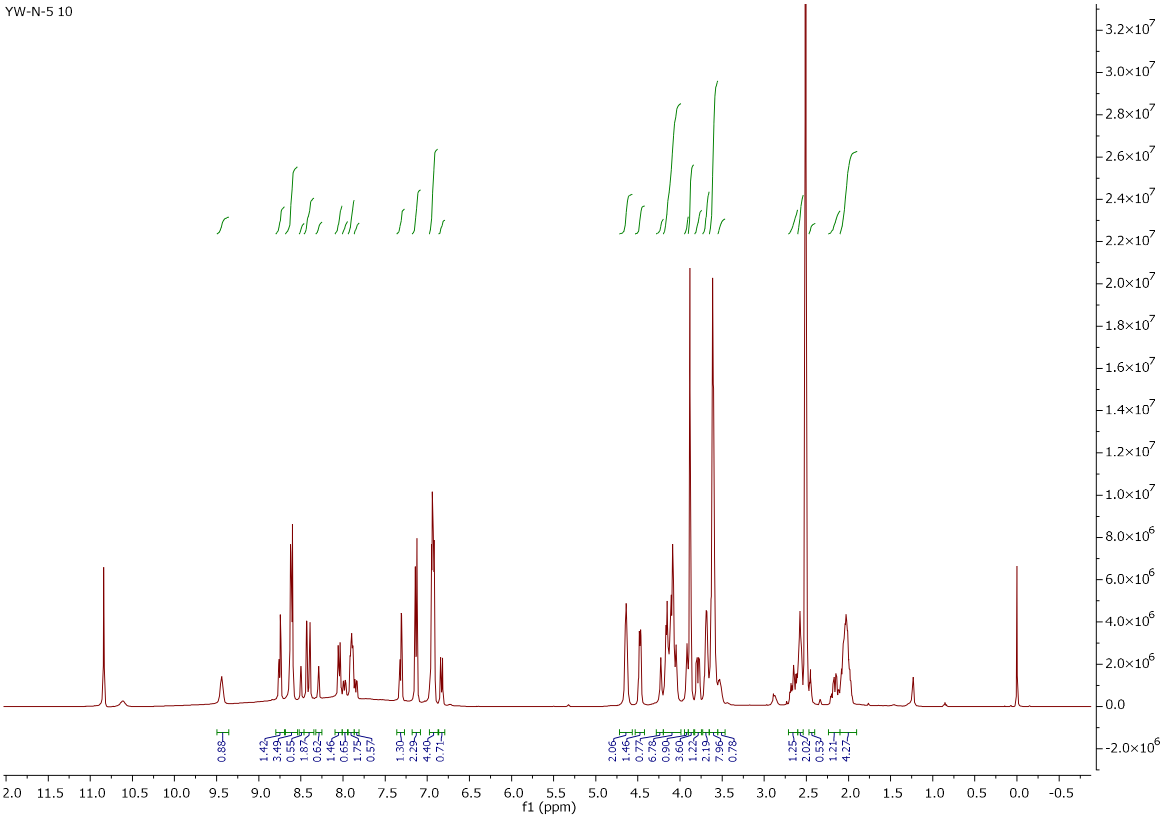
YW-N-5 10
0.88
1.42
3.49
0.55
1.87
0.62
1.46
0.65
1.75
0.57
1.30
2.29
4.40
0.71
2.06
1.46
0.77
6.78
0.90
3.60
1.22
2.19
7.96
0.78
1.25
2.02
0.53
1.21
4.27
f1 (ppm)

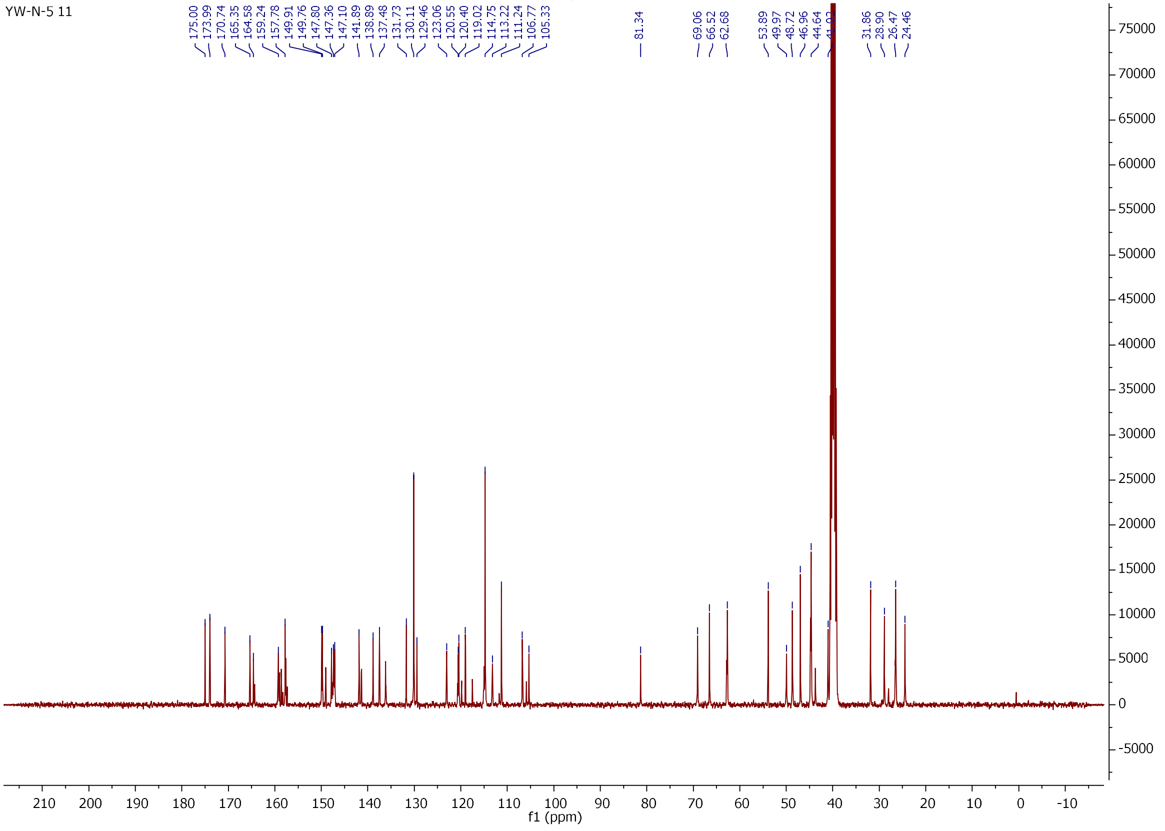
YW-N-5 11
175.00
173.99
170.74
165.35
164.58
159.24
157.78
149.91
149.76
147.80
147.36
147.10
141.89
138.89
137.48
131.73
130.11
129.46
123.06
120.55
120.40
119.02
114.75
113.22
111.24
106.77
105.33
81.34
69.06
66.52
62.68
53.89
49.97
48.72
46.96
44.64
31.86
28.90
26.47
24.46
f1 (ppm)

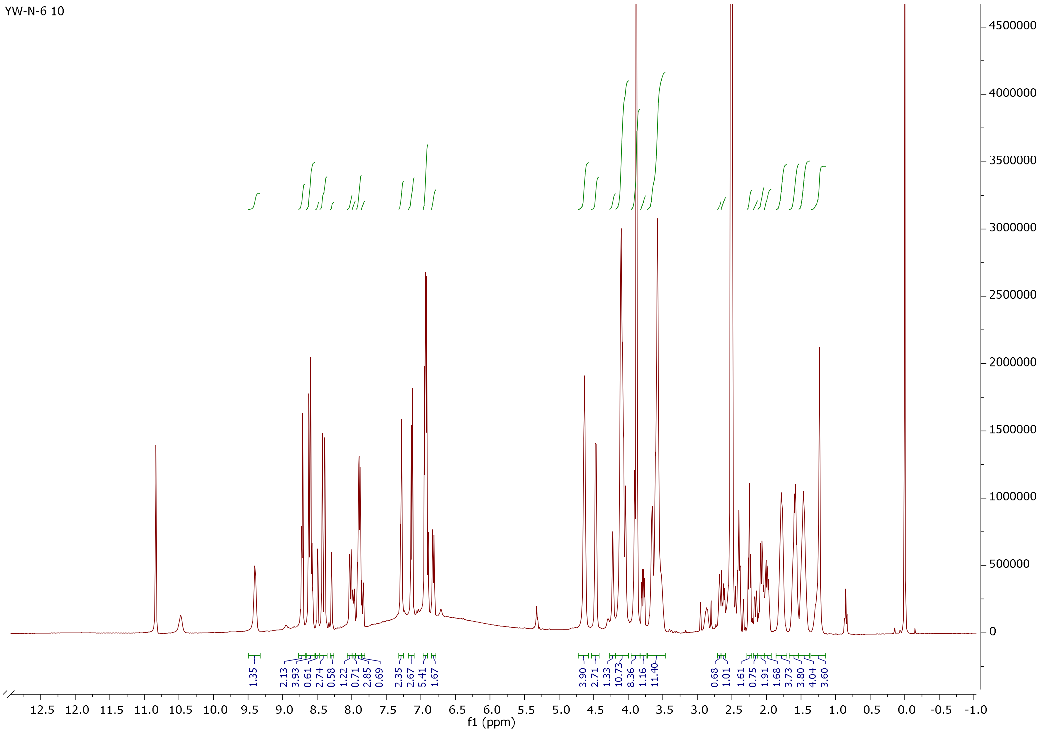
YW-N-6 10
1.35
2.13
3.93
0.61
2.74
0.58
1.22
0.71
2.85
0.69
2.35
2.67
5.41
1.67
3.90
2.71
1.33
10.73
8.36
1.16
11.40
0.68
1.01
1.61
0.75
1.91
1.68
3.73
3.80
4.04
3.60
f1 (ppm)

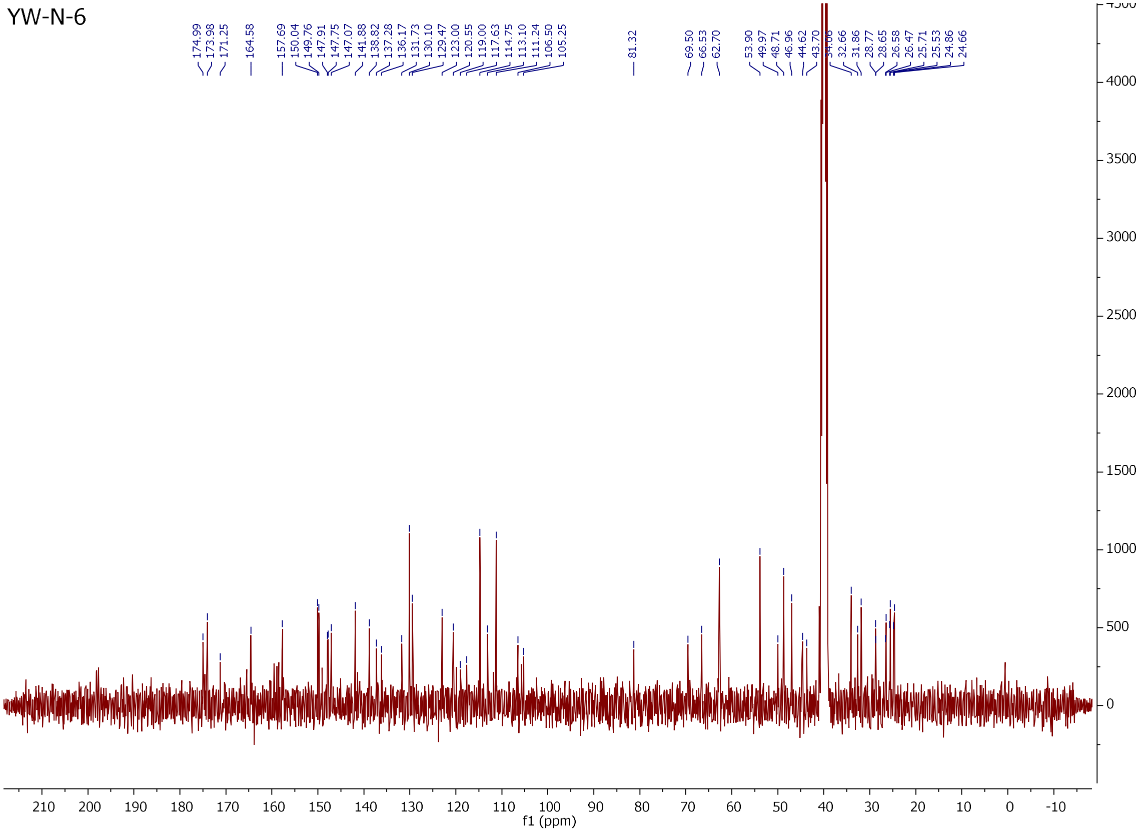
YW-N-6
174.99
173.98
171.25
164.58
157.69
150.04
149.76
147.91
147.75
147.07
141.88
138.82
137.28
136.17
131.73
130.10
129.47
123.00
120.55
119.00
117.63
114.75
113.10
111.24
106.50
105.25
81.32
69.50
66.53
62.70
53.90
49.97
48.71
46.96
44.62
43.70
34.06
32.66
31.86
28.77
28.65
26.58
26.47
25.71
25.53
24.86
24.66
f1 (ppm)

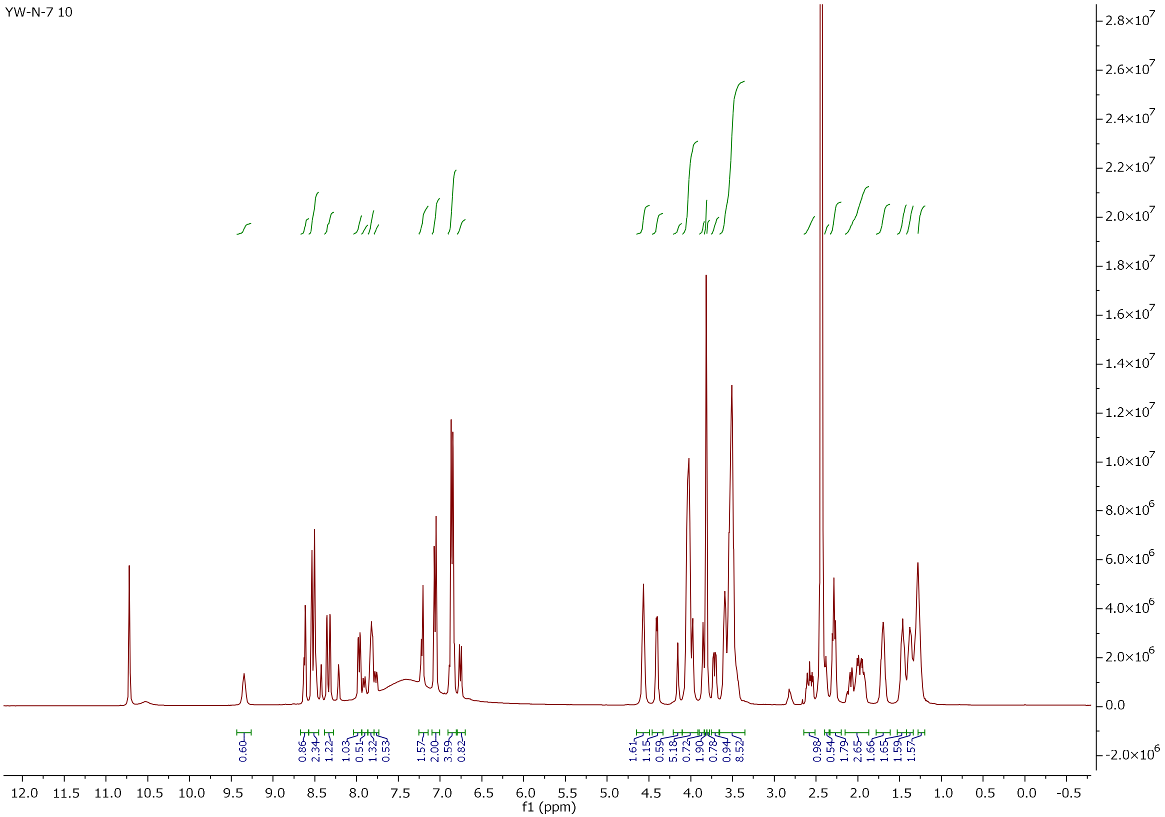
YW-N-7 10
0.60
0.86
2.34
1.22
1.03
0.51
1.32
0.53
1.57
2.00
3.59
0.82
1.61
1.15
0.59
5.18
0.72
1.90
0.78
0.94
8.52
0.98
0.54
1.79
2.65
1.66
1.65
1.59
1.57
12.0 11.5 11.0 10.5 10.0 9.5 9.0 8.5 8.0 7.5 7.0 6.5 6.0 5.5 5.0 4.5 4.0 3.5 3.0 2.5 2.0 1.5 1.0 0.5 0.0 -0.5
f1 (ppm)
2.8×10^7 2.6×10^7 2.4×10^7 2.2×10^7 2.0×10^7 1.8×10^7 1.6×10^7 1.4×10^7 1.2×10^7 1.0×10^7 8.0×10^6 6.0×10^6 4.0×10^6 2.0×10^6 0.0 -2.0×10^6

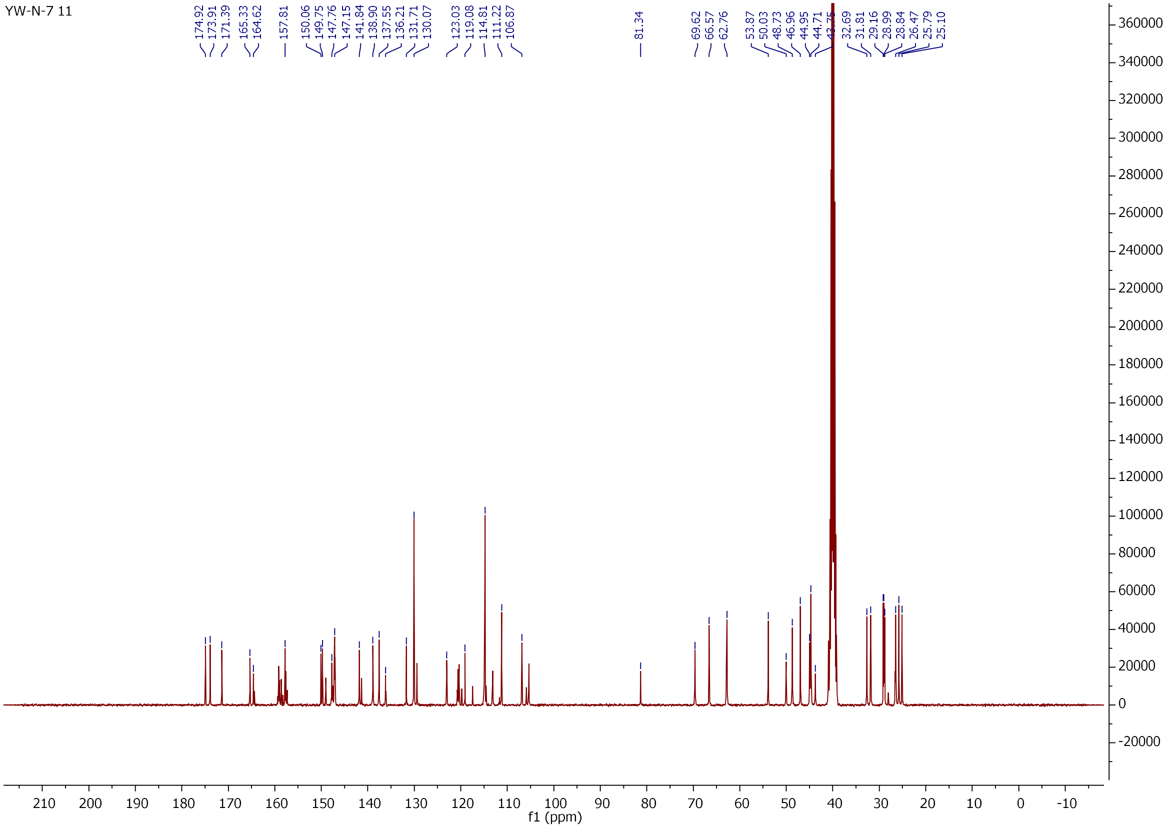
YW-N-7 11
174.92
173.91
171.39
165.33
164.62
157.81
150.06
149.75
147.76
147.15
141.84
138.90
137.55
136.21
131.71
130.07
123.03
119.08
114.81
111.22
106.87
81.34
69.62
66.57
62.76
53.87
50.03
48.73
46.96
44.95
44.71
43.75
32.69
31.81
29.16
28.99
28.84
26.47
25.79
25.10
210 200 190 180 170 160 150 140 130 120 110 100 90 80 70 60 50 40 30 20 10 0 -10
f1 (ppm)
360000 340000 320000 300000 280000 260000 240000 220000 200000 180000 160000 140000 120000 100000 80000 60000 40000 20000 0 -20000

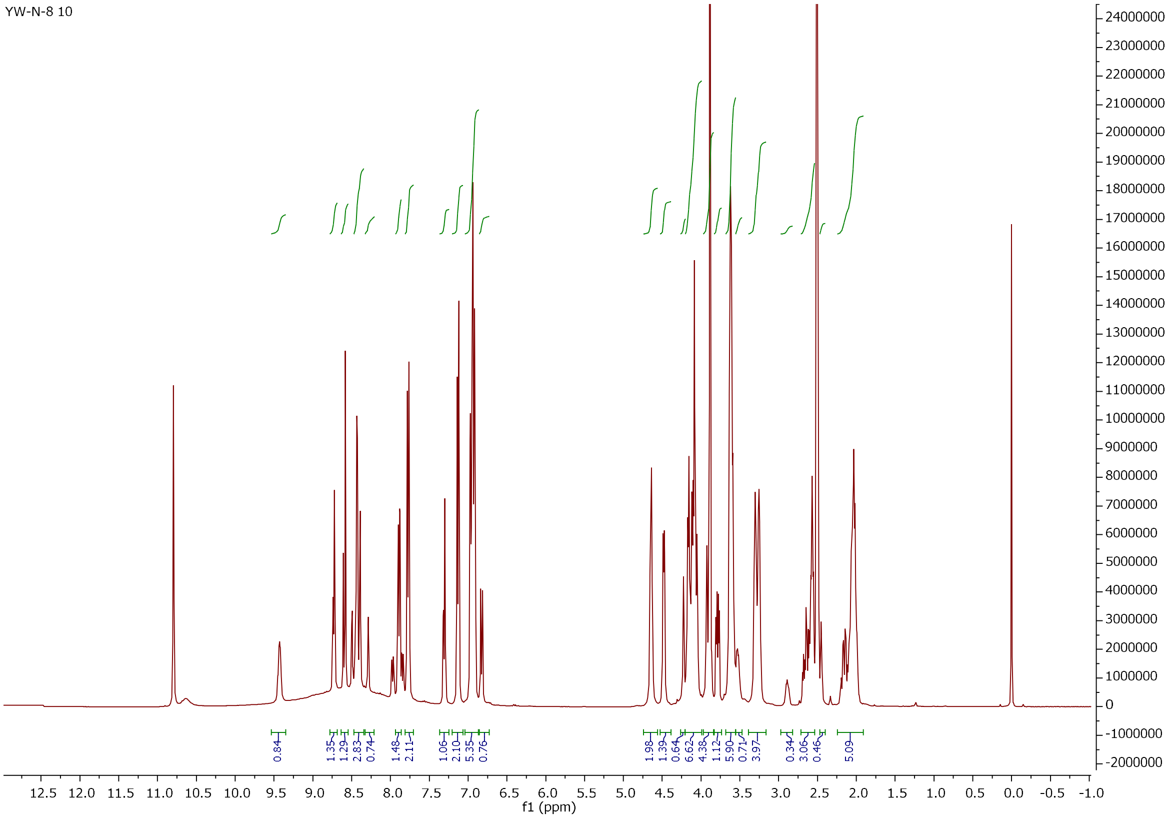
YW-N-8 10
0.84
1.35
1.29
2.83
0.74
1.48
2.11
1.06
2.10
5.35
0.76
1.98
1.39
0.64
6.62
4.38
1.12
5.90
0.71
3.97
0.34
3.06
0.46
5.09
24000000
23000000
22000000
21000000
20000000
19000000
18000000
17000000
16000000
15000000
14000000
13000000
12000000
11000000
10000000
9000000
8000000
7000000
6000000
5000000
4000000
3000000
2000000
1000000
0
-1000000
-2000000
12.5 12.0 11.5 11.0 10.5 10.0 9.5 9.0 8.5 8.0 7.5 7.0 6.5 6.0 5.5 5.0 4.5 4.0 3.5 3.0 2.5 2.0 1.5 1.0 0.5 0.0 -0.5 -1.0
f1 (ppm)

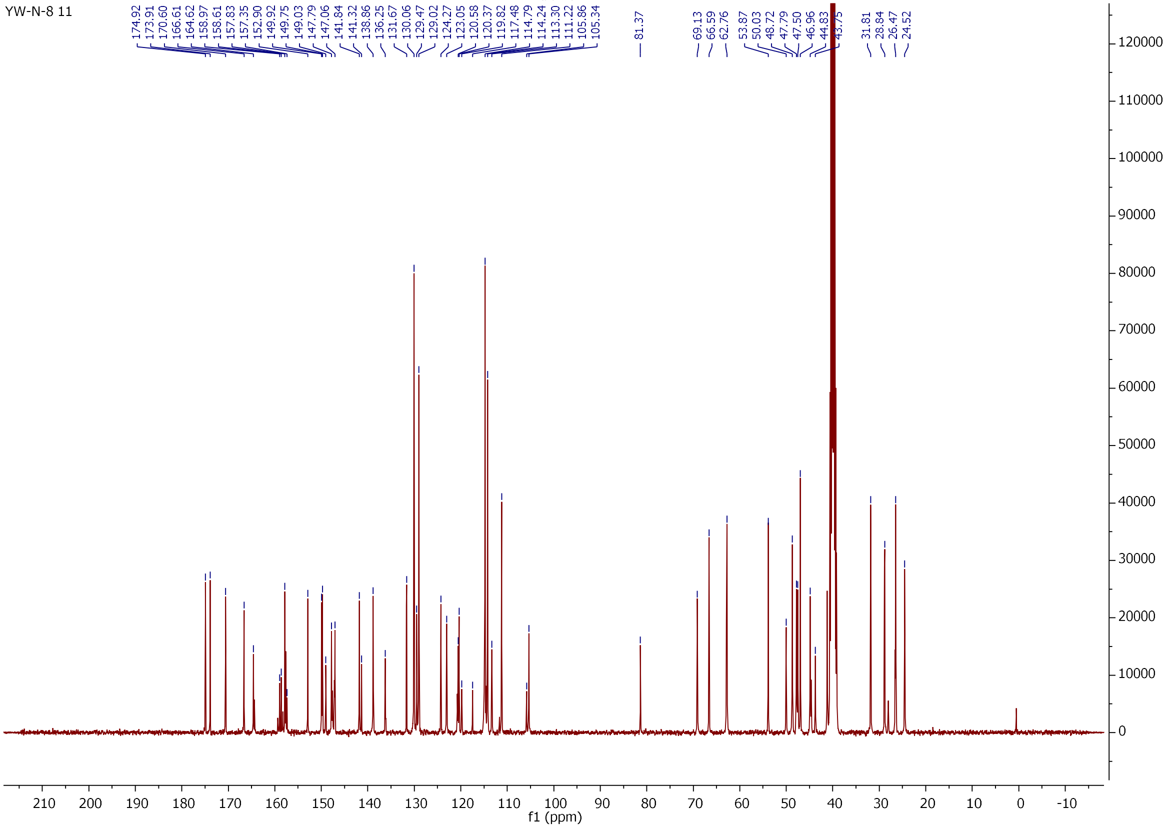
YW-N-8 11
174.92
173.91
170.60
166.61
164.62
158.97
158.61
157.83
157.35
152.90
149.92
149.75
149.03
147.79
147.06
141.84
141.32
138.86
136.25
131.67
130.06
129.47
129.02
124.27
123.05
120.58
120.37
119.82
117.48
114.79
114.24
113.30
111.22
105.86
105.34
81.37
69.13
66.59
62.76
53.87
50.03
48.72
47.79
47.50
46.96
44.83
43.75
31.81
28.84
26.47
24.52
120000
110000
100000
90000
80000
70000
60000
50000
40000
30000
20000
10000
0
210 200 190 180 170 160 150 140 130 120 110 100 90 80 70 60 50 40 30 20 10 0 -10
f1 (ppm)

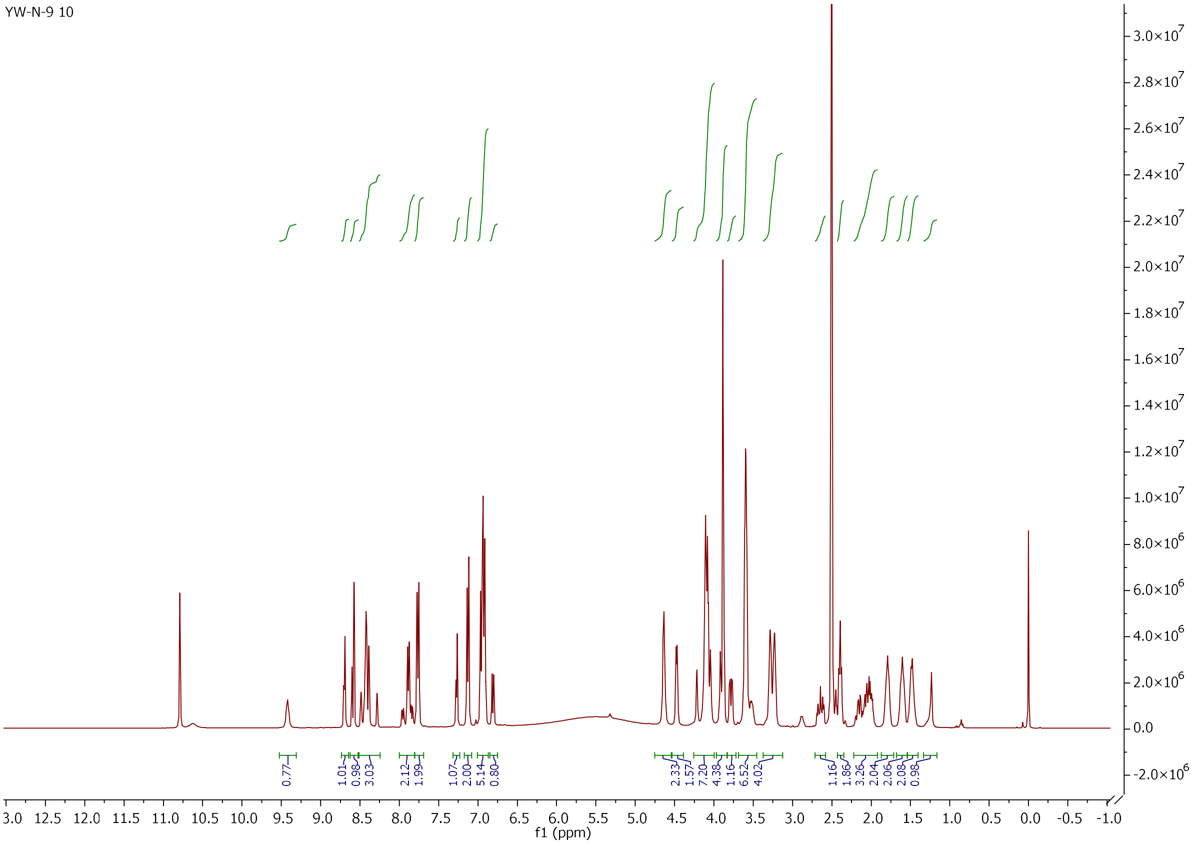
YW-N-9 10
0.77
1.01
0.98
3.03
2.12
1.99
1.07
2.00
5.14
0.80
2.33
1.57
7.20
4.38
1.16
6.52
4.02
1.16
1.86
3.26
2.04
2.06
2.08
0.98
3.0 12.5 12.0 11.5 11.0 10.5 10.0 9.5 9.0 8.5 8.0 7.5 7.0 6.5 6.0 5.5 5.0 4.5 4.0 3.5 3.0 2.5 2.0 1.5 1.0 0.5 0.0 -0.5 -1.0
f1 (ppm)
3.0×10^7
2.8×10^7
2.6×10^7
2.4×10^7
2.2×10^7
2.0×10^7
1.8×10^7
1.6×10^7
1.4×10^7
1.2×10^7
1.0×10^7
8.0×10^6
6.0×10^6
4.0×10^6
2.0×10^6
0.0
-2.0×10^6

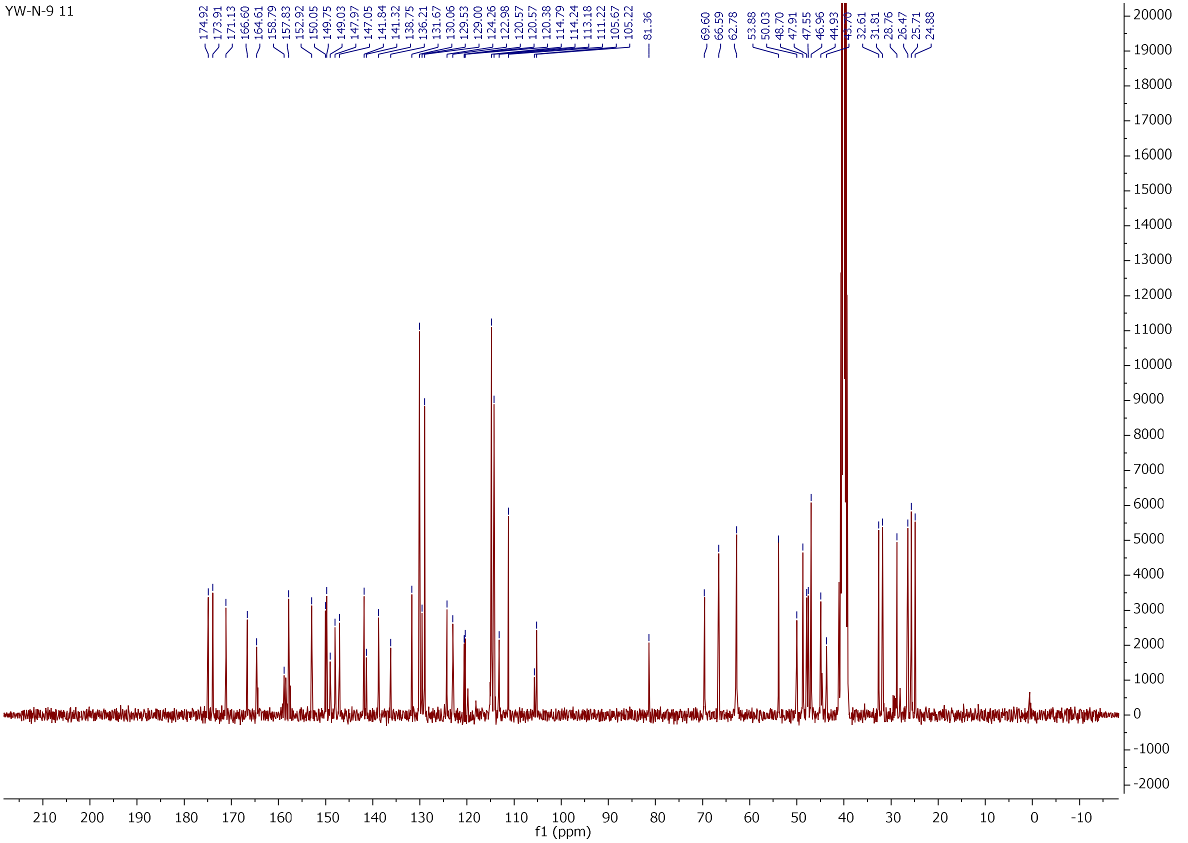
YW-N-9 11
174.92
173.91
171.13
166.60
164.61
158.79
157.83
152.92
150.05
149.75
149.03
147.97
147.05
141.84
141.32
138.75
136.21
131.67
130.06
129.53
129.00
124.26
122.98
120.57
120.57
120.38
114.79
114.24
113.18
111.22
105.67
105.22
81.36
69.60
66.59
62.78
53.88
50.03
48.70
47.91
47.55
46.96
44.93
43.70
32.61
31.81
28.76
26.47
25.71
24.88
210 200 190 180 170 160 150 140 130 120 110 100 90 80 70 60 50 40 30 20 10 0 -10
f1 (ppm)
20000
19000
18000
17000
16000
15000
14000
13000
12000
11000
10000
9000
8000
7000
6000
5000
4000
3000
2000
1000
0
-1000
-2000

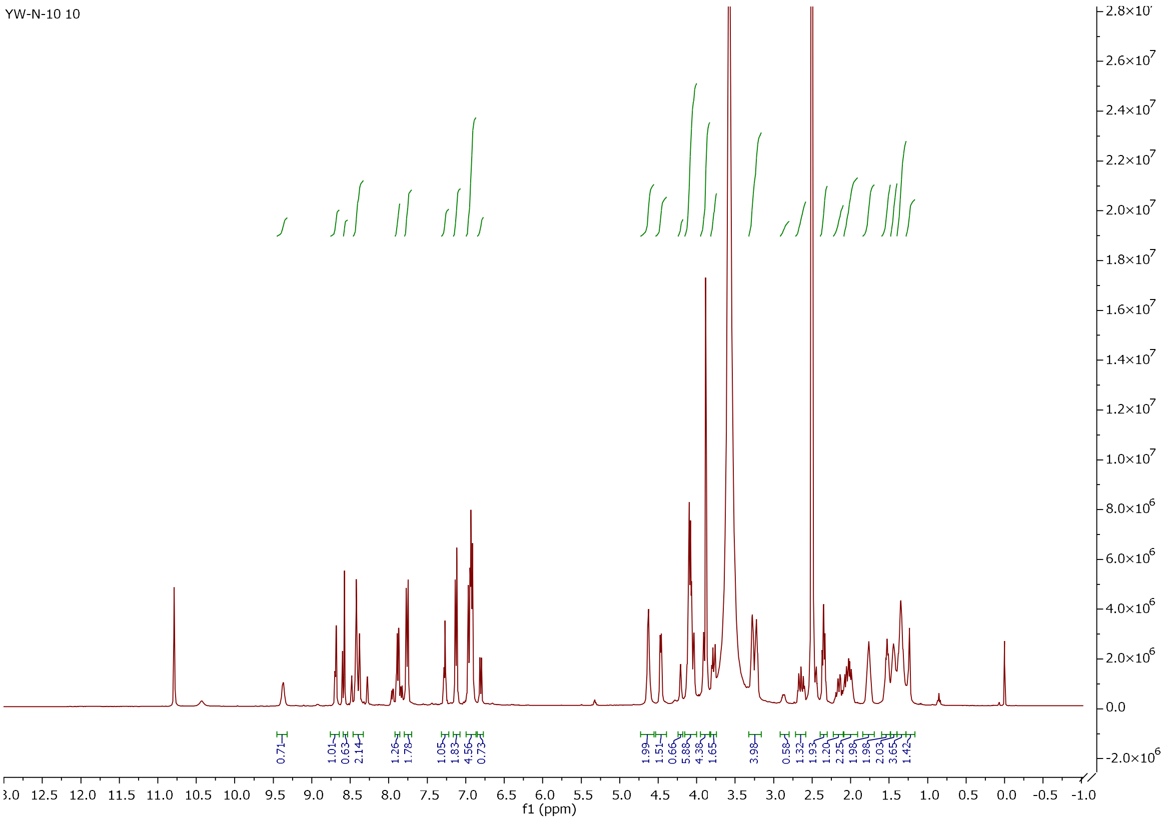
YW-N-10 10
0.71
1.01
0.63
2.14
1.26
1.78
1.05
1.83
4.56
0.73
1.99
1.51
0.66
5.88
4.38
1.65
3.98
0.58
1.32
1.93
1.20
2.25
1.98
1.98
2.03
3.65
1.42
f1 (ppm)
3.0 12.5 12.0 11.5 11.0 10.5 10.0 9.5 9.0 8.5 8.0 7.5 7.0 6.5 6.0 5.5 5.0 4.5 4.0 3.5 3.0 2.5 2.0 1.5 1.0 0.5 0.0 -0.5 -1.0
2.8×10^7
2.6×10^7
2.4×10^7
2.2×10^7
2.0×10^7
1.8×10^7
1.6×10^7
1.4×10^7
1.2×10^7
1.0×10^7
8.0×10^6
6.0×10^6
4.0×10^6
2.0×10^6
0.0
-2.0×10^6

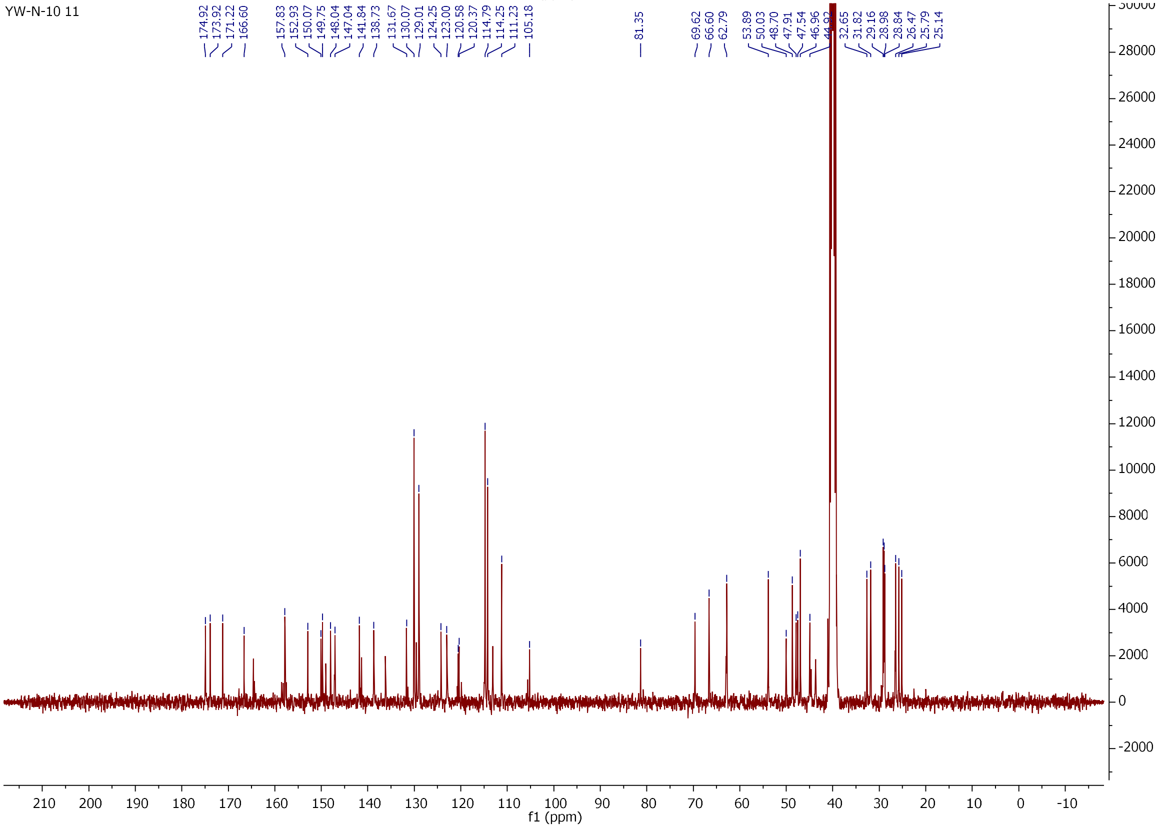
YW-N-10 11
174.92
173.92
171.22
166.60
157.83
152.93
150.07
149.75
148.04
147.04
141.84
138.73
131.67
130.07
129.01
124.25
123.00
120.58
120.37
114.79
114.25
111.23
105.18
81.35
69.62
66.60
62.79
53.89
50.03
48.70
47.91
47.54
46.96
44.92
32.65
31.82
29.16
28.98
28.84
26.47
25.79
25.14
f1 (ppm)
210 200 190 180 170 160 150 140 130 120 110 100 90 80 70 60 50 40 30 20 10 0 -10
30000
28000
26000
24000
22000
20000
18000
16000
14000
12000
10000
8000
6000
4000
2000
0
-2000

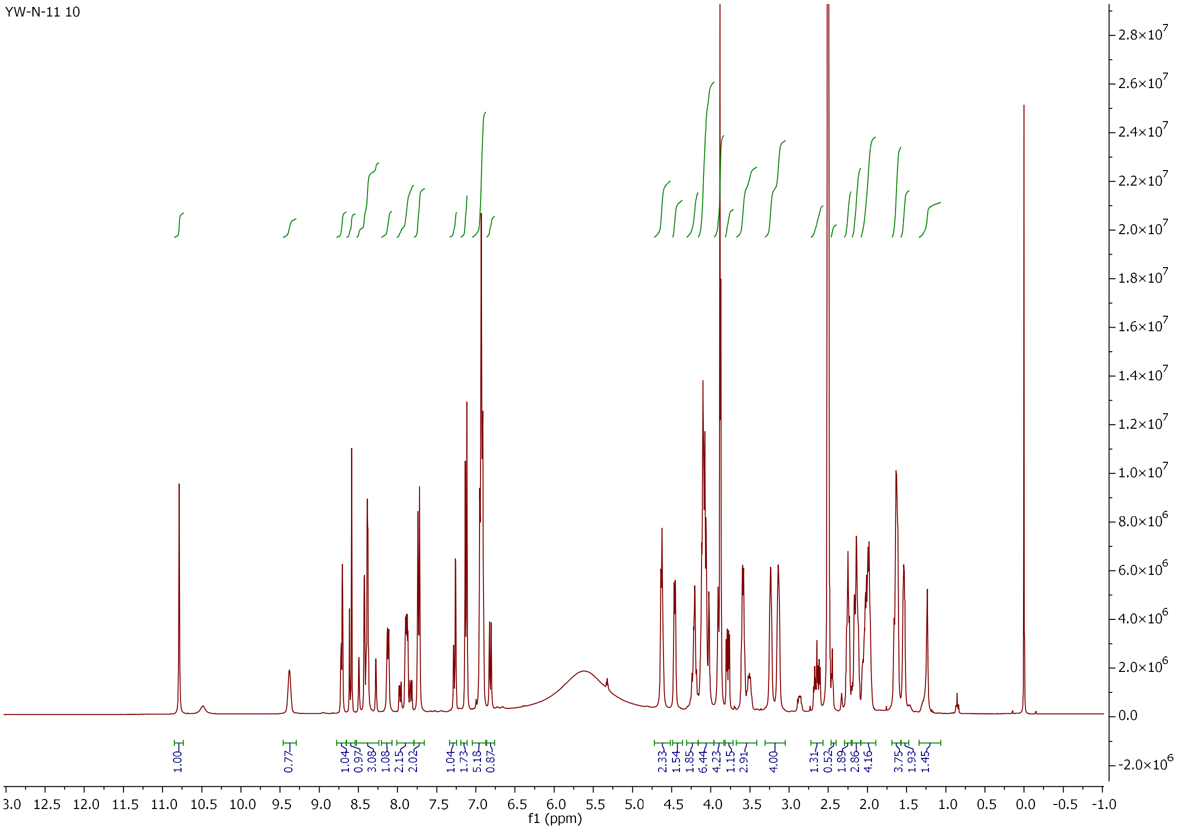
YW-N-11 10
1.00
0.77
1.04
0.97
3.08
1.08
2.15
2.02
1.04
1.73
5.18
0.87
2.33
1.54
1.85
6.44
4.23
1.15
2.91
4.00
1.31
0.52
1.89
2.86
4.16
3.75
1.93
1.45
3.0 12.5 12.0 11.5 11.0 10.5 10.0 9.5 9.0 8.5 8.0 7.5 7.0 6.5 6.0 5.5 5.0 4.5 4.0 3.5 3.0 2.5 2.0 1.5 1.0 0.5 0.0 -0.5 -1.0
f1 (ppm)
2.8×10^7
2.6×10^7
2.4×10^7
2.2×10^7
2.0×10^7
1.8×10^7
1.6×10^7
1.4×10^7
1.2×10^7
1.0×10^7
8.0×10^6
6.0×10^6
4.0×10^6
2.0×10^6
0.0
-2.0×10^6

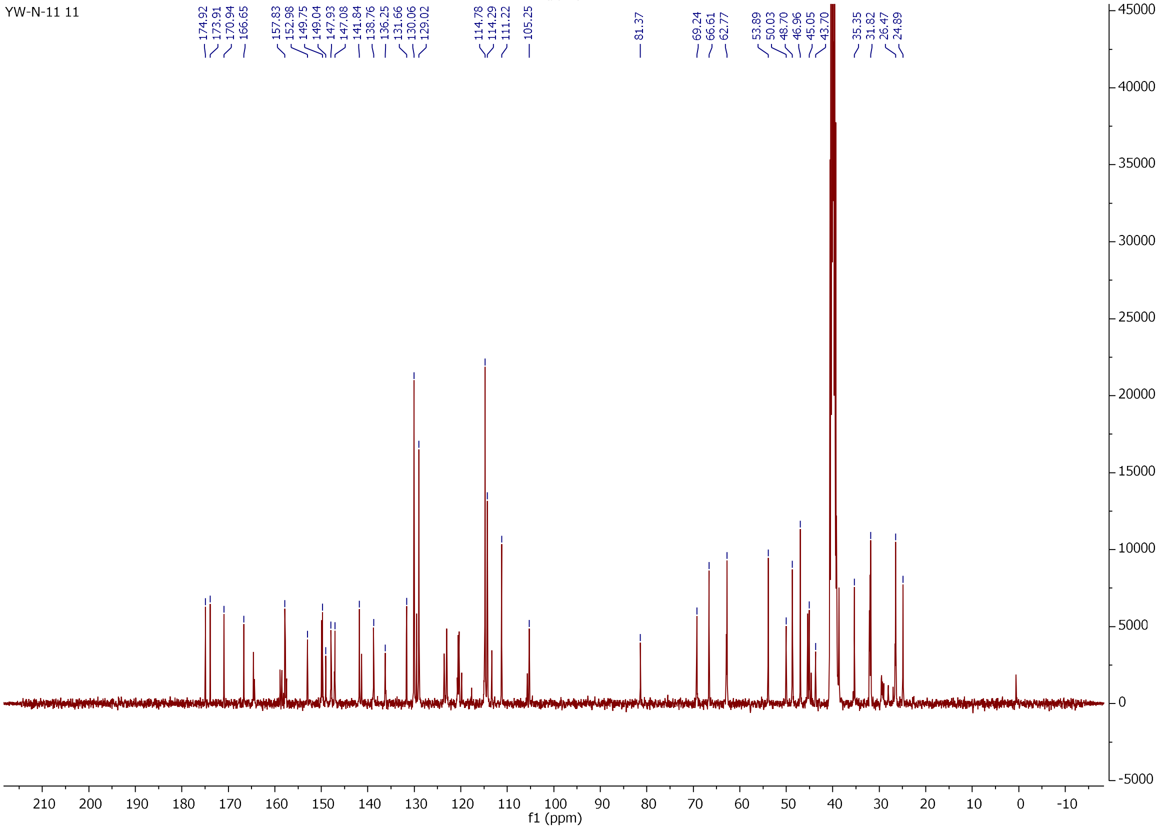
YW-N-11 11
174.92
173.91
170.94
166.65
157.83
152.98
149.75
149.04
147.93
147.08
141.84
138.76
136.25
131.66
130.06
129.02
114.78
114.29
111.22
105.25
81.37
69.24
66.61
62.77
53.89
50.03
48.70
46.96
45.05
43.70
35.35
31.82
26.47
24.89
210 200 190 180 170 160 150 140 130 120 110 100 90 80 70 60 50 40 30 20 10 0 -10
f1 (ppm)
45000
40000
35000
30000
25000
20000
15000
10000
5000
0
-5000

S1.2. HRMS data

Table 1.2. HRMS data

Compound name	Exact Mass	HRMS
YW-L-1	874.3915	875.4016
YW-L-2	916.4384	917.4439
YW-L-3	958.4854	959.4893
YW-L-4	1004.4909	1005.4914
YW-L-5	936.3919	937.3947
YW-L-6	980.4181	981.4232
YW-L-7	1024.4443	1025.4492
YW-L-8	1034.4551	1035.4603
YW-L-9	1062.4864	1063.4966
YW-L-10	1088.5021	1089.5102
YW-L-11	1112.5021	1113.5224
YW-L-12	1140.5334	1141.4944
YW-N-1	769.3336	770.3434
YW-N-2	797.3649	798.3754
YW-N-3	825.3962	826.4066
YW-N-4	867.4432	868.4533
YW-N-5	958.4238	959.4336
YW-N-6	986.4551	987.4647
YW-N-7	1014.4864	1015.4968
YW-N-8	957.4286	958.4385
YW-N-9	985.4599	986.4700
YW-N-10	1013.4912	1014.5008
YW-N-11	1011.4755	1012.4851

YW-L-1

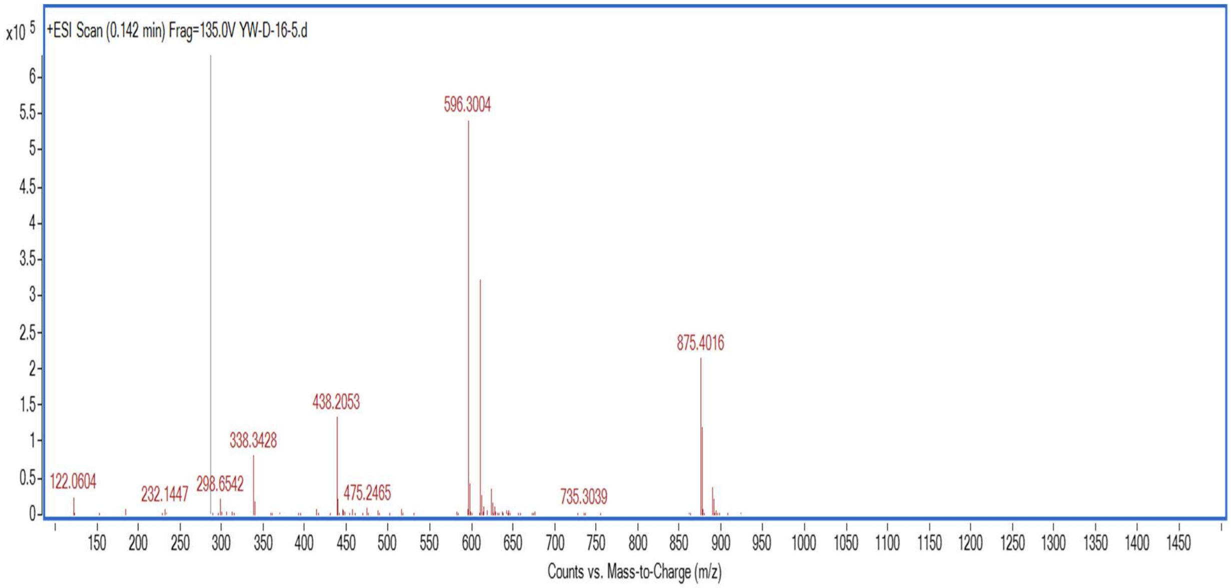
x10 5
+ESI Scan (0.142 min) Frag=135.0V YW-D-16-5.d
596.3004
875.4016
438.2053
338.3428
122.0604
232.1447
298.6542
475.2465
735.3039
Counts vs. Mass-to-Charge (m/z)

YW-L-2

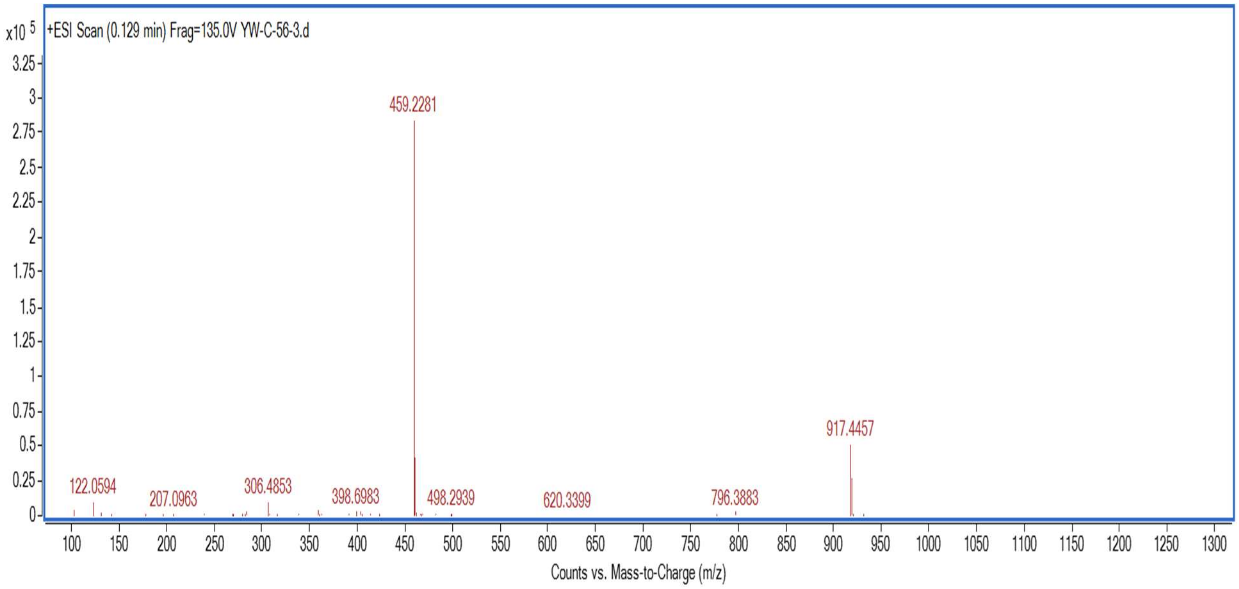
x10 5
+ESI Scan (0.129 min) Frag=135.0V YW-C-56-3.d
459.2281
917.4457
122.0594
207.0963
306.4853
398.6983
498.2939
620.3399
796.3883
Counts vs. Mass-to-Charge (m/z)

YW-L-3

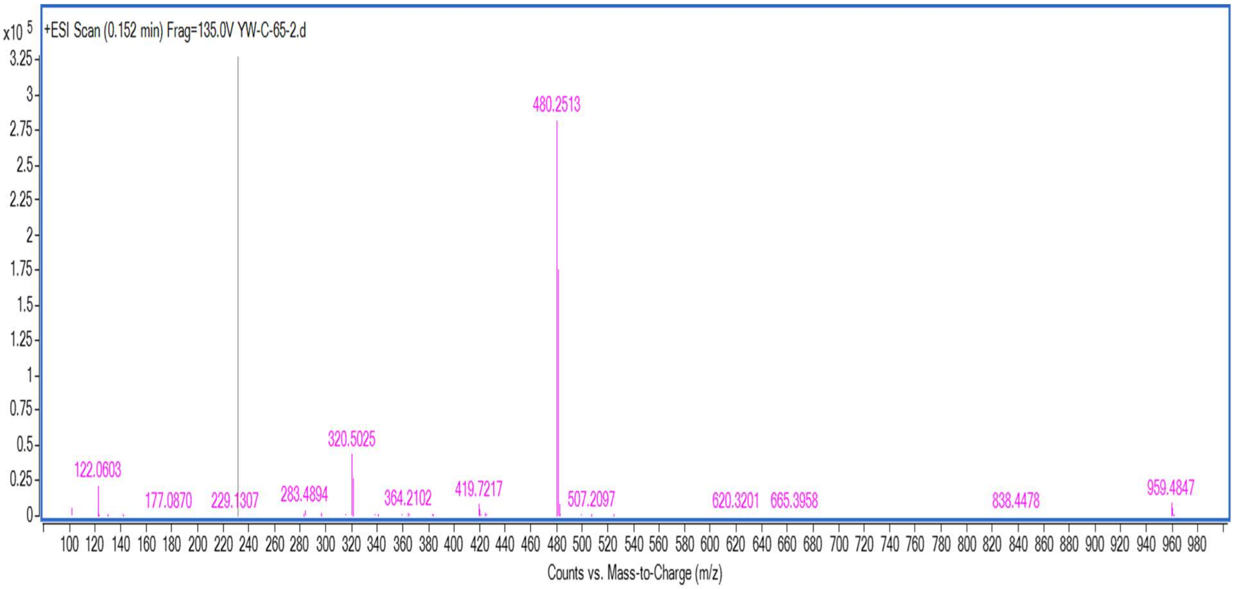
x10 5
+ESI Scan (0.152 min) Frag=135.0V YW-C-65-2.d
3.25
3
2.75
2.5
2.25
2
1.75
1.5
1.25
1
0.75
0.5
0.25
0
480.2513
320.5025
122.0603
177.0870
229.1307
283.4894
364.2102
419.7217
507.2097
620.3201
665.3958
838.4478
959.4847
100 120 140 160 180 200 220 240 260 280 300 320 340 360 380 400 420 440 460 480 500 520 540 560 580 600 620 640 660 680 700 720 740 760 780 800 820 840 860 880 900 920 940 960 980
Counts vs. Mass-to-Charge (m/z)

YW-L-4

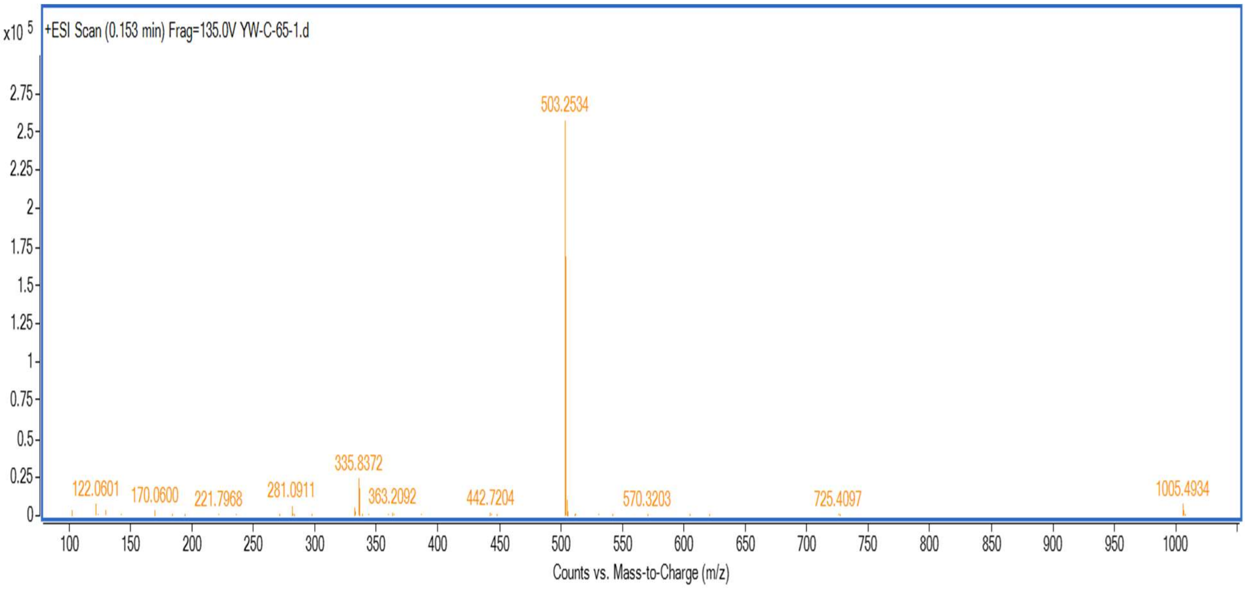
x10 5
+ESI Scan (0.153 min) Frag=135.0V YW-C-65-1.d
2.75
2.5
2.25
2
1.75
1.5
1.25
1
0.75
0.5
0.25
0
503.2534
335.8372
122.0601
170.0600
221.7968
281.0911
363.2092
442.7204
570.3203
725.4097
1005.4934
100 150 200 250 300 350 400 450 500 550 600 650 700 750 800 850 900 950 1000
Counts vs. Mass-to-Charge (m/z)

YW-L-5

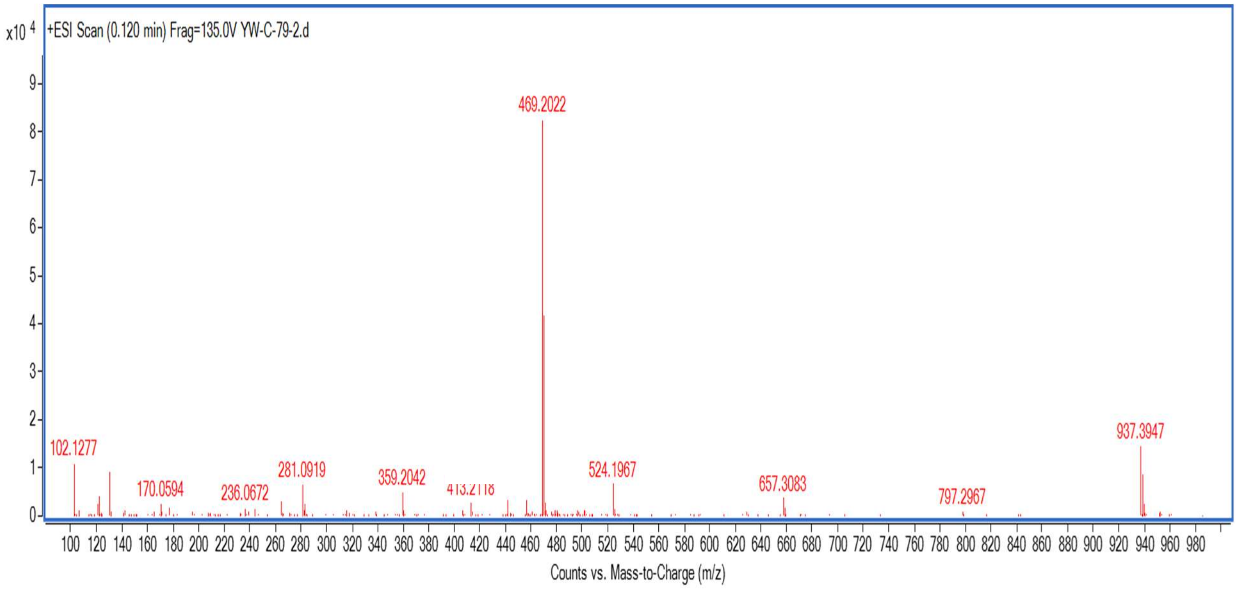
x10 4
+ESI Scan (0.120 min) Frag=135.0V YW-C-79-2.d
469.2022
937.3947
102.1277
170.0594
236.0672
281.0919
359.2042
413.2118
524.1967
657.3083
797.2967
0
1
2
3
4
5
6
7
8
9
100 120 140 160 180 200 220 240 260 280 300 320 340 360 380 400 420 440 460 480 500 520 540 560 580 600 620 640 660 680 700 720 740 760 780 800 820 840 860 880 900 920 940 960 980
Counts vs. Mass-to-Charge (m/z)

YW-L-9

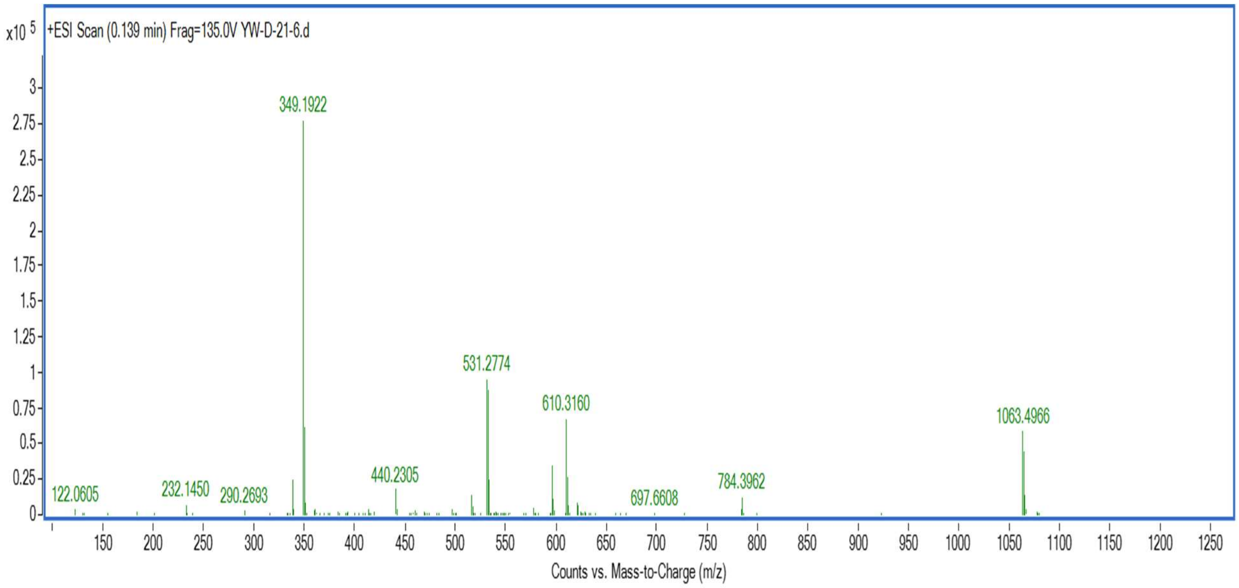
x10 5
+ESI Scan (0.139 min) Frag=135.0V YW-D-21-6.d
349.1922
531.2774
610.3160
1063.4966
122.0605
232.1450
290.2693
440.2305
697.6608
784.3962
0
0.25
0.5
0.75
1
1.25
1.5
1.75
2
2.25
2.5
2.75
3
150 200 250 300 350 400 450 500 550 600 650 700 750 800 850 900 950 1000 1050 1100 1150 1200 1250
Counts vs. Mass-to-Charge (m/z)

YW-L-11

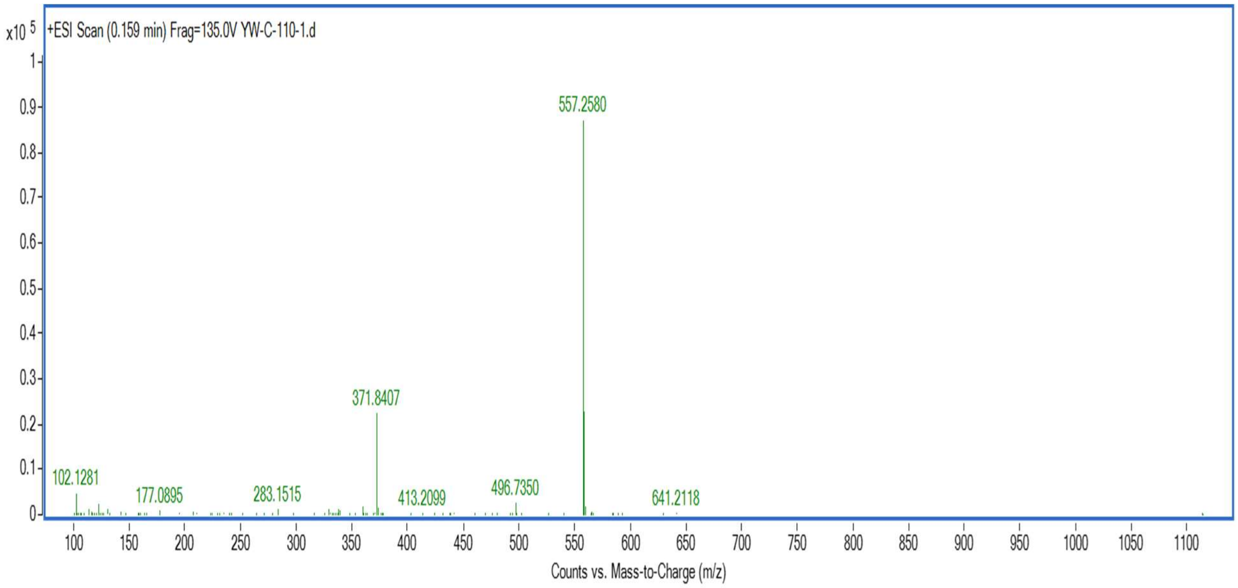

x10 5
+ESI Scan (0.159 min) Frag=135.0V YW-C-110-1.d
557.2580
371.8407
102.1281
177.0895
283.1515
413.2099
496.7350
641.2118
Counts vs. Mass-to-Charge (m/z)

YW-N-1

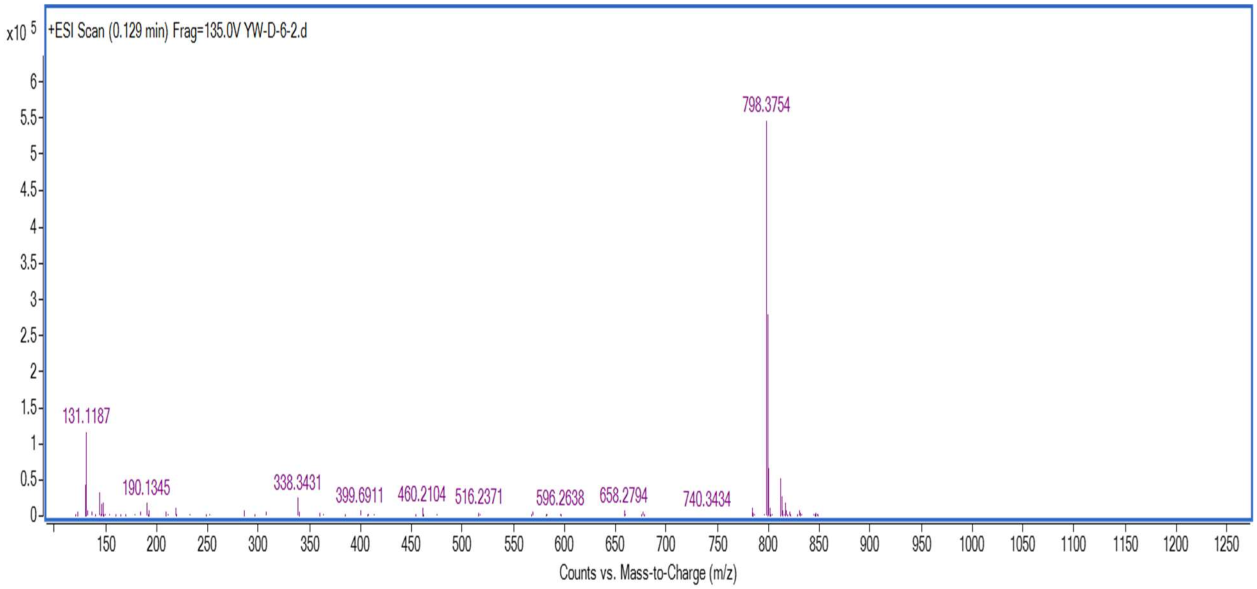

x10 5
+ESI Scan (0.129 min) Frag=135.0V YW-D-6-2.d
798.3754
131.1187
190.1345
338.3431
399.6911
460.2104
516.2371
596.2638
658.2794
740.3434
Counts vs. Mass-to-Charge (m/z)

YW-N-2

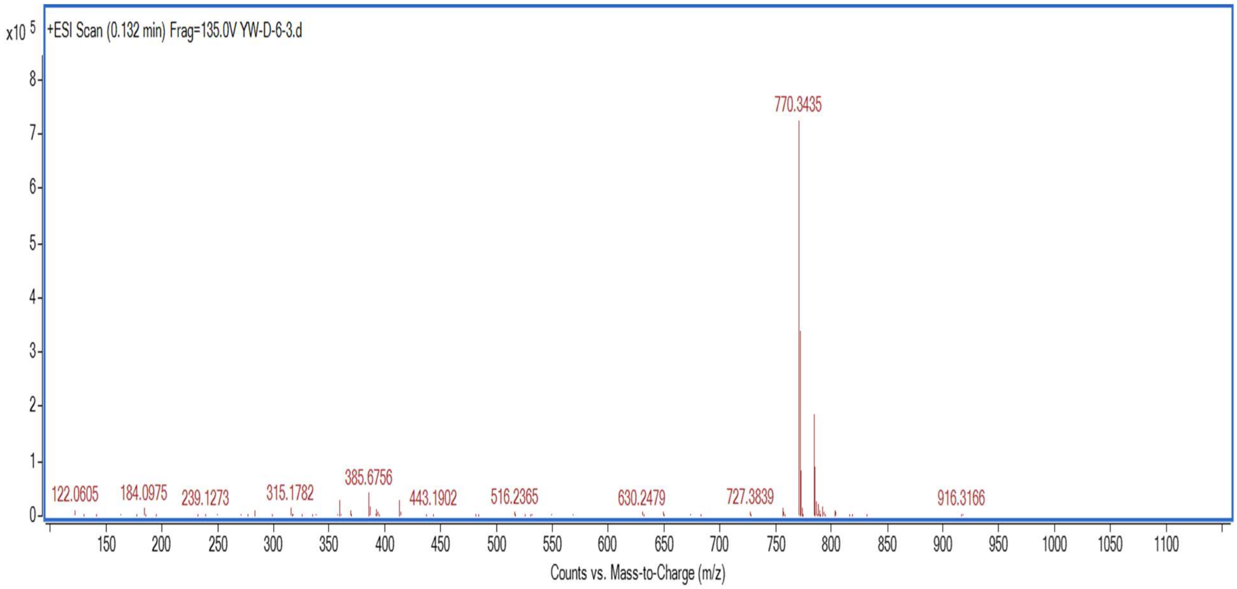
x10 5
+ESI Scan (0.132 min) Frag=135.0V YW-D-6-3.d
770.3435
122.0605
184.0975
239.1273
315.1782
385.6756
443.1902
516.2365
630.2479
727.3839
916.3166
0 1 2 3 4 5 6 7 8
150 200 250 300 350 400 450 500 550 600 650 700 750 800 850 900 950 1000 1050 1100
Counts vs. Mass-to-Charge (m/z)

YW-N-3

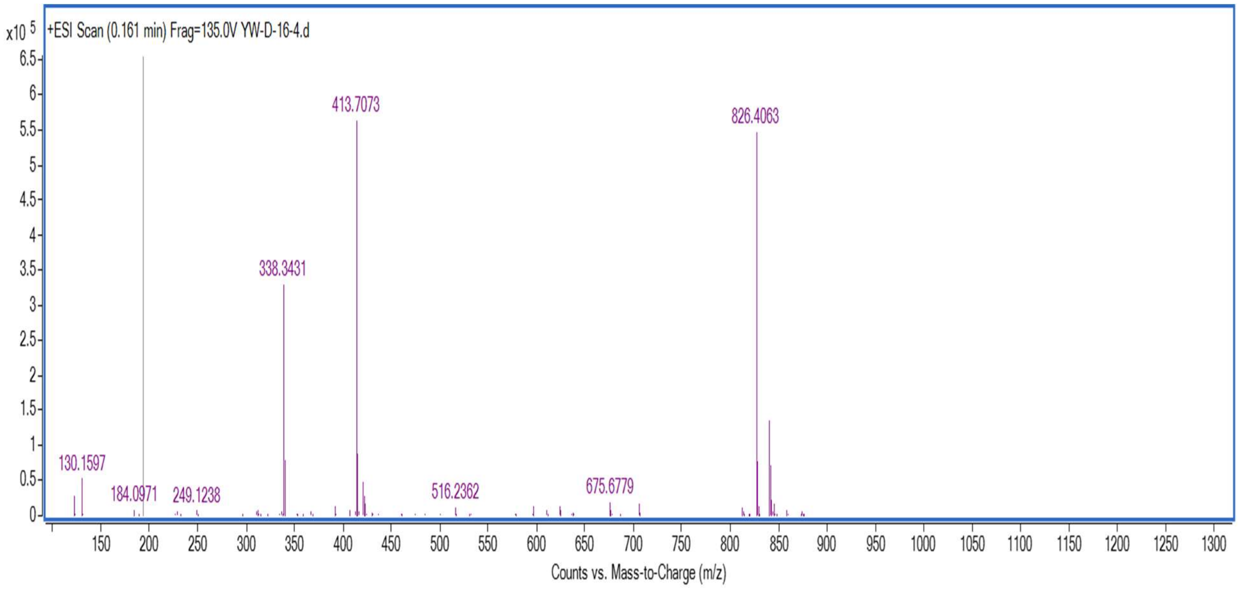
x10 5
+ESI Scan (0.161 min) Frag=135.0V YW-D-16-4.d
413.7073
826.4063
338.3431
130.1597
184.0971
249.1238
516.2362
675.6779
0 0.5 1 1.5 2 2.5 3 3.5 4 4.5 5 5.5 6 6.5
150 200 250 300 350 400 450 500 550 600 650 700 750 800 850 900 950 1000 1050 1100 1150 1200 1250 1300
Counts vs. Mass-to-Charge (m/z)

YW-N-4

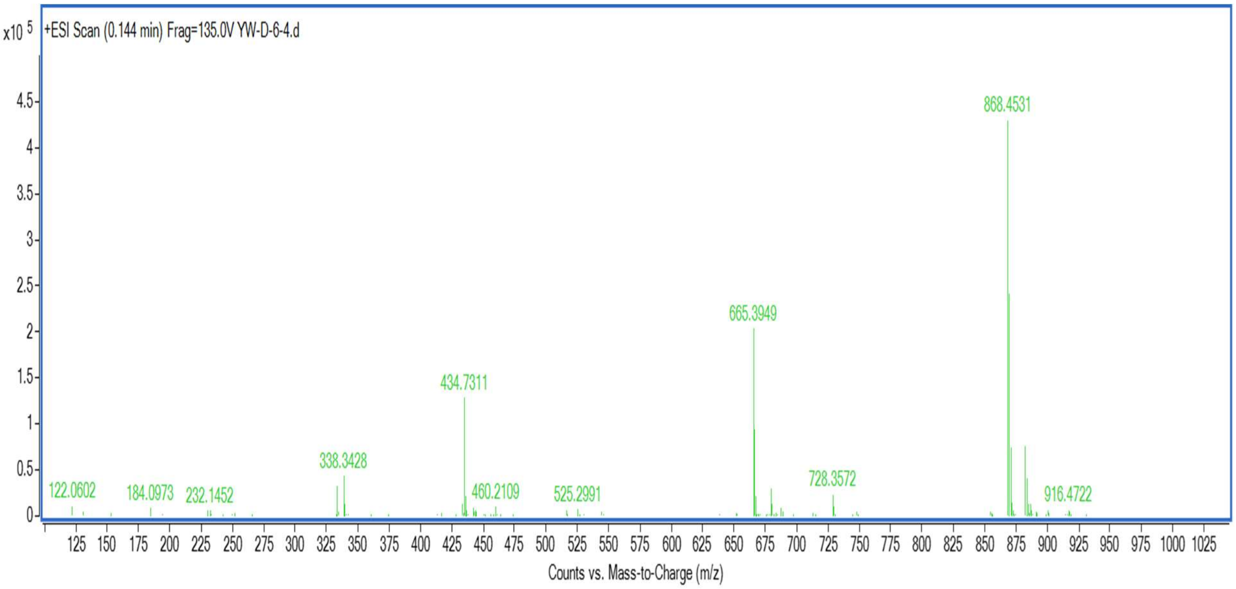
x10 5
+ESI Scan (0.144 min) Frag=135.0V YW-D-6-4.d
4.5
4
3.5
3
2.5
2
1.5
1
0.5
0
868.4531
665.3949
434.7311
338.3428
728.3572
122.0602
184.0973
232.1452
460.2109
525.2991
916.4722
125 150 175 200 225 250 275 300 325 350 375 400 425 450 475 500 525 550 575 600 625 650 675 700 725 750 775 800 825 850 875 900 925 950 975 1000 1025
Counts vs. Mass-to-Charge (m/z)

YW-N-5

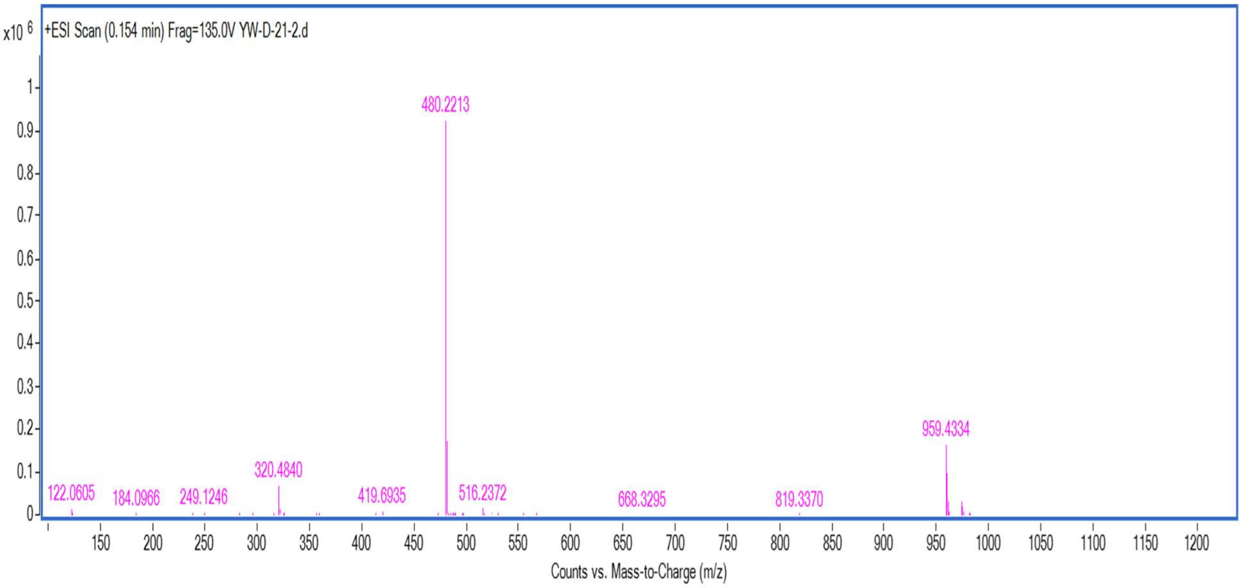
x10 6
+ESI Scan (0.154 min) Frag=135.0V YW-D-21-2.d
1
0.9
0.8
0.7
0.6
0.5
0.4
0.3
0.2
0.1
0
480.2213
959.4334
320.4840
122.0605
184.0966
249.1246
419.6935
516.2372
668.3295
819.3370
150 200 250 300 350 400 450 500 550 600 650 700 750 800 850 900 950 1000 1050 1100 1150 1200
Counts vs. Mass-to-Charge (m/z)

YW-N-6

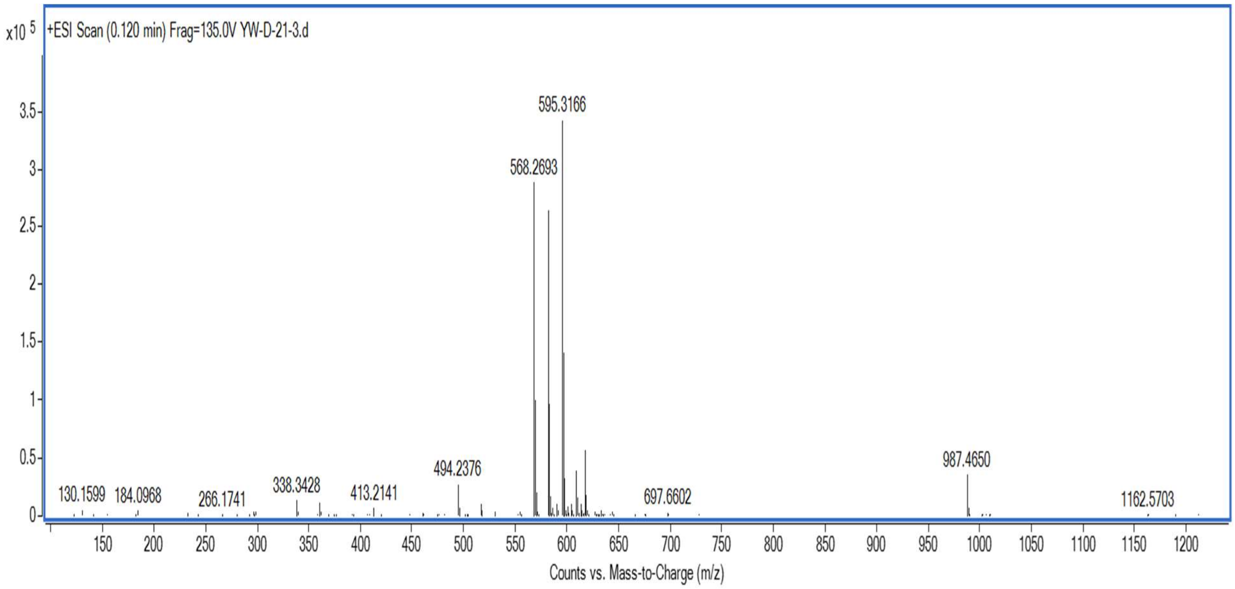
x10 5
+ESI Scan (0.120 min) Frag=135.0V YW-D-21-3.d
3.5
3
2.5
2
1.5
1
0.5
0
595.3166
568.2693
494.2376
987.4650
130.1599
184.0968
266.1741
338.3428
413.2141
697.6602
1162.5703
150 200 250 300 350 400 450 500 550 600 650 700 750 800 850 900 950 1000 1050 1100 1150 1200
Counts vs. Mass-to-Charge (m/z)

YW-N-7

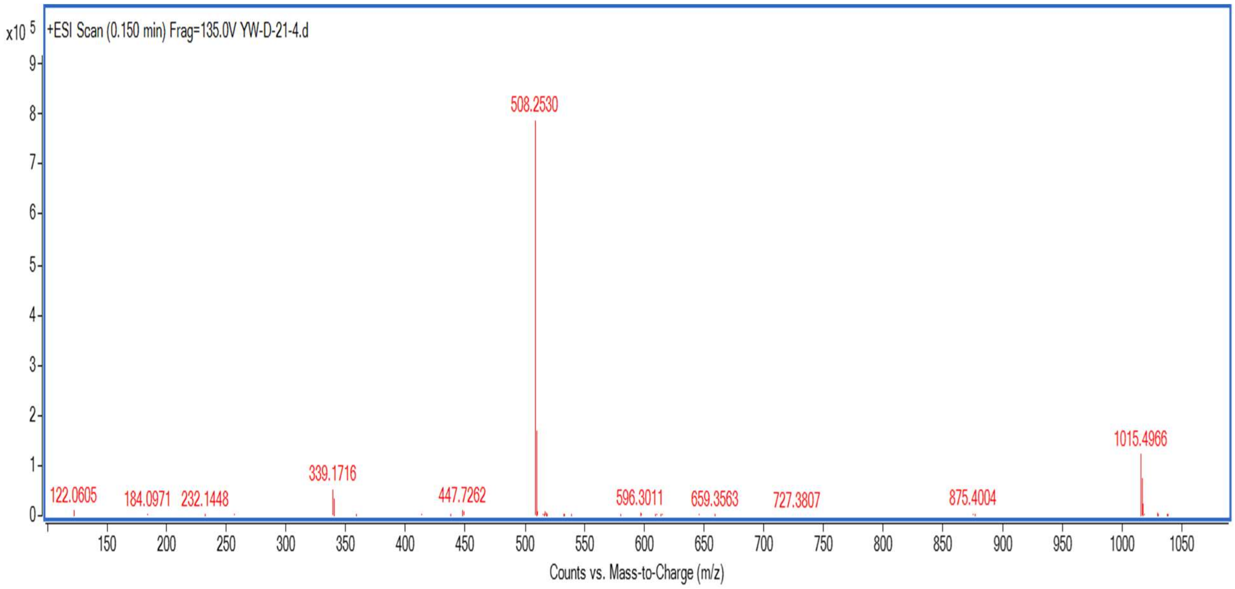
x10 5
+ESI Scan (0.150 min) Frag=135.0V YW-D-21-4.d
9
8
7
6
5
4
3
2
1
0
508.2530
1015.4966
339.1716
122.0605
184.0971
232.1448
447.7262
596.3011
659.3563
727.3807
875.4004
150 200 250 300 350 400 450 500 550 600 650 700 750 800 850 900 950 1000 1050
Counts vs. Mass-to-Charge (m/z)

YW-N-8

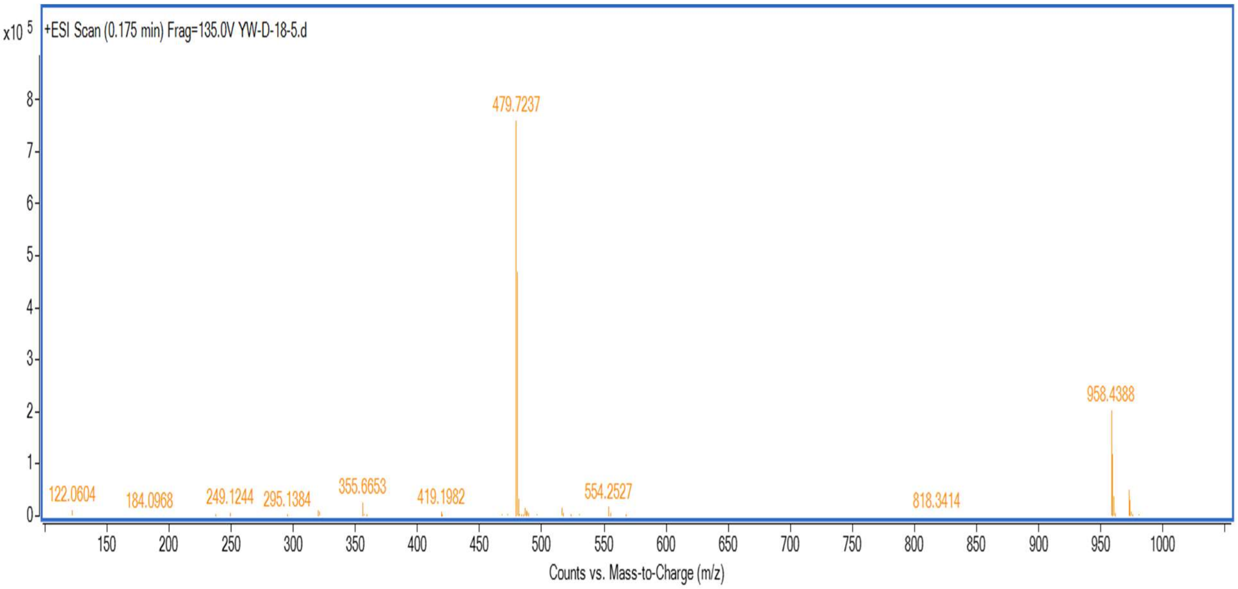
x10 5
+ESI Scan (0.175 min) Frag=135.0V YW-D-18-5.d
479.7237
958.4388
122.0604
184.0968
249.1244
295.1384
355.6653
419.1982
554.2527
818.3414
Counts vs. Mass-to-Charge (m/z)

YW-N-9

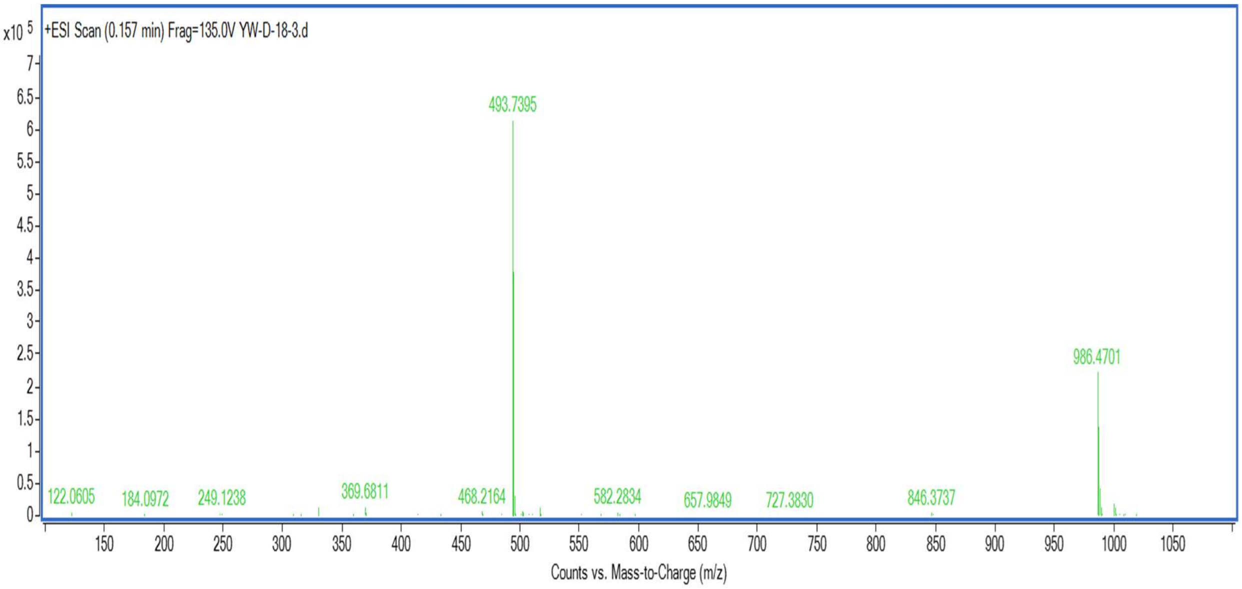
x10 5
+ESI Scan (0.157 min) Frag=135.0V YW-D-18-3.d
493.7395
986.4701
122.0605
184.0972
249.1238
369.6811
468.2164
582.2834
657.9849
727.3830
846.3737
Counts vs. Mass-to-Charge (m/z)

YW-N-10

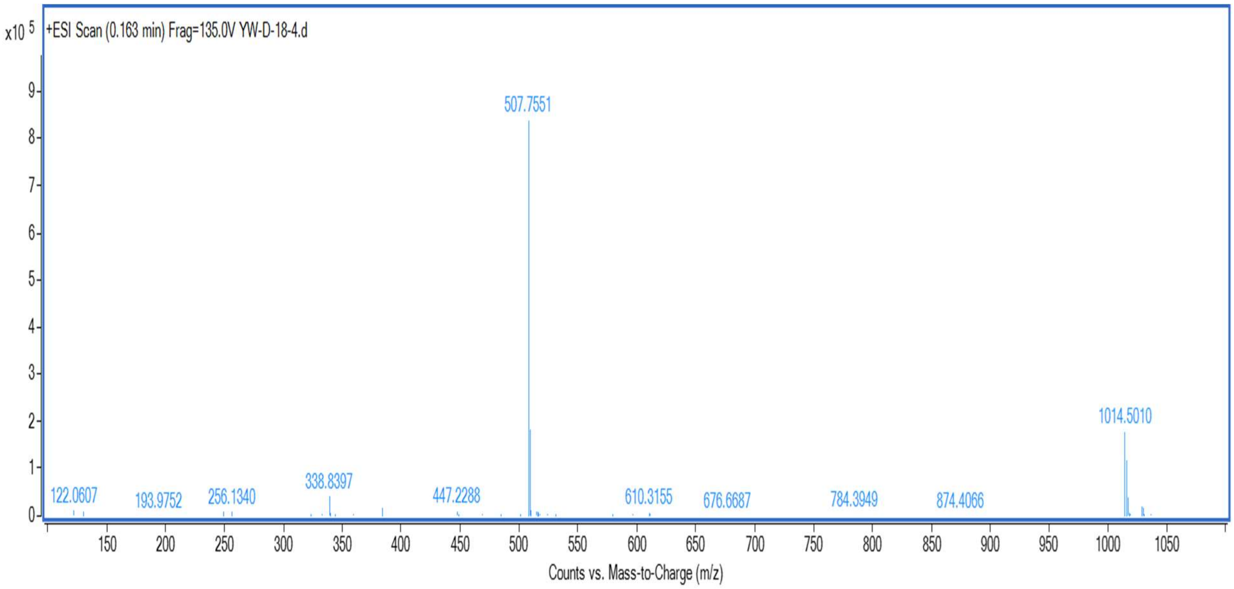

x10 5
+ESI Scan (0.163 min) Frag=135.0V YW-D-18-4.d
9
8
7
6
5
4
3
2
1
0
507.7551
1014.5010
122.0607
193.9752
256.1340
338.8397
447.2288
610.3155
676.6687
784.3949
874.4066
150
200
250
300
350
400
450
500
550
600
650
700
750
800
850
900
950
1000
1050
Counts vs. Mass-to-Charge (m/z)

YW-N-11

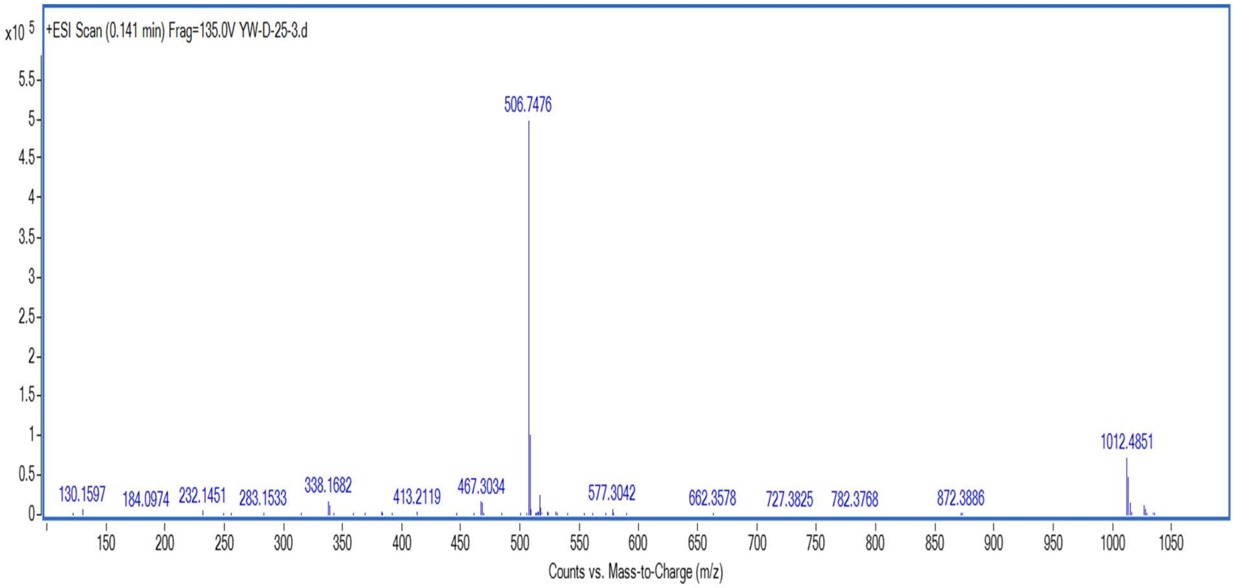

x10 5
+ESI Scan (0.141 min) Frag=135.0V YW-D-25-3.d
5.5
5
4.5
4
3.5
3
2.5
2
1.5
1
0.5
0
506.7476
1012.4851
130.1597
184.0974
232.1451
283.1533
338.1682
413.2119
467.3034
577.3042
662.3578
727.3825
782.3768
872.3886
150
200
250
300
350
400
450
500
550
600
650
700
750
800
850
900
950
1000
1050
Counts vs. Mass-to-Charge (m/z)

YW-T-1

^{1}H NMR (400 MHz, DMSO-d_6) δ 9.41 (s, 1H), 8.64 (s, 1H), 8.56 (s, 1H), 8.40 (d, *J* = 7.5 Hz, 1H), 8.13 (s, 1H), 7.88 (t, *J* = 7.5 Hz, 2H), 7.77 (t, *J* = 7.9 Hz, 1H), 7.52 (d, *J* = 8.5 Hz, 1H), 7.42 (d, *J* = 7.2 Hz, 1H), 7.26 (s, 1H), 6.93 (d, *J* = 8.4 Hz, 1H), 6.81 (d, *J* = 8.8 Hz, 1H), 5.08 (d, *J* = 7.5 Hz, 2H), 4.63 (s, 3H), 4.48 (d, *J* = 6.1 Hz, 2H), 4.24 (d, *J* = 12.6 Hz, 3H), 4.07 (d, *J* = 23.7 Hz, 5H), 3.92 (s, 1H), 3.88 (d, *J* = 4.3 Hz, 4H), 3.49 (s, 3H), 2.88 (d, *J* = 7.3 Hz, 2H), 2.60 (s, 2H), 2.30 (s, 2H), 2.00 (s, 4H).

^{13}C NMR (101 MHz, DMSO-d_6) δ 173.25, 172.40, 170.39, 167.23, 165.71, 164.62, 157.73, 156.16, 149.90, 149.75, 149.03, 147.90, 147.03, 141.84, 138.76, 137.43, 136.20, 136.10, 133.69, 129.48, 122.98, 120.49, 116.91, 115.93, 113.24, 111.22, 105.25, 81.36, 69.06, 67.95, 62.77, 53.88, 50.46, 50.03, 49.21, 48.71, 38.44, 31.88, 31.41, 26.60, 24.89, 22.47.

YW-T-2

^{1}H NMR (400 MHz, Chloroform-*d*) δ 10.50 (s, 1H), 9.39 (s, 1H), 8.67 (s, 1H), 8.57 (s, 1H), 8.40 (d, *J* = 14.9 Hz, 1H), 8.00 (t, *J* = 5.3 Hz, 1H), 7.88 (d, *J* = 8.6 Hz, 1H), 7.83 – 7.75 (m, 1H), 7.54 (d, *J* = 8.5 Hz, 1H), 7.45 (d, *J* = 7.2 Hz, 1H), 7.26 (s, 1H), 6.93 (d, *J* = 8.3 Hz, 1H), 6.81 (d, *J* = 8.8 Hz, 1H), 5.07 (d, *J* = 12.8 Hz, 1H), 4.63 (s, 4H), 4.46 (s, 3H), 4.26 – 4.18 (m, 3H), 4.15 – 4.00 (m, 5H), 3.91 (s, 1H), 3.87 (d, *J* = 4.4 Hz, 3H), 3.43 (d, *J* = 5.6 Hz, 2H), 2.89 (s, 1H), 2.58 (d, *J* = 17.6 Hz, 1H), 2.06 (t, *J* = 7.3 Hz, 3H), 1.74 (s, 2H), 1.44 (d, *J* = 23.5 Hz, 4H), 1.35 – 1.27 (m, 2H), 1.22 (s, 7H).

^{13}C NMR (101 MHz, Chloroform-*d*) δ 177.99, 177.89, 175.12, 172.01, 169.37, 162.48, 160.98, 154.81, 154.50, 153.79, 152.68, 151.78, 146.59, 143.54, 142.23, 138.49, 134.25, 127.76, 125.48, 125.33, 121.70, 120.74, 117.88, 115.97, 110.00, 86.09, 74.38, 72.69, 67.67, 58.63, 54.78, 53.97, 53.46, 48.46, 43.14, 40.47, 36.16, 34.16, 34.07, 33.90, 33.83, 33.64, 31.35, 30.63, 30.39, 27.24.

YW-T-3

^{1}H NMR (400 MHz, DMSO-d_6) δ 9.38 (s, 1H), 8.66 (d, *J* = 5.2 Hz, 1H), 8.59 (d, *J* = 10.6 Hz, 1H), 8.40 (d, *J* = 11.6 Hz, 1H), 8.07 (t, *J* = 5.0 Hz, 1H), 7.88 (d, *J* = 8.6 Hz, 1H), 7.56 (t, *J* = 7.8 Hz, 1H), 7.26 (d, *J* = 8.2 Hz, 1H), 7.16 (d, *J* = 8.6 Hz, 1H), 7.00 (d, *J* = 7.0 Hz, 1H), 6.93 (d, *J* = 8.5 Hz, 1H), 6.81 (d, *J* = 8.8 Hz, 1H), 6.71 (s, 1H), 5.04 (dd, *J* = 12.8, 5.3 Hz, 1H), 4.64 (d, *J* = 5.2 Hz, 3H), 4.47 (d, *J* = 6.1 Hz, 2H), 4.08 (dd, *J* = 15.9, 10.2 Hz, 6H), 3.60 – 3.46 (m, 1H), 3.45 – 3.32 (m, 2H), 3.25 (d, *J* = 5.6 Hz, 2H), 2.87 (t, *J* = 12.9 Hz, 2H), 2.58 (s, 1H), 2.53 (s, 1H), 2.15 (s, 2H), 2.04 (dd, *J* = 28.2, 9.6 Hz, 2H), 1.70 (d, *J* = 8.8 Hz, 5H).

^{13}C NMR (101 MHz, DMSO-d_6) δ 173.26, 173.12 (d, *J* = 29.5 Hz), 170.55, 169.19, 167.75, 164.62, 157.77, 150.00, 149.88 (d, *J* = 24.9 Hz), 149.05, 147.99, 147.05, 146.94 (d, *J* = 22.5 Hz), 138.74, 136.64, 136.21, 132.66, 129.52, 122.99, 117.61, 113.09, 111.11 (d, *J* = 23.6 Hz), 105.21, 81.36, 69.33, 62.95, 62.79, 53.89, 50.03, 48.85 (d, *J* = 28.5 Hz), 41.96, 38.47, 35.25, 31.44, 28.34, 26.60, 22.40 (d, *J* = 45.6 Hz).

YW-T-4

^{1}H NMR (400 MHz, DMSO-d_6) δ 9.39 (s, 1H), 8.66 (s, 1H), 8.57 (s, 1H), 8.40 (d, *J* = 10.0 Hz, 1H), 7.88 (d, *J* = 8.6 Hz, 1H), 7.78 (t, *J* = 4.9 Hz, 1H), 7.56 (t, *J* = 7.8 Hz, 1H), 7.26 (s, 1H), 7.03 (dd, *J* = 25.5, 7.8 Hz, 2H), 6.93 (d, *J* = 8.3 Hz, 1H), 6.81 (d, *J* = 8.8 Hz, 1H), 6.51 (s, 1H), 5.04 (dd, *J* = 12.8, 5.3 Hz, 1H), 4.63 (s, 2H), 4.47 (d, *J* = 6.1 Hz, 2H), 4.07 (d, *J* = 24.0 Hz, 4H), 3.97 – 3.81 (m, 4H), 3.58 – 3.45 (m, 1H), 3.27 (s, 2H), 3.03 (d, *J* = 6.0 Hz, 2H), 2.88 (t, *J* = 12.9 Hz, 1H), 2.58 (d, *J* = 17.6 Hz, 1H), 2.21 – 1.94 (m, 4H), 1.80 – 1.61 (m, 4H), 1.60 – 1.49 (m, 2H), 1.45 – 1.19 (m, 5H).

^{13}C NMR (101 MHz, DMSO-d_6) δ 173.29, 172.11, 170.57, 169.42, 164.62, 157.75, 150.01, 149.75, 147.96, 146.86, 141.84, 138.74, 136.73, 136.20, 132.65, 129.52, 122.99, 120.37, 117.59, 114.92, 113.12, 111.22, 110.84, 109.47, 105.22, 81.36, 69.36, 62.78, 53.88, 50.03, 49.01, 48.70, 42.24, 35.34, 31.45, 29.58, 29.09, 28.40, 26.60, 26.49, 22.62, 22.33.

YW-T-6

^{1}H NMR (400 MHz, DMSO-d_6) δ 9.37 (s, 1H), 8.71 (d, *J* = 4.4 Hz, 1H), 8.59 (d, *J* = 10.4 Hz, 1H), 8.40 (d, *J* = 13.9 Hz, 1H), 8.07 (t, *J* = 5.2 Hz, 1H), 7.88 (dd, *J* = 8.7, 2.2 Hz, 1H), 7.63 – 7.51 (m, 1H), 7.31 (d, *J* = 7.3 Hz, 1H), 7.15 (d, *J* = 8.6 Hz, 1H), 7.02 (d, *J* = 7.0 Hz, 1H), 6.93 (d, *J* = 8.4 Hz, 1H), 6.81 (d, *J* = 8.8 Hz, 1H), 6.71 (s, 1H), 5.05 (dd, *J* = 12.8, 5.2 Hz, 1H), 4.63 (s, 2H), 4.47 (d, *J* = 6.0 Hz, 2H), 4.25 (s, 3H), 4.15 – 4.01 (m, 5H), 3.88 (d, *J* = 4.5 Hz, 5H), 3.79 (s, 4H), 3.61 – 3.40 (m, 16H), 3.40 – 3.30 (m, 2H), 3.23 (d, *J* = 5.7 Hz, 2H), 2.88 (t, *J* = 13.0 Hz, 2H), 2.69 – 2.55 (m, 2H), 2.29 (t, *J* = 6.4 Hz, 2H), 2.04 (dt, *J* = 13.1, 6.2 Hz, 2H).

^{13}C NMR (101 MHz, DMSO-d_6) δ 173.28, 171.12, 170.55, 169.18, 167.76, 164.62, 157.79, 149.75, 149.05, 148.04, 147.09, 146.94 (d, *J* = 29.7 Hz), 141.84, 138.72, 136.67, 129.55, 122.97, 120.56, 117.61, 114.91, 113.32, 111.12 (d, *J* = 20.5 Hz), 81.39, 70.70 – 69.72 (m), 69.15, 67.18, 62.79, 53.89, 50.03, 48.85 (d, *J* = 28.9 Hz), 41.89, 38.50, 36.57, 31.45, 26.60, 22.63.

YW-V-1

^{1}H NMR (400 MHz, DMSO-d_6) δ 10.48 (s, 1H), 9.39 (s, 1H), 9.00 (s, 1H), 8.69 (s, 1H), 8.64 – 8.47 (m, 2H), 8.42 (d, *J* = 14.7 Hz, 1H), 8.02 – 7.81 (m, 3H), 7.41 (d, *J* = 8.2 Hz, 4H), 7.29 (s, 1H), 6.94 (d, *J* = 8.2 Hz, 1H), 6.83 (d, *J* = 8.8 Hz, 1H), 4.65 (s, 4H), 4.58 (d, *J* = 8.8 Hz, 3H), 4.37 (s, 2H), 4.23 (s, 3H), 4.18 – 3.99 (m, 6H), 3.91 (d, *J* = 11.5 Hz, 5H), 3.67 (s, 2H), 3.53 (s, 1H), 2.46 (s, 3H), 2.41 – 2.31 (m, 1H), 2.25 (s, 1H), 2.06 (d, *J* = 9.9 Hz, 2H), 1.92 (s, 1H), 1.73 (d, *J* = 22.0 Hz, 4H), 0.95 (s, 9H). ^{13}C NMR (101 MHz, DMSO-d_6) δ 172.41, 170.15, 164.63, 157.76, 151.95, 149.90 (d, *J* = 28.3 Hz), 147.99, 147.06, 141.85, 139.99, 129.53, 129.11, 127.89, 123.05, 113.17, 111.23, 105.23, 81.36, 69.34, 62.79, 59.17, 56.86, 53.89, 48.72, 42.12, 38.45, 35.28 (d, *J* = 90.0 Hz), 28.41, 26.86, 22.47, 16.41.

YW-V-2

^{1}H NMR (400 MHz, DMSO-d_6) δ 10.33 (s, 1H), 9.30 (s, 1H), 8.91 (s, 1H), 8.61 (s, 1H), 8.53 (s, 2H), 8.33 (d, *J* = 13.5 Hz, 2H), 8.21 (s, 1H), 7.82 (d, *J* = 8.5 Hz, 1H), 7.76 (d, *J* = 9.2 Hz, 1H), 7.33 (q, *J* = 8.0 Hz, 4H), 7.19 (s, 1H), 6.86 (d, *J* = 8.5 Hz, 1H), 6.74 (d, *J* = 8.8 Hz, 1H), 4.61 – 4.52 (m, 3H), 4.47 (d, *J* = 9.3 Hz, 2H), 4.39 (s, 5H), 4.35 (s, 3H), 4.28 (s, 5H), 4.16 (s, 7H), 4.06 – 3.98 (m, 7H), 3.97 (s, 2H), 3.84 (s, 1H), 3.81 (d, *J* = 3.8 Hz, 4H), 3.57 (s, 2H), 3.50 – 3.38 (m, 1H), 2.60 (s, 1H), 2.37 (s, 3H), 2.26 (s, 1H), 2.21 (s, 1H), 1.99 (s, 4H), 1.83 (s, 1H), 1.69 (s, 3H), 1.36 (s, 5H), 1.19 (s, 11H), 0.86 (s, 9H).

^{13}C NMR (101 MHz, DMSO-d_6) δ 172.55, 172.41, 170.17, 165.01, 158.77, 158.42, 157.75, 151.94, 150.07, 149.75, 147.98, 147.04, 141.84, 141.36, 139.99, 138.76, 136.21, 131.64, 130.09, 129.52, 129.10, 127.89, 123.01, 113.13, 111.23, 105.22, 81.34, 69.63, 69.32, 62.95, 62.79, 59.16, 56.81, 56.73, 53.88, 50.03, 48.71, 43.70, 42.11, 38.43, 35.69, 35.32, 29.40, 29.21, 29.16, 29.12, 28.90, 26.84, 25.90, 16.40.

YW-V-3

^{1}H NMR (400 MHz, DMSO-d_6) δ 10.65 (s, 1H), 9.46 (s, 1H), 9.00 (d, *J* = 2.9 Hz, 1H), 8.74 (d, *J* = 7.1 Hz, 1H), 8.42 (d, *J* = 13.4 Hz, 1H), 7.91 (d, *J* = 9.0 Hz, 3H), 7.41 (q, *J* = 7.9 Hz, 4H), 7.33 (d, *J* = 8.1 Hz, 1H), 6.94 (q, *J* = 7.8 Hz, 1H), 6.84 (d, *J* = 8.8 Hz, 1H), 4.65 (d, *J* = 6.4 Hz, 2H), 4.56 (d, *J* = 9.0 Hz, 1H), 4.52 – 4.39 (m, 3H), 4.36 (s, 1H), 4.32 – 4.18 (m, 4H), 4.17 – 4.01 (m, 3H), 3.94 (s, 1H), 3.89 (d, *J* = 3.9 Hz, 3H), 3.81 (t, *J* = 4.3 Hz, 2H), 3.73 – 3.39 (m, 16H), 2.90 (q, *J* = 7.7, 6.5 Hz, 1H), 2.45 (d, *J* = 3.1 Hz, 3H), 2.41 – 2.27 (m, 1H), 2.06 (q, *J* = 9.5 Hz, 2H), 1.91 (ddt, *J* = 12.7, 8.1, 3.8 Hz, 1H), 0.94 (s, 9H).

^{13}C NMR (101 MHz, DMSO-d_6) δ 172.40, 170.42, 170.00, 164.62, 157.86, 151.97, 149.93, 149.76, 148.12, 147.83, 147.09, 141.86, 141.36, 140.00, 138.86, 131.67, 130.08, 129.49, 129.11, 127.90, 123.02, 120.38, 117.45, 114.92, 113.37, 111.22, 105.34, 81.40, 70.37, 70.26, 70.17, 69.94, 69.33, 69.17, 67.41, 62.76, 59.19, 56.77, 53.88, 50.03, 48.72, 43.74, 42.12, 38.42, 36.12, 35.83, 26.79, 16.38.

YW-V-4

^{1}H NMR (400 MHz, DMSO-d_6) δ 9.40 (s, 1H), 8.99 (d, *J* = 2.5 Hz, 1H), 8.73 (d, *J* = 6.9 Hz, 1H), 8.59 (d, *J* = 7.4 Hz, 1H), 8.41 (d, *J* = 14.6 Hz, 1H), 8.00 – 7.80 (m, 3H), 7.41 (q, *J* = 8.0 Hz, 4H), 7.32 (d, *J* = 8.3 Hz, 1H), 6.94 (d, *J* = 8.5 Hz, 1H), 6.83 (d, *J* = 8.8 Hz, 1H), 4.65 (d, *J* = 5.5 Hz, 2H), 4.56 (d, *J* = 9.0 Hz, 1H), 4.47 (t, *J* = 7.1 Hz, 2H), 4.43 (d, *J* = 7.6 Hz, 1H), 4.36 (s, 1H), 4.24 (d, *J* = 6.0 Hz, 4H), 4.16 – 4.01 (m, 3H), 3.89 (d, *J* = 3.5 Hz, 3H), 3.79 (t, *J* = 4.4 Hz, 2H), 3.72 – 3.42 (m, 9H), 2.45 (d, *J* = 2.7 Hz, 3H), 2.38 (dd, *J* = 14.1, 7.0 Hz, 1H), 2.06 (q, *J* = 10.4, 9.4 Hz, 2H), 1.91 (tt, *J* = 9.7, 4.2 Hz, 1H), 0.93 (s, 9H).

^{13}C NMR (101 MHz, DMSO-d_6) δ 172.40, 170.41, 170.00, 164.62, 158.88, 157.72, 151.95, 149.93, 149.76, 149.05, 148.14, 147.92, 147.08, 141.84, 141.35, 139.98, 138.79, 136.29, 131.65, 130.09, 129.51, 129.10, 127.89, 123.00, 120.57, 120.38, 114.92, 113.31, 111.22, 105.28, 81.40, 70.34, 69.98, 69.33, 69.17, 67.45, 62.92, 62.78, 59.19, 56.85, 56.75, 53.88, 50.03, 48.72, 43.72, 42.12, 38.42, 36.12, 35.84, 26.79, 16.39.

W-2-3 C_4

^{1}H NMR (400 MHz, DMSO-d_6) δ 12.24 (s, 1H), 9.49 (s, 1H), 8.70 (s, 1H), 8.59 (s, 1H), 8.43 (t, *J* = 17.2 Hz, 2H), 7.89 (d, *J* = 7.9 Hz, 2H), 7.29 (s, 1H), 6.91 (s, 1H), 6.82 (d, *J* = 8.4 Hz, 1H), 4.56 (d, *J* = 68.6 Hz, 3H), 4.20 – 4.10 (m, 2H), 4.06 (d, *J* = 11.5 Hz, 2H), 3.90 (d, *J* = 16.5 Hz, 4H), 3.45 (d, *J* = 56.9 Hz, 6H), 3.17 (s, 1H), 2.43 (t, *J* = 7.1 Hz, 2H), 2.12 – 2.04 (m, 1H), 2.04 – 1.94 (m, 2H).

^{13}C NMR (101 MHz, DMSO-d_6) δ 174.48, 164.61, 157.82, 149.90, 147.58 (d, *J* = 96.9 Hz), 141.83, 136.25, 129.61, 122.95, 120.55, 114.95, 113.26, 111.19, 105.17, 81.38, 68.83, 62.77, 53.86, 50.01, 48.67, 43.75, 30.46, 26.60, 24.41.

W-2-3 C_6

^{1}H NMR (400 MHz, DMSO-d_6) δ 12.04 (s, 1H), 9.45 (s, 1H), 8.69 (s, 1H), 8.59 (s, 1H), 8.41 (d, *J* = 18.8 Hz, 2H), 8.19 (s, 1H), 7.89 (d, *J* = 8.8 Hz, 2H), 7.81 (d, *J* = 10.7 Hz, 1H), 7.28 (s, 1H), 6.98 – 6.76 (m, 2H), 4.56 (d, *J* = 68.0 Hz, 3H), 4.10 (t, *J* = 6.4 Hz, 3H), 3.92 (s, 2H), 3.87 (s, 5H), 3.52 (s, 1H), 2.25 (t, *J* = 7.3 Hz, 2H), 2.07 (d, *J* = 10.3 Hz, 1H), 1.77 (p, *J* = 6.9 Hz, 2H), 1.59 (p, *J* = 7.3 Hz, 2H), 1.45 (p, *J* = 7.8 Hz, 3H).

^{13}C NMR (101 MHz, DMSO-d_6) δ 174.90, 157.87, 153.16 – 146.68 (m), 138.66, 136.21, 129.59, 122.91, 121.74 (d, *J* = 236.3 Hz), 114.99, 113.16, 111.16, 105.17, 81.35, 69.55,62.77, 53.81, 50.08, 48.68, 34.08, 28.64, 25.52, 24.66.

W-2-3 C_8

^{1}H NMR (400 MHz, DMSO-d_6) δ 12.03 (s, 1H), 9.50 (s, 1H), 8.68 (s, 1H), 8.59 (s, 1H), 8.41 (q, *J* = 13.4, 11.7 Hz, 2H), 7.89 (d, *J* = 8.7 Hz, 2H), 7.28 (s, 1H), 6.99 – 6.76 (m, 2H), 4.56 (d, *J* = 69.1 Hz, 3H), 4.18 – 3.98 (m, 5H), 3.97 – 3.78 (m, 6H), 3.53 (s, 1H), 2.21 (t, *J* = 7.3 Hz, 2H), 1.76 (p, *J* = 6.7 Hz, 2H), 1.51 (p, *J* = 7.5 Hz, 2H), 1.43 (q, *J* = 7.2 Hz, 2H), 1.39 – 1.23 (m, *J* = 6.9 Hz, 5H).

^{13}C NMR (101 MHz, DMSO-d_6) δ 174.96, 164.60, 157.83, 150.08, 148.06, 147.07, 141.84, 138.68, 129.60, 122.94, 120.53, 14.99, 113.09 (t, *J* = 191.9 Hz), 105.18, 81.35, 69.61, 62.77, 53.83, 50.01, 48.65, 34.11, 28.90 (d, *J* = 9.7 Hz), 25.76, 24.90.

L-2-2

^{1}H NMR (400 MHz, DMSO-d_6) δ 12.54 (s, 1H), 8.64 (s, 1H), 7.95 (d, *J* = 8.9 Hz, 1H), 6.86 (d, *J* = 9.0 Hz, 1H), 3.71 – 3.54 (m, 4H), 3.51 – 3.37 (m, 4H), 1.43 (s, 9H).

^{13}C NMR (101 MHz, DMSO-d_6) δ 167.03, 160.60, 154.37, 150.79， 138.82, 115.44, 106.22, 79.58, 44.33, 28.53.

L-3-2

^{1}H NMR (400 MHz, DMSO-d_6) δ 12.44 (s, 1H), 7.78 (d, *J* = 8.4 Hz, 2H), 6.96 (d, *J* = 8.6 Hz, 2H), 3.45 (t, *J* = 5.2 Hz, 4H), 1.42 (s, 9H).

^{13}C NMR (101 MHz, DMSO-d_6) δ 167.70, 154.33, 153.98, 131.33, 120.22, 114.10, 79.54, 47.11, 28.53.

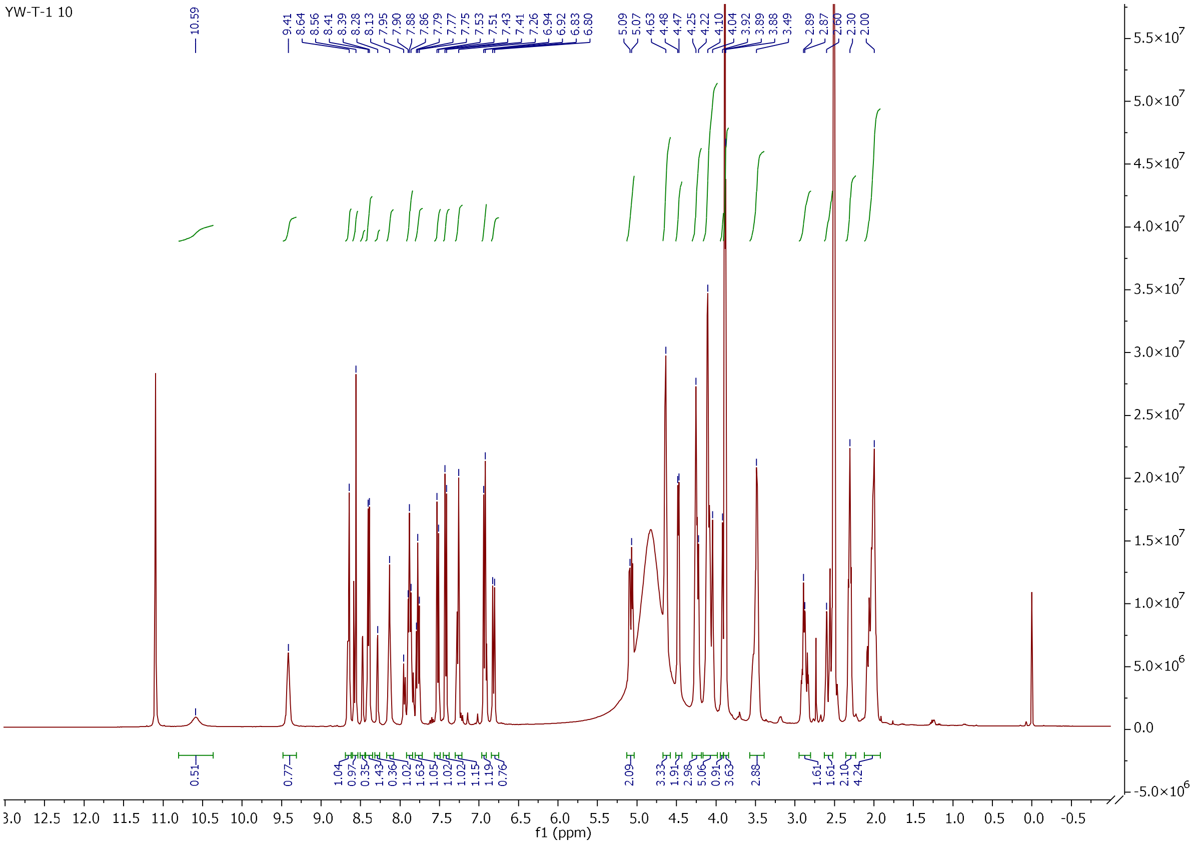
YW-T-1 10
10.59
9.41
8.64
8.56
8.41
8.39
8.28
8.13
7.95
7.90
7.88
7.86
7.79
7.77
7.75
7.53
7.51
7.43
7.41
7.26
6.94
6.92
6.83
6.80
5.09
5.07
4.63
4.48
4.47
4.25
4.22
4.10
4.04
3.92
3.89
3.88
3.49
2.89
2.87
2.60
2.30
2.00
0.51
0.77
1.04
0.97
0.35
1.43
0.36
1.02
1.63
1.05
1.02
1.02
1.15
1.19
0.76
2.09
3.33
1.91
2.98
5.06
0.91
3.63
2.88
1.61
1.61
2.10
4.24
f1 (ppm)

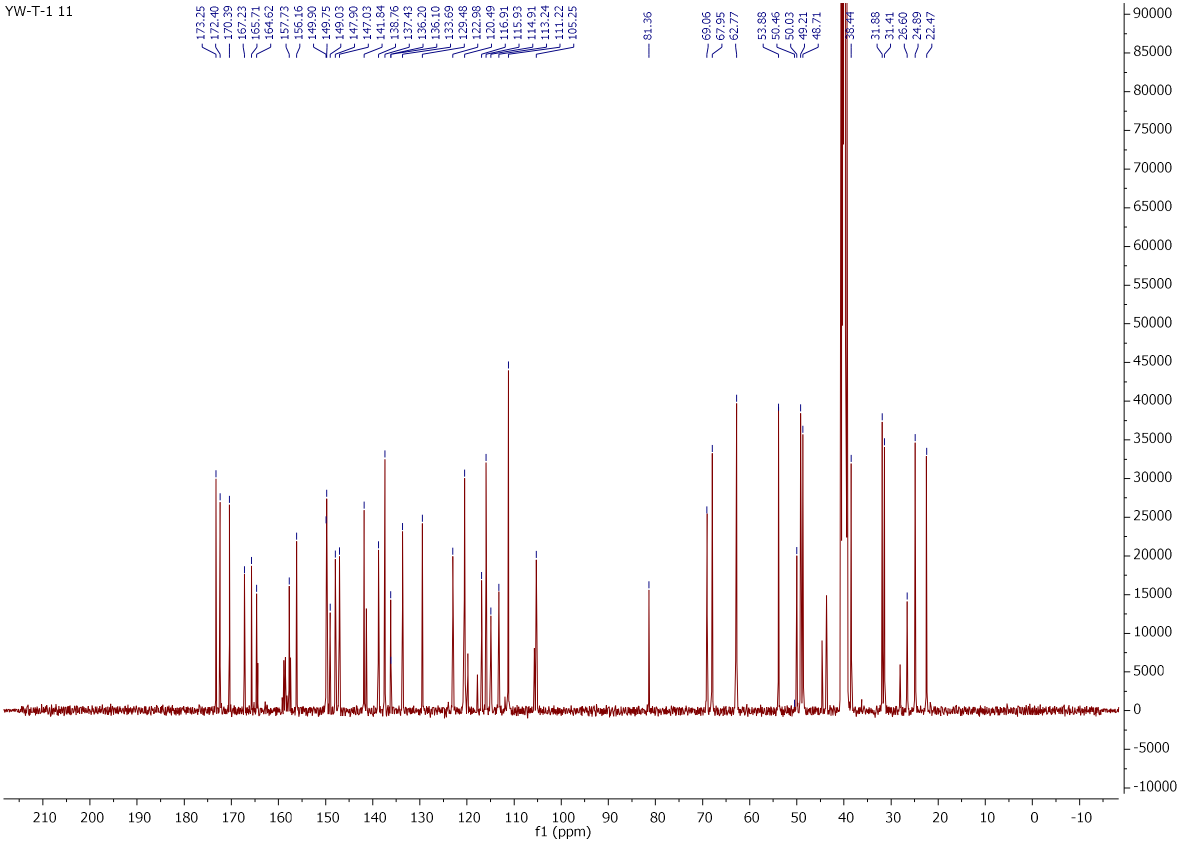
YW-T-1 11
173.25
172.40
170.39
167.23
165.71
164.62
157.73
156.16
149.90
149.75
149.03
147.90
147.03
141.84
138.76
137.43
136.20
136.10
133.69
129.48
122.98
120.49
116.91
115.93
114.91
113.24
111.22
105.25
81.36
69.06
67.95
62.77
53.88
50.46
50.03
49.21
48.71
38.44
31.88
31.41
26.60
24.89
22.47
f1 (ppm)

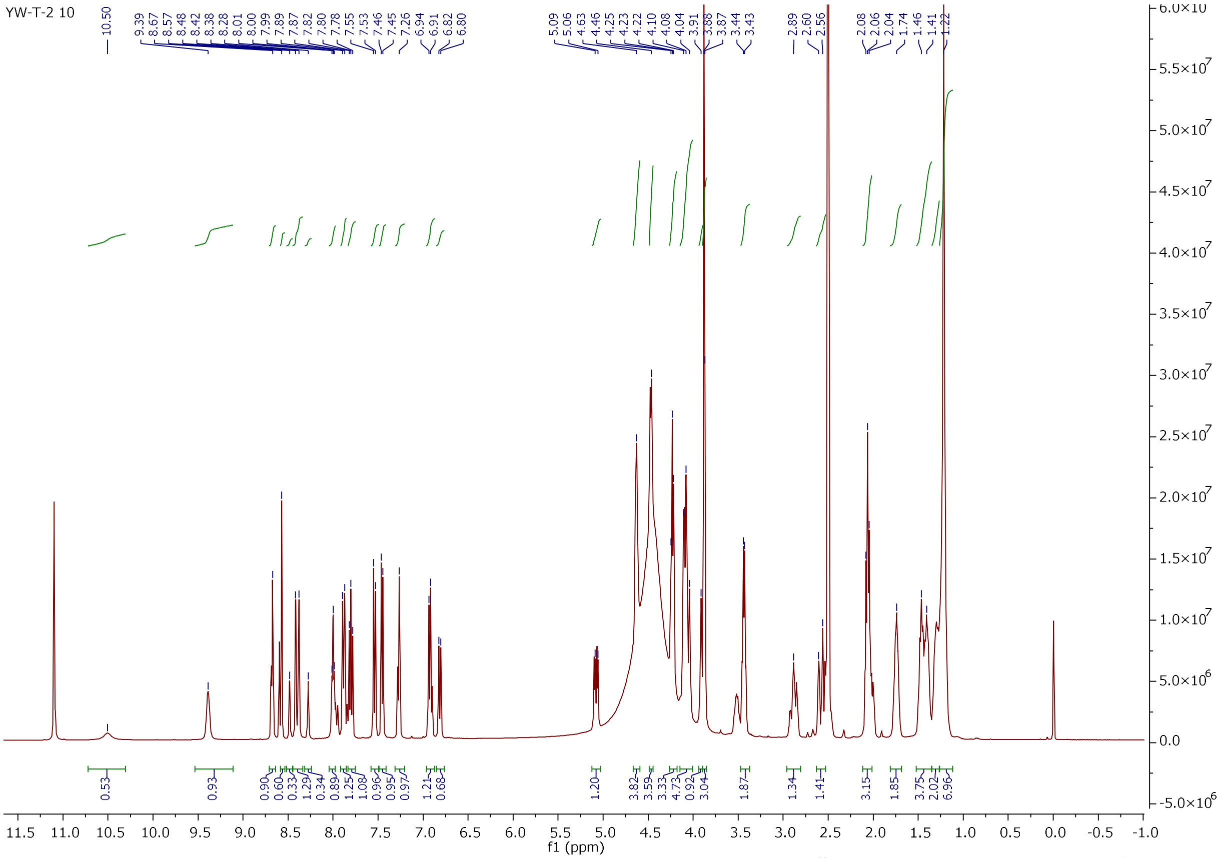
YW-T-2 10
10.50
9.39
8.67
8.57
8.48
8.42
8.38
8.28
8.01
8.00
7.99
7.89
7.87
7.82
7.80
7.78
7.55
7.53
7.46
7.45
7.26
6.94
6.91
6.82
6.80
5.09
5.06
4.63
4.46
4.25
4.23
4.22
4.10
4.08
4.04
3.91
3.88
3.87
3.44
3.43
2.89
2.60
2.56
2.08
2.06
2.04
1.74
1.46
1.41
1.22
0.53
0.93
0.90
0.60
0.33
1.29
0.34
0.89
1.25
1.08
0.96
0.95
0.97
1.21
0.68
1.20
3.82
3.59
3.33
4.73
0.92
3.04
1.87
1.34
1.41
3.15
1.85
3.75
2.02
6.96
11.5 11.0 10.5 10.0 9.5 9.0 8.5 8.0 7.5 7.0 6.5 6.0 5.5 5.0 4.5 4.0 3.5 3.0 2.5 2.0 1.5 1.0 0.5 0.0 -0.5 -1.0
f1 (ppm)
6.0×10^7
5.5×10^7
5.0×10^7
4.5×10^7
4.0×10^7
3.5×10^7
3.0×10^7
2.5×10^7
2.0×10^7
1.5×10^7
1.0×10^7
5.0×10^6
0.0
-5.0×10^6

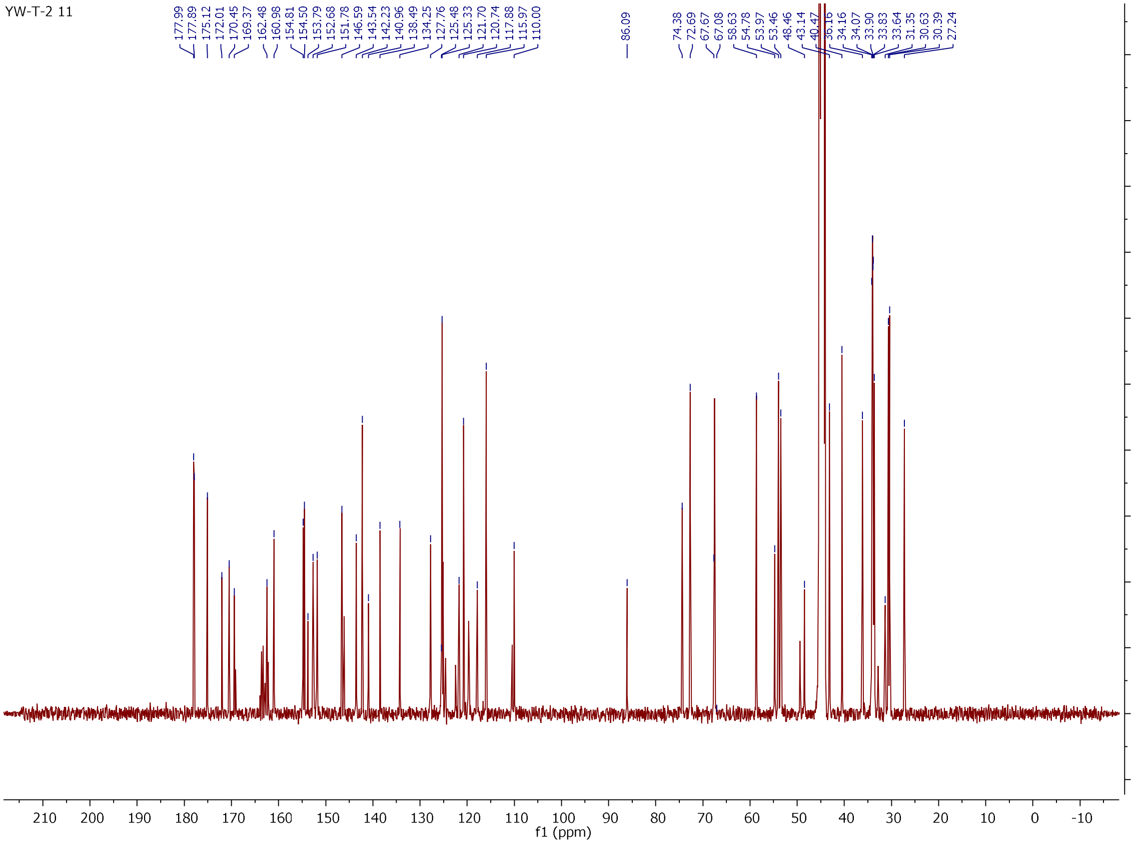
YW-T-2 11
177.99
177.89
175.12
172.01
170.45
169.37
162.48
160.98
154.81
154.50
153.79
152.68
151.78
146.59
143.54
142.23
140.96
138.49
134.25
127.76
125.48
125.33
121.70
120.74
117.88
115.97
110.00
86.09
74.38
72.69
67.67
67.08
58.63
54.78
53.97
53.46
48.46
43.14
40.47
36.16
34.16
34.07
33.90
33.83
33.64
31.35
30.63
30.39
27.24
210 200 190 180 170 160 150 140 130 120 110 100 90 80 70 60 50 40 30 20 10 0 -10
f1 (ppm)
50000
45000
40000
35000
30000
25000
20000
15000
10000
5000
0
-5000

YW-T-3 10

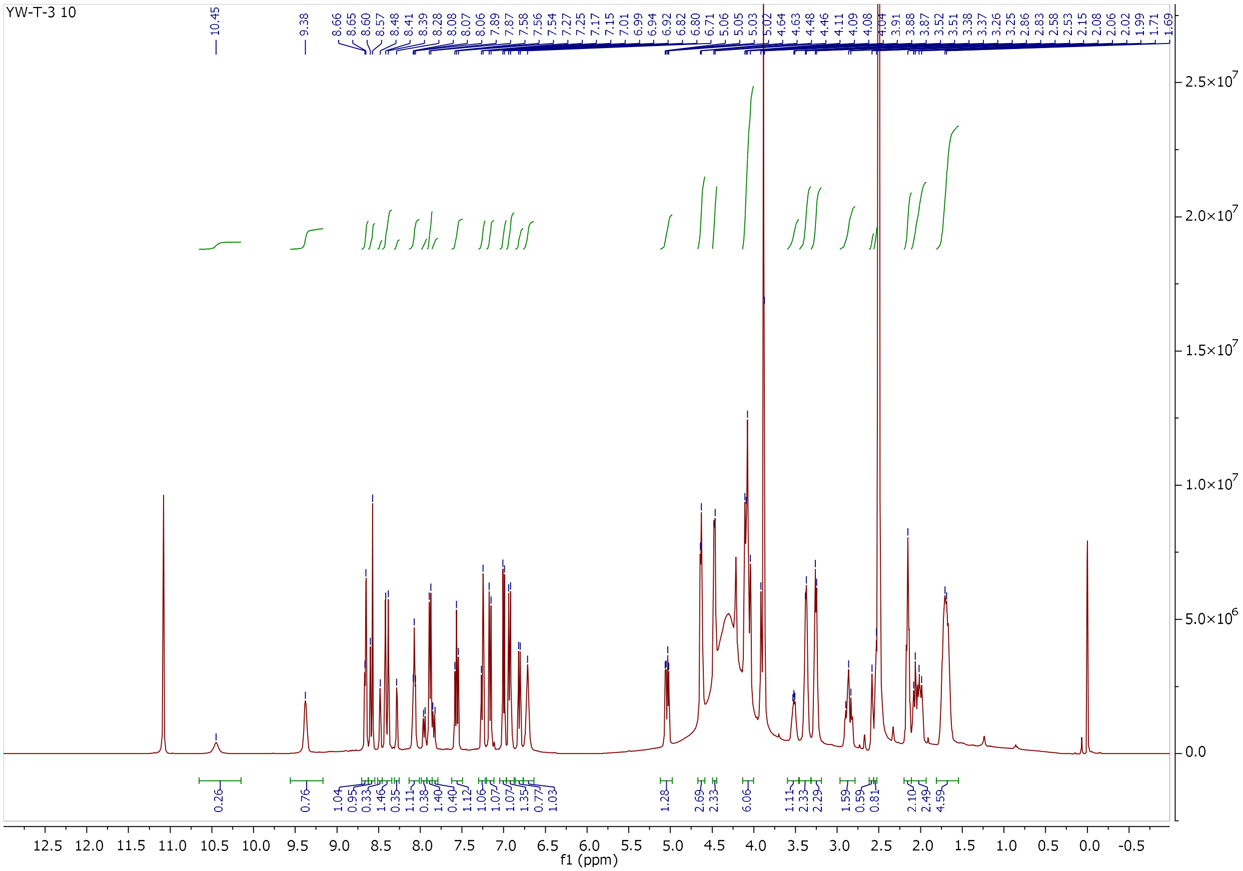

YW-T-3 11

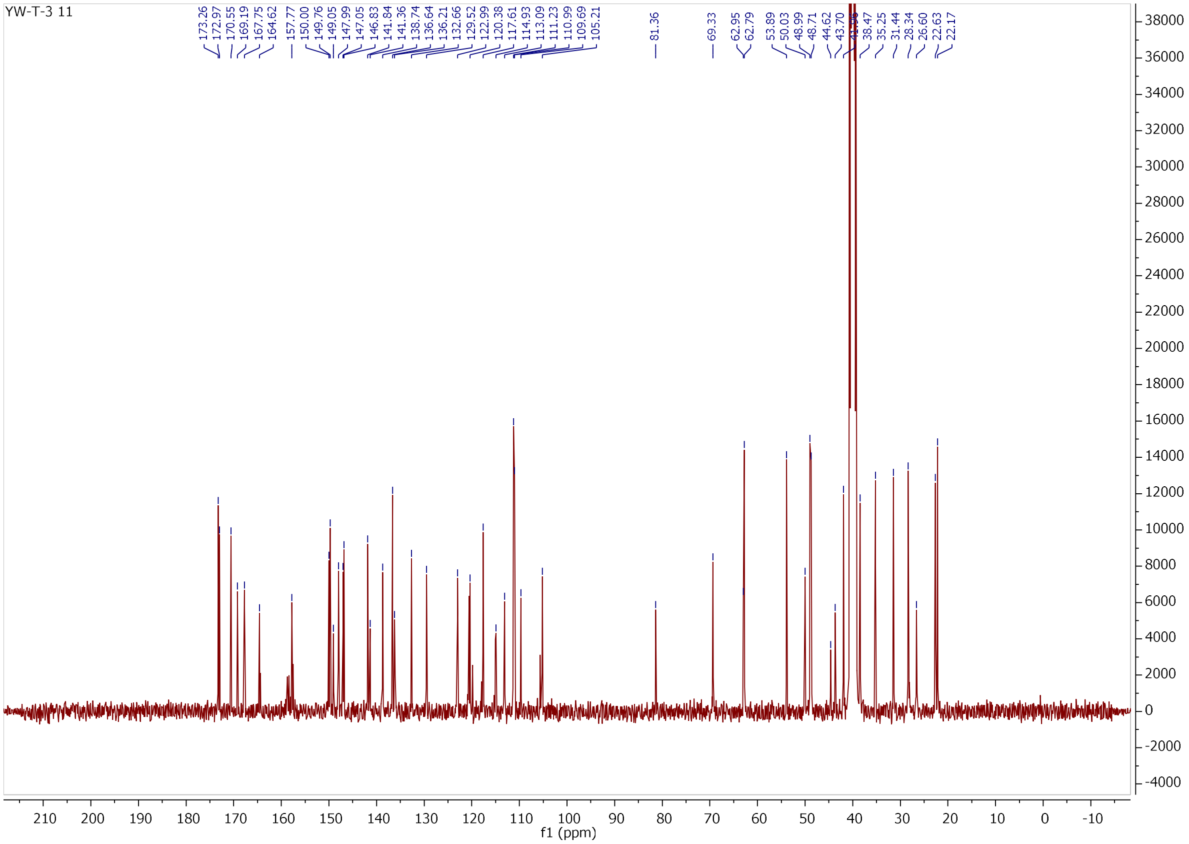

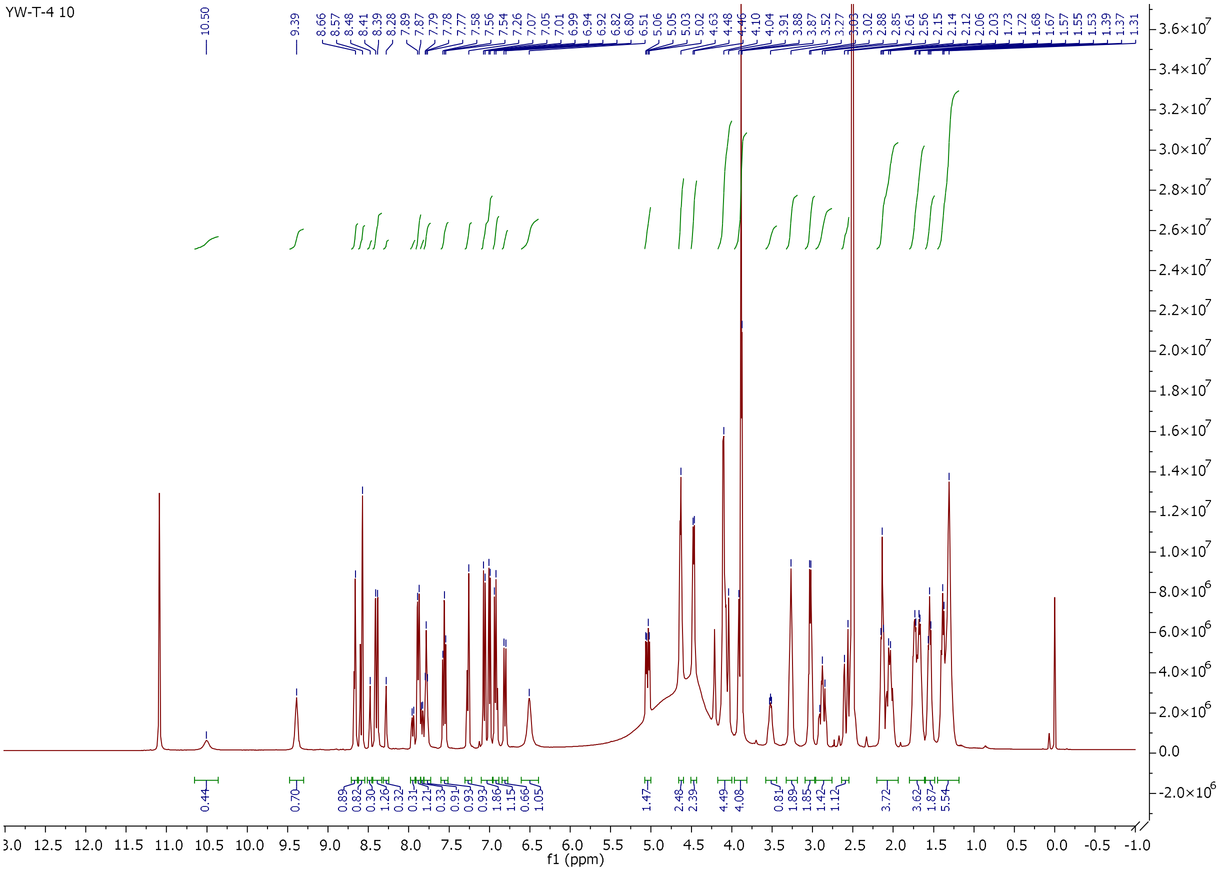
YW-T-4 10
10.50
9.39
8.66
8.57
8.48
8.41
8.39
8.28
7.89
7.87
7.79
7.78
7.77
7.58
7.56
7.54
7.26
7.07
7.05
7.01
6.99
6.94
6.92
6.82
6.80
6.51
5.06
5.05
5.03
5.02
4.63
4.48
4.46
4.10
4.04
3.91
3.88
3.87
3.52
3.27
3.03
3.02
2.88
2.85
2.61
2.56
2.15
2.14
2.12
2.06
2.03
1.73
1.72
1.68
1.67
1.57
1.55
1.53
1.39
1.37
1.31
0.44
0.70
0.89
0.82
0.30
1.26
0.32
0.31
1.21
0.33
0.91
0.93
1.86
1.15
0.66
1.05
1.47
2.48
2.39
4.49
4.08
0.81
1.89
1.85
1.42
1.12
3.72
3.62
1.87
5.54
3.6×10^7
3.4×10^7
3.2×10^7
3.0×10^7
2.8×10^7
2.6×10^7
2.4×10^7
2.2×10^7
2.0×10^7
1.8×10^7
1.6×10^7
1.4×10^7
1.2×10^7
1.0×10^7
8.0×10^6
6.0×10^6
4.0×10^6
2.0×10^6
0.0
-2.0×10^6
3.0
12.5
12.0
11.5
11.0
10.5
10.0
9.5
9.0
8.5
8.0
7.5
7.0
6.5
6.0
5.5
5.0
4.5
4.0
3.5
3.0
2.5
2.0
1.5
1.0
0.5
0.0
-0.5
-1.0
f1 (ppm)

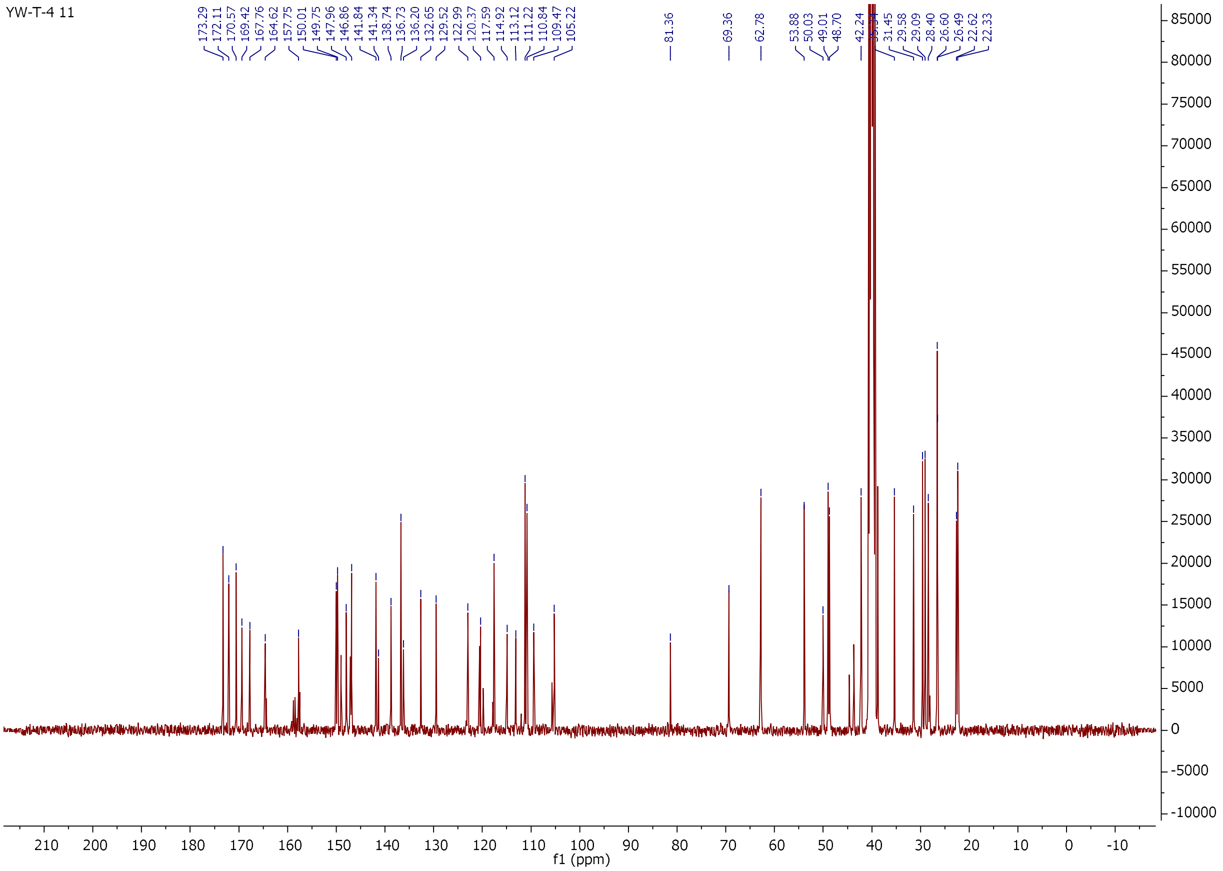
YW-T-4 11
173.29
172.11
170.57
169.42
167.76
164.62
157.75
150.01
149.75
147.96
146.86
141.84
141.34
138.74
136.73
136.20
132.65
129.52
122.99
120.37
117.59
114.92
113.12
111.22
110.84
109.47
105.22
81.36
69.36
62.78
53.88
50.03
49.01
48.70
42.24
35.34
31.45
29.58
29.09
28.40
26.60
26.49
22.62
22.33
85000
80000
75000
70000
65000
60000
55000
50000
45000
40000
35000
30000
25000
20000
15000
10000
5000
0
-5000
-10000
210
200
190
180
170
160
150
140
130
120
110
100
90
80
70
60
50
40
30
20
10
0
-10
f1 (ppm)

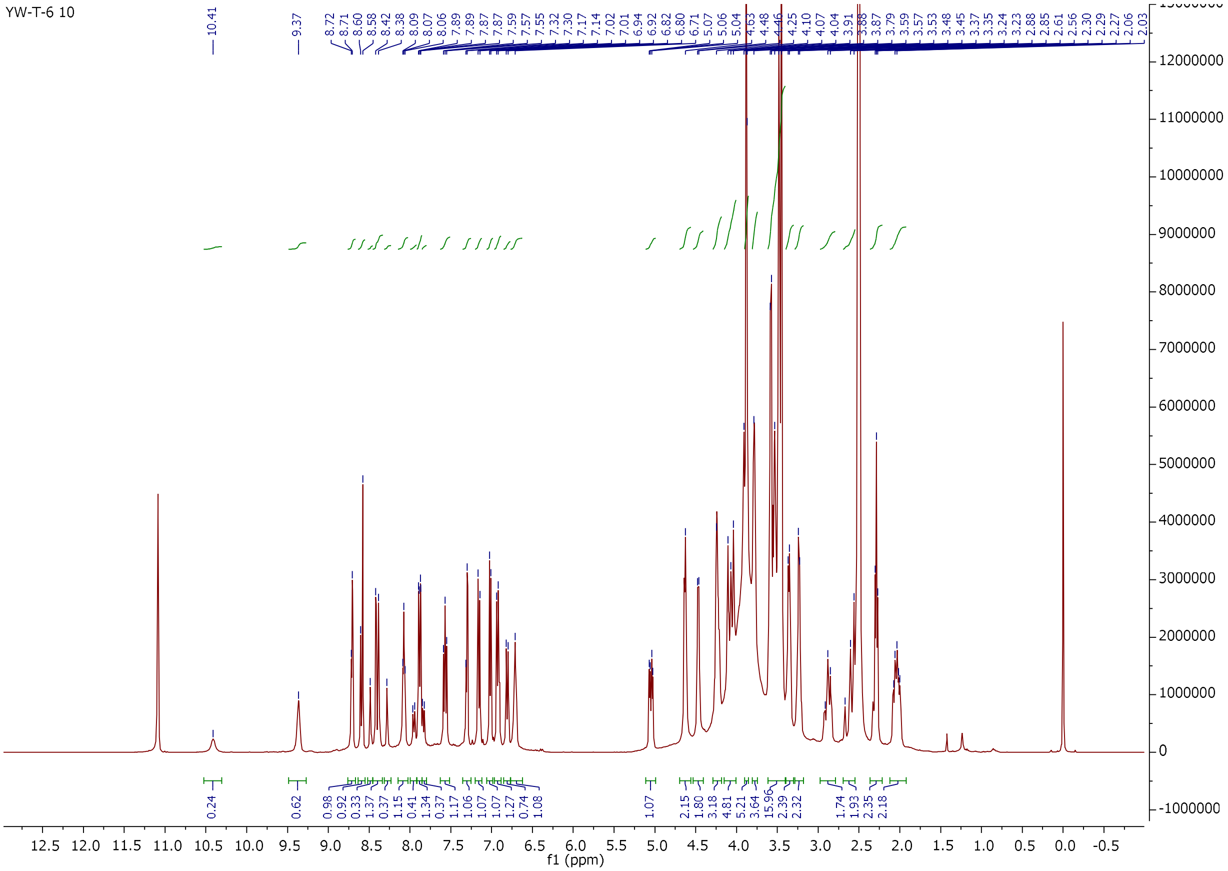
YW-T-6 10
10.41
9.37
8.72
8.71
8.60
8.58
8.42
8.38
8.09
8.07
8.06
7.89
7.89
7.87
7.87
7.59
7.57
7.55
7.32
7.30
7.17
7.14
7.02
7.01
6.94
6.92
6.82
6.80
6.71
5.07
5.06
5.04
4.63
4.48
4.46
4.25
4.10
4.07
4.04
3.91
3.88
3.87
3.79
3.59
3.57
3.53
3.48
3.45
3.37
3.35
3.24
3.23
2.88
2.85
2.61
2.56
2.30
2.29
2.27
2.06
2.03
0.24
0.62
0.98
0.92
0.33
1.37
0.37
1.15
0.41
1.34
0.37
1.17
1.06
1.07
1.07
1.27
0.74
1.08
1.07
2.15
1.80
3.18
4.81
5.21
3.64
15.96
2.39
2.32
1.74
1.93
2.35
2.18
12.5 12.0 11.5 11.0 10.5 10.0 9.5 9.0 8.5 8.0 7.5 7.0 6.5 6.0 5.5 5.0 4.5 4.0 3.5 3.0 2.5 2.0 1.5 1.0 0.5 0.0 -0.5
f1 (ppm)
12000000
11000000
10000000
9000000
8000000
7000000
6000000
5000000
4000000
3000000
2000000
1000000
0
-1000000

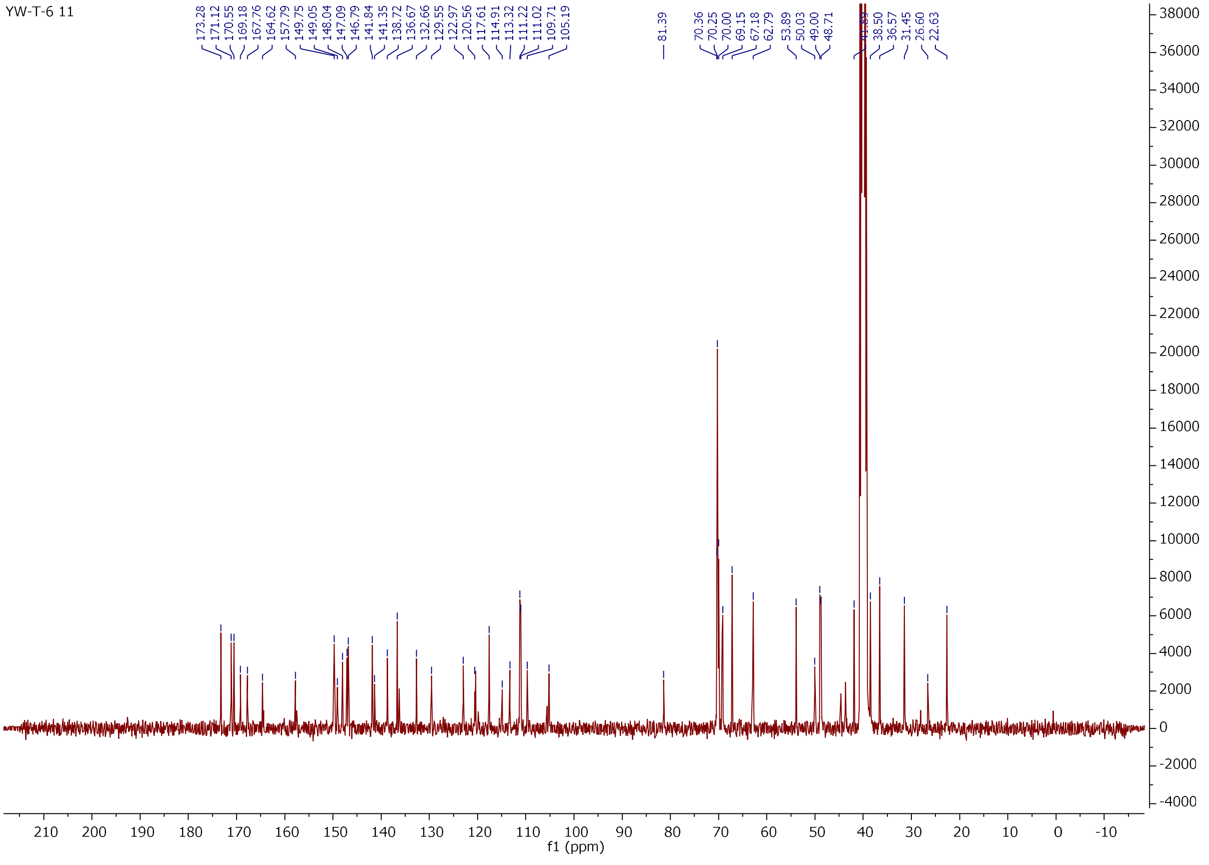
YW-T-6 11
173.28
171.12
170.55
169.18
167.76
164.62
157.79
149.75
149.05
148.04
147.09
146.79
141.84
141.35
138.72
136.67
132.66
129.55
122.97
120.56
117.61
114.91
113.32
111.22
111.02
109.71
105.19
81.39
70.36
70.25
70.00
69.15
67.18
62.79
53.89
50.03
49.00
48.71
38.50
36.57
31.45
26.60
22.63
210 200 190 180 170 160 150 140 130 120 110 100 90 80 70 60 50 40 30 20 10 0 -10
f1 (ppm)
38000
36000
34000
32000
30000
28000
26000
24000
22000
20000
18000
16000
14000
12000
10000
8000
6000
4000
2000
0
-2000
-4000

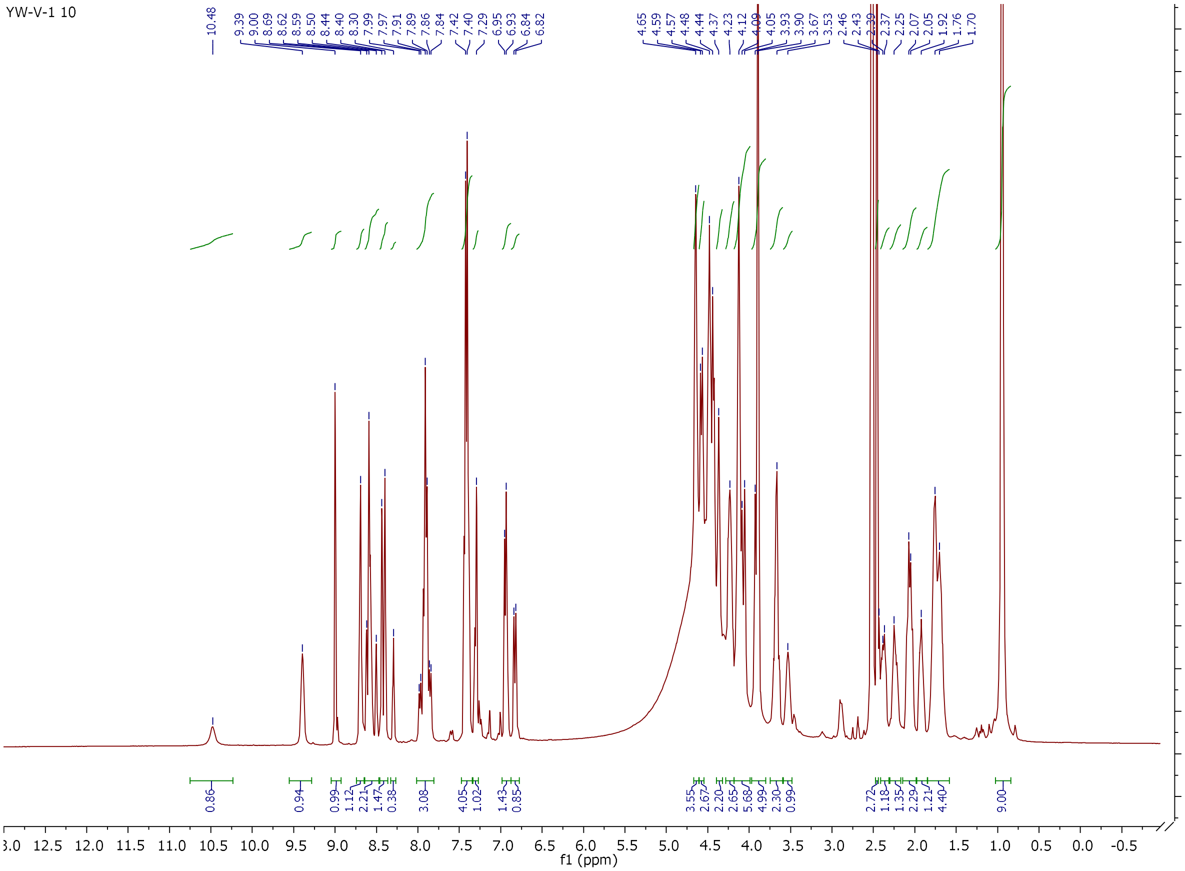
YW-V-1 10
10.48
9.39
9.00
8.69
8.62
8.59
8.50
8.44
8.40
8.30
7.99
7.97
7.91
7.89
7.86
7.84
7.42
7.40
7.29
6.95
6.93
6.84
6.82
4.65
4.59
4.57
4.48
4.44
4.37
4.23
4.12
4.09
4.05
3.93
3.90
3.67
3.53
2.46
2.43
2.39
2.37
2.25
2.07
2.05
1.92
1.76
1.70
0.86
0.94
0.99
1.12
2.21
1.47
0.38
3.08
4.05
1.02
1.43
0.85
3.55
2.67
2.20
2.65
5.68
4.99
2.30
0.99
2.72
1.18
1.35
2.29
1.21
4.40
9.00
f1 (ppm)
17000000
16000000
15000000
14000000
13000000
12000000
11000000
10000000
9000000
8000000
7000000
6000000
5000000
4000000
3000000
2000000
1000000
0
-1000000

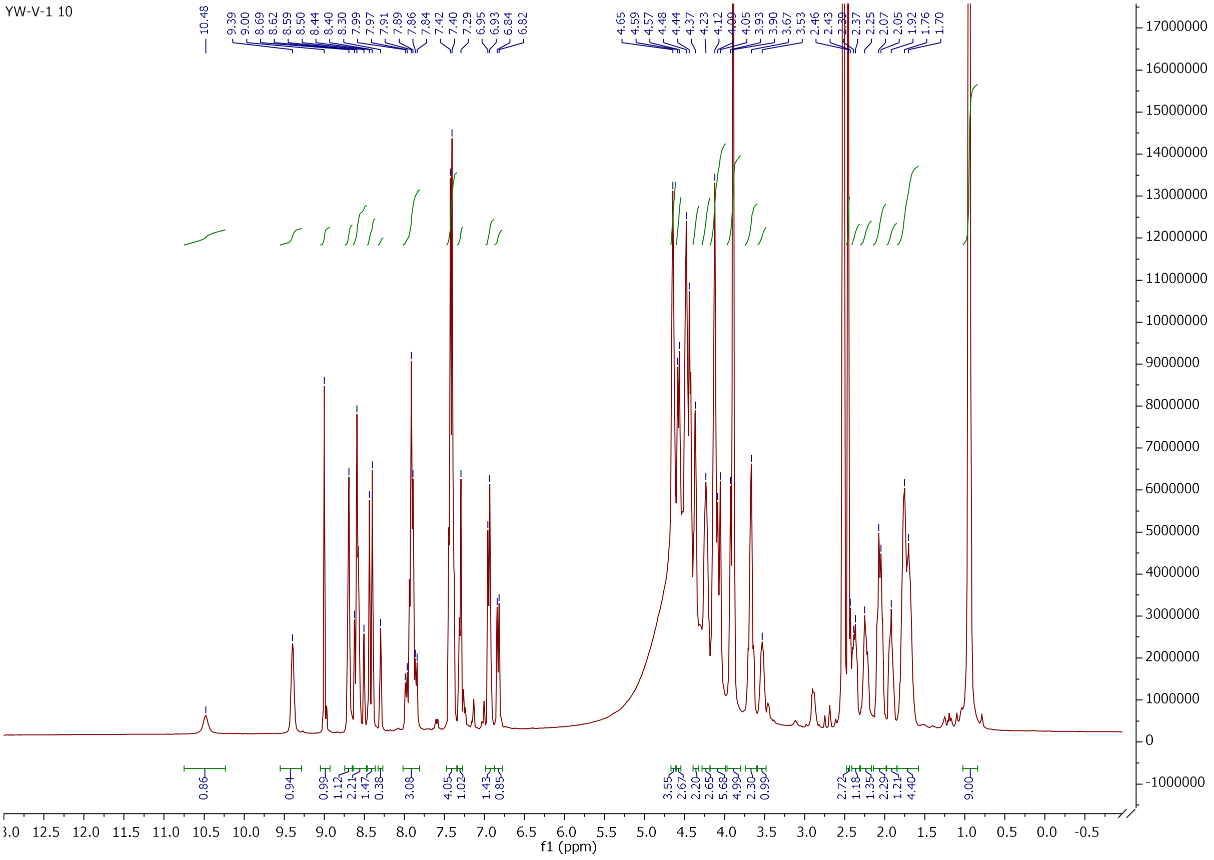
YW-V-1 10
10.48
9.39
9.00
8.69
8.62
8.59
8.50
8.44
8.40
8.30
7.99
7.97
7.91
7.89
7.86
7.84
7.42
7.40
7.29
6.95
6.93
6.84
6.82
4.65
4.59
4.57
4.48
4.44
4.37
4.23
4.12
4.09
4.05
3.93
3.90
3.67
3.53
2.46
2.43
2.39
2.37
2.25
2.07
2.05
1.92
1.76
1.70
0.86
0.94
0.99
1.12
2.21
1.47
0.38
3.08
4.05
1.02
1.43
0.85
3.55
2.67
2.20
2.65
5.68
4.99
2.30
0.99
2.72
1.18
1.35
2.29
1.21
4.40
9.00
f1 (ppm)
17000000
16000000
15000000
14000000
13000000
12000000
11000000
10000000
9000000
8000000
7000000
6000000
5000000
4000000
3000000
2000000
1000000
0
-1000000

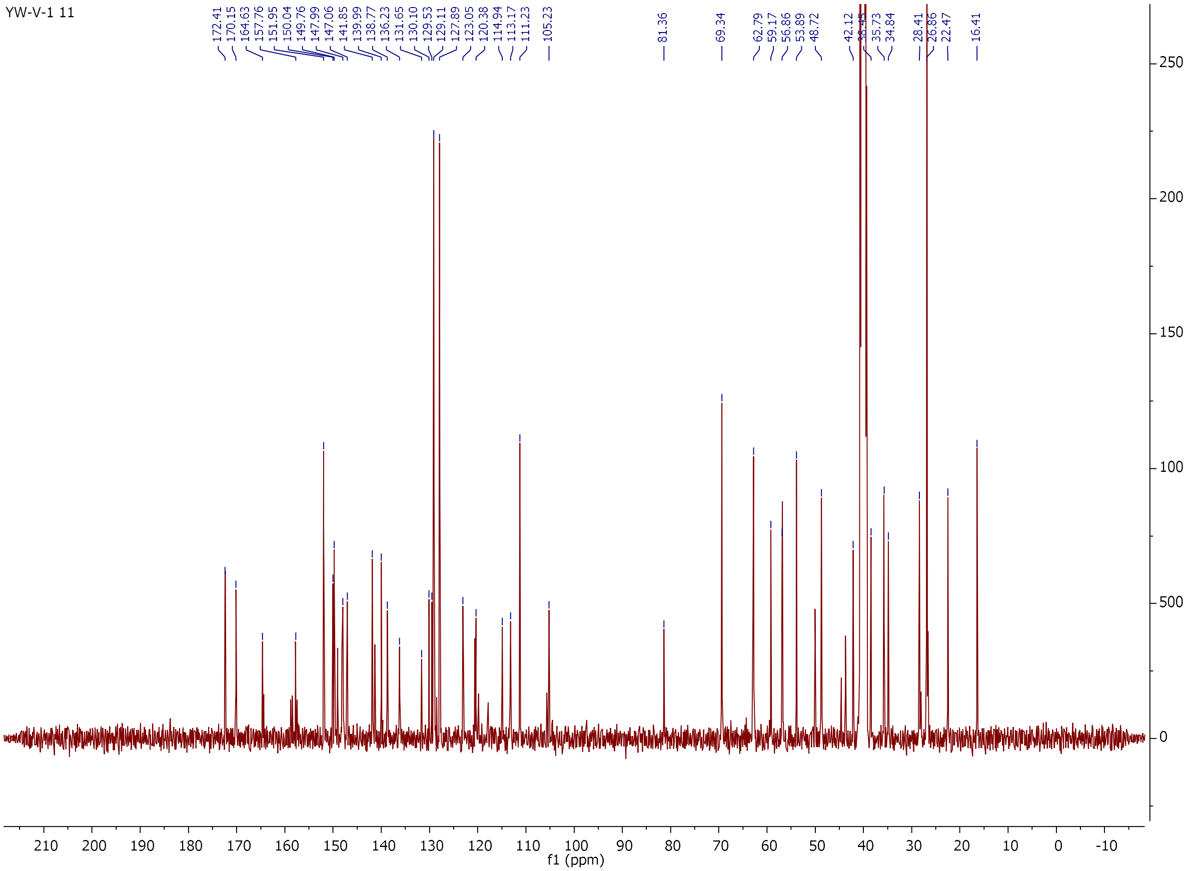
YW-V-1 11
172.41
170.15
164.63
157.76
151.95
150.04
149.76
147.99
147.06
141.85
139.99
138.77
136.23
131.65
130.10
129.53
129.11
127.89
123.05
120.38
114.94
113.17
111.23
105.23
81.36
69.34
62.79
59.17
56.86
53.89
48.72
42.12
38.45
35.73
34.84
28.41
26.86
22.47
16.41
25000
20000
15000
10000
5000
0
210 200 190 180 170 160 150 140 130 120 110 100 90 80 70 60 50 40 30 20 10 0 -10
f1 (ppm)

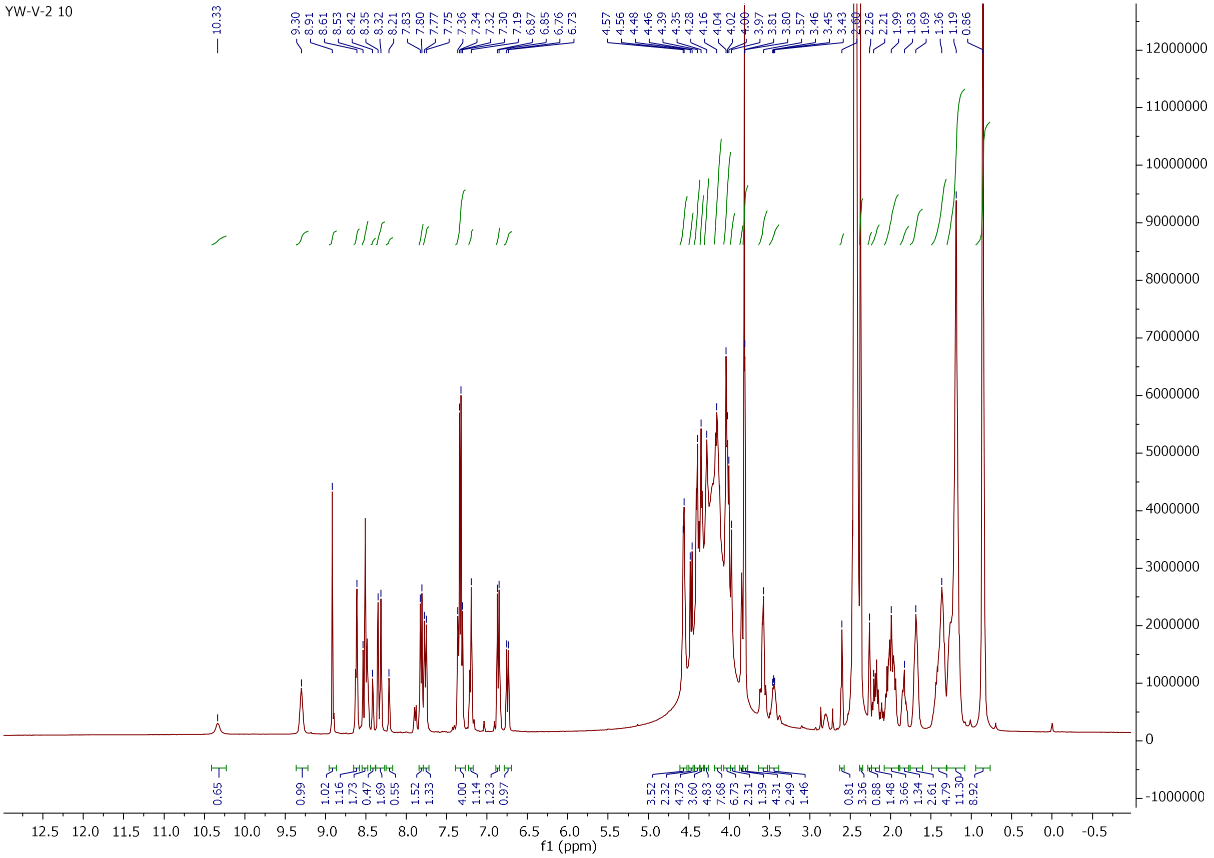
YW-V-2 10
10.33
9.30
8.91
8.61
8.53
8.42
8.35
8.32
8.21
7.83
7.80
7.77
7.75
7.36
7.34
7.32
7.30
7.19
6.87
6.85
6.76
6.73
4.57
4.56
4.48
4.46
4.39
4.35
4.28
4.16
4.04
4.02
4.00
3.97
3.81
3.80
3.57
3.46
3.45
3.43
2.60
2.26
2.21
1.99
1.83
1.69
1.36
1.19
0.86
12000000
11000000
10000000
9000000
8000000
7000000
6000000
5000000
4000000
3000000
2000000
1000000
0
-1000000
0.65
0.99
1.02
1.16
1.73
0.47
1.69
0.55
1.52
1.33
4.00
1.14
1.23
0.97
3.52
2.32
4.73
3.60
4.83
7.68
6.73
2.31
1.39
4.31
2.49
1.46
0.81
3.36
0.88
1.48
3.66
1.34
2.61
4.79
11.30
8.92
12.5 12.0 11.5 11.0 10.5 10.0 9.5 9.0 8.5 8.0 7.5 7.0 6.5 6.0 5.5 5.0 4.5 4.0 3.5 3.0 2.5 2.0 1.5 1.0 0.5 0.0 -0.5
f1 (ppm)

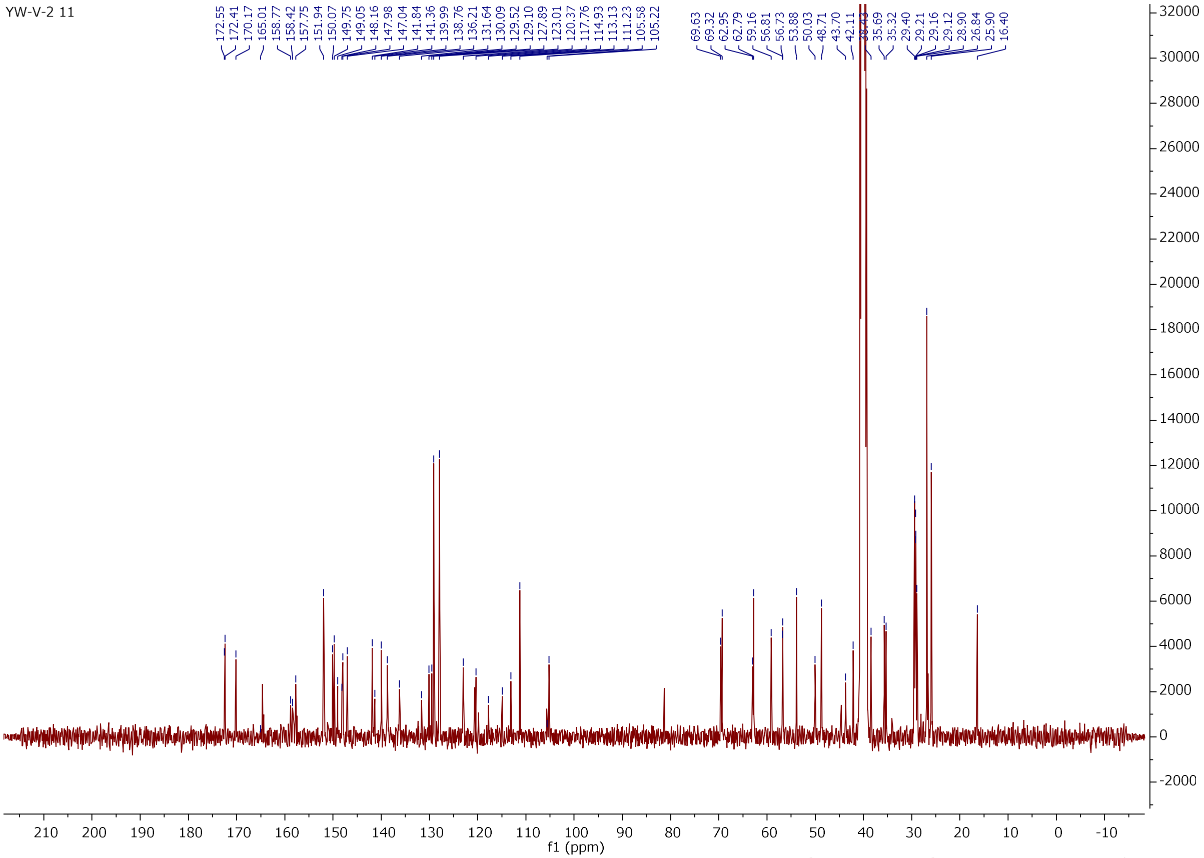
YW-V-2 11
172.55
172.41
170.17
165.01
158.77
158.42
157.75
151.94
150.07
149.75
149.05
148.16
147.98
147.04
141.84
141.36
139.99
138.76
136.21
131.64
130.09
129.52
129.10
127.89
123.01
120.37
117.76
114.93
113.13
111.23
105.58
105.22
69.63
69.32
62.95
62.79
59.16
56.81
56.73
53.88
50.03
48.71
43.70
42.11
38.43
35.69
35.32
29.40
29.21
29.16
29.12
28.90
26.84
25.90
16.40
32000
30000
28000
26000
24000
22000
20000
18000
16000
14000
12000
10000
8000
6000
4000
2000
0
-2000
210 200 190 180 170 160 150 140 130 120 110 100 90 80 70 60 50 40 30 20 10 0 -10
f1 (ppm)

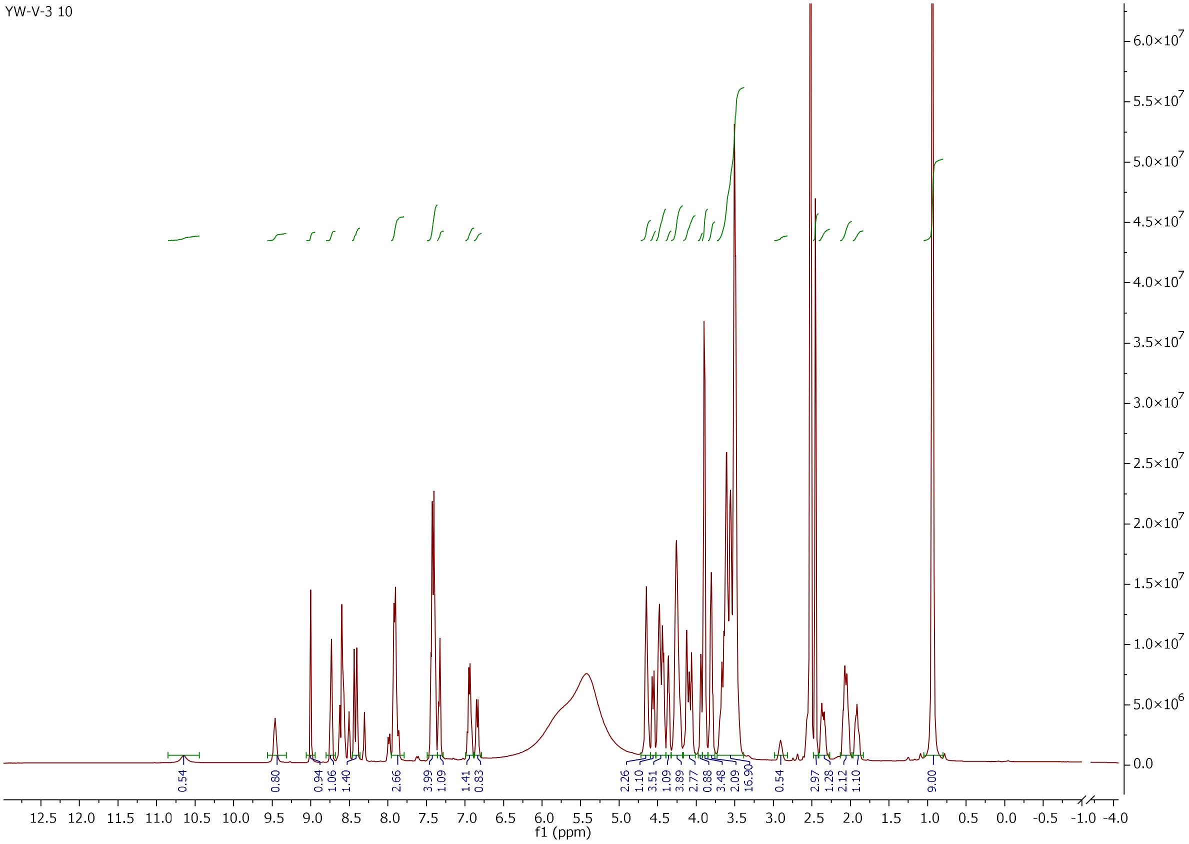
YW-V-3 10
6.0×10^7
5.5×10^7
5.0×10^7
4.5×10^7
4.0×10^7
3.5×10^7
3.0×10^7
2.5×10^7
2.0×10^7
1.5×10^7
1.0×10^7
5.0×10^6
0.0
0.54
0.80
0.94
1.06
1.40
2.66
3.99
1.09
1.41
0.83
2.26
1.10
3.51
1.09
3.89
2.77
0.88
3.48
2.09
16.90
0.54
2.97
1.28
2.12
1.10
9.00
12.5 12.0 11.5 11.0 10.5 10.0 9.5 9.0 8.5 8.0 7.5 7.0 6.5 6.0 5.5 5.0 4.5 4.0 3.5 3.0 2.5 2.0 1.5 1.0 0.5 0.0 -0.5 -1.0 -4.0
f1 (ppm)

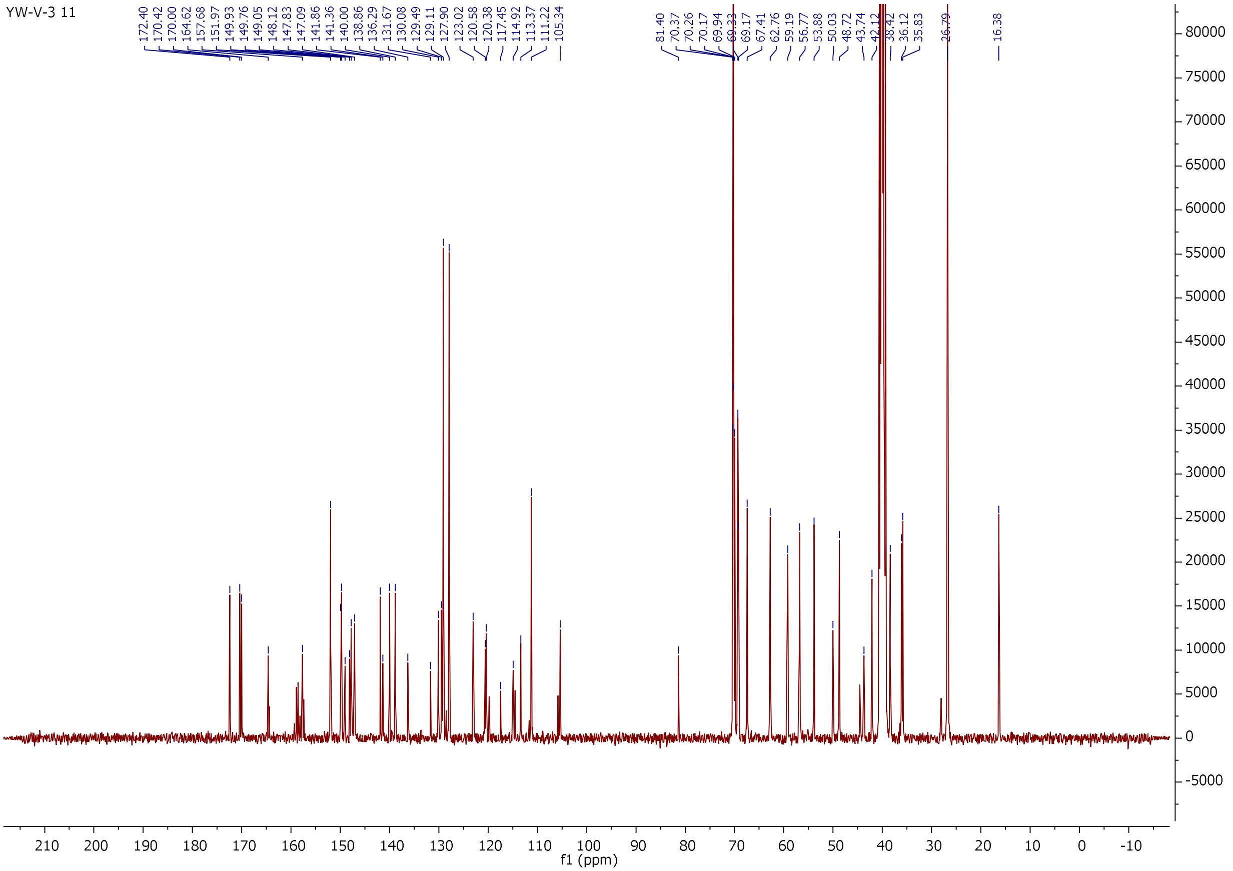
YW-V-3 11
172.40
170.42
170.00
164.62
157.68
151.97
149.93
149.76
149.05
148.12
147.83
147.09
141.86
141.36
140.00
138.86
136.29
131.67
130.08
129.49
129.11
127.90
123.02
120.58
120.38
117.45
114.92
113.37
111.22
105.34
81.40
70.37
70.26
70.17
69.94
69.33
69.17
67.41
62.76
59.19
56.77
53.88
50.03
48.72
43.74
42.12
38.42
36.12
35.83
26.79
16.38
80000
75000
70000
65000
60000
55000
50000
45000
40000
35000
30000
25000
20000
15000
10000
5000
0
-5000
210 200 190 180 170 160 150 140 130 120 110 100 90 80 70 60 50 40 30 20 10 0 -10
f1 (ppm)

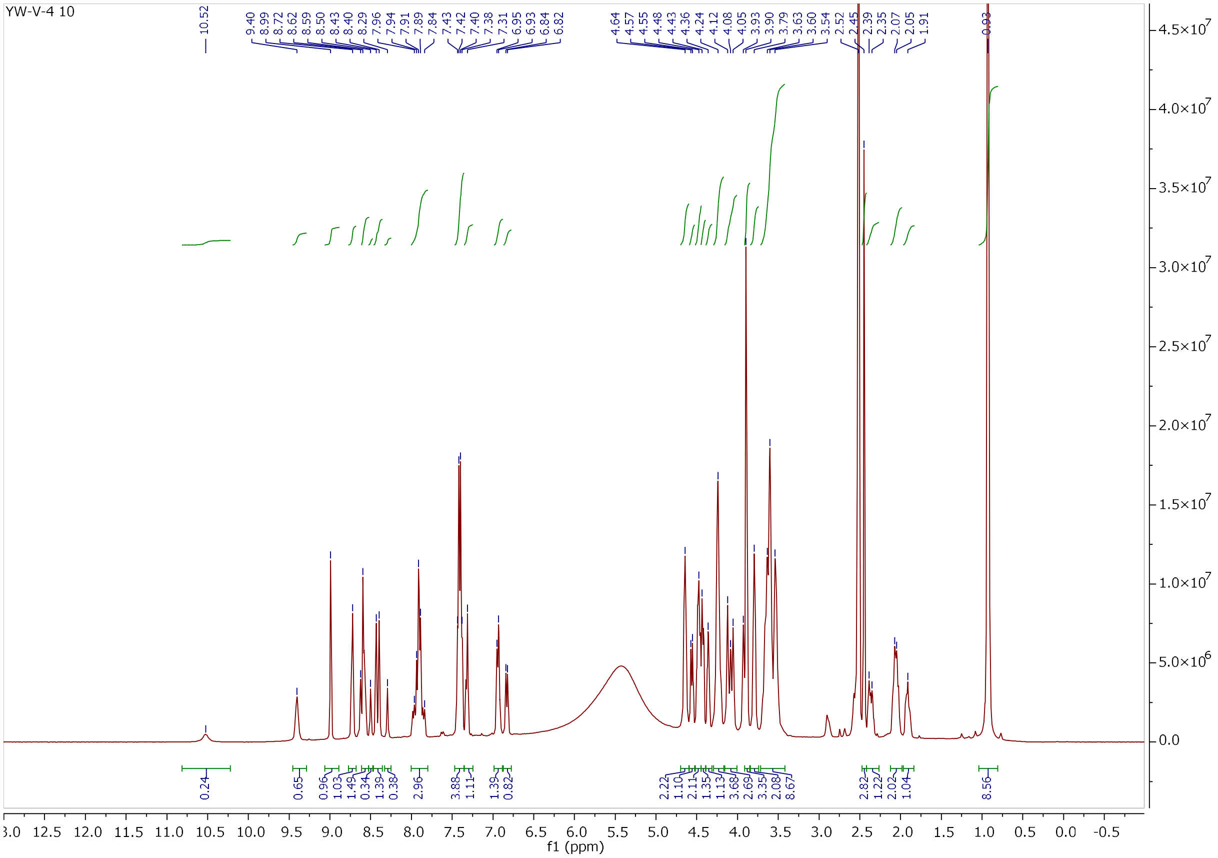
YW-V-4 10
10.52
9.40
8.99
8.72
8.62
8.59
8.50
8.43
8.40
8.29
7.96
7.94
7.91
7.89
7.84
7.43
7.42
7.40
7.38
7.31
6.95
6.93
6.84
6.82
4.64
4.57
4.55
4.48
4.43
4.36
4.24
4.12
4.08
4.05
3.93
3.90
3.79
3.63
3.60
3.54
2.52
2.45
2.39
2.35
2.07
2.05
1.91
0.93
0.24
0.65
0.96
1.03
1.49
0.34
1.39
0.38
2.96
3.88
1.11
1.39
0.82
2.22
1.10
2.11
1.35
1.13
3.68
2.69
3.35
2.08
8.67
2.82
1.22
2.02
1.04
8.56
4.5×10^7
4.0×10^7
3.5×10^7
3.0×10^7
2.5×10^7
2.0×10^7
1.5×10^7
1.0×10^7
5.0×10^6
0.0
3.0 12.5 12.0 11.5 11.0 10.5 10.0 9.5 9.0 8.5 8.0 7.5 7.0 6.5 6.0 5.5 5.0 4.5 4.0 3.5 3.0 2.5 2.0 1.5 1.0 0.5 0.0 -0.5
f1 (ppm)

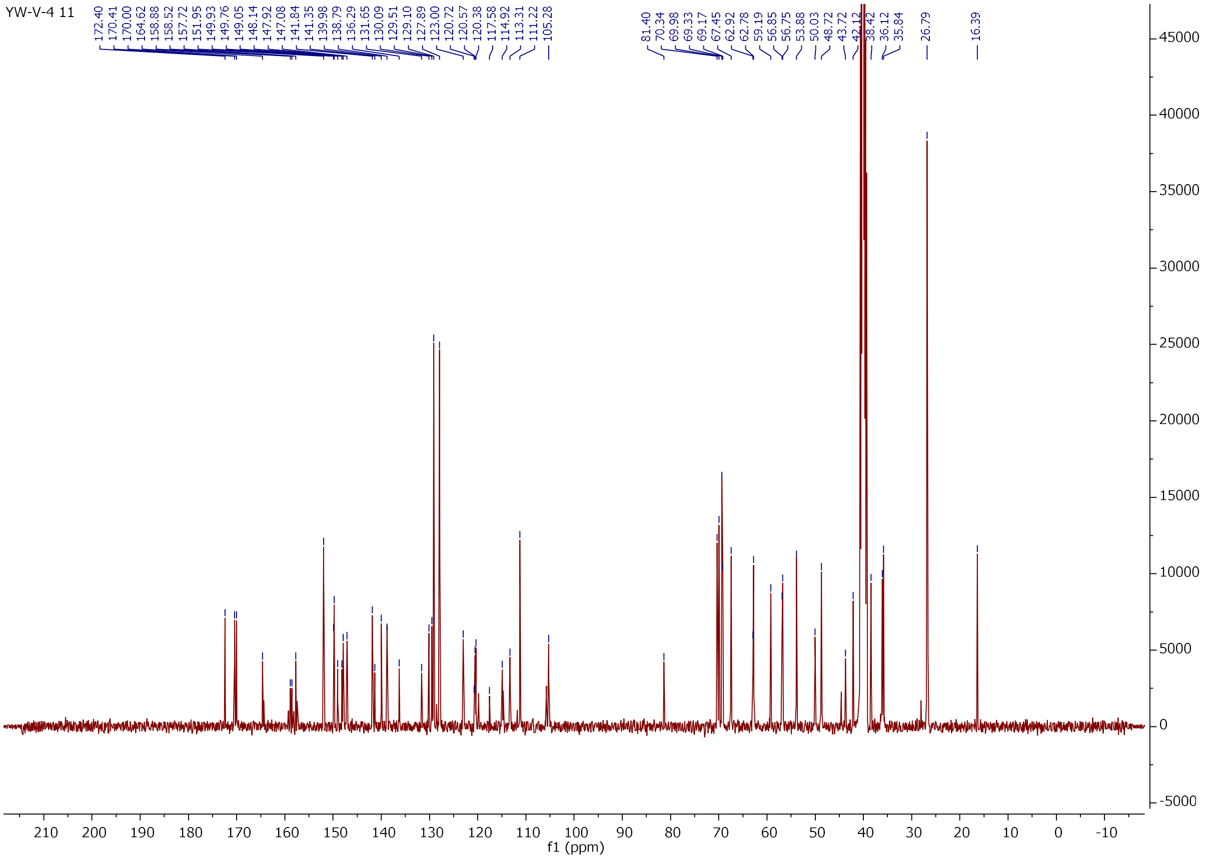
YW-V-4 11
172.40
170.41
170.00
164.62
158.88
158.52
157.72
151.95
149.93
149.76
149.05
148.14
147.92
147.08
141.84
141.35
139.98
138.79
136.29
131.65
130.09
129.51
129.10
127.89
123.00
120.72
120.57
120.38
117.58
114.92
113.31
111.22
105.28
81.40
70.34
69.98
69.33
69.17
67.45
62.92
62.78
59.19
56.85
56.75
53.88
50.03
48.72
43.72
42.12
38.42
36.12
35.84
26.79
16.39
45000
40000
35000
30000
25000
20000
15000
10000
5000
0
-5000
210
200
190
180
170
160
150
140
130
120
110
100
90
80
70
60
50
40
30
20
10
0
-10
f1 (ppm)

W-2-3 (C_4, C_6, C_8, C_{10}, C_{11}**)**

W-2-3 C_4

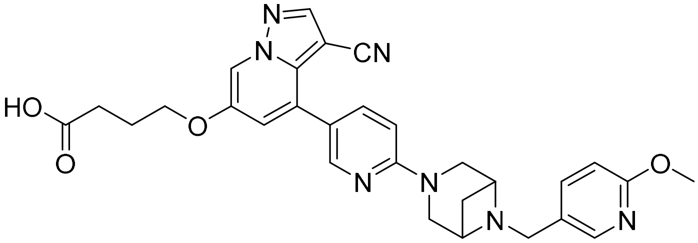

N
N
CN
HO
O
O
N
N
N
O
N

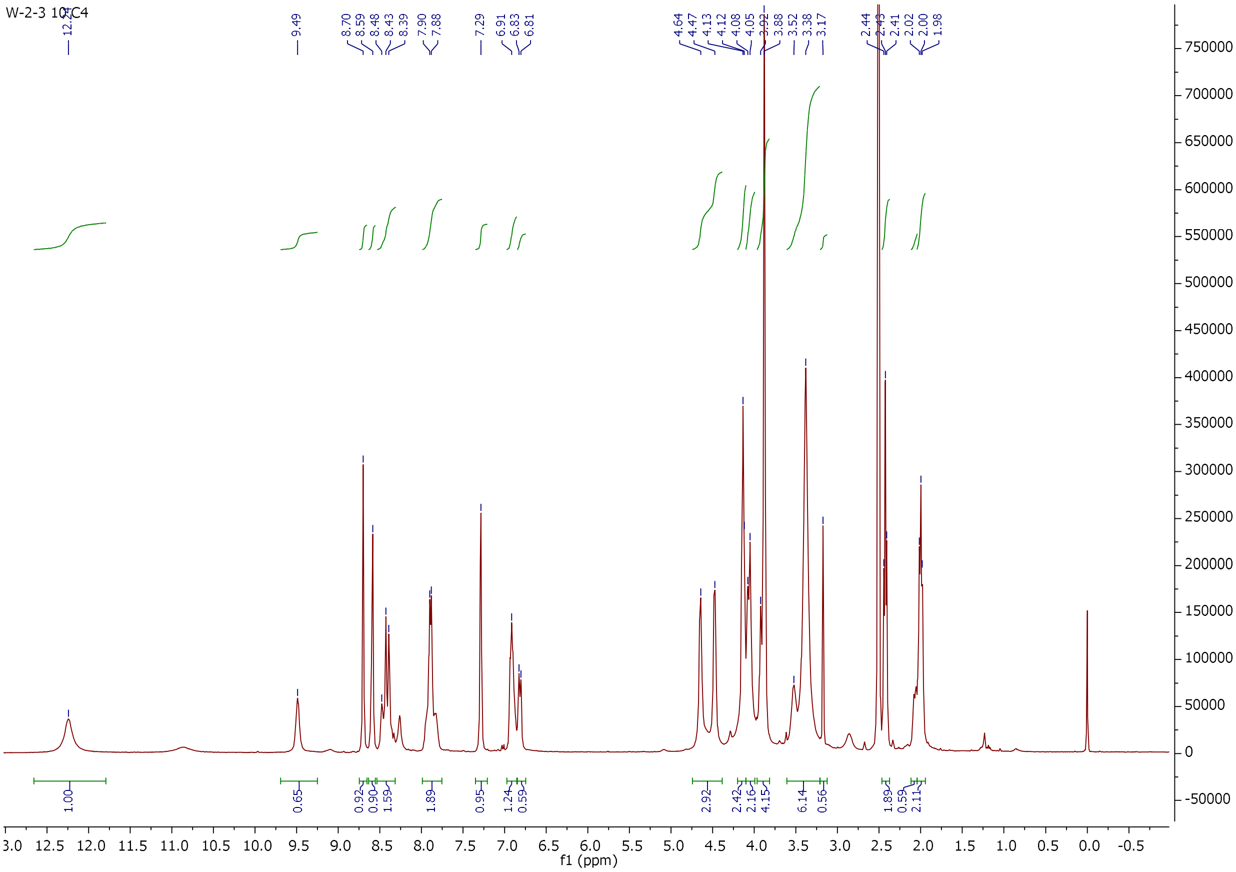

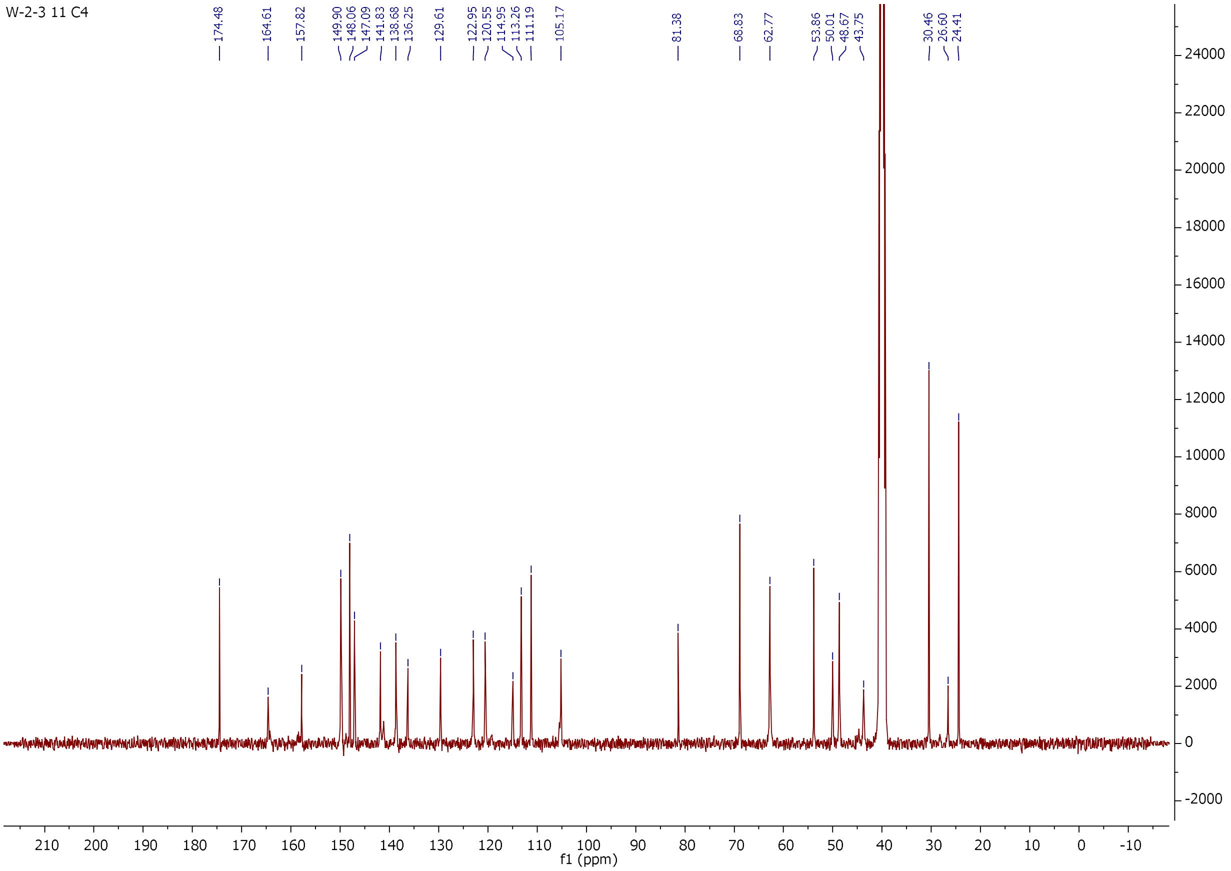
W-2-3 11 C4
174.48
164.61
157.82
149.90
148.06
147.09
141.83
138.68
136.25
129.61
122.95
120.55
114.95
113.26
111.19
105.17
81.38
68.83
62.77
53.86
50.01
48.67
43.75
30.46
26.60
24.41
24000
22000
20000
18000
16000
14000
12000
10000
8000
6000
4000
2000
0
-2000
210
200
190
180
170
160
150
140
130
120
110
100
90
80
70
60
50
40
30
20
10
0
-10
f1 (ppm)

W-2-3 C_6

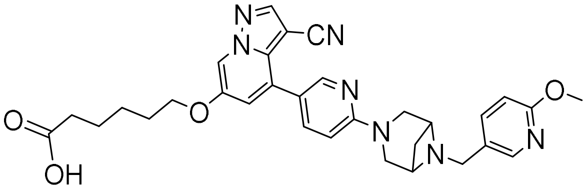
N
N
CN
O
O
OH
N
N
N
O
N

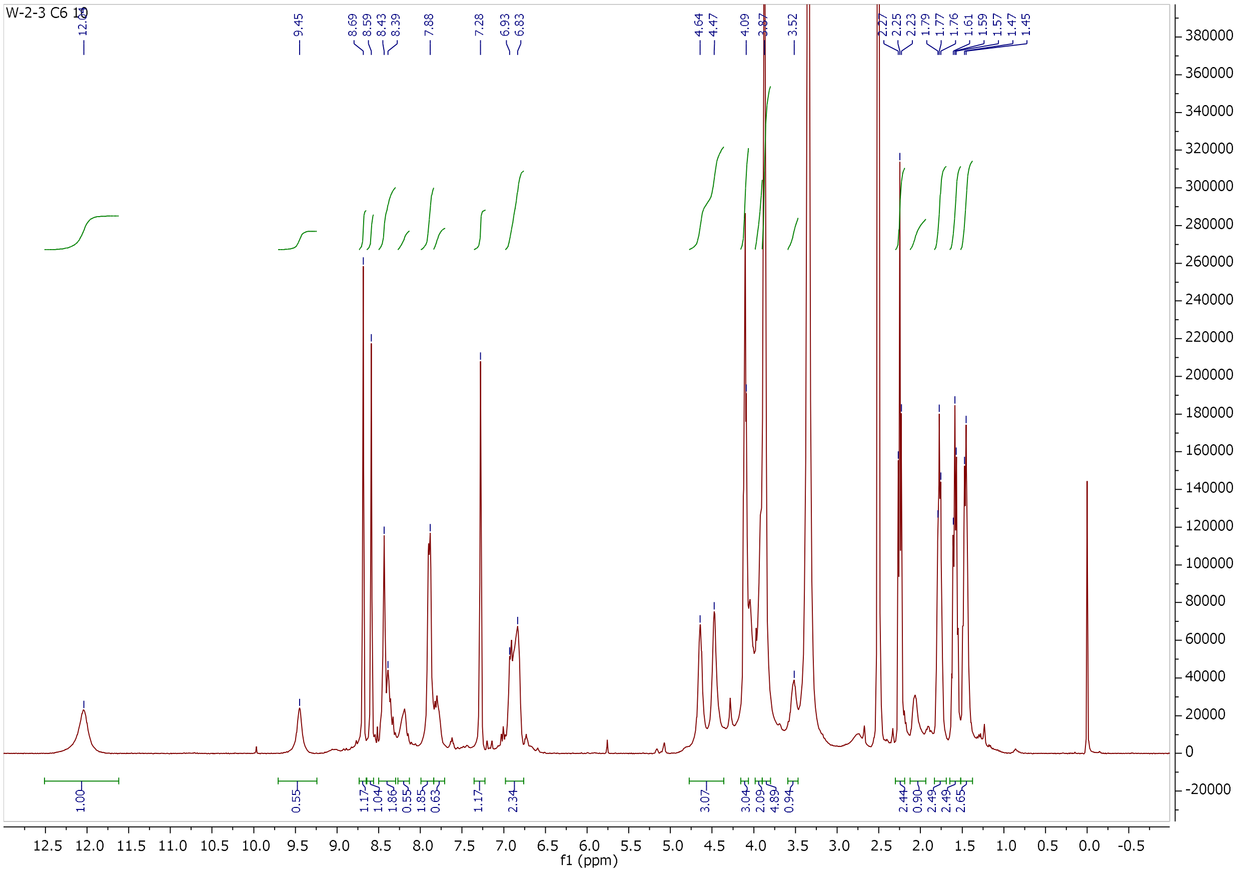
W-2-3 C6 1H
12.05
9.45
8.69
8.59
8.43
8.39
7.88
7.28
6.93
6.83
4.64
4.47
4.09
3.87
3.52
2.27
2.25
2.23
1.79
1.77
1.76
1.61
1.59
1.57
1.47
1.45
1.00
0.55
1.17
1.04
1.86
0.55
1.85
0.63
1.17
2.34
3.07
3.04
2.09
4.89
0.94
2.44
0.90
2.49
2.49
2.65
380000
360000
340000
320000
300000
280000
260000
240000
220000
200000
180000
160000
140000
120000
100000
80000
60000
40000
20000
0
-20000
12.5
12.0
11.5
11.0
10.5
10.0
9.5
9.0
8.5
8.0
7.5
7.0
6.5
6.0
5.5
5.0
4.5
4.0
3.5
3.0
2.5
2.0
1.5
1.0
0.5
0.0
-0.5
f1 (ppm)

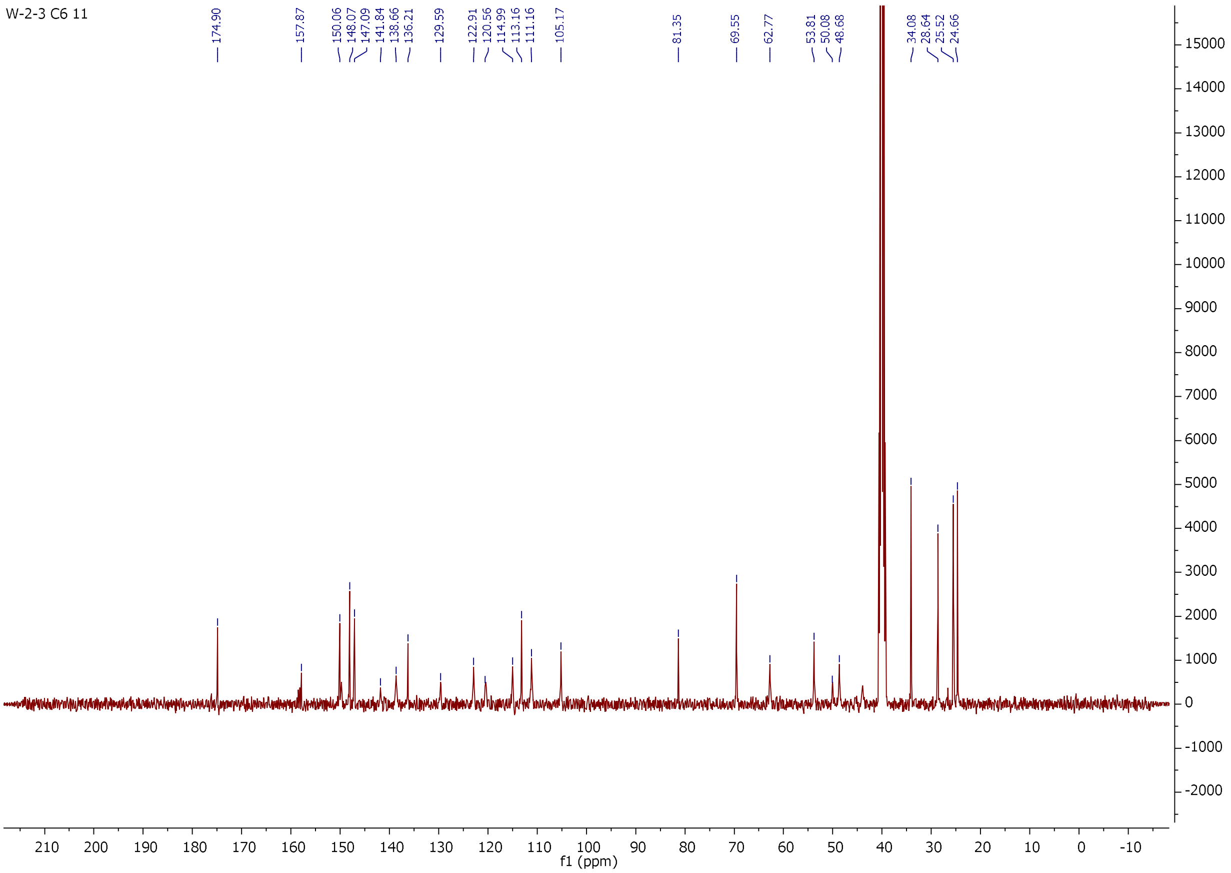
W-2-3 C6 11
174.90
157.87
150.06
148.07
147.09
141.84
138.66
136.21
129.59
122.91
120.56
114.99
113.16
111.16
105.17
81.35
69.55
62.77
53.81
50.08
48.68
34.08
28.64
25.52
24.66
15000
14000
13000
12000
11000
10000
9000
8000
7000
6000
5000
4000
3000
2000
1000
0
-1000
-2000
210
200
190
180
170
160
150
140
130
120
110
100
90
80
70
60
50
40
30
20
10
0
-10
f1 (ppm)

W-2-3 C_8

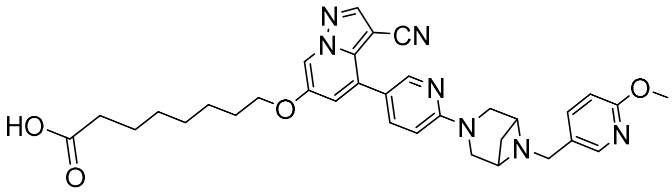

N
N
CN
N
HO
O
O
N
N
N
O

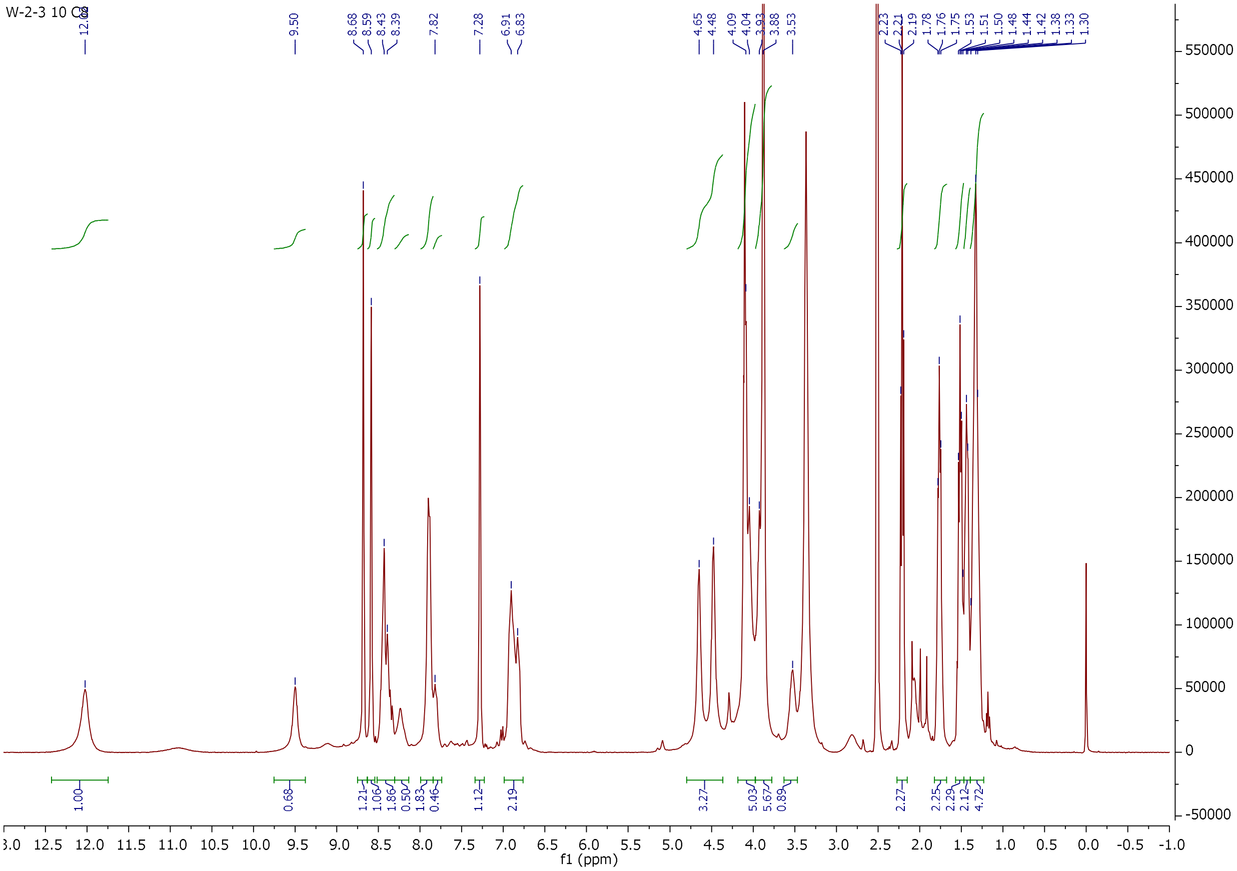

W-2-3 10 C8
12.00
9.50
8.68
8.59
8.43
8.39
7.82
7.28
6.91
6.83
4.65
4.48
4.09
4.04
3.93
3.88
3.53
2.23
2.21
2.19
1.78
1.76
1.75
1.53
1.51
1.50
1.48
1.44
1.42
1.38
1.33
1.30
1.00
0.68
1.21
1.06
1.86
0.50
1.83
0.46
1.12
2.19
3.27
5.03
5.67
0.89
2.27
2.25
2.29
2.12
4.72
550000
500000
450000
400000
350000
300000
250000
200000
150000
100000
50000
0
-50000
3.0
12.5
12.0
11.5
11.0
10.5
10.0
9.5
9.0
8.5
8.0
7.5
7.0
6.5
6.0
5.5
5.0
4.5
4.0
3.5
3.0
2.5
2.0
1.5
1.0
0.5
0.0
-0.5
-1.0
f1 (ppm)

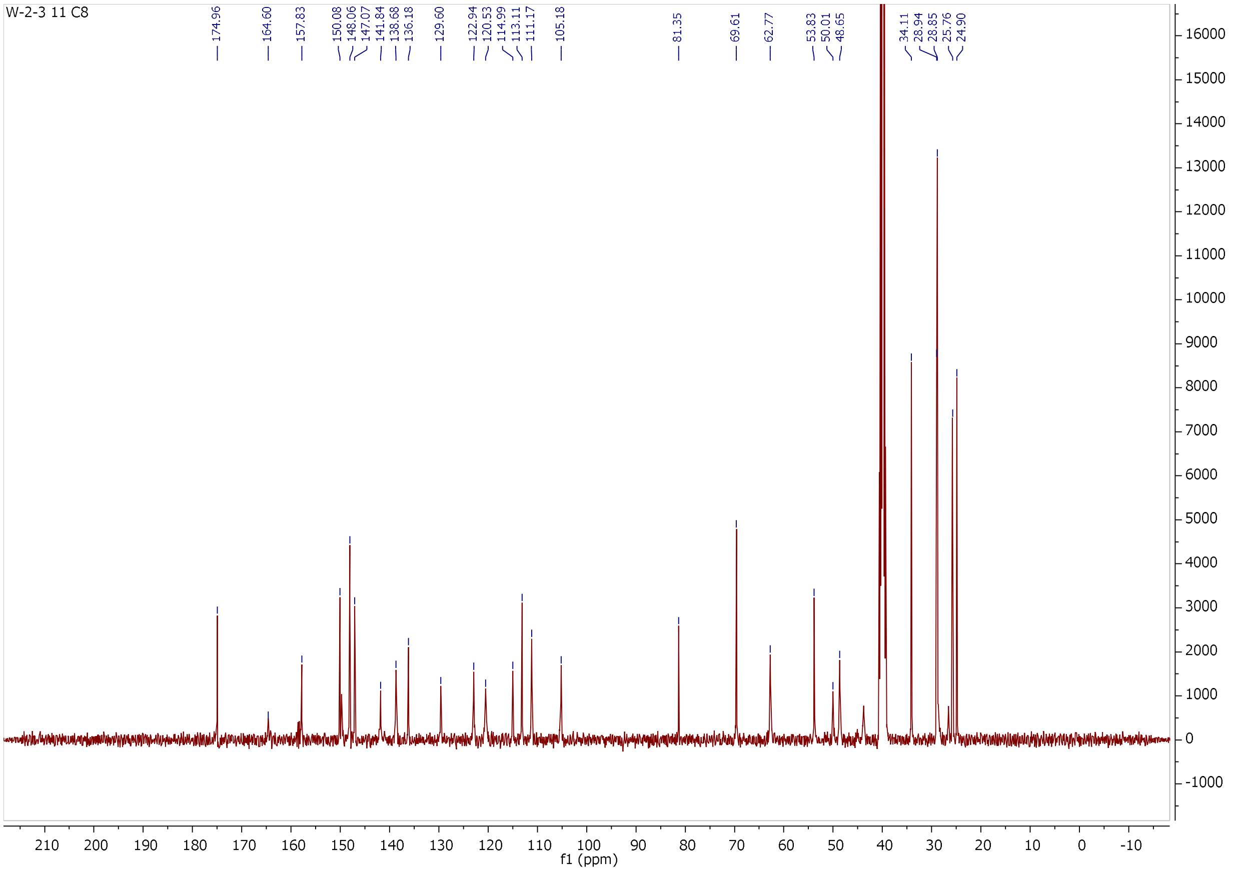
W-2-3 11 C8
174.96
164.60
157.83
150.08
148.06
147.07
141.84
138.68
136.18
129.60
122.94
120.53
114.99
113.11
111.17
105.18
81.35
69.61
62.77
53.83
50.01
48.65
34.11
28.94
28.85
25.76
24.90
16000
15000
14000
13000
12000
11000
10000
9000
8000
7000
6000
5000
4000
3000
2000
1000
0
-1000
210
200
190
180
170
160
150
140
130
120
110
100
90
80
70
60
50
40
30
20
10
0
-10
f1 (ppm)

L-2-2

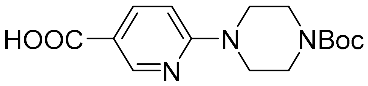
HOOC
N
NBoc
N

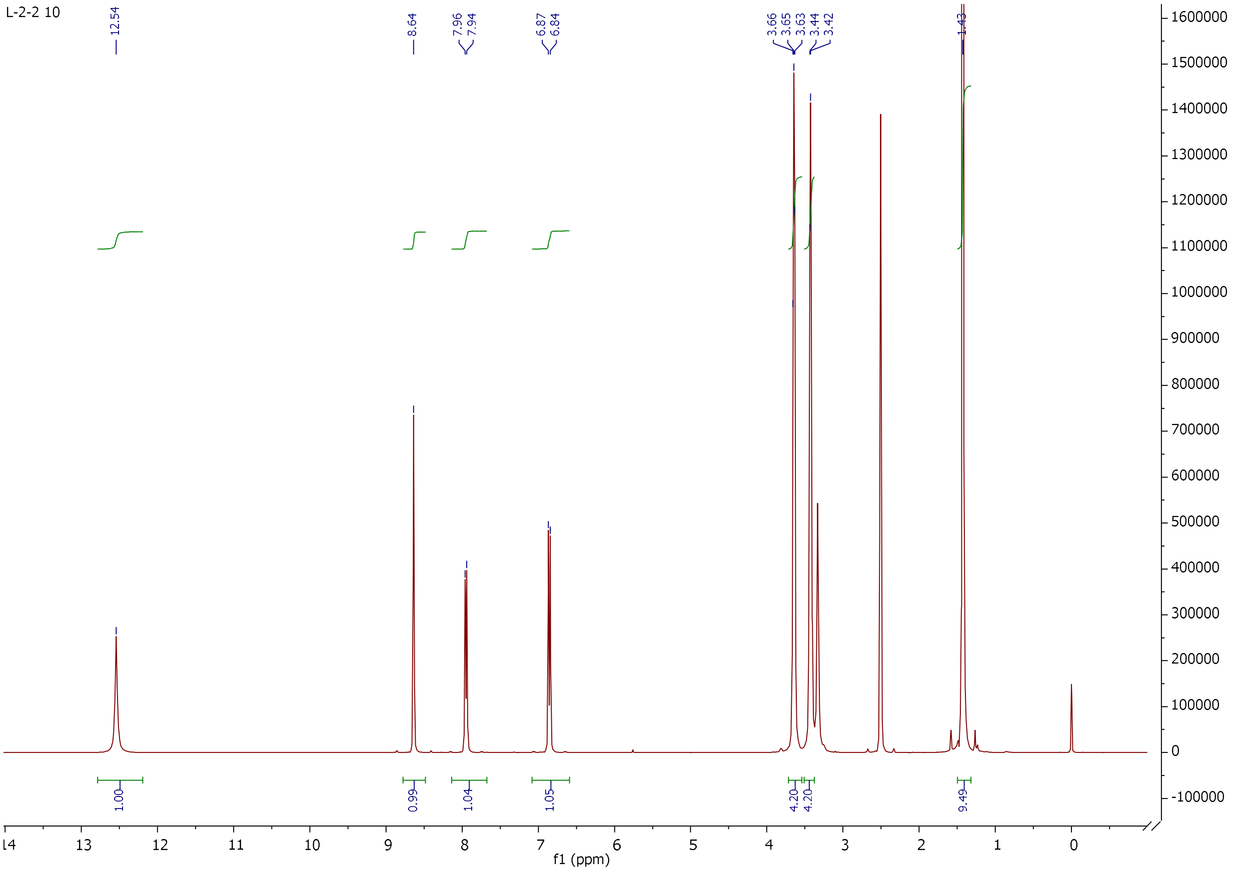
L-2-2 10
12.54
8.64
7.96
7.94
6.87
6.84
3.66
3.65
3.63
3.44
3.42
1.42
1.00
0.99
1.04
1.05
4.20
4.20
9.49
14
13
12
11
10
9
8
7
6
5
4
3
2
1
0
f1 (ppm)
1600000
1500000
1400000
1300000
1200000
1100000
1000000
900000
800000
700000
600000
500000
400000
300000
200000
100000
0
-100000

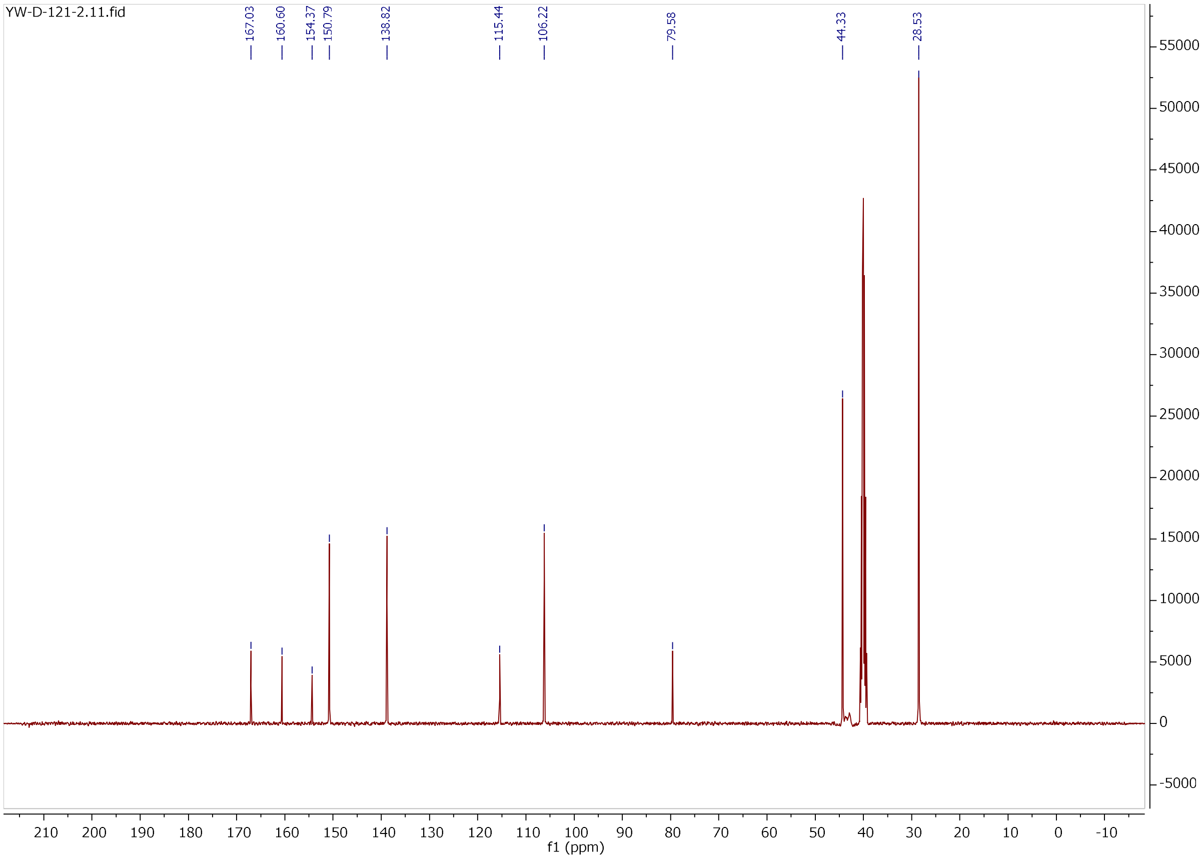
YW-D-121-2.11.fid
167.03
160.60
154.37
150.79
138.82
115.44
106.22
79.58
44.33
28.53
55000
50000
45000
40000
35000
30000
25000
20000
15000
10000
5000
0
-5000
210
200
190
180
170
160
150
140
130
120
110
100
90
80
70
60
50
40
30
20
10
0
-10
f1 (ppm)

L-3-2

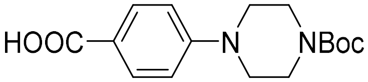
HOOC
N
NBoc

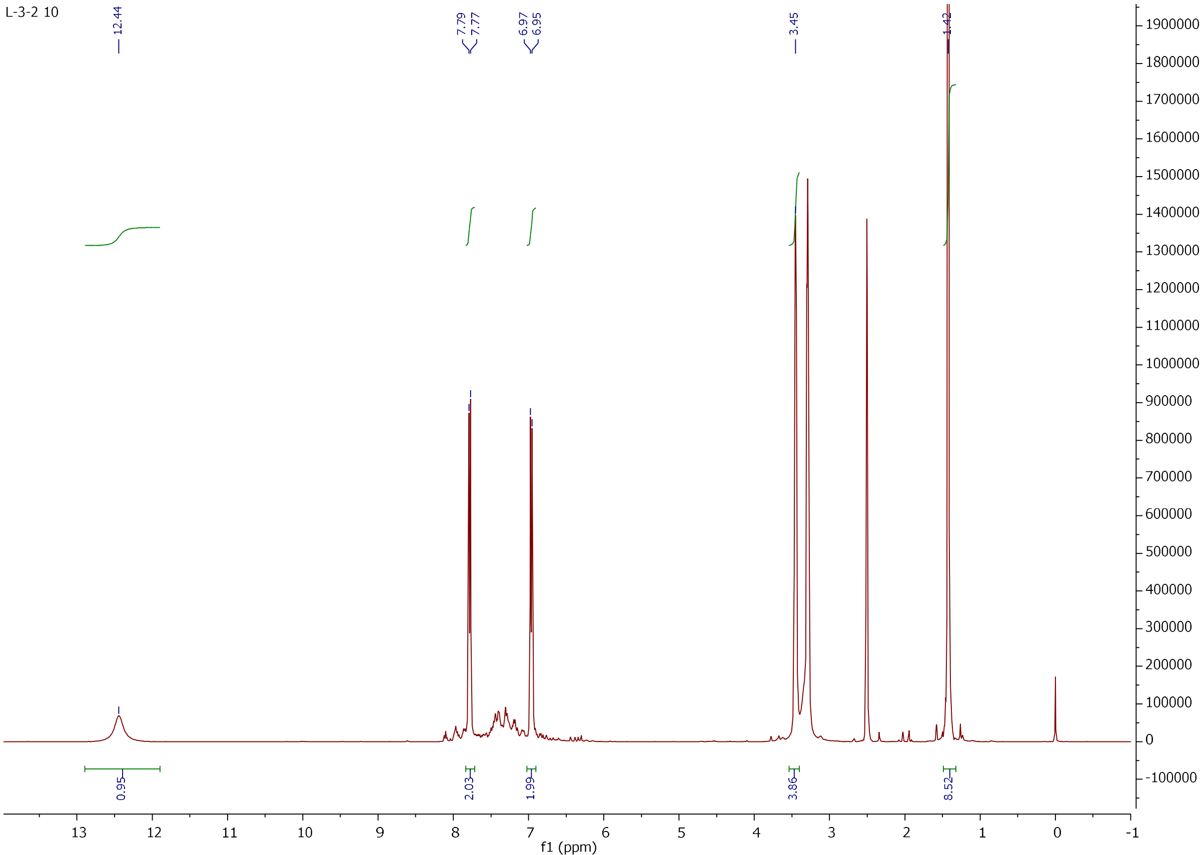
L-3-2 10
12.44
7.79
7.77
6.97
6.95
3.45
1.42
0.95
2.03
1.99
3.86
8.52
13
12
11
10
9
8
7
6
5
4
3
2
1
0
-1
f1 (ppm)
1900000
1800000
1700000
1600000
1500000
1400000
1300000
1200000
1100000
1000000
900000
800000
700000
600000
500000
400000
300000
200000
100000
0
-100000

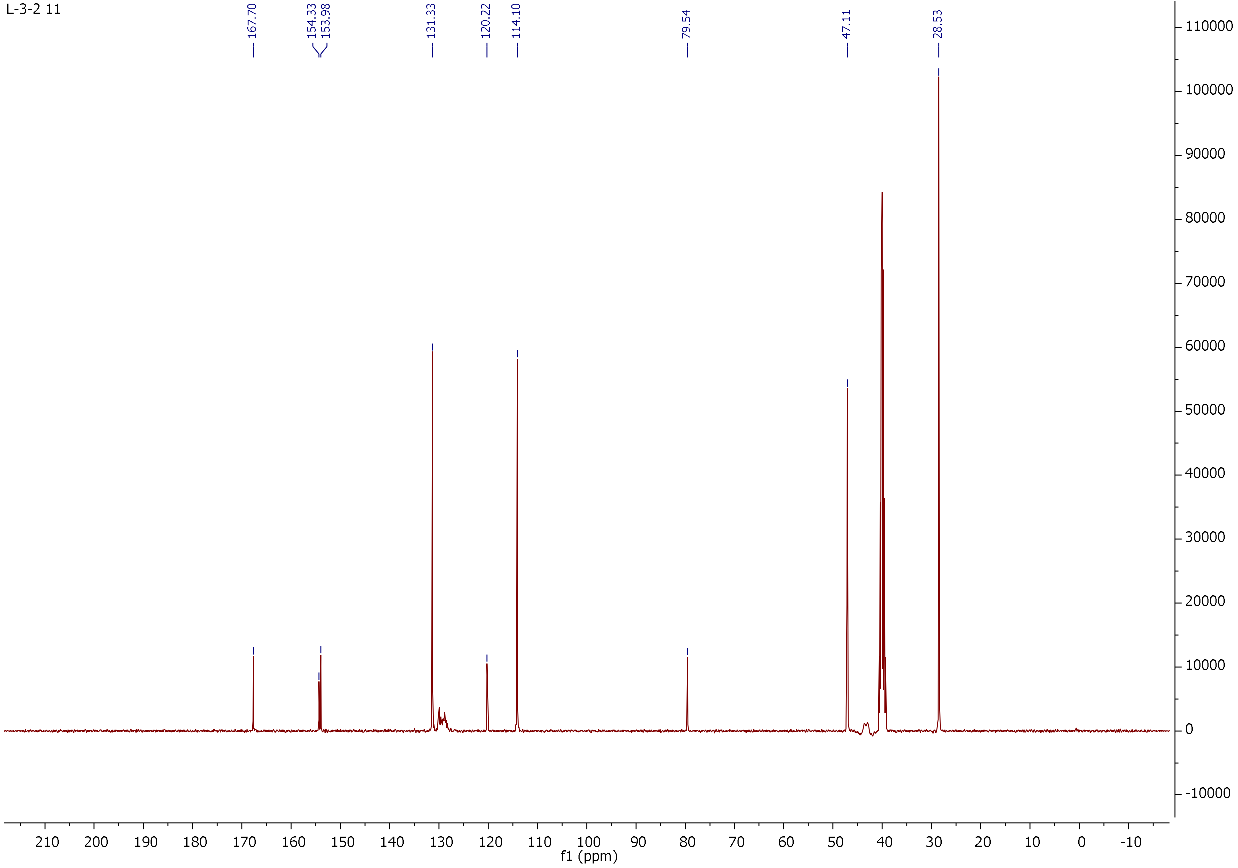
L-3-2 11
167.70
154.33
153.98
131.33
120.22
114.10
79.54
47.11
28.53
210
200
190
180
170
160
150
140
130
120
110
100
90
80
70
60
50
40
30
20
10
0
-10
f1 (ppm)
110000
100000
90000
80000
70000
60000
50000
40000
30000
20000
10000
0
-10000

Appendix B: ^{1}H-NMR and ^{13}C-NMR

YW-D-50-2

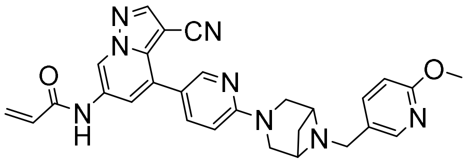

^{1}H NMR (400 MHz, DMSO-d$_6$) δ 9.55 (s, 1H), 9.42 (s, 1H), 8.64 (s, 1H), 8.54 – 8.25 (m, 2H), 8.02 – 7.80 (m, 2H), 7.49 (d, J = 17.2 Hz, 1H), 6.90 (dd, J = 29.6, 8.6 Hz, 3H), 6.47 (d, J = 6.7 Hz, 1H), 6.39 – 6.30 (m, 1H), 5.87 (d, J = 9.9 Hz, 1H), 4.64 (s, 2H), 4.48 (d, J = 6.1 Hz, 1H), 4.23 (s, 1H), 4.17 – 4.02 (m, 2H), 3.98 – 3.83 (m, 4H), 3.53 (s, 1H), 2.08 (s, 1H).

^{13}C NMR (101 MHz, DMSO-*d*$_6$) δ 164.62, 164.30, 158.56, 157.82, 149.76, 149.05, 147.79, 147.58, 141.85, 141.34, 138.67, 137.24, 131.27, 129.43, 129.19, 128.73, 123.28, 120.68, 120.39, 118.97, 114.77, 111.22, 105.93, 105.43, 81.74, 62.77, 53.88, 50.03, 48.74, 44.60, 43.74.

YW-D-50-6

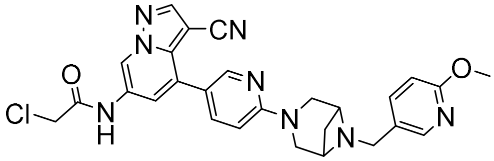

^{1}H NMR (400 MHz, DMSO-*d*$_6$) δ 9.40 (s, 1H), 8.66 (s, 1H), 8.41 (d, *J* = 15.1 Hz, 1H), 7.89 (d, *J* = 9.1 Hz, 1H), 7.48 (d, *J* = 16.9 Hz, 1H), 6.93 (q, *J* = 7.2, 6.6 Hz, 1H), 6.85 (d, *J* = 8.8 Hz, 1H), 4.64 (s, 2H), 4.48 (d, *J* = 6.1 Hz, 1H), 4.38 (d, *J* = 5.2 Hz, 2H), 4.23 (s, 1H), 4.12 (s, 1H), 4.07 (d, *J* = 12.7 Hz, 1H), 3.93 (s, 1H), 3.89 (s, 2H), 3.88 (s, 1H), 3.59 – 3.46 (m, 1H), 2.08 (s, 1H).

^{13}C NMR (101 MHz, DMSO-*d*$_6$) δ 166.00, 164.62, 157.85, 149.75, 149.04, 147.67, 141.85, 141.34, 138.64, 137.44, 129.56, 128.70, 123.24, 120.61, 120.39, 119.22, 114.70, 111.22, 105.89, 105.41, 81.86, 62.77, 53.88, 50.03, 48.73, 44.60, 43.63.

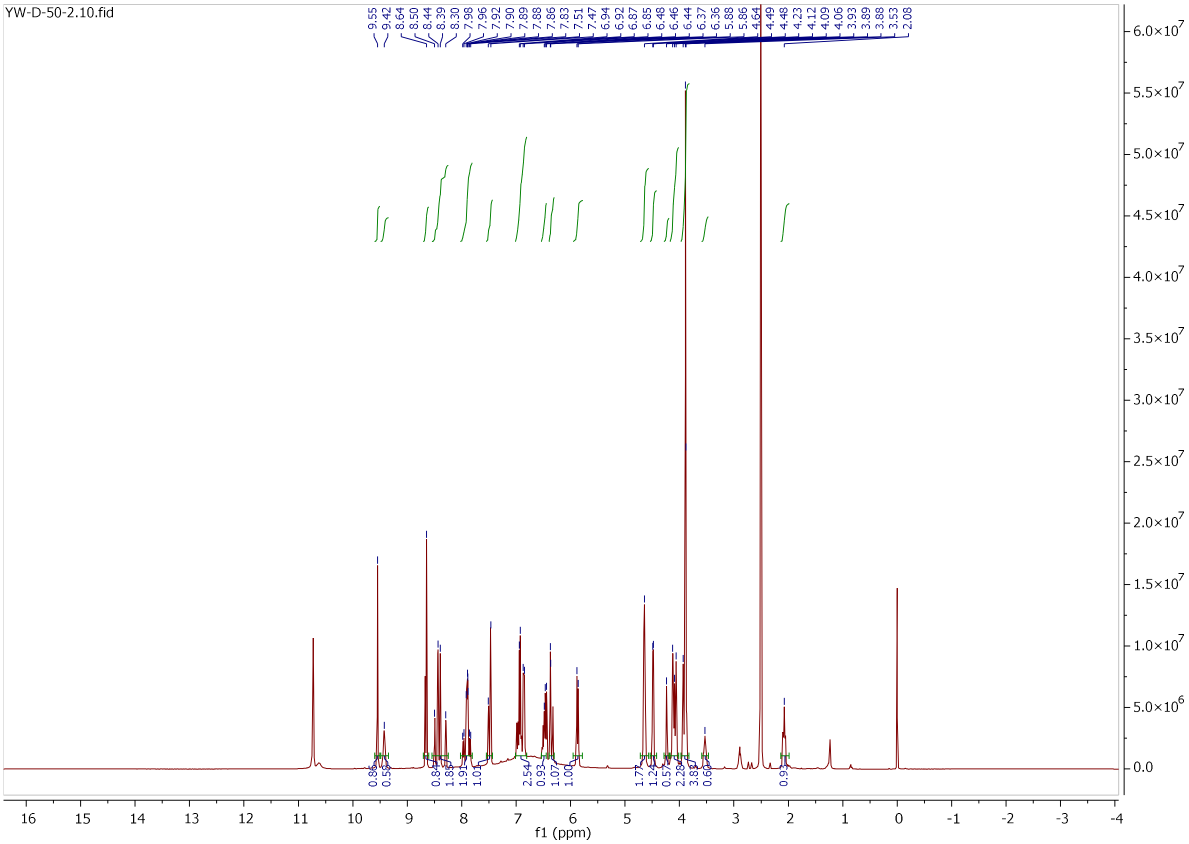
YW-D-50-2.10.fid
9.55
9.42
8.64
8.50
8.44
8.39
8.30
7.98
7.96
7.92
7.90
7.89
7.88
7.86
7.83
7.51
7.47
6.94
6.92
6.87
6.85
6.48
6.46
6.44
6.37
6.36
5.88
5.86
4.64
4.49
4.48
4.23
4.12
4.09
4.05
3.93
3.89
3.88
3.53
2.08
0.86
0.58
0.84
1.85
1.91
1.01
2.54
0.93
1.07
1.00
1.77
1.24
0.57
2.28
3.83
0.60
0.93
16
15
14
13
12
11
10
9
8
7
6
5
4
3
2
1
0
-1
-2
-3
-4
f1 (ppm)
6.0×10^7
5.5×10^7
5.0×10^7
4.5×10^7
4.0×10^7
3.5×10^7
3.0×10^7
2.5×10^7
2.0×10^7
1.5×10^7
1.0×10^7
5.0×10^6
0.0

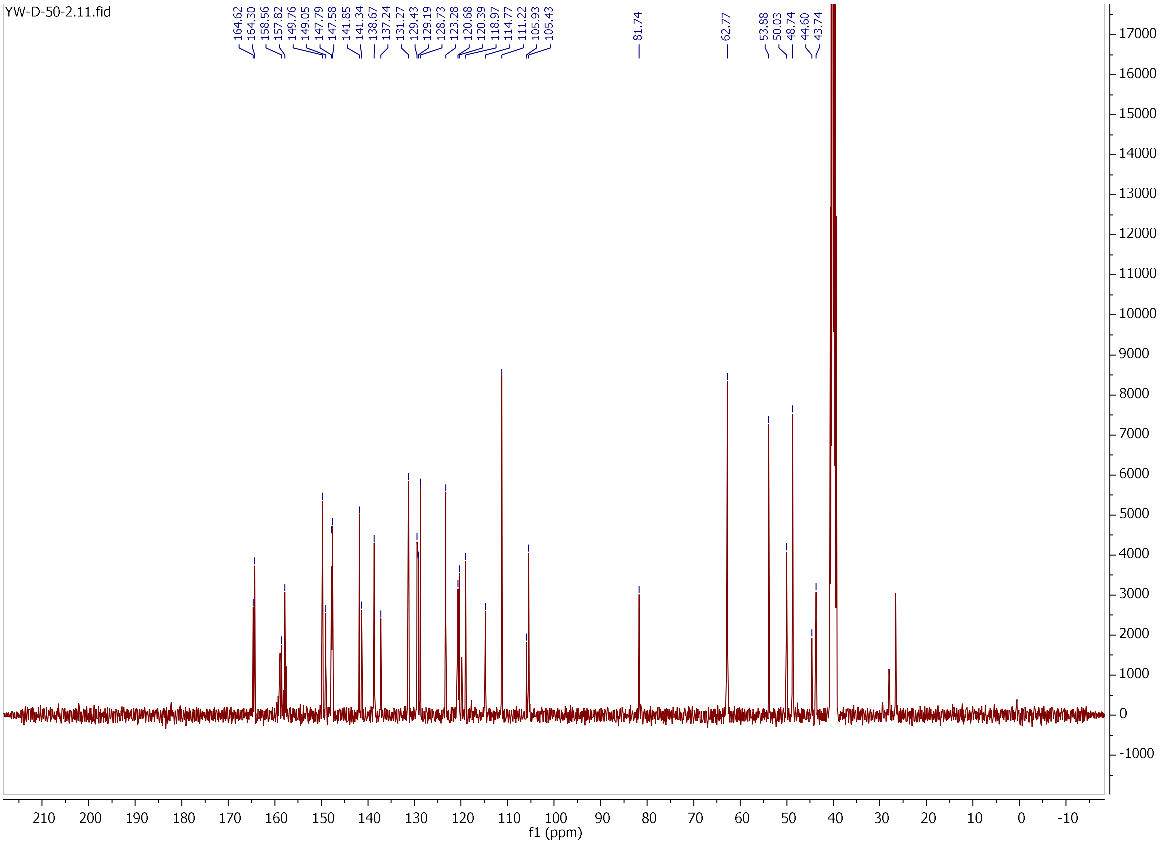
YW-D-50-2.11.fid
164.62
164.30
158.56
157.82
149.76
149.05
147.79
147.58
141.85
141.34
138.67
137.24
131.27
129.43
129.19
128.73
123.28
120.68
120.39
118.97
114.77
111.22
105.93
105.43
81.74
62.77
53.88
50.03
48.74
44.60
43.74
210 200 190 180 170 160 150 140 130 120 110 100 90 80 70 60 50 40 30 20 10 0 -10
f1 (ppm)
17000 16000 15000 14000 13000 12000 11000 10000 9000 8000 7000 6000 5000 4000 3000 2000 1000 0 -1000

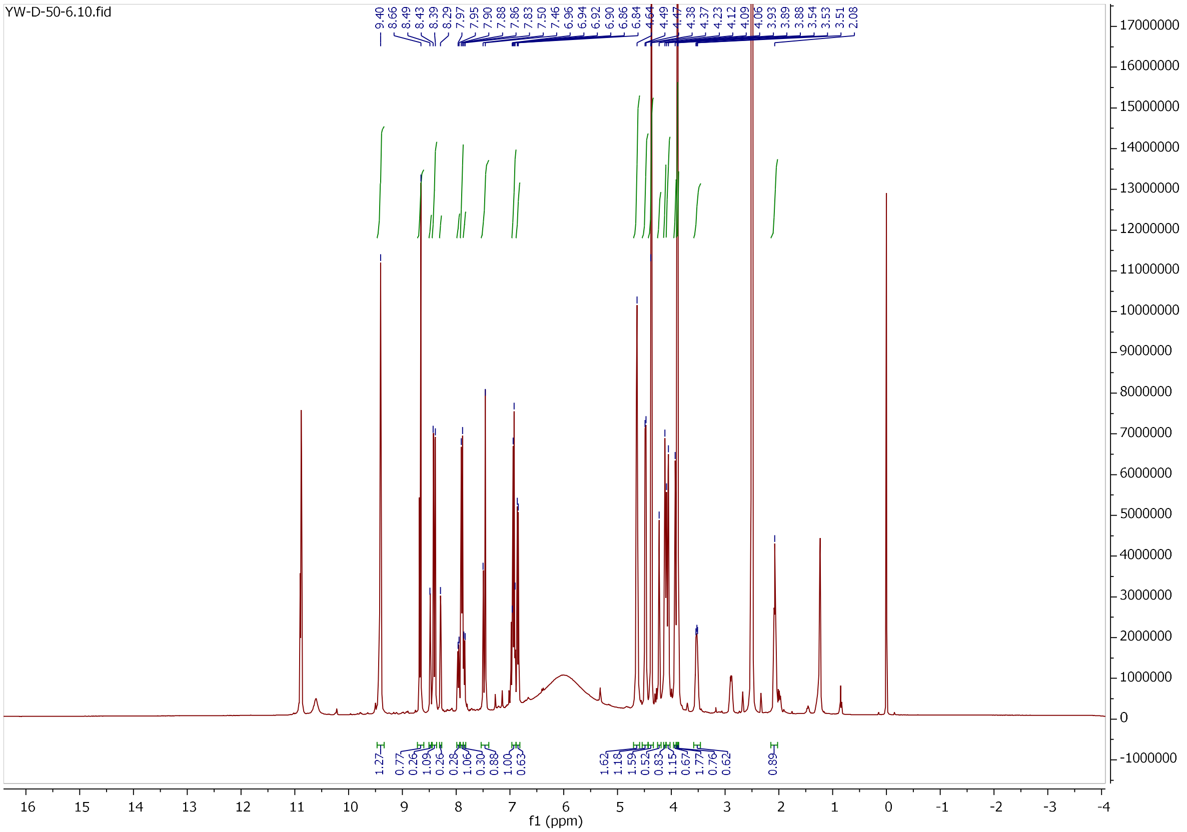
YW-D-50-6.10.fid
9.40
8.66
8.49
8.43
8.39
8.29
7.97
7.95
7.90
7.88
7.86
7.83
7.50
7.46
6.96
6.94
6.92
6.90
6.86
6.84
4.64
4.49
4.47
4.38
4.37
4.23
4.12
4.09
4.06
3.93
3.89
3.88
3.54
3.53
3.51
2.08
1.27
0.77
0.26
1.09
0.26
0.28
1.06
0.30
0.88
1.00
0.63
1.62
1.18
1.59
0.52
0.83
1.15
0.67
1.77
0.76
0.62
0.89
16 15 14 13 12 11 10 9 8 7 6 5 4 3 2 1 0 -1 -2 -3 -4
f1 (ppm)
17000000 16000000 15000000 14000000 13000000 12000000 11000000 10000000 9000000 8000000 7000000 6000000 5000000 4000000 3000000 2000000 1000000 0 -1000000

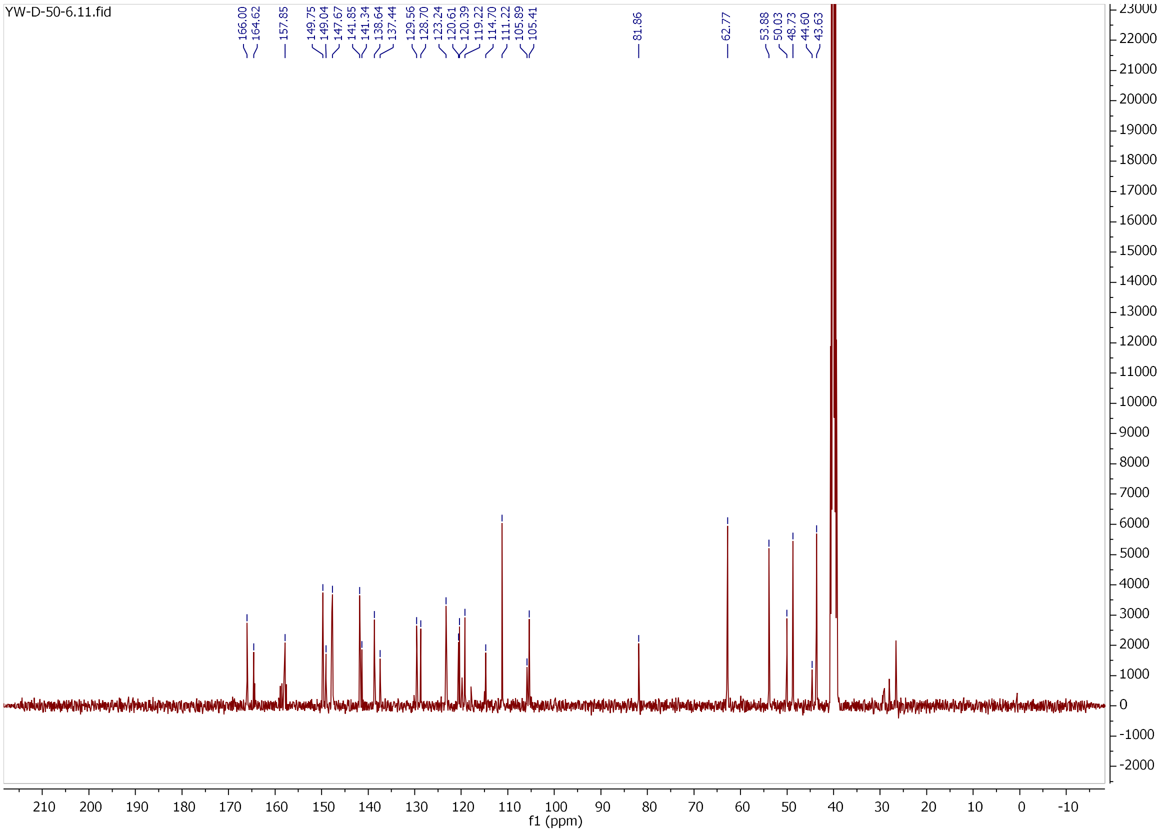
YW-D-50-6.11.fid
166.00
164.62
157.85
149.75
149.04
147.67
141.85
141.34
138.64
137.44
129.56
128.70
123.24
120.61
120.39
119.22
114.70
111.22
105.89
105.41
81.86
62.77
53.88
50.03
48.73
44.60
43.63
23000
22000
21000
20000
19000
18000
17000
16000
15000
14000
13000
12000
11000
10000
9000
8000
7000
6000
5000
4000
3000
2000
1000
0
-1000
-2000
210
200
190
180
170
160
150
140
130
120
110
100
90
80
70
60
50
40
30
20
10
0
-10
f1 (ppm)

Appendix C: HPLC data , ^{1}HNMR, and ^{13}C NMR spectrum

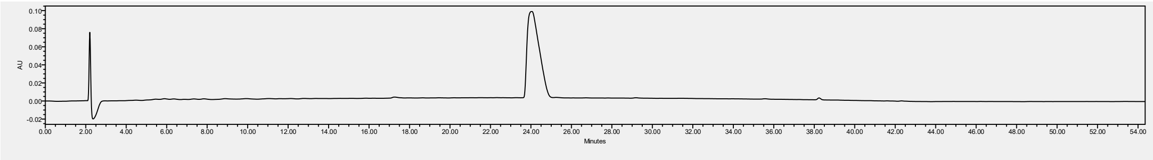

YW-1

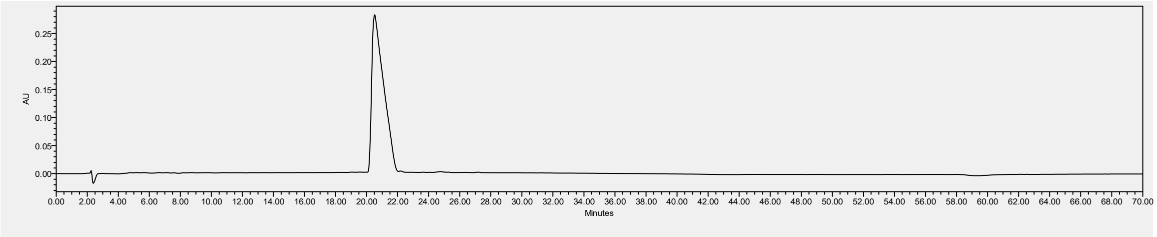

YW-2

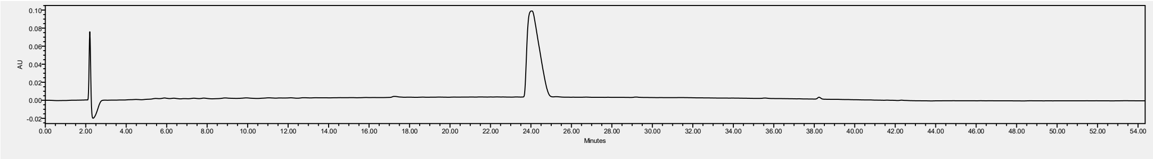

YW-3

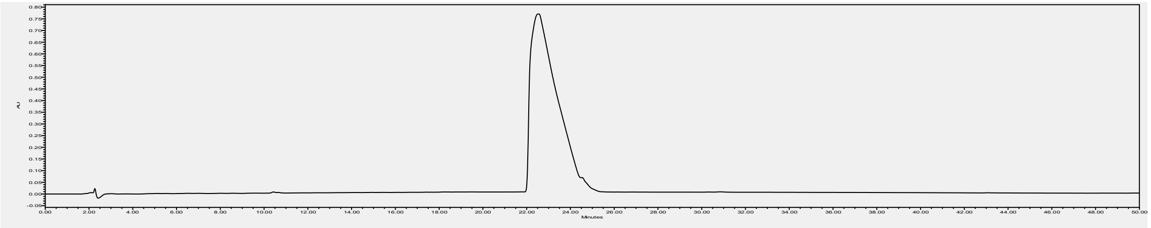

YW-4

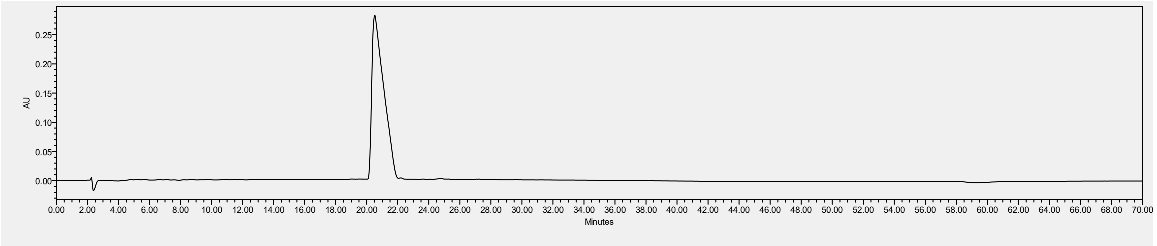

YW-5

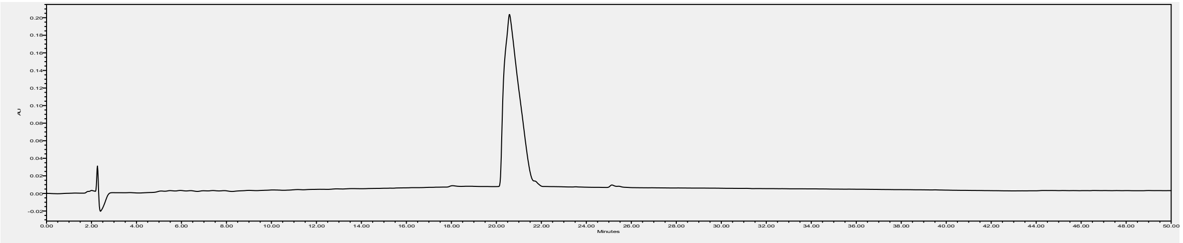

YW-6

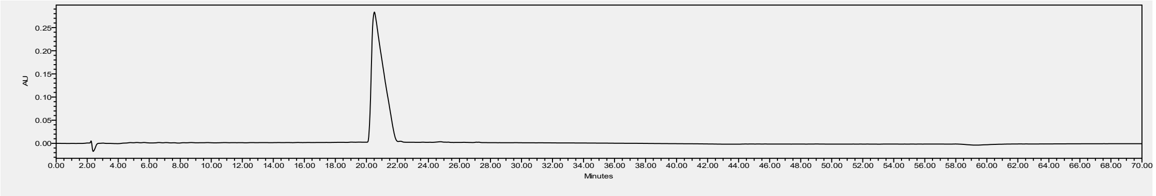

YW-7

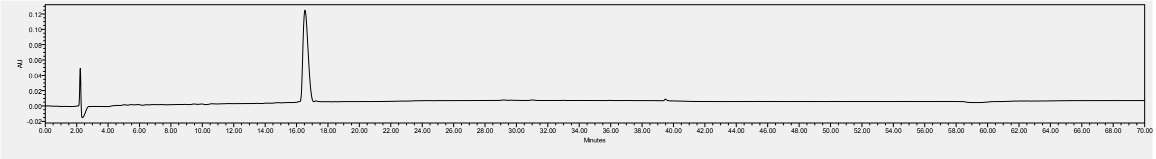

YW-8

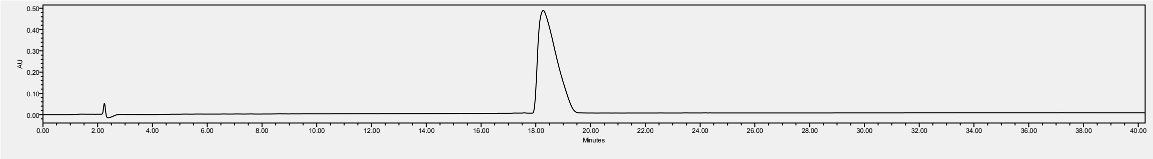

YW-9

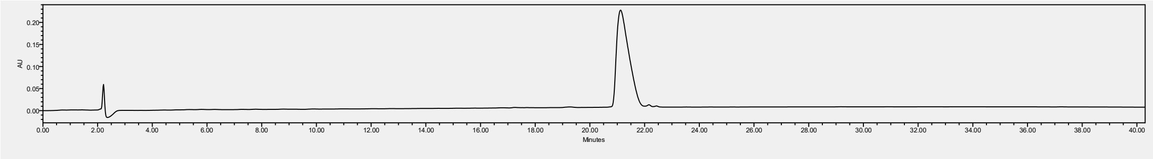

YW-10

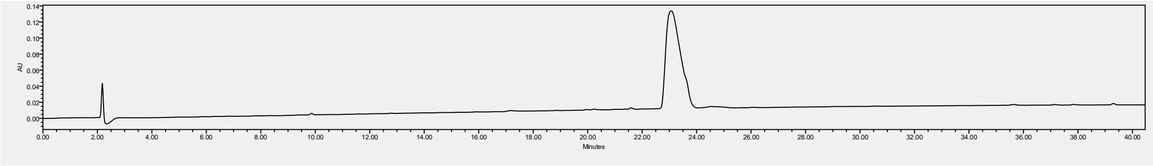

YW-11

YW-1:

^{1}H NMR (600 MHz, DMSO-d6) δ 8.09 (s, 1H), 7.96 – 7.71 (m, 9H), 7.57 (d, J = 8.9 Hz, 1H), 7.37 (d, J = 22.1 Hz, 1H), 7.17 (d, J = 12.8 Hz, 1H), 6.99 (d, J = 14.9 Hz, 1H), 4.10 – 3.88 (m, 3H), 3.74 (d, J = 16.5 Hz, 1H), 3.50 (ddd, J = 33.1, 14.7, 7.5 Hz, 4H), 3.26 – 3.16 (m, 1H), 3.02 (qd, J = 6.4, 3.2 Hz, 2H), 2.75 (dddd, J = 28.1, 13.9, 6.9, 3.1 Hz, 5H), 2.11 – 1.95 (m, 2H), 1.64 – 1.30 (m, 10H), 1.24 (s, 26H), 0.89 – 0.83 (m, 6H), 0.80 (dd, J = 10.4, 6.5 Hz, 3H).

^{13}C NMR (151 MHz, DMSO-d6) δ 172.72, 172.49, 170.78, 158.82, 158.61, 38.94, 36.02, 35.73, 31.74, 30.46, 29.50, 29.15, 28.97, 27.14, 24.78, 23.80, 22.55, 22.01, 21.72, 14.41.

YW-2:

^{1}H NMR (600 MHz, DMSO-d6) δ 8.20 – 7.96 (m, 1H), 7.94 – 7.71 (m, 9H), 7.30 – 7.10 (m, 6H), 4.27 – 4.09 (m, 1H), 4.08 – 3.94 (m, 1H), 3.93 – 3.75 (m, 1H), 3.56 (ddd, J = 87.1, 13.0, 5.8 Hz, 4H), 3.02 (p, J = 6.4 Hz, 2H), 2.94 (dd, J = 13.4, 7.4 Hz, 1H), 2.85 – 2.53 (m, 7H), 2.45 (q, J = 7.0 Hz, 1H), 1.93 (td, J = 7.3, 4.0 Hz, 2H), 1.53 (dtt, J = 17.2, 10.4, 5.2 Hz, 4H), 1.45 – 1.10 (m, 27H), 1.09 – 0.94 (m, 2H), 0.85 (t, J = 6.9 Hz, 3H).

^{13}C NMR (151 MHz, DMSO-d6) δ 171.27, 170.78, 158.54, 129.45, 128.50, 128.39, 118.54, 116.71,49.99, 47.31, 44.32, 38.95, 31.75, 29.52, 29.38, 29.16, 27.17, 25.67, 22.55, 22.02, 14.42.

YW-3:

^{1}H NMR (600 MHz, DMSO-d6) δ 7.95 – 7.69 (m, 9H), 4.07 – 3.76 (m, 3H), 3.50 (dd, J = 17.8, 10.9 Hz, 4H), 3.24 (dd, J = 7.3, 3.6 Hz, 1H), 3.01 (h, J = 6.2 Hz, 2H), 2.85 – 2.63 (m, 5H), 2.02 (dq, J = 12.1, 7.0 Hz, 2H), 1.62 – 1.49 (m, J = 6.5 Hz, 4H), 1.49 – 1.35 (m, 4H), 1.24 (s, 24H), 1.05 (d, J = 6.7 Hz, 1H), 0.97 (d, J = 6.7 Hz, 1H), 0.85 (t, J = 6.9 Hz, 3H).

^{13}C NMR (151 MHz, DMSO-d6) δ 172.19, 171.93, 158.82, 158.62, 117.72, 116.43, 49.91, 47.31, 43.58, 38.95, 35.74, 31.75, 30.39, 29.51, 29.47, 29.16, 27.16, 25.70, 22.55, 22.01, 18.70, 18.46, 14.42.

YW-4

^{1}H NMR (600 MHz, DMSO-d6) δ 8.11 (d, J = 7.8 Hz, 1H), 7.98 – 7.68 (m, 9H), 7.03 – 6.91 (m, 3H), 6.67 – 6.58 (m, 2H), 4.17 – 3.75 (m, 3H), 3.57 (td, J = 13.7, 6.2 Hz, 2H), 3.41 – 3.28 (m, 3H), 3.25 (dd, J = 15.1, 9.2 Hz, 1H), 3.01 (h, J = 6.2 Hz, 2H), 2.92 (dd, J = 13.4, 7.7 Hz, 1H), 2.83 – 2.56 (m, 6H), 2.43 (dd, J = 13.5, 9.3 Hz, 1H), 1.95 (tt, J = 7.6, 3.1 Hz, 2H), 1.55 (tt, J = 14.0, 5.2 Hz, 4H), 1.46 – 1.30 (m, 4H), 1.30 – 1.13 (m, 22H), 1.09 (h, J = 7.0 Hz, 2H), 0.85 (t, J = 7.0 Hz, 3H).

^{13}C NMR (151 MHz, DMSO-d6) δ 172.62, 171.79, 170.95, 158.97, 158.76, 156.14, 130.27, 128.92, 118.51, 116.53, 115.34, 115.23, 49.92, 47.40, 38.93, 37.31, 36.07, 35.72, 31.75, 29.47, 29.17, 27.16, 25.68, 22.55, 22.02, 14.41.

YW-5

^{1}H NMR (600 MHz, DMSO-d6) δ 8.03 (s, 1H), 7.89 – 7.63 (m, 9H), 4.08 – 3.76 (m, 4H), 3.57 – 3.38 (m, 6H), 3.03 (dp, J = 17.3, 6.8, 6.0 Hz, 3H), 2.84 – 2.63 (m, 6H), 2.10 – 1.99 (m, 2H), 1.53 (h, J = 6.4, 5.4 Hz, 4H), 1.43 (dt, J = 30.3, 7.3 Hz, 4H), 1.24 (s, 24H), 0.86 (t, J = 6.9 Hz, 3H).

^{13}C NMR (151 MHz, DMSO-d6) δ 172.75, 171.00, 159.29, 158.54, 50.10,49.42, 38.97, 35.75, 31.75, 30.40, 29.53, 29.31, 29.17, 27.18, 25.72, 22.56, 14.42.

YW-6:

^{1}H NMR (600 MHz, DMSO-d6) δ 8.06 (s, 1H), 7.78 (d, J = 31.6 Hz, 13H), 3.95 (dd, J = 20.6, 4.1 Hz, 2H), 3.88 (d, J = 14.1 Hz, 1H), 3.72 (d, J = 16.5 Hz, 1H), 3.58 – 3.40 (m, 4H), 3.01 (s, 2H), 2.95 (dd, J = 13.7, 8.3 Hz, 1H), 2.76 (dtd, J = 31.4, 17.3, 14.7, 7.3 Hz, 8H), 2.45 – 2.35 (m, 1H), 2.03 (dq, J = 9.5, 7.0, 6.6 Hz, 2H), 1.62 – 1.36 (m, 13H), 1.24 (s, 31H), 0.86 (t, J = 6.9 Hz, 3H). ^{13}C NMR (151 MHz, DMSO-d6) δ 171.75, 169.58, 159.06, 158.32, 47.62, 45.31, 43.94, 39.03, 31.75, 29.54, 29.17, 22.55, 14.42.

YW-7:

^{1}H NMR (600 MHz, DMSO-d6) δ 8.05 (s, 1H), 7.95 – 7.53 (m, 11H), 4.09 – 3.84 (m, 3H), 3.73 (d, J = 16.5 Hz, 1H), 3.51 (s, 6H), 3.25 (s, 2H), 3.10 – 2.88 (m, 4H), 2.85 – 2.63 (m, 5H), 2.46 – 2.35 (m, 1H), 2.02 (dq, J = 10.1, 6.9 Hz, 2H), 1.60 – 1.05 (m, 38H), 0.85 (t, J = 6.9 Hz, 3H). ^{13}C NMR (151 MHz, DMSO-d6) δ 172.04, 171.95, 158.82, 158.66, 157.24, 118.85, 117.36, 50.22, 47.53, 44.10, 39.00, 36.22, 36.07, 35.73, 31.75, 29.54, 29.17, 22.55, 14.42.

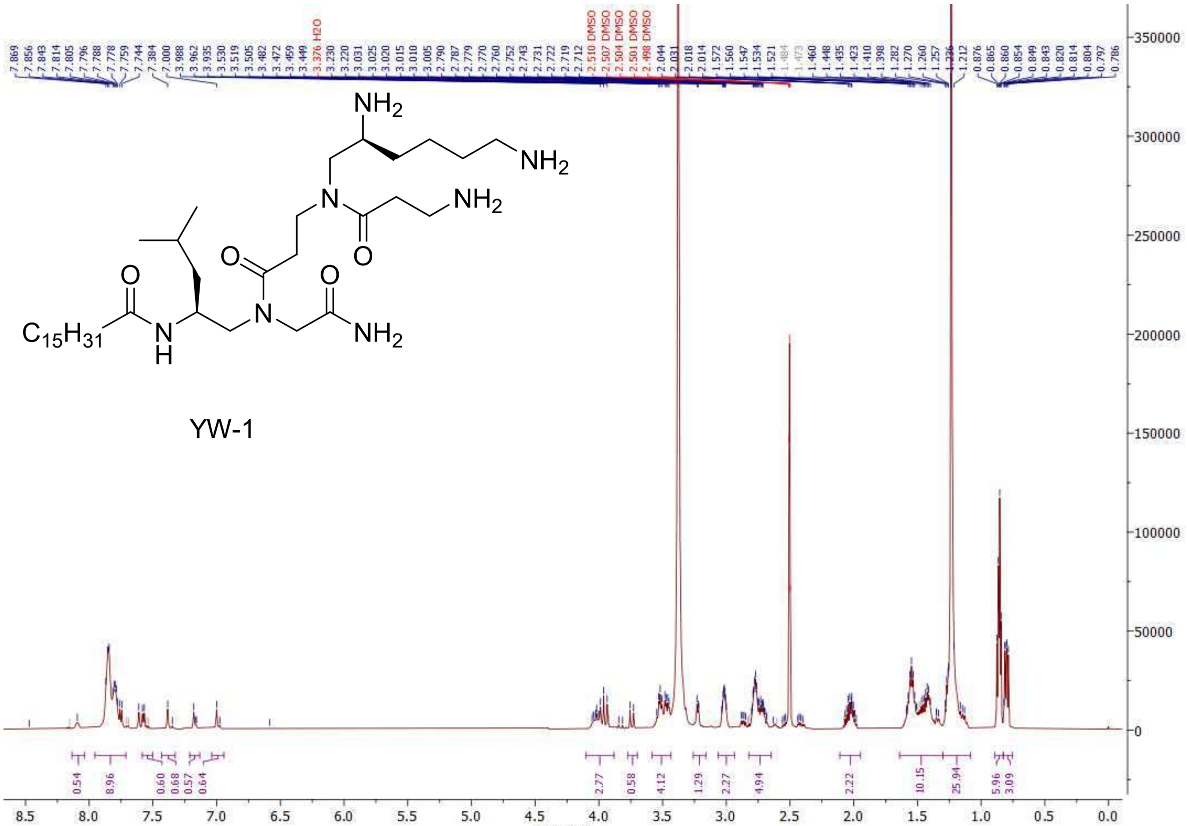
7.869
7.856
7.843
7.814
7.805
7.796
7.788
7.778
7.759
7.744
7.384
7.000
3.988
3.962
3.935
3.530
3.519
3.505
3.482
3.472
3.459
3.449
3.376 H2O
3.230
3.220
3.031
3.025
3.020
3.015
3.010
3.005
2.790
2.787
2.779
2.770
2.760
2.752
2.743
2.731
2.722
2.719
2.712
2.510 DMSO
2.507 DMSO
2.504 DMSO
2.501 DMSO
2.498 DMSO
2.044
2.031
2.018
2.014
1.572
1.560
1.547
1.534
1.521
1.484
1.473
1.460
1.448
1.435
1.423
1.410
1.398
1.282
1.270
1.260
1.257
1.236
1.212
0.876
0.865
0.860
0.854
0.849
0.843
0.820
0.814
0.804
0.797
0.786
NH2
NH2
N
NH2
O
O
O
O
C15H31
N
H
N
NH2
0.54
8.96
0.60
0.68
0.57
0.64
2.77
0.58
4.12
1.29
2.27
4.94
2.22
10.15
25.94
5.96
3.09
8.5
8.0
7.5
7.0
6.5
6.0
5.5
5.0
4.5
4.0
3.5
3.0
2.5
2.0
1.5
1.0
0.5
0.0
f1 (ppm)
350000
300000
250000
200000
150000
100000
50000
0

YW-1

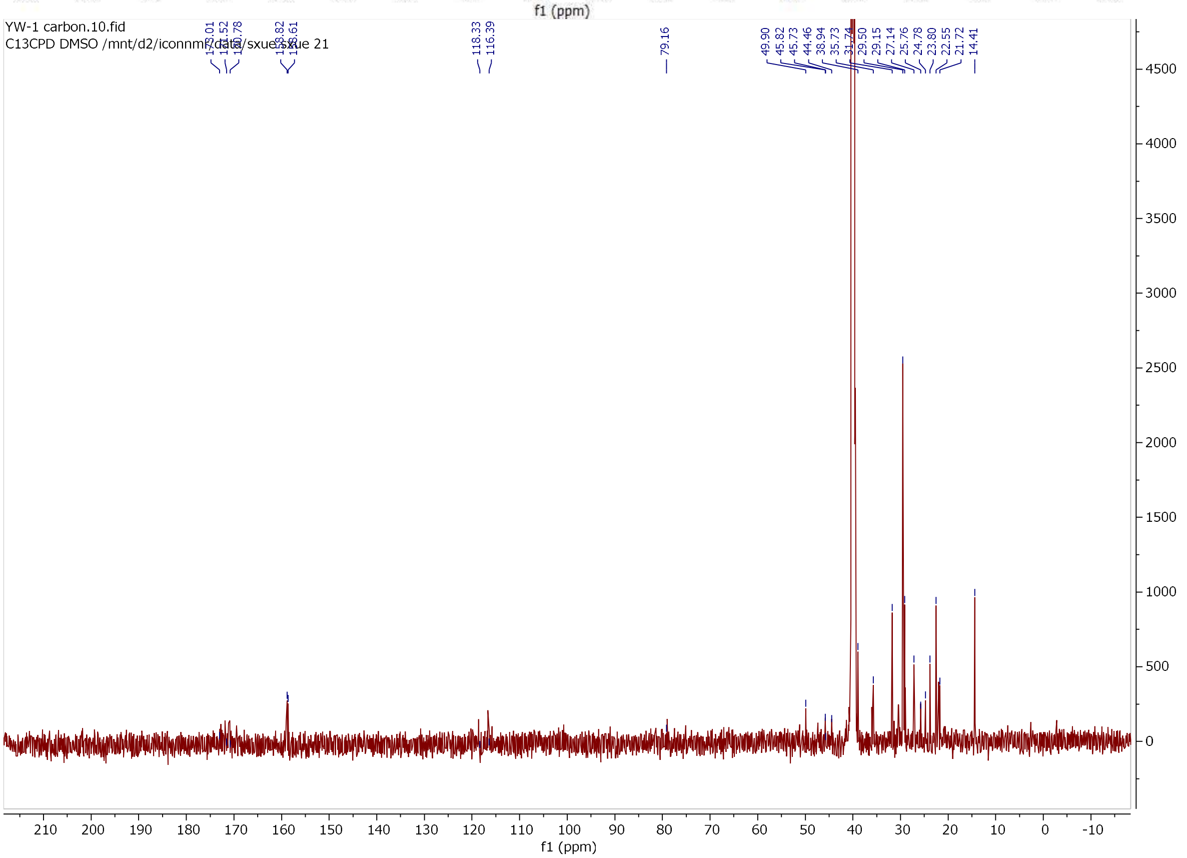
YW-1 carbon.10.fid
C13CPD DMSO /mnt/d2/iconnmr/data/sxue sxue 21
173.01
171.52
170.78
158.82
158.61
118.33
116.39
79.16
49.90
45.82
45.73
44.46
38.94
35.73
31.74
29.50
29.15
27.14
25.76
24.78
23.80
22.55
21.72
14.41
4500
4000
3500
3000
2500
2000
1500
1000
500
0
210
200
190
180
170
160
150
140
130
120
110
100
90
80
70
60
50
40
30
20
10
0
-10
f1 (ppm)

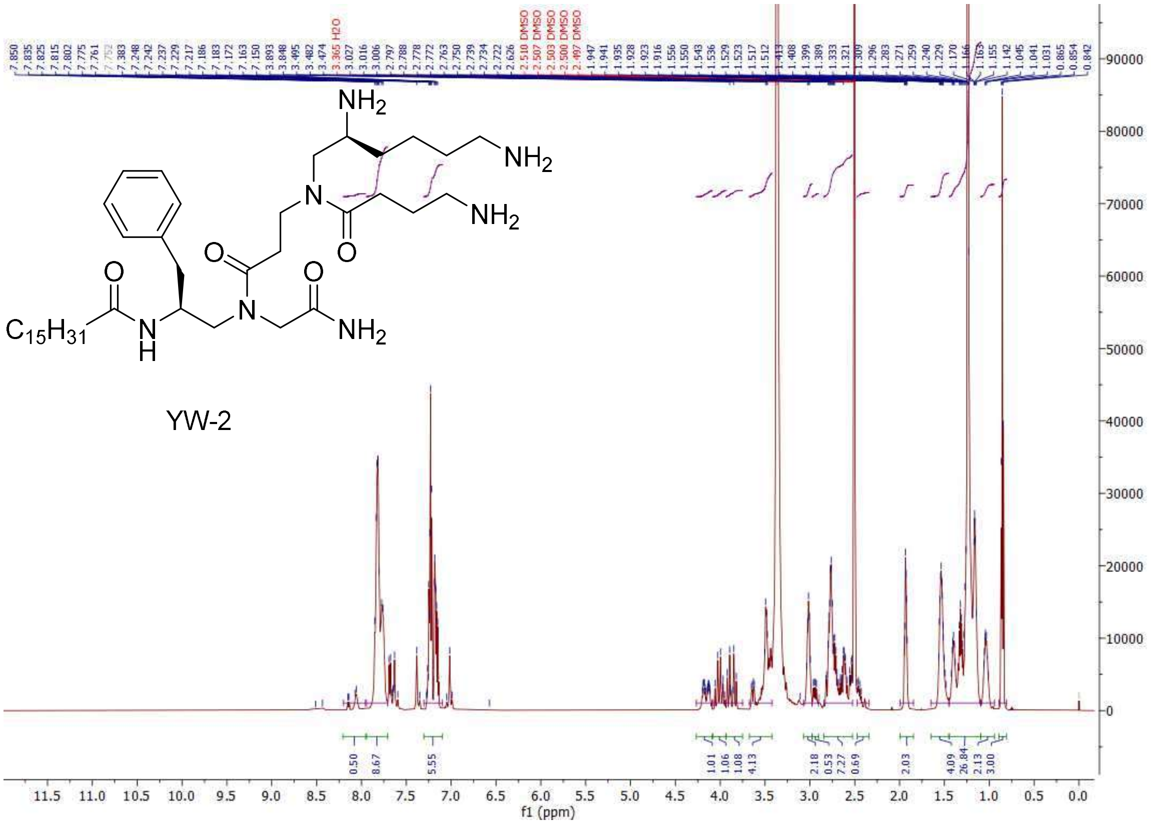
7.850 7.835 7.825 7.815 7.802 7.775 7.761 7.752 7.383 7.248 7.242 7.237 7.229 7.217 7.186 7.183 7.172 7.163 7.150 3.893 3.848 3.495 3.482 3.474 3.365 H2O 3.027 3.016 3.006 2.797 2.788 2.778 2.772 2.763 2.750 2.739 2.734 2.722 2.626 2.510 DMSO 2.507 DMSO 2.503 DMSO 2.500 DMSO 2.497 DMSO 1.947 1.941 1.935 1.928 1.923 1.916 1.556 1.550 1.543 1.536 1.529 1.523 1.517 1.512 1.413 1.408 1.399 1.389 1.333 1.321 1.309 1.296 1.283 1.271 1.259 1.240 1.229 1.170 1.166 1.163 1.155 1.142 1.045 1.041 1.031 0.865 0.854 0.842
NH2
NH2
N
NH2
O
O
O
O
C15H31
N
H
N
NH2
YW-2
90000 80000 70000 60000 50000 40000 30000 20000 10000 0
0.50 8.67 5.55 1.01 1.06 1.08 4.13 2.18 0.53 7.27 0.69 2.03 4.09 26.84 2.13 3.00
11.5 11.0 10.5 10.0 9.5 9.0 8.5 8.0 7.5 7.0 6.5 6.0 5.5 5.0 4.5 4.0 3.5 3.0 2.5 2.0 1.5 1.0 0.5 0.0
f1 (ppm)

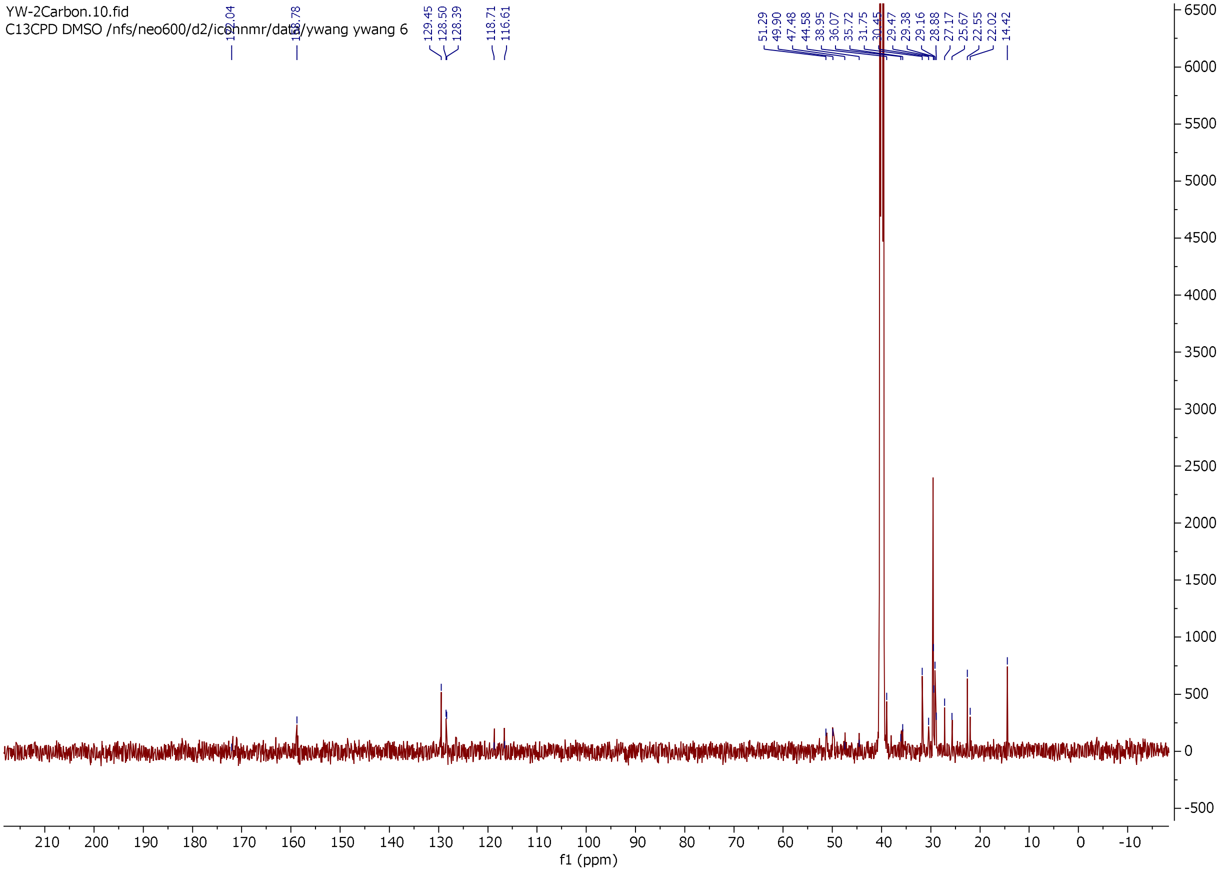
YW-2Carbon.10.fid
C13CPD DMSO /nfs/neo600/d2/icbnmr/data/ywang ywang 6
172.04 158.78 129.45 128.50 128.39 118.71 116.61 51.29 49.90 47.48 44.58 38.95 36.07 35.72 31.75 30.45 29.47 29.38 29.16 28.88 27.17 25.67 22.55 22.02 14.42
6500 6000 5500 5000 4500 4000 3500 3000 2500 2000 1500 1000 500 0 -500
210 200 190 180 170 160 150 140 130 120 110 100 90 80 70 60 50 40 30 20 10 0 -10
f1 (ppm)

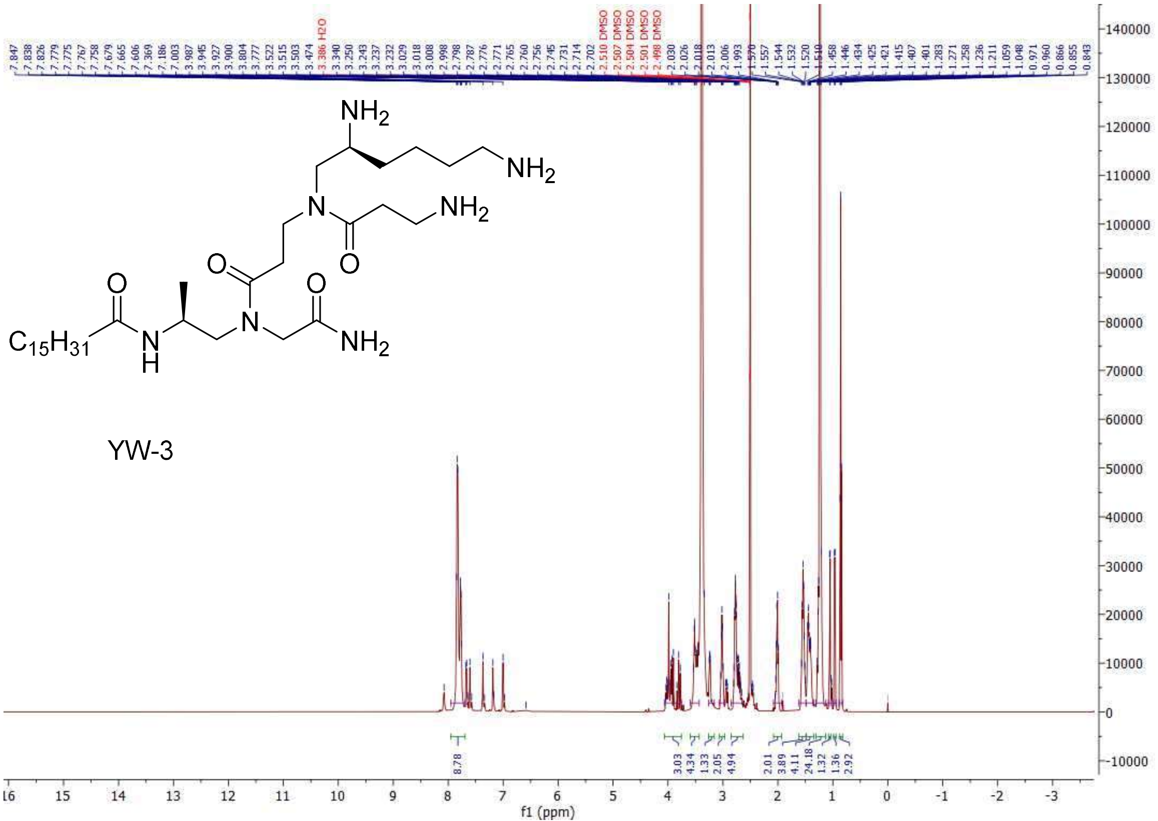
7.847
7.838
7.826
7.779
7.775
7.767
7.758
7.679
7.665
7.606
7.369
7.186
7.003
3.987
3.945
3.927
3.900
3.804
3.777
3.522
3.515
3.503
3.474
3.386 H2O
3.340
3.250
3.243
3.237
3.232
3.029
3.018
3.008
2.998
2.798
2.787
2.776
2.771
2.765
2.760
2.756
2.745
2.731
2.714
2.702
2.510 DMSO
2.507 DMSO
2.504 DMSO
2.501 DMSO
2.498 DMSO
2.030
2.026
2.018
2.013
2.006
1.993
1.570
1.557
1.544
1.532
1.520
1.510
1.458
1.446
1.434
1.425
1.421
1.415
1.407
1.401
1.283
1.271
1.258
1.236
1.211
1.059
1.048
0.971
0.960
0.866
0.855
0.843
NH2
NH2
N
NH2
O
O
O
O
C15H31
N
H
N
NH2
8.78
3.03
4.34
1.33
2.05
4.94
2.01
3.89
4.11
24.18
1.32
1.36
2.92
16 15 14 13 12 11 10 9 8 7 6 5 4 3 2 1 0 -1 -2 -3
f1 (ppm)
140000
130000
120000
110000
100000
90000
80000
70000
60000
50000
40000
30000
20000
10000
0
-10000

YW-3

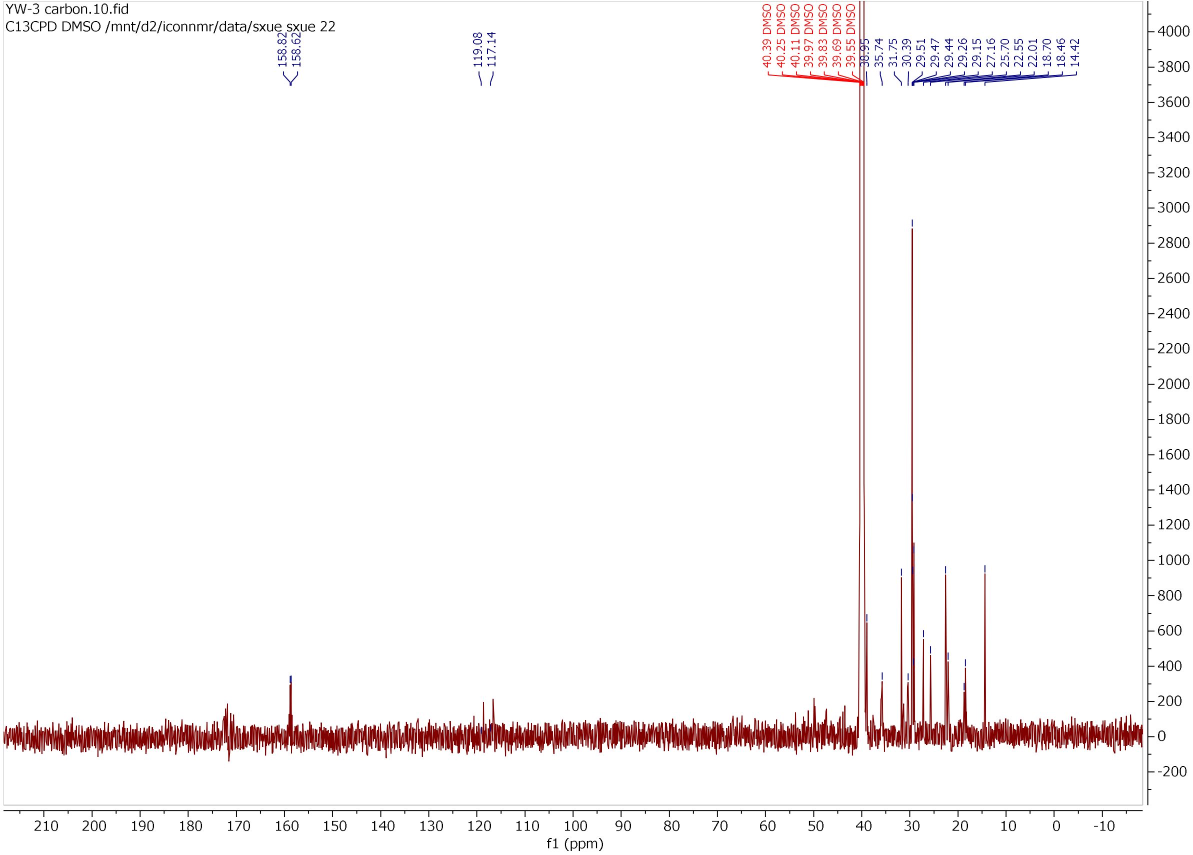
YW-3 carbon.10.fid
C13CPD DMSO /mnt/d2/iconnmr/data/sxue sxue 22
158.82
158.62
119.08
117.14
40.39 DMSO
40.25 DMSO
40.11 DMSO
39.97 DMSO
39.83 DMSO
39.69 DMSO
39.55 DMSO
38.95
35.74
31.75
30.39
29.51
29.47
29.44
29.26
29.15
27.16
25.70
22.55
22.01
18.70
18.46
14.42
210 200 190 180 170 160 150 140 130 120 110 100 90 80 70 60 50 40 30 20 10 0 -10
f1 (ppm)
4000
3800
3600
3400
3200
3000
2800
2600
2400
2200
2000
1800
1600
1400
1200
1000
800
600
400
200
0
-200

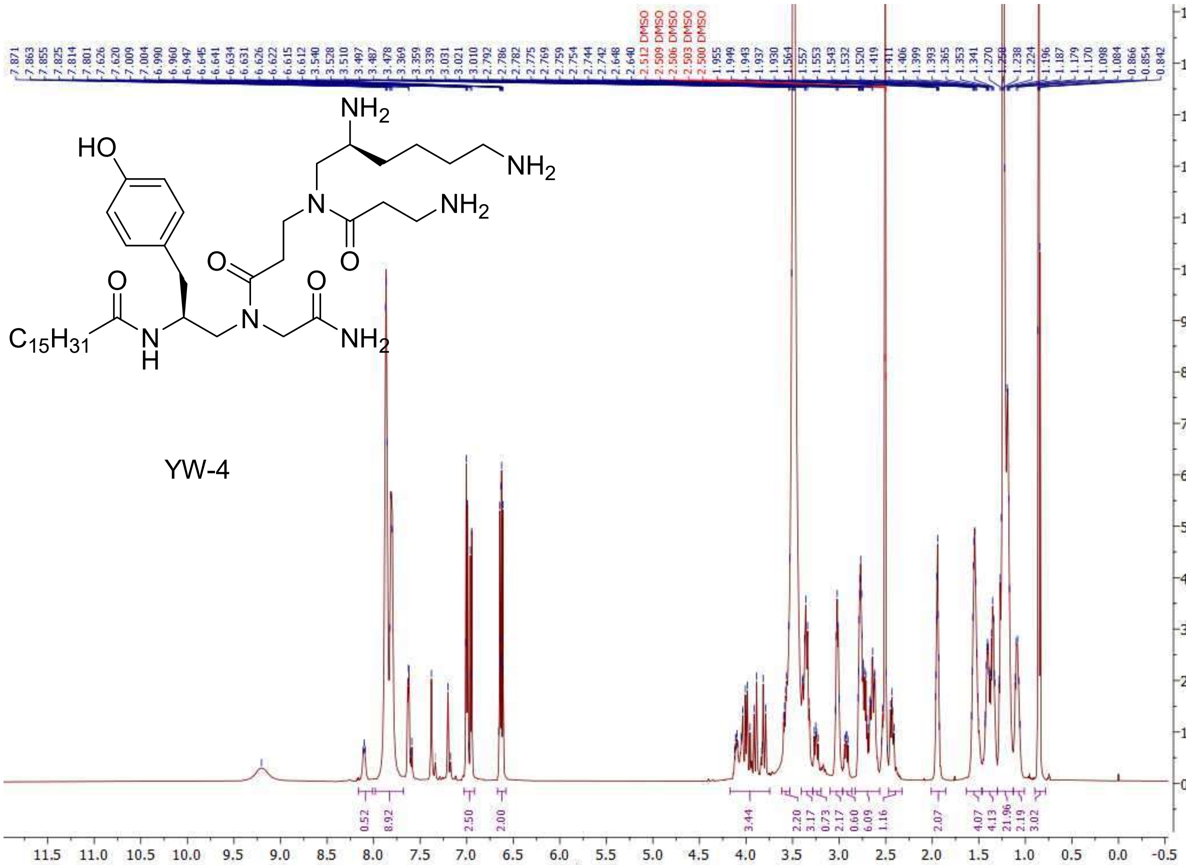
7.871
7.863
7.855
7.825
7.814
7.801
7.626
7.620
7.009
7.004
6.990
6.960
6.947
6.645
6.641
6.634
6.631
6.626
6.622
6.615
6.612
3.540
3.528
3.510
3.497
3.487
3.478
3.369
3.359
3.339
3.031
3.021
3.010
2.792
2.786
2.782
2.775
2.769
2.759
2.754
2.744
2.742
2.648
2.640
2.512 DMSO
2.509 DMSO
2.506 DMSO
2.503 DMSO
2.500 DMSO
1.955
1.949
1.943
1.937
1.930
1.564
1.557
1.553
1.543
1.532
1.520
1.419
1.411
1.406
1.399
1.393
1.365
1.353
1.341
1.270
1.258
1.238
1.224
1.196
1.187
1.179
1.170
1.098
1.084
0.866
0.854
0.842
HO
NH2
NH2
N
NH2
O
O
O
N
O
C15H31
N
H
NH2
YW-4
0.52
8.92
2.50
2.00
3.44
2.20
3.17
0.73
2.17
0.60
6.09
1.16
2.07
4.07
4.13
21.96
2.19
3.02
11.5 11.0 10.5 10.0 9.5 9.0 8.5 8.0 7.5 7.0 6.5 6.0 5.5 5.0 4.5 4.0 3.5 3.0 2.5 2.0 1.5 1.0 0.5 0.0 -0.5
f1 (ppm)
150000 140000 130000 120000 110000 100000 90000 80000 70000 60000 50000 40000 30000 20000 10000 0

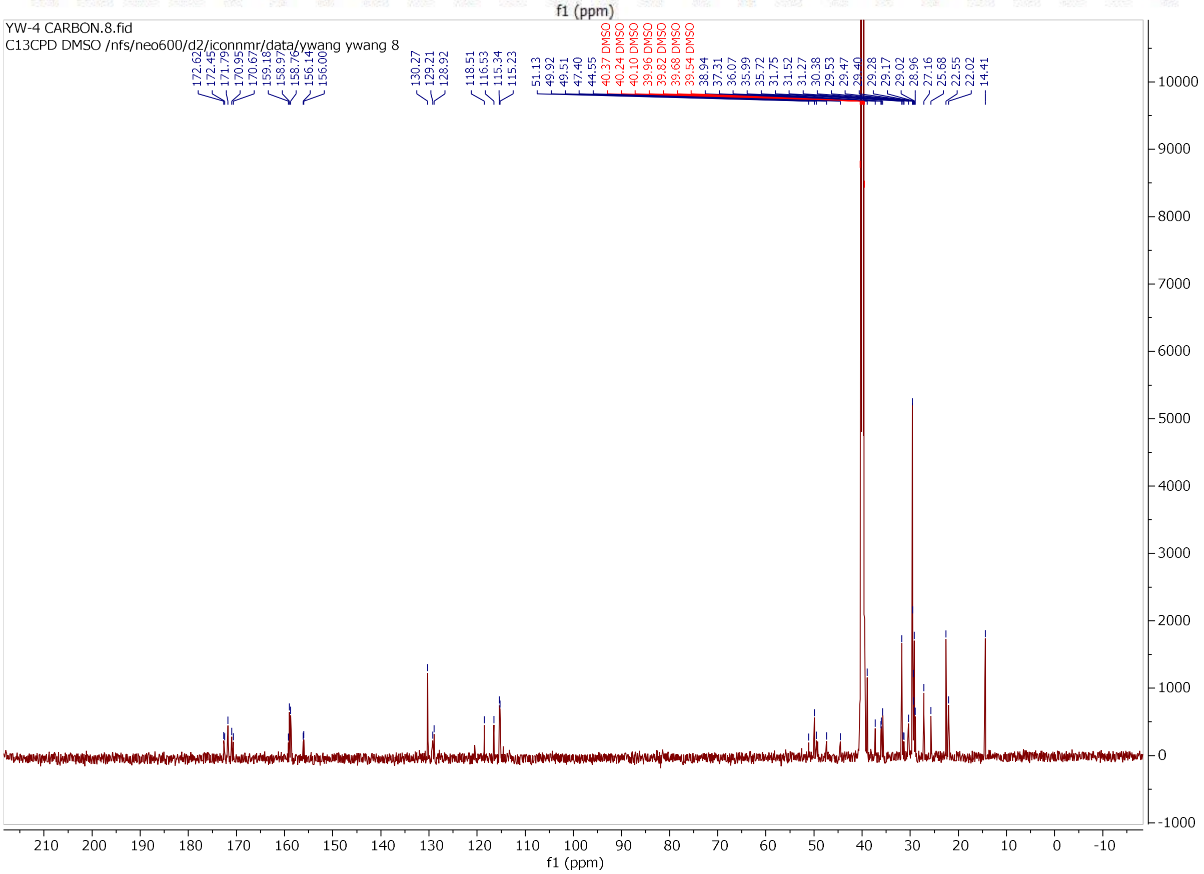
YW-4 CARBON.8.fid
C13CPD DMSO /nfs/neo600/d2/iconnmr/data/ywang ywang 8
172.62
172.45
171.79
170.95
170.67
159.18
158.97
158.76
156.14
156.00
130.27
129.21
128.92
118.51
116.53
115.34
115.23
51.13
49.92
49.51
47.40
44.55
40.37 DMSO
40.24 DMSO
40.10 DMSO
39.96 DMSO
39.82 DMSO
39.68 DMSO
39.54 DMSO
38.94
37.31
36.07
35.99
35.72
31.75
31.52
31.27
30.38
29.53
29.47
29.40
29.28
29.17
29.02
28.96
27.16
25.68
22.55
22.02
14.41
210 200 190 180 170 160 150 140 130 120 110 100 90 80 70 60 50 40 30 20 10 0 -10
f1 (ppm)
10000 9000 8000 7000 6000 5000 4000 3000 2000 1000 0 -1000

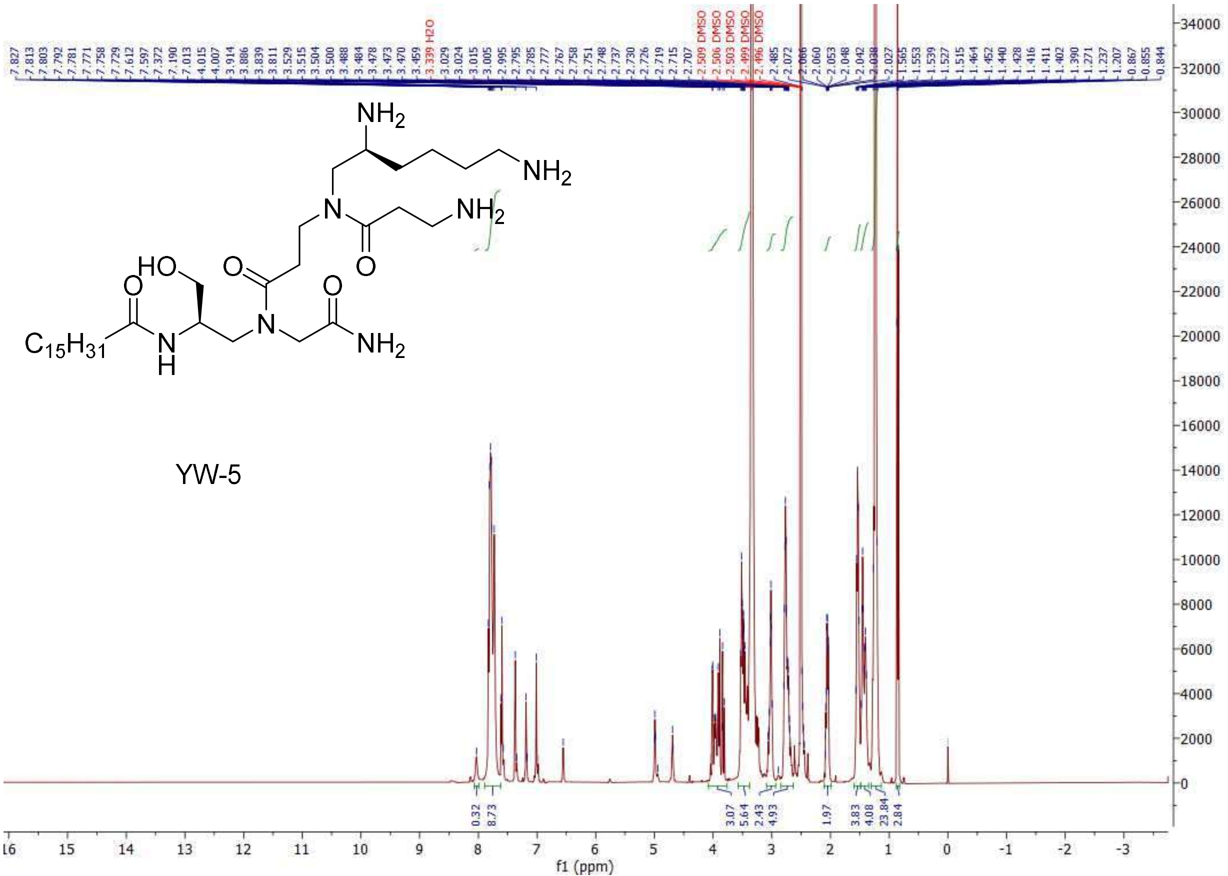
7.827
7.813
7.803
7.792
7.781
7.771
7.758
7.729
7.612
7.597
7.372
7.190
7.013
4.015
4.007
3.914
3.886
3.839
3.811
3.529
3.515
3.504
3.500
3.488
3.484
3.478
3.473
3.470
3.459
3.339 H2O
3.029
3.024
3.015
3.005
2.995
2.795
2.785
2.777
2.767
2.758
2.751
2.748
2.737
2.730
2.726
2.719
2.715
2.707
2.509 DMSO
2.506 DMSO
2.503 DMSO
2.499 DMSO
2.496 DMSO
2.485
2.072
2.066
2.060
2.053
2.048
2.042
2.038
2.027
1.565
1.553
1.539
1.527
1.515
1.464
1.452
1.440
1.428
1.416
1.411
1.402
1.390
1.271
1.237
1.207
0.867
0.855
0.844
NH2
NH2
N
NH2
O
HO
O
O
O
C15H31
N
H
N
NH2
0.32
8.73
3.07
5.64
2.43
4.93
1.97
3.83
4.08
23.84
2.84
16 15 14 13 12 11 10 9 8 7 6 5 4 3 2 1 0 -1 -2 -3
f1 (ppm)
34000 32000 30000 28000 26000 24000 22000 20000 18000 16000 14000 12000 10000 8000 6000 4000 2000 0

YW-5

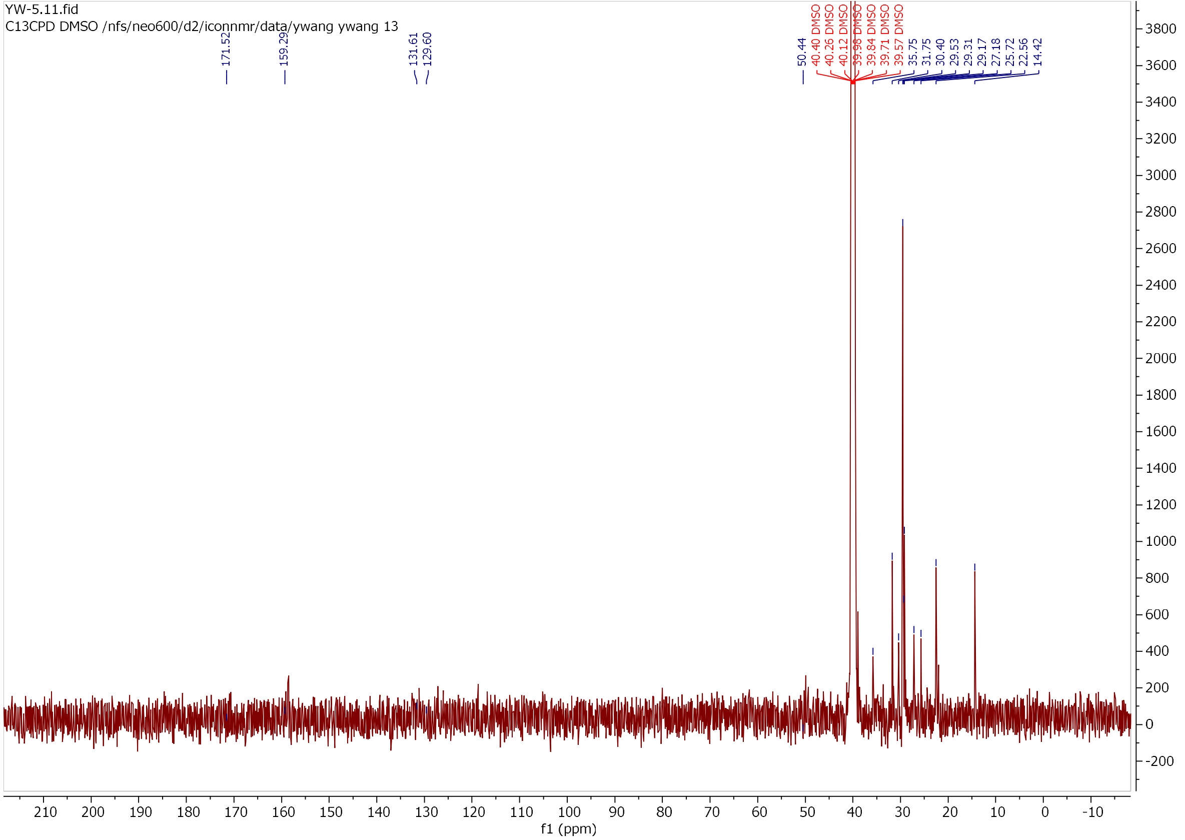
YW-5.11.fid
C13CPD DMSO /nfs/neo600/d2/iconnmr/data/ywang ywang 13
171.52
159.29
131.61
129.60
50.44
40.40 DMSO
40.26 DMSO
40.12 DMSO
39.98 DMSO
39.84 DMSO
39.71 DMSO
39.57 DMSO
35.75
31.75
30.40
29.53
29.31
29.17
27.18
25.72
22.56
14.42
210 200 190 180 170 160 150 140 130 120 110 100 90 80 70 60 50 40 30 20 10 0 -10
f1 (ppm)
3800 3600 3400 3200 3000 2800 2600 2400 2200 2000 1800 1600 1400 1200 1000 800 600 400 200 0 -200

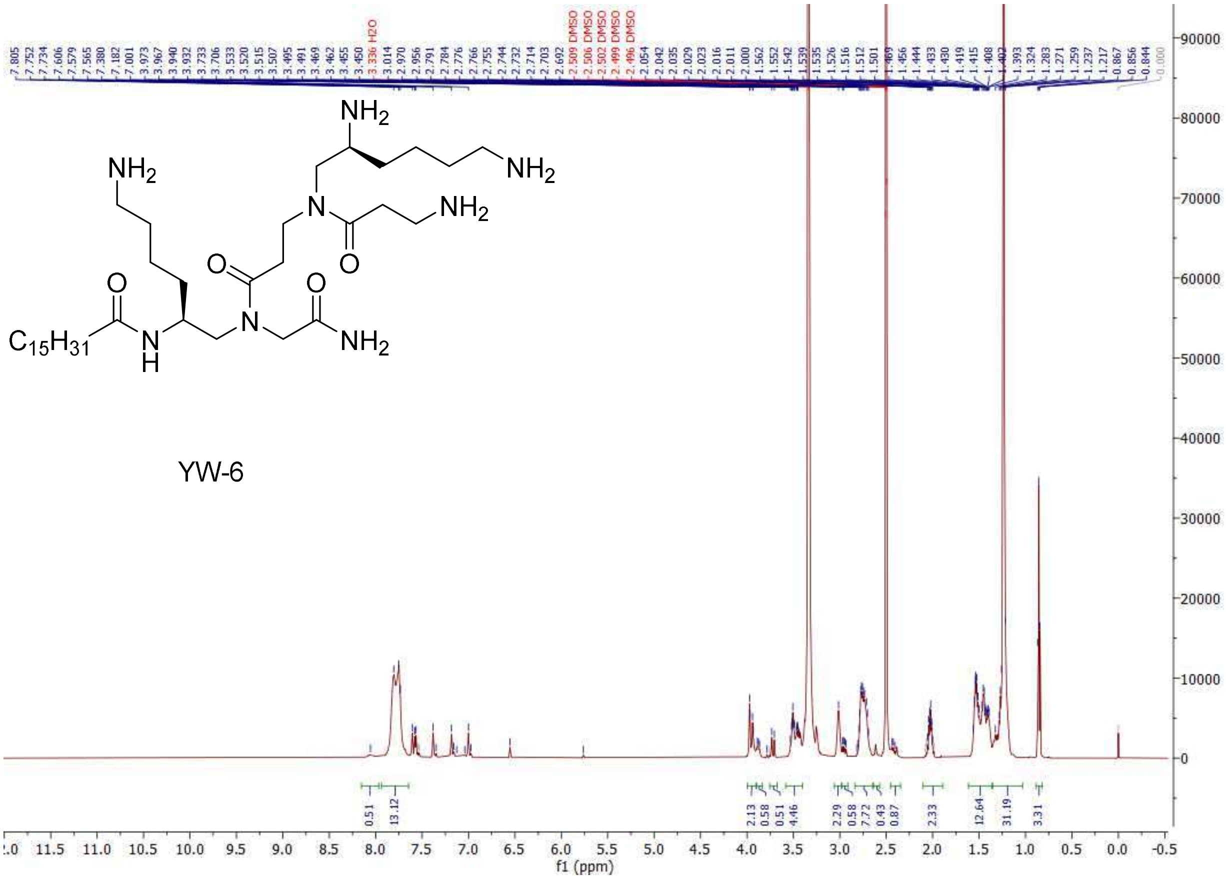
YW-6

7.805
7.752
7.734
7.606
7.579
7.565
7.380
7.182
7.001
3.973
3.967
3.940
3.932
3.733
3.706
3.533
3.520
3.515
3.507
3.495
3.491
3.469
3.462
3.455
3.450
3.336 H2O
3.014
2.970
2.956
2.791
2.784
2.776
2.766
2.755
2.744
2.732
2.714
2.703
2.692
2.509 DMSO
2.506 DMSO
2.502 DMSO
2.499 DMSO
2.496 DMSO
2.054
2.042
2.035
2.029
2.023
2.016
2.011
2.000
1.562
1.552
1.542
1.539
1.535
1.526
1.516
1.512
1.501
1.469
1.456
1.444
1.433
1.430
1.419
1.415
1.408
1.402
1.393
1.324
1.283
1.271
1.259
1.237
1.217
0.867
0.856
0.844
0.000
NH2
NH2
NH2
NH2
NH2
N
N
O
O
O
O
C15H31
N
H
0.51
13.12
2.13
0.58
0.51
4.46
2.29
0.58
7.72
0.43
0.87
2.33
12.64
31.19
3.31
12.0
11.5
11.0
10.5
10.0
9.5
9.0
8.5
8.0
7.5
7.0
6.5
6.0
5.5
5.0
4.5
4.0
3.5
3.0
2.5
2.0
1.5
1.0
0.5
0.0
-0.5
f1 (ppm)
90000
80000
70000
60000
50000
40000
30000
20000
10000
0

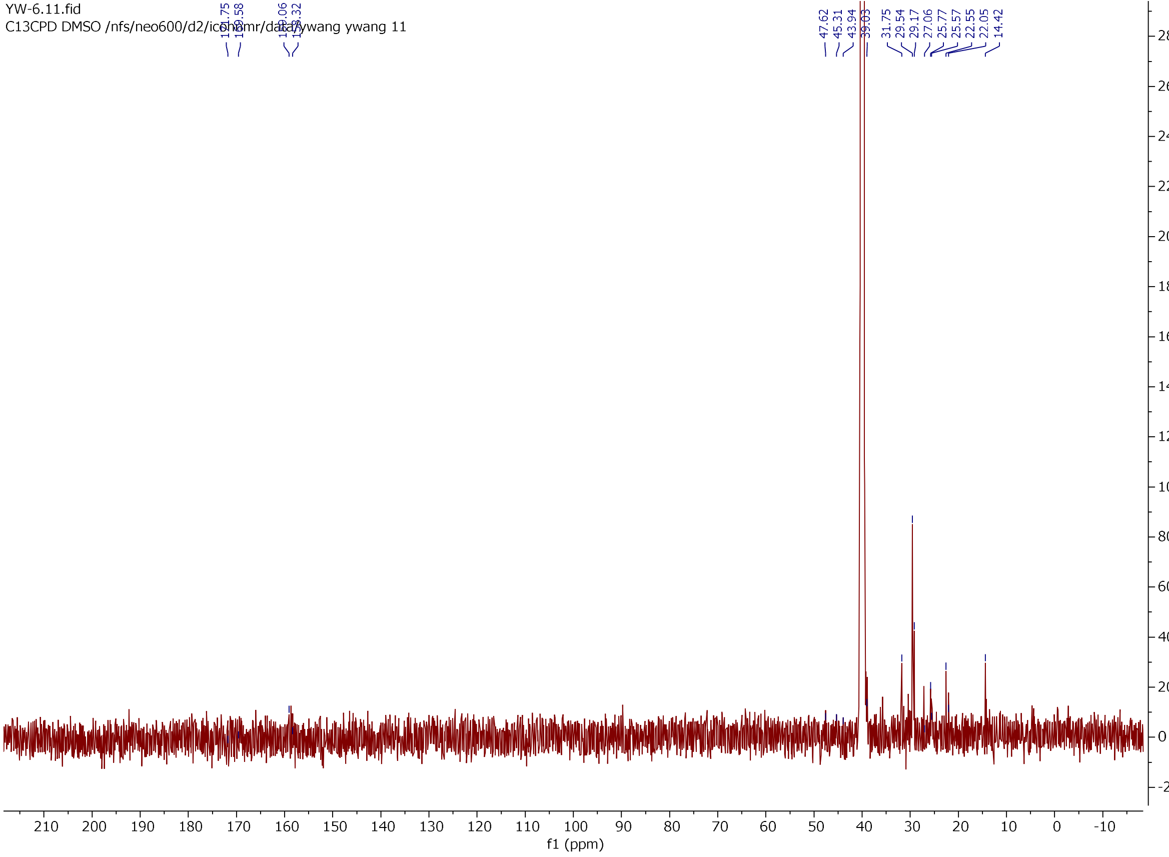
YW-6.11.fid
C13CPD DMSO /nfs/neo600/d2/icchemr/data/ywang ywang 11
171.75
169.58
159.06
158.32
47.62
45.31
43.94
39.03
31.75
29.54
29.17
27.06
25.77
25.57
22.55
22.05
14.42
210
200
190
180
170
160
150
140
130
120
110
100
90
80
70
60
50
40
30
20
10
0
-10
f1 (ppm)
2800
2600
2400
2200
2000
1800
1600
1400
1200
1000
800
600
400
200
0
-200

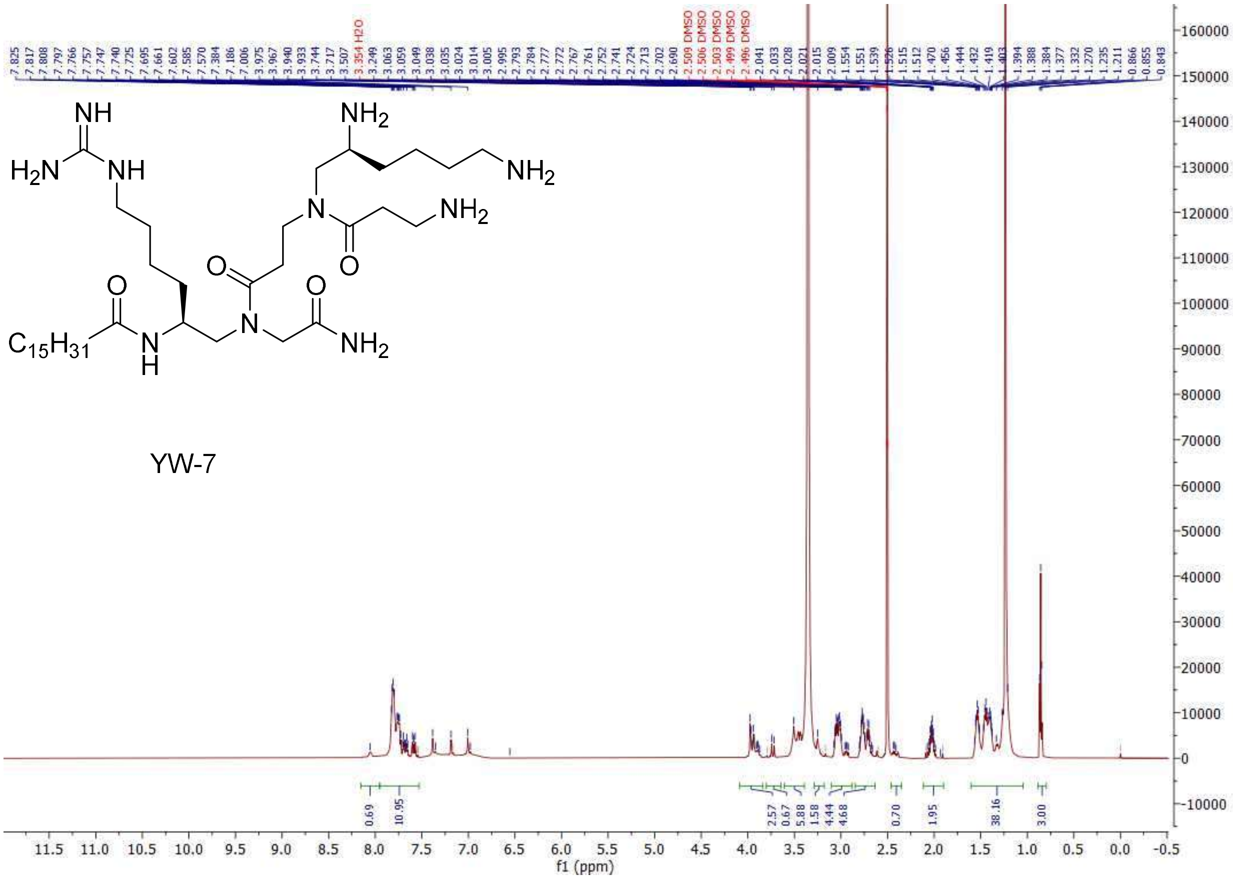
7.825
7.817
7.808
7.797
7.766
7.757
7.747
7.740
7.725
7.695
7.661
7.602
7.585
7.570
7.384
7.186
7.006
3.975
3.967
3.940
3.933
3.744
3.717
3.507
3.354 H2O
3.249
3.063
3.059
3.049
3.038
3.035
3.024
3.014
3.005
2.995
2.793
2.784
2.777
2.772
2.767
2.761
2.752
2.741
2.724
2.713
2.702
2.690
2.509 DMSO
2.506 DMSO
2.503 DMSO
2.499 DMSO
2.496 DMSO
2.041
2.033
2.028
2.021
2.015
2.009
1.554
1.551
1.539
1.526
1.515
1.512
1.470
1.456
1.444
1.432
1.419
1.403
1.394
1.388
1.384
1.377
1.332
1.270
1.235
1.211
0.866
0.855
0.843
NH
H2N
NH
NH2
NH2
N
NH2
O
O
O
O
C15H31
N
H
N
NH2
YW-7
0.69
10.95
2.57
0.67
5.88
1.58
4.44
4.68
0.70
1.95
38.16
3.00
160000
150000
140000
130000
120000
110000
100000
90000
80000
70000
60000
50000
40000
30000
20000
10000
0
-10000
11.5 11.0 10.5 10.0 9.5 9.0 8.5 8.0 7.5 7.0 6.5 6.0 5.5 5.0 4.5 4.0 3.5 3.0 2.5 2.0 1.5 1.0 0.5 0.0 -0.5
f1 (ppm)

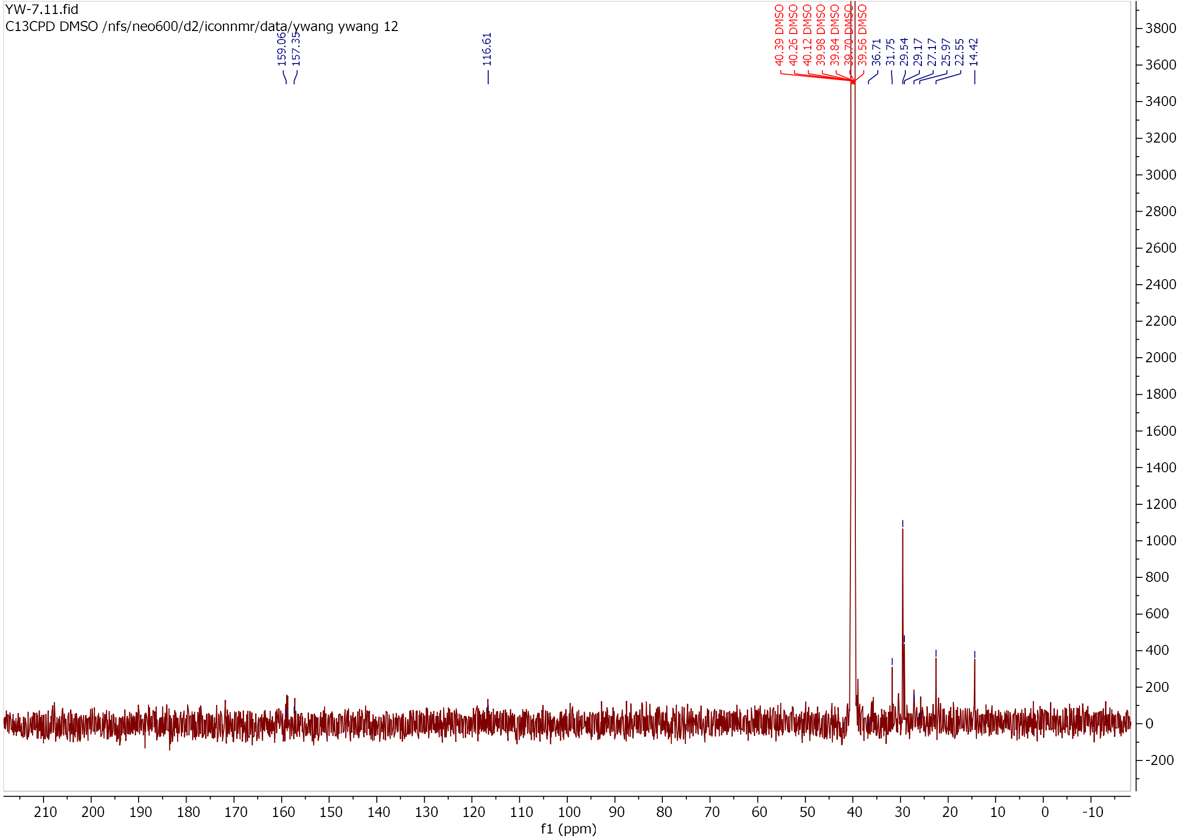
YW-7.11.fid
C13CPD DMSO /nfs/neo600/d2/iconnmr/data/ywang ywang 12
159.06
157.35
116.61
40.39 DMSO
40.26 DMSO
40.12 DMSO
39.98 DMSO
39.84 DMSO
39.70 DMSO
39.56 DMSO
36.71
31.75
29.54
29.17
27.17
25.97
22.55
14.42
3800
3600
3400
3200
3000
2800
2600
2400
2200
2000
1800
1600
1400
1200
1000
800
600
400
200
0
-200
210 200 190 180 170 160 150 140 130 120 110 100 90 80 70 60 50 40 30 20 10 0 -10
f1 (ppm)

Appendix D: ESI-MS Data

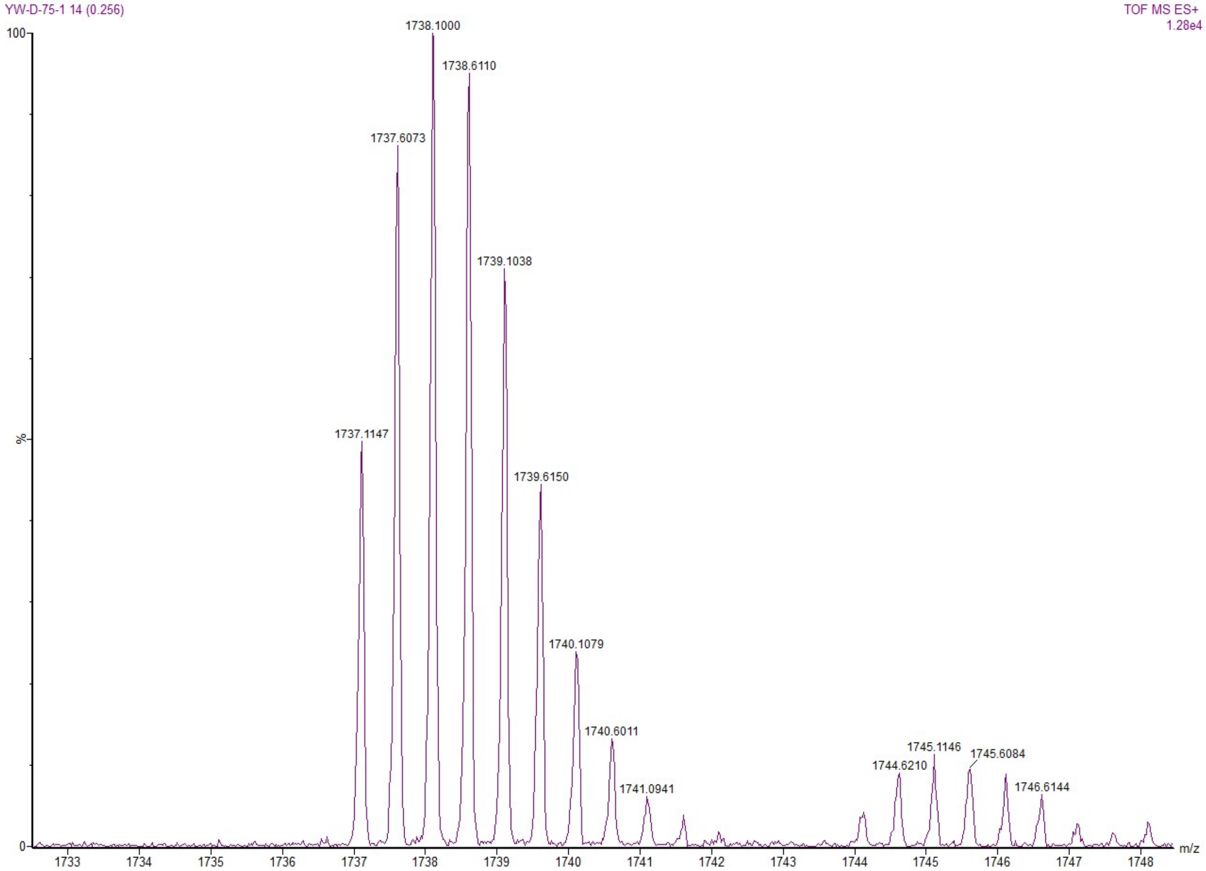

YW-D-75-1 ((E.M.+2)/2)
Chemical Formula: $C_{141}H_{258}N_{40}O_{38}S_{11}$
Exact Mass: 3471.6414

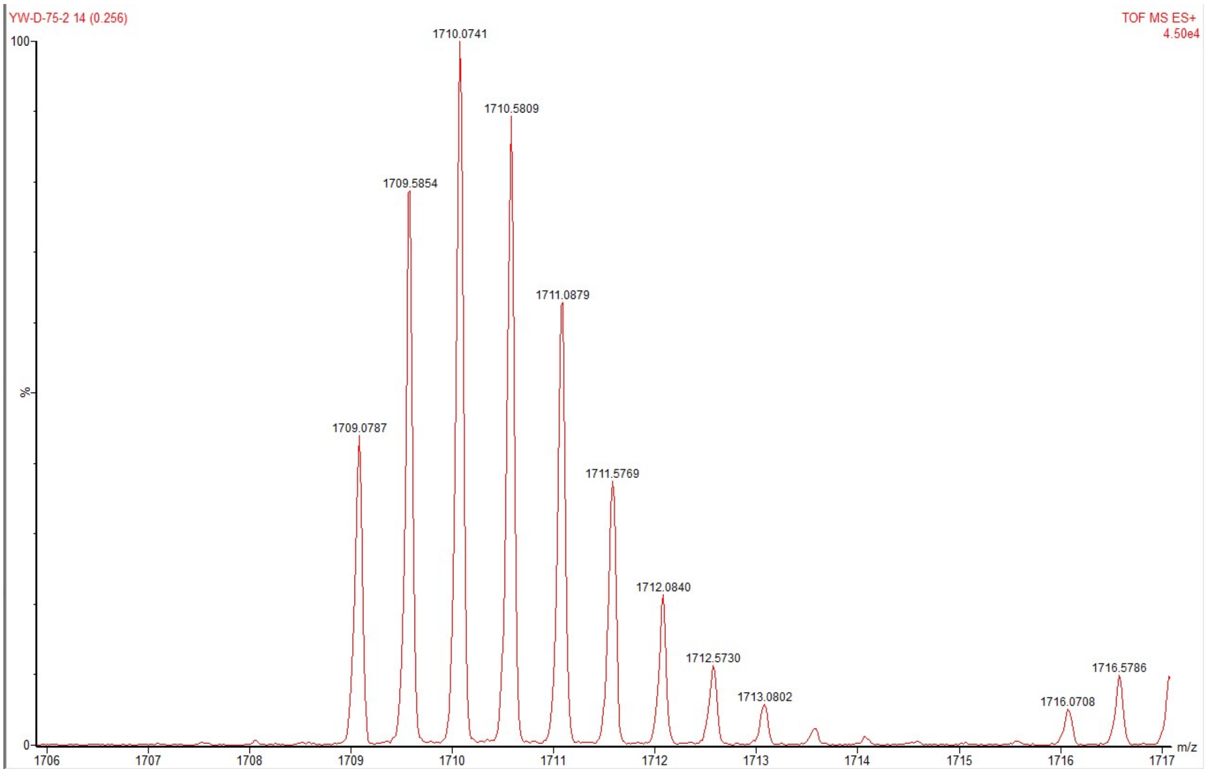

YW-D-75-2 ((E.M.+2)/2)
Chemical Formula: $C_{137}H_{250}N_{40}O_{38}S_{11}$
Exact Mass: 3415.5788

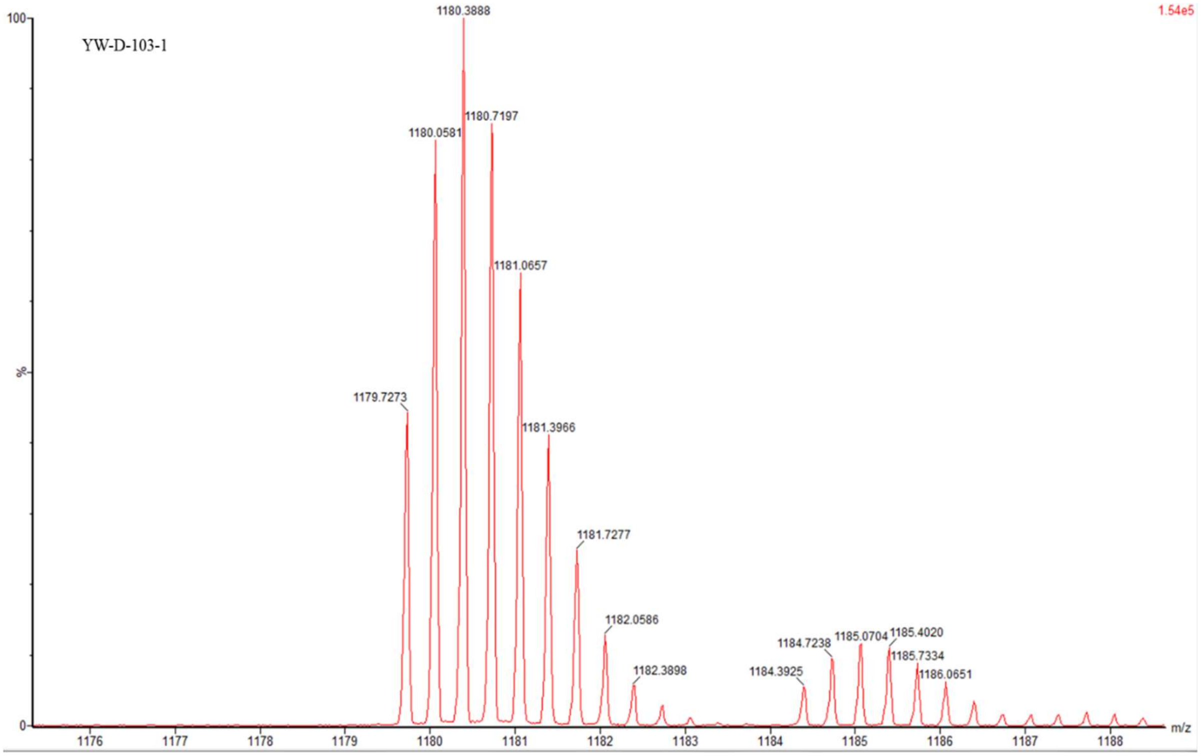

YW-D-103-1 ((E.M.+2)/2)
Chemical Formula: $C_{141}H_{258}N_{40}O_{42}S_{11}$
Exact Mass: 3535.6210
Molecular Weight: 3538.5130

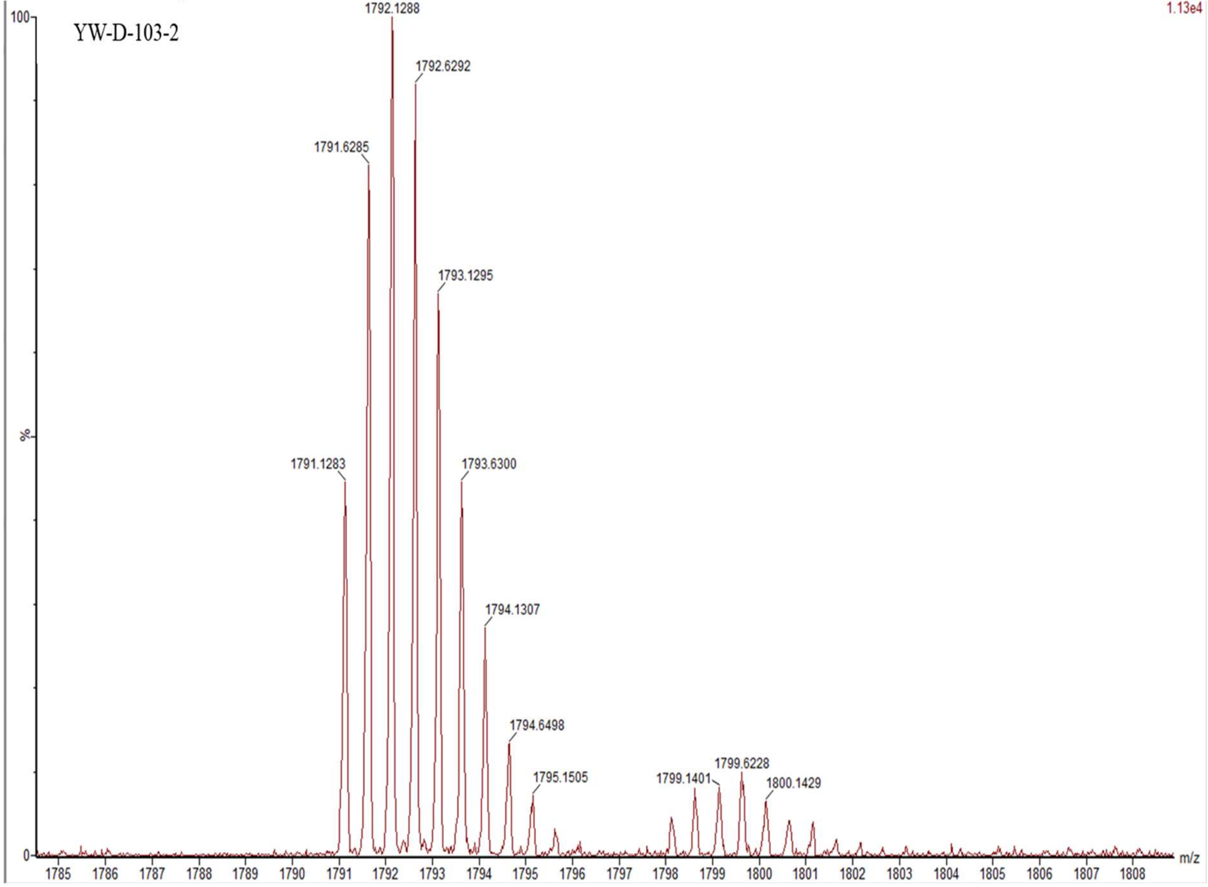

YW-D-103-2 ((E.M.+2)/2)
Chemical Formula: $C_{143}H_{262}N_{40}O_{43}S_{11}$
Exact Mass: 3579.6472
Molecular Weight: 3582.5660

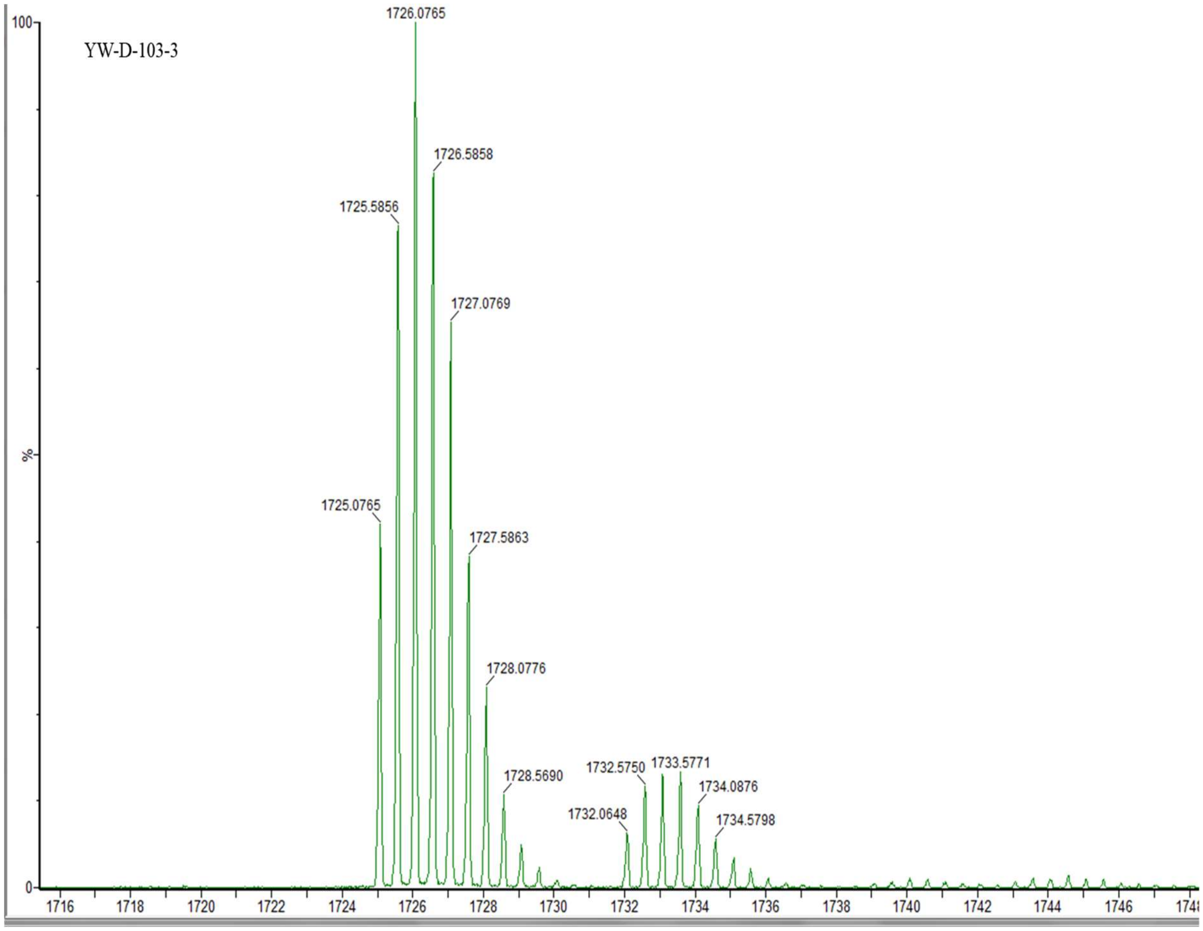

YW-D-103-3 ((E.M.+2)/2)
Chemical Formula: $C_{137}H_{250}N_{40}O_{40}S_{11}$
Exact Mass: 3447.5686
Molecular Weight: 3450.4070

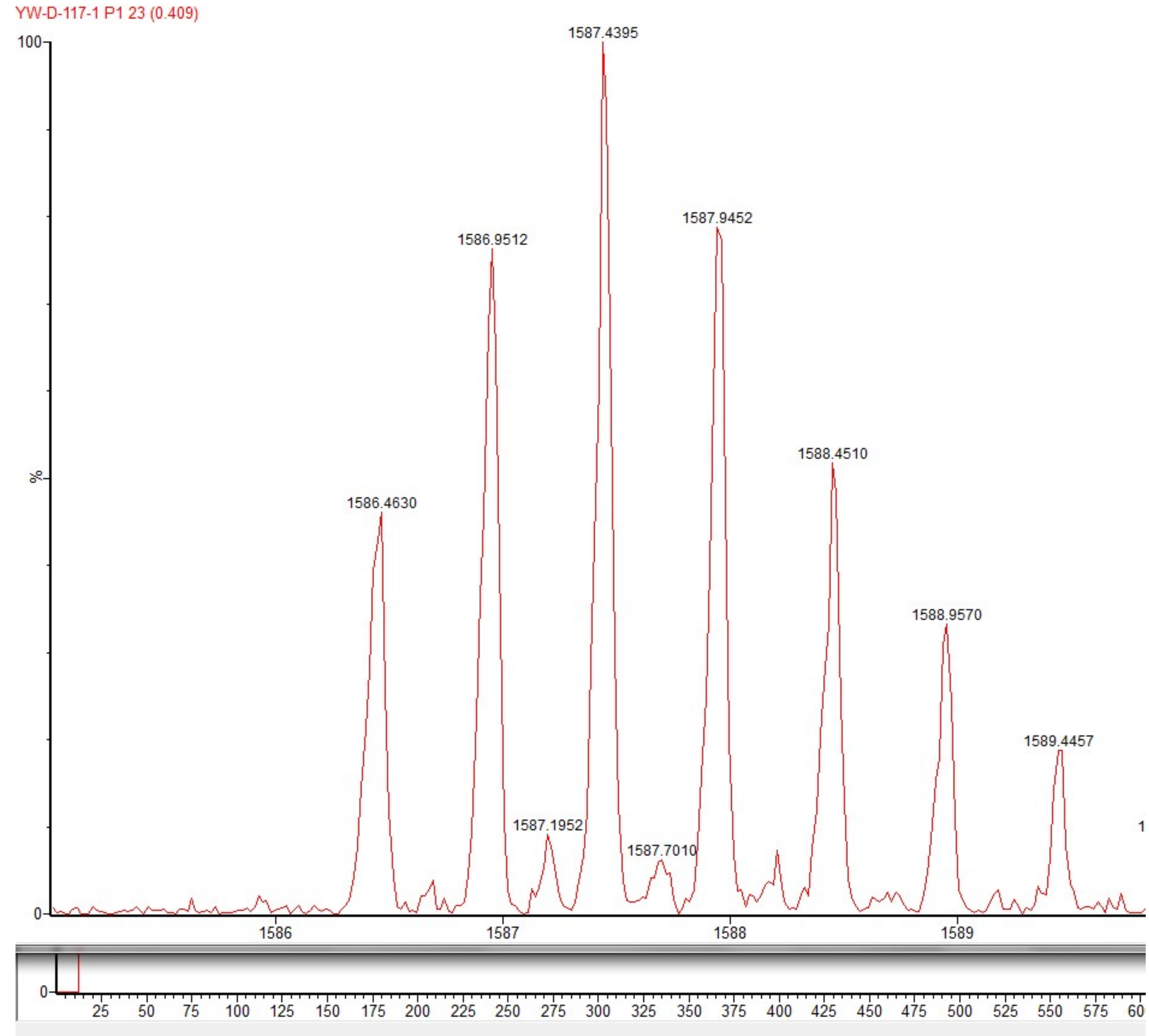

YW-D-117-1 ((E.M.+2)/2)
Chemical Formula: $C_{124}H_{231}N_{40}O_{40}S_{10}$
Exact Mass: 3170.4325

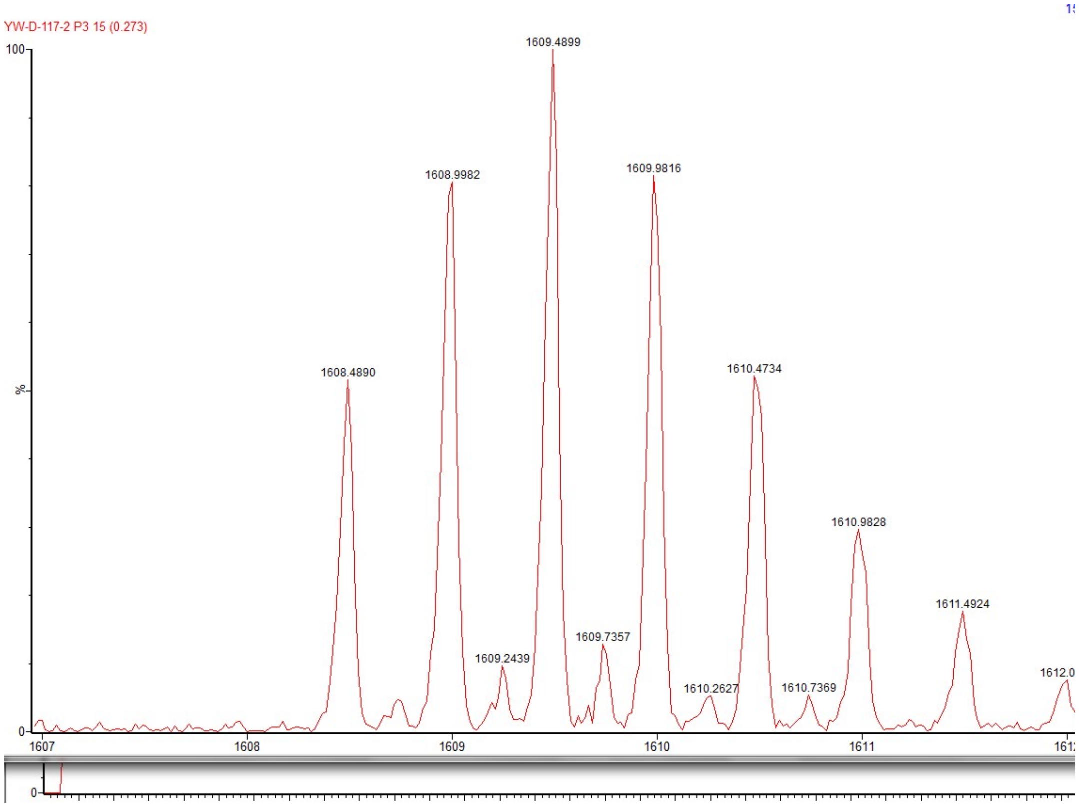

YW-D-117-2 ((E.M.+2)/2)
Chemical Formula: $C_{126}H_{235}N_{35}O_{41}S_{10}$
Exact Mass: 3214.4587

Appendix E: LC-MS and ESI-MS data

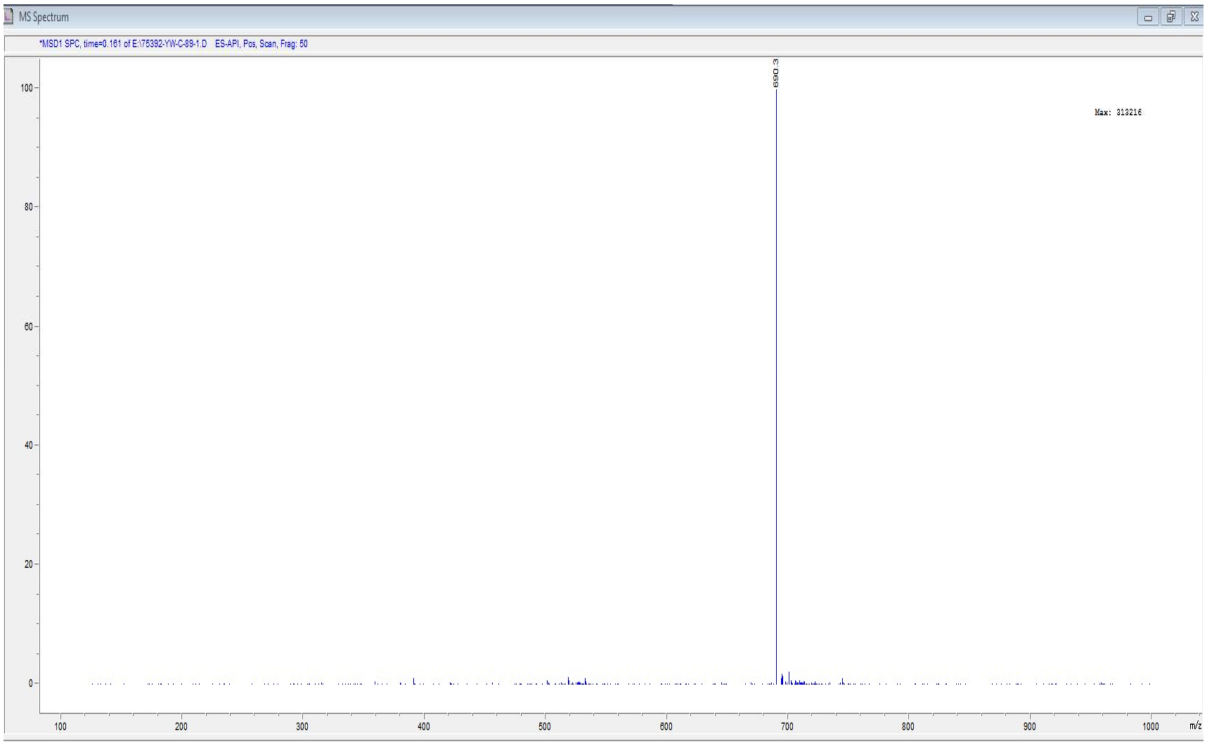

YW-C-89-1
((M.W.+3)/3)

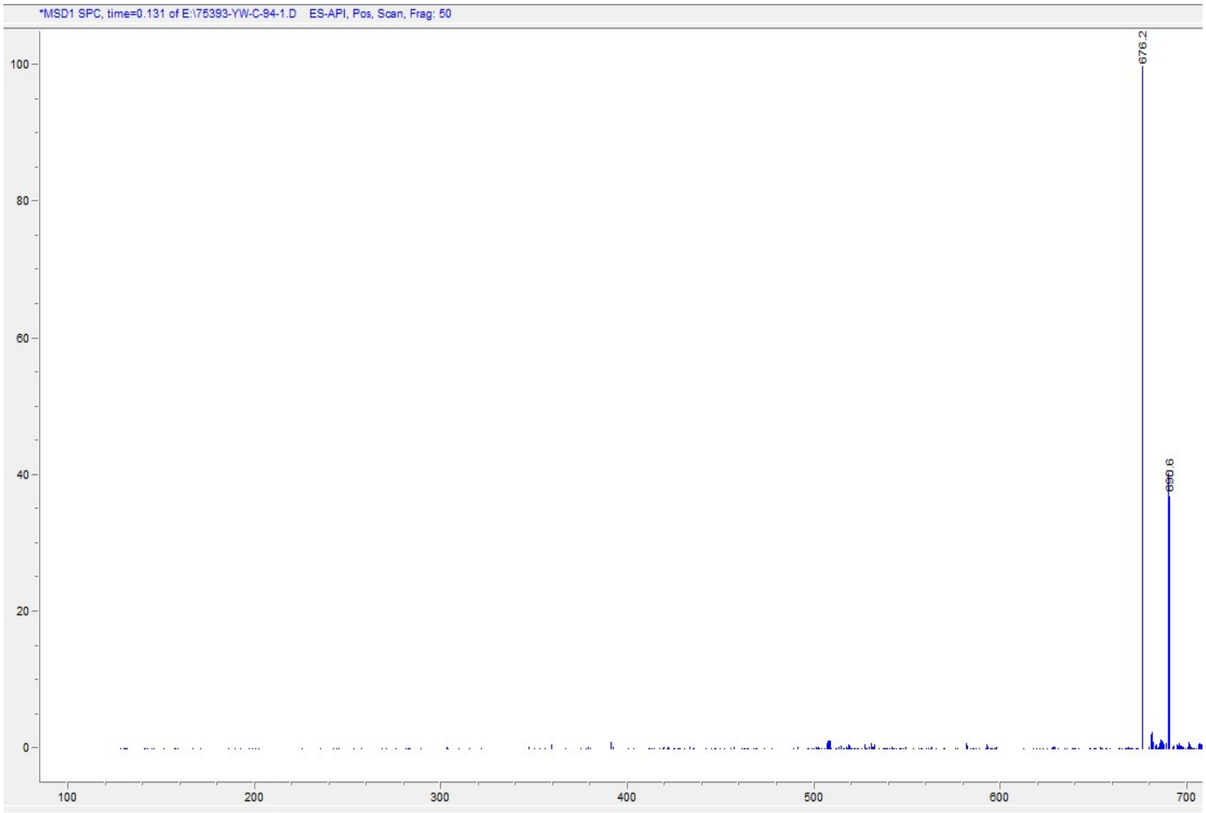
*MSD1 SPC, time=0.131 of E:\75393-YW-C-94-1.D ES-API, Pos, Scan, Frag: 50
676.2
690.6
100
80
60
40
20
0
100
200
300
400
500
600
700

YW-C-94-1
((M.W.+3)/3)

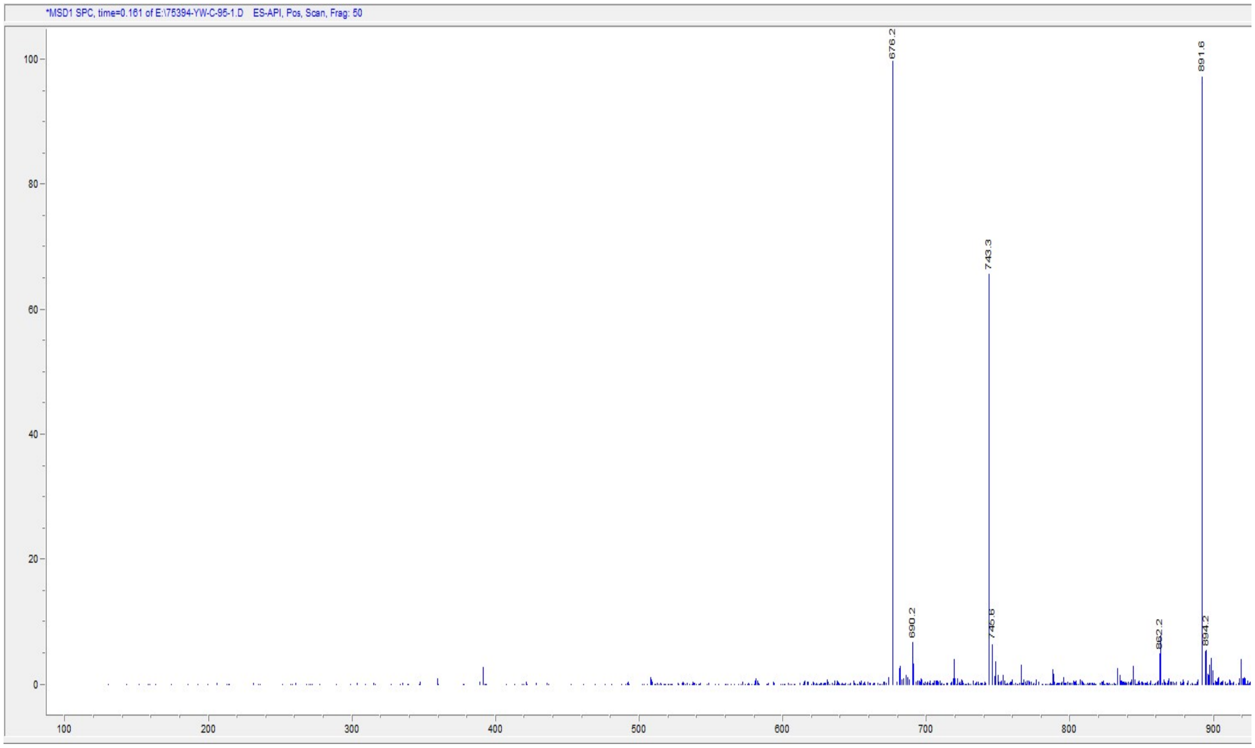
*MSD1 SPC, time=0.161 of E:\75394-YW-C-95-1.D ES-API, Pos, Scan, Frag: 50
100
80
60
40
20
0
676.2
891.6
743.3
690.2
745.6
862.2
894.2
100
200
300
400
500
600
700
800
900

YW-C-95-1
((M.W.+6)/6)

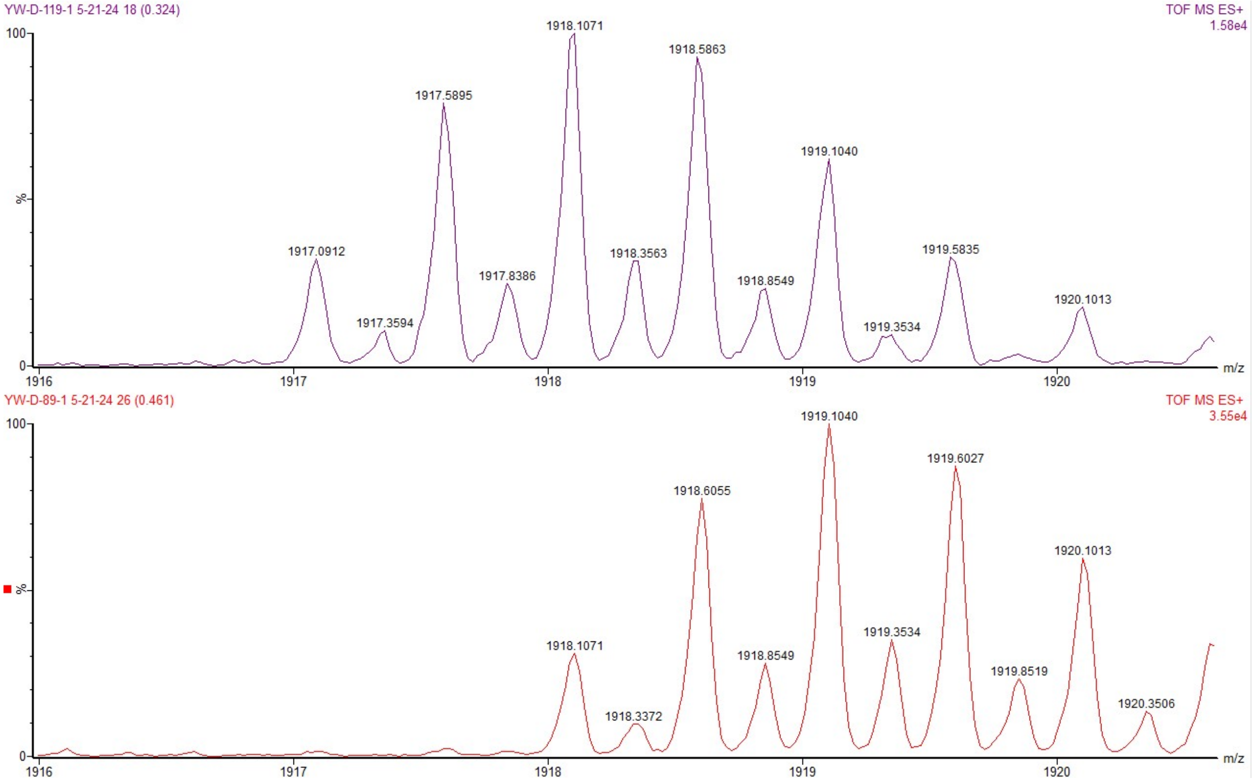

YW-D-119-1
((E.M.+2)/2)

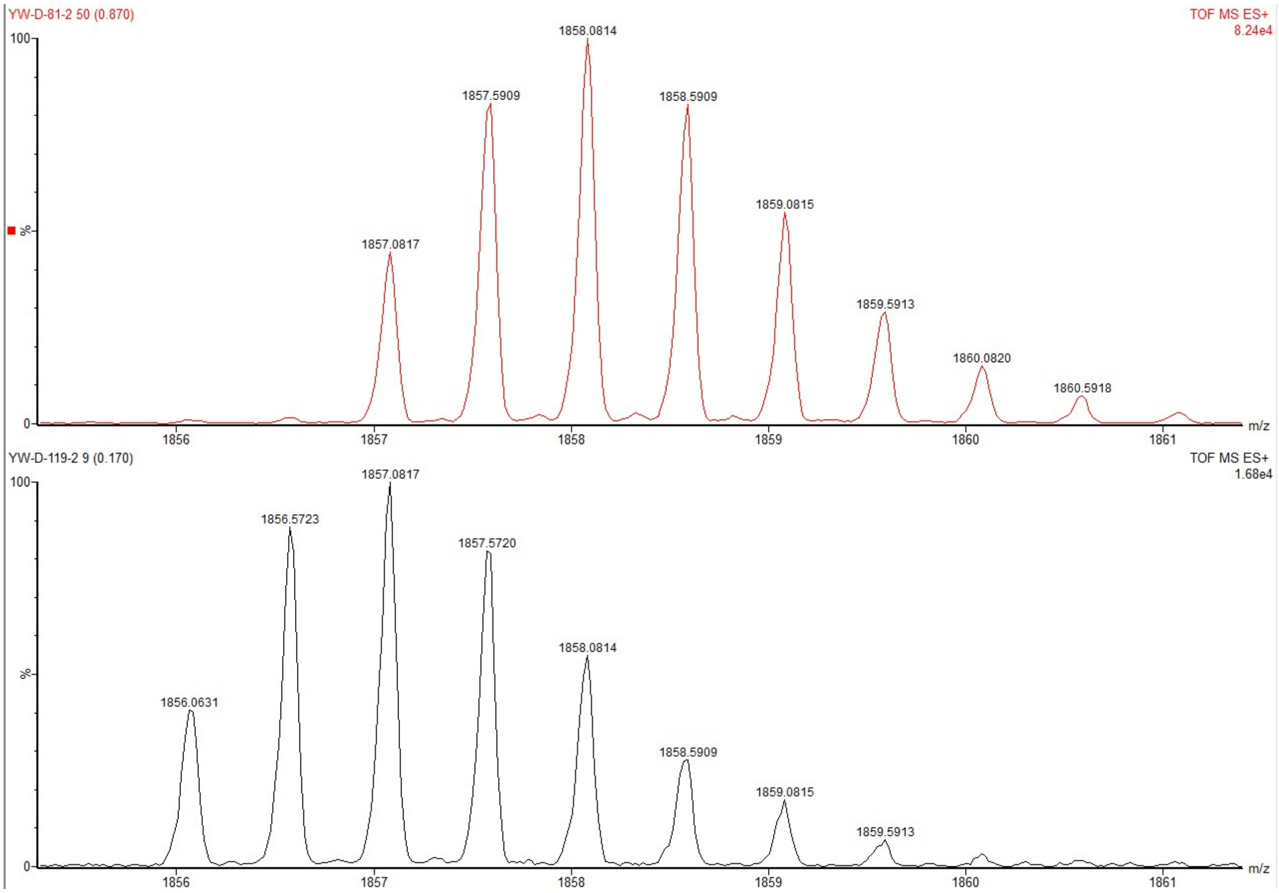

YW-D-81-2 50 (0.870)
TOF MS ES+
8.24e4
100
%
0
1857.0817
1857.5909
1858.0814
1858.5909
1859.0815
1859.5913
1860.0820
1860.5918
1856
1857
1858
1859
1860
1861
m/z
YW-D-119-2 9 (0.170)
TOF MS ES+
1.68e4
100
%
0
1856.0631
1856.5723
1857.0817
1857.5720
1858.0814
1858.5909
1859.0815
1859.5913
1856
1857
1858
1859
1860
1861
m/z

YW-D-119-2
((E.M.+2)